Advanced controller design for quasi-LPV systems applied to automotive engine control

Thomas Laurain

N° d'ordre : 17/35

UNIVERSITE DE VALENCIENNES ET DU HAINAUT-CAMBRESIS

THESE

présentée en vue d'obtenir le grade de

DOCTEUR

en

AUTOMATIQUE

par

Thomas LAURAIN

"Advanced controller design for quasi-LPV systems applied to automotive engine control"

"Synthèse de contrôleurs avancés pour les systèmes quasi-LPV appliqués au contrôle de moteurs automobiles"

Soutenue le 04 décembre 2017 à Valenciennes devant le jury d'examen :

Rapporteur	*Lars Eriksson, Professeur, Vehicular Systems, Linköping, Suède*
Rapporteur	*Said Mammar, Professeur, IBISC, Evry Val d'Essonne, France*
Président	*Thierry-Marie Guerra, Professeur, LAMIH, Valenciennes, France*
Membre	*Daniela Chrenko, MdC HDR, DRIVE, Nevers (Bourgogne), France*
Membre	*Zsofia Lendek, MdC HDR, UTCN, Cluj-Napoca, Roumanie*
Membre	*Miguel Bernal, Professeur, ITSON, Sonora, Mexique*
Directeur de thèse	*Jimmy Lauber, Professeur, LAMIH, Valenciennes, France*
Directeur de thèse	*Reinaldo Palhares, Professeur, UFMG, Belo-Horizonte, Brésil*

Thèse préparée dans le Laboratoire LAMIH (UMR CNRS 8201)

Ecole Doctorale SPI 072 (Lille I, Lille III, Artois, ULCO, UVHC, EC Lille)

The most merciful thing in the world, I think, is the inability of the human mind to correlate all its contents […]The sciences, each straining in its own direction, have hitherto harmed us little; but some day the piecing together of dissociated knowledge will open up such terrifying vistas of reality, and of our frightful position therein.

H. P. Lovecraft*, The Call of Cthulhu*

REMERCIEMENTS

No Gods or Kings. Only Man

Andrew Ryan in 2K's *Bioshock*

The special thanks will be divided into a french part and an english part (for non-french speakers, even if it is the most beautiful language of the world…)

En premier lieu, il me paraît évident de remercier celle qui a supporté dans son quotidien un thésard en pleine rédaction, avec ce que ça implique de stress et d'angoisse (RIP Chapitre 3…). Je lui suis très reconnaissant, car à naviguer dans les ténèbres sans lanterne, on risque de perdre la raison. Merci.

Je tenais ensuite à remercier ma famille qui m'a soutenu pendant ses trois ans, même s'ils n'ont pas tout compris ce que je fabriquais, en particulier ma mère Sylvie et mon père Eric, ainsi que mon frère Alexis, mes grands-parents, Raphaël et Victor, ma marraine, Jean-Seb, Ilan et Lucie.

Je voulais sincèrement remercier Elodie et François pour l'amitié qu'ils me témoignent et pour le soutien incommensurable qu'ils m'ont apporté. Je leur dois la survie de mon moral en ces années troubles.

Un jour, on m'a demandé ce qui était le plus important dans une thèse. J'ai répondu : « l'encadrement. Avec un bon encadrant, même avec un sujet pas forcément passionnant, ça se passera bien. Alors qu'un sujet génial avec un mauvais encadrant, ça donnera une mauvaise thèse ». Aujourd'hui, après trois ans à travailler avec Jimmy, je ne peux que réaffirmer cette phrase. Cet homme incarne l'optimisme et la force tranquille, et en cas d'invasion zombie, c'est le coéquipier idéal, juste pour entendre « c'est bon, ça va le faire ! » même dans les pires moments (enfin, presque, sauf en plein déluge néo-zélandais avec des dieux maoris déchaînés…). Je ne le remercierai jamais assez pour ses conseils scientifiques « Est-ce que les fils sont tous connectés ? », « C'est quoi les entrées, c'est quoi les sorties ? » ou « ouais, vas-y, soumets, on s'en tape ! » que pour ses remarques moins scientifiques « Chebi ! », « T'es allé au cinéma cette semaine ? », remarques généralement précédées d'une entrée nonchalante le mug à la main. Sans oublier les blagues d'un niveau lauberien dont la liste serait bien trop longue et qui pourrait constituer une nouvelle thèse tant elles sont « révolutionnaires ». Je voulais également adresser mes plus chaleureux remerciements à la tribu Lauber, à Séverine pour son soutien (« c'est minuit la deadline et vous n'avez pas encore fini le papier à 23h ? c'est n'importe quoi ! »), et à leurs enfants Emma, Clément et Nicolas.

A la manière de Batman et Robin, j'ai pu apprécier le soutien humain et attentionné de Mathias durant ces 3 ans de thèse (au vue des gabarits, aucun doute sur qui est qui…). Un ami, un sourire, une épaule, une licorne, un partenaire de ping-pong (le terme est volontairement choisi), un bobo-coco, un vampire, Mathias, c'est tout ça. Je le remercie chaleureusement, voire même « pouletteusement », lui ainsi que sa tribu définie croissante (donc instable au sens de Lyapunov…)

Un peu comme un dresseur d'ours, Mathias est parfois accompagné d'un barbu trapu qui gesticule en grognant. Nom scientifique : Thierry-Maris Barbus Guerrae. H-index : 41. Rapport de force : Mâle alpha du LAMIH. Son vocabulaire oral semble se résumer à « elle est où ma publi ? » et « Biomaaaaaan ! ». Je le remercie pour toute l'aide qu'il m'a apporté et la considération qu'il me porte. Je remercie également sa chère et tendre tricoteuse de bonnet Murielle. J'adresse également mes remerciements les plus sincères à son fils et mon doppelgänger Jérémie (et à ses fichiers Excel), lui aussi fervent cultiste du laubérisme qui n'emprunte pas la route la plus longue, et à Angie, avec qui je ne me suis pas marié.

Je remercie également tous mes collègues doctorants du laboratoire, en particulier Anh-Tu (la sagesse à la vietnamienne !), Ciska et ses regards incendiaires quand je l'embête alors qu'elle travaille, Victoria et le vent d'Avignon, Tariq l'indien contre le monde, Michael, Guoxi (« comment on organise un anniversaire ? »), Braulio (« Professor Güera »), Serhii, Pippit, Mohammed, Van Anh, Anis et le bureau des bioméca (où ça rigole plus souvent que ça ne travaille ;) Lydia (« je mets quoi comme chaussures pour la conf ? »), Amir, Salvatore et ceux que j'oublie de la cave.

Sans oublier les anciens du labo, mon ami et ancien partenaire de bureau (mais pas que ;) Rémi (« deliver us !!!!! »), Raphaël dit Raton, Victor, Reymundo, Ben et Thach.

Je tenais également à remercier les permanents de ce laboratoire dont j'ai arpenté les couloirs pendant trois ans tel un zombie, en particulier Michel (merci pour les voyages ! euh… déplacements professionnels…), Seb D. (« Billy boy ! »), Seb P. (le magicien), Sami la roulette, Serge (« regarde tes mails ! »), Thierry (« T'as une petite mine »), Mappy, JC, Chouki, Philippe, Jérôme, Patrice, Patrick, Mohammed et Michaël, les bioméca et tous ceux que j'oublie par inadvertance.

J'adresse mes sincères remerciements plein de sirops d'érable au Professeur Dany Gagnon.

Enfin, il me paraissait important de remercier Mélanie, Isabelle, Josèphe et Sylvie pour m'avoir supporté (les 21 OM…). Courage les filles, je pars bientôt…

I would like to warmly thank Reinaldo, my advisor from Brazil for his valuable scientific advice 'Thomas, at the end of the third year, maybe you can do some state of the art, what do you think ?' and non-scientific advice : 'don't forget your sunblock !'. He made my stay in Belo Horizonte unforgettable, particularly the trip to Serra do Cipo (nice hat by the way !) or the one to the Parque das Mangabeiras ('of course it's open !'). As welcoming as Reinaldo, I would like to thank the Palhares' family, Velusca (with who I tasted my first caipirinha), Lionel ('are you happy ?') and Natasha ('starting by T… Thanks ! your turn !'). Obrigado para você !

I would like to thank all my friends in BH, particularly my roomates of this wonderful appartment, Tiago ('maladif'), Rafael ('Bacon is life !'), Aéçio (twin brothers !) and Luisa (Doctor Luisa !). My warm thanks are going to Wagner ('Mister Happy !') and his family for being so welcome and kind with me ; the DIFCOM team: Fernando and Leonardo (I liked our discussions on SF movies !), Heitor (Prof-Heitor !), Fulvia ('I don't want to touch the bat !'), Rosileide ('la cachoeira de açai'), Klenilmar ('16 :00 CREME DE ACAI !!!!'), Ramon (Ouro Preto, the city of crazyness !), Douglas, Antoniel, Pedro, Guilherme (don't kill me !) and those I forgot to mention. I would like also the thank the professors

from the other laboratories with who I discussed and collaborated, Prof. Pujatti and Carlos from CTM and Prof. Pereira from the robotics lab.

I would like to coldly (winter in Romania…) thank Zsofi, my non-official advisor from the land of vampires for being so kind and so thoughtful with me, even if you are a little terrifying sometimes (when you think I didn't correct a paper but I did, for example ;) or when you kindly asked me to move from another line at the pool ;) Thank you very much for everything, for scientific advice (covering the papers in red, fully) and non-scientific advice : 'go home !' I don't have enough vocabulary to say thanks, so, Multumesc !

Also, I want to thank the ROCON team, Lucian ('Why a man is naked in the desert ?'), Paula, Tassos, the two 'French' visitors from Nancy, Jihene (official guide of Salina Turda) and Mathieu, my dear friend Zoli ('We are in Hawaii !'), Reka, the traditional hungarian dance group, Vlad and Ioana the (lazy) funny vampires and those I forgot to mention. See you in AQTR 2018 to eat Kovacs Kalacs and Papanasi !!

Finally, I would like to end the english part by thanking Pr. Lars Eriksson and Pr. Said Mammar for accepting to review my thesis manuscript and for their expertise, and Daniela Chrenko and Miguel Bernal (JFC) for being members of my committee.

Je dédie cette thèse à Chloé, à Lola et à la petite Céleste.

OUTLINE

GENERAL INTRODUCTION

He often wondered if all these advances, which never ceased to revolutionize the world, would not eventually deprive humanity of what life had of its originality and its peculiarities.

M. Chattam, *Léviatemps*

Even if alternatives are investigated, cars remain the main part of the transport system in the world: for example, the 2016th edition of the "Energy, transport and environment indicators" report of the European Union figures that in 2013, among the 28 countries, passenger cars represent an average proportion of 83.2% of the ground transport (Fig. 1). The number of motor ground vehicles to carry passengers has increased from 2005 to 2014 in all the countries of the EU, except in Lithuania and Germany. For instance, in 2014, there is one car per two inhabitants in countries like Finland.

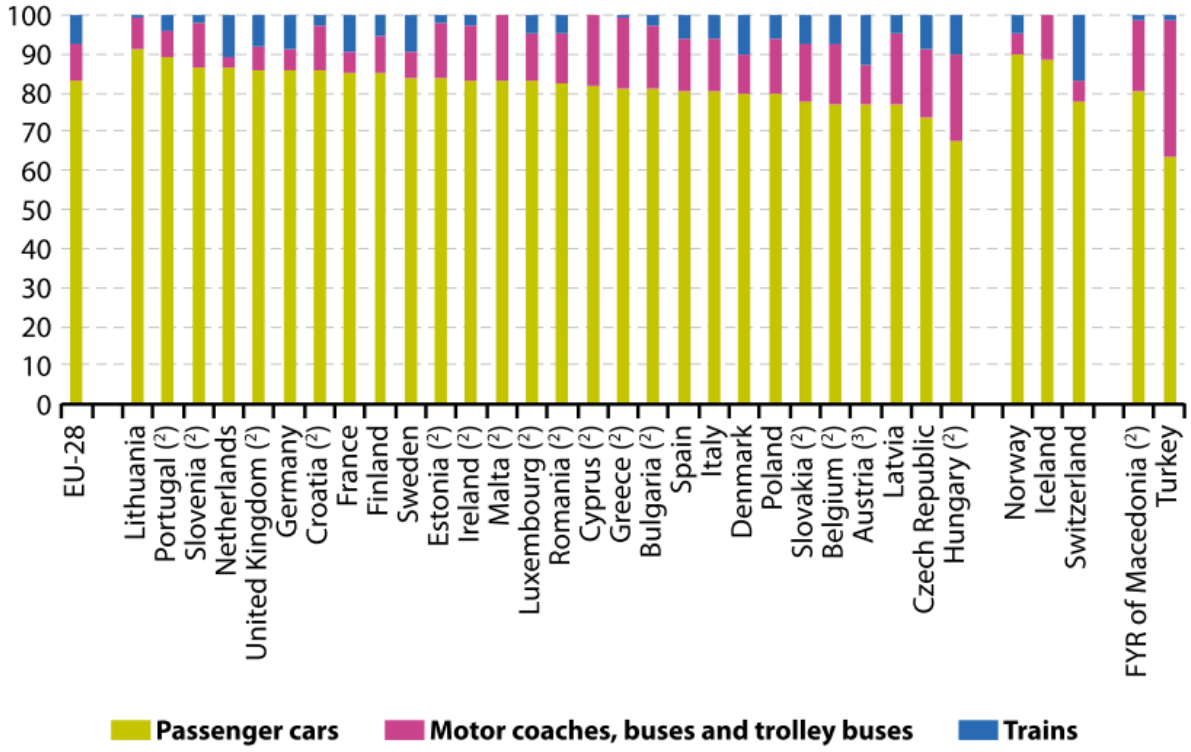

(1) Excluding powered two-wheelers. Cyprus, Malta and Iceland: railways not applicable.
(2) Includes estimates or provisional data.
(3) The railway in Liechtenstein is owned and operated by the Austrian ÖBB and included in their statistics.

Source: Eurostat (online data code: tran_hv_psmod)

Fig. 1. Split of ground passenger transport mode in 2013 (% of the total passenger-Km)

In addition to the passengers flow along Europe, the transport of goods follows the same scheme: In 2014, 74.9% of the freight transportation was ensured using trucks and ground vehicles (even if this number is slowly reducing). For the European Union, the ground transport sector is a multi-domain

challenge. Indeed, road transport represents an important part (27.3%) in the total consumption of energy for the whole European Union (Fig. 2) and road transport becomes an energetic problem.

Moreover, 40% of the energy produced in Europe comes from petroleum products (352.9 millions of tons of oil equivalent, Mtoe) (Fig. 3). Considering the price of the different fuels that are increasing (Fig. 4) and the global consumption for road transport that has increased by around 20% in the last thirty years (Fig. 5), the road transport is an economic issue.

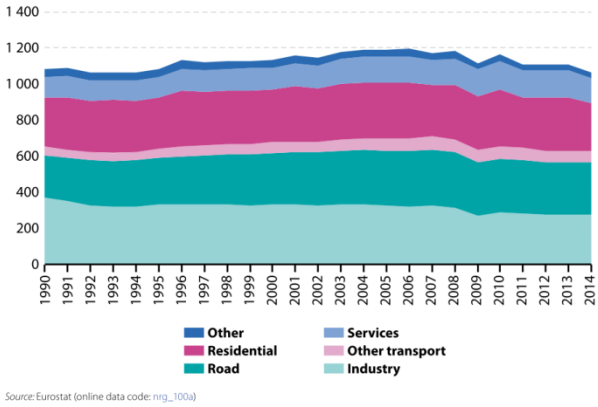

Fig. 2. Final energy consumption, by sector (Mtoe) (Eurostat:nrg_100a)

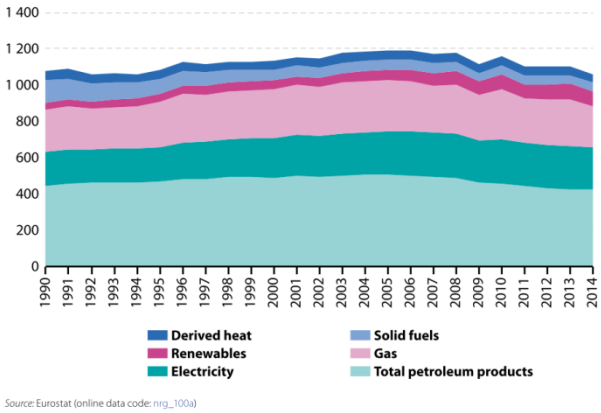

Fig. 3. Final energy consumption, by fuel, (Mtoe) (Eurostat:nrg_100a)

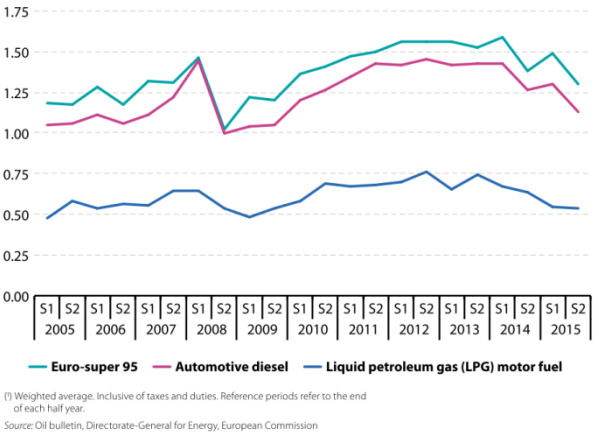

Fig. 4. Consumer prices of petroleum products (EUR/liter) (Oil bulletin, European Commission)

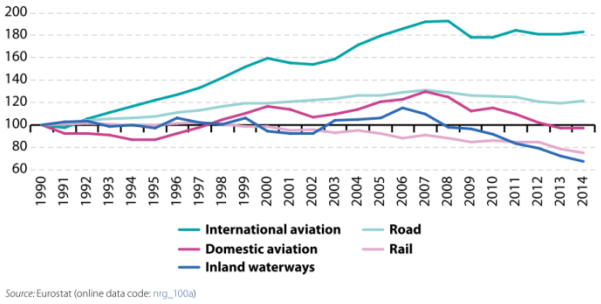

Fig. 5. Energy consumption by transport mode (based on the index of the year 1990) (Eurostat:nrg_100a)

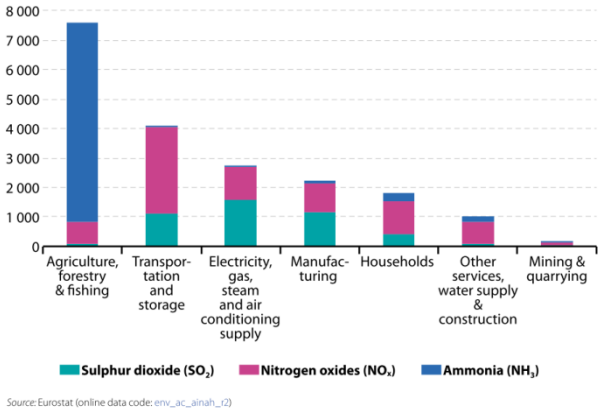

Fig. 6. Emissions of acidifying gases, by sector (equivalent of 1000 tons of SO_2) (Eurostat:env_ac_ainah_r2)

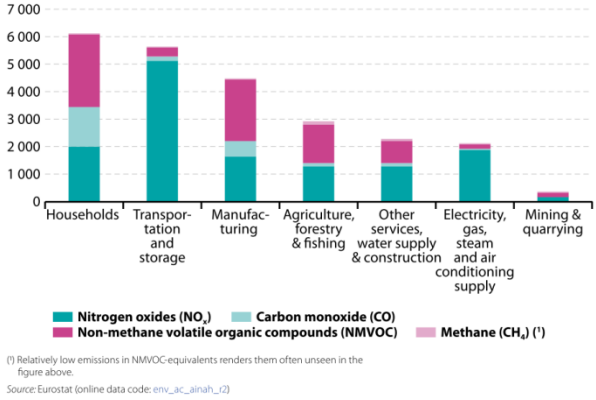

Fig. 7. Emissions of ozone precursors, by sector (equivalent of 1000 tons of SO_2) (Eurostat:env_ac_ainah_r2)

If the engine consumes fuel, it also rejects pollution: In addition to the CO_2 exhausted by the combustion of the engines, the transport represents the most important part of all activity sectors for the nitrogen oxides NO_x by considering the two classes of polluting gases, the acidifying gases and the ozone precursors (Fig. 6 and Fig. 7). Studies have been realized in several countries to evaluate the consequences of air pollution caused by the car engines, such as in Portugal (Sa et al., 2015), Canada (Jordaan et al., 2017) or China (Lang et al., 2016). Considering the disastrous impact that engine emission gases have on the planet, that makes road transport an ecologic and environment problem. And because the pollution gases emitted by the ground vehicles may damage the lung tissues and cause respiratory diseases (emphysema, bronchitis), heart diseases or premature death, road transport may be a concern for the mankind.

How can the advanced control tools reduce the consumption of the fuel and the emission of polluted gases with adequate solutions according to the industry constraints?

The manuscript is composed of 4 chapters and a conclusion. Chapter 1 introduces the functioning of the gasoline engine and focuses on the different controllers that have been already developed and tested, highlighting the advantage and inconvenient of each solution. Among the designed control laws, two main methodologies are used, including or not a model. After the statement of the existing solutions, the choice is made to consider a model-based controller, managing the nonlinearities with the Takagi-Sugeno (TS) representation.

Chapter 2 is dedicated to the modelling process of the engine. The transformation realized on the hybrid model of (Balluchi et al., 2010) is detailed, as well as the crank-angle domain conversion. The model is then reduced to be suitable for controller design (control-oriented model). The identification phase is presented, providing values to the constant parameters depending on the engine. Datasets from the engine test bench located in the LAMIH, University of Valenciennes, are used to the identification and the validation of the model. Fig. 8 depicts a photo of the engine equipment used along the thesis (@Alexis Chézière)

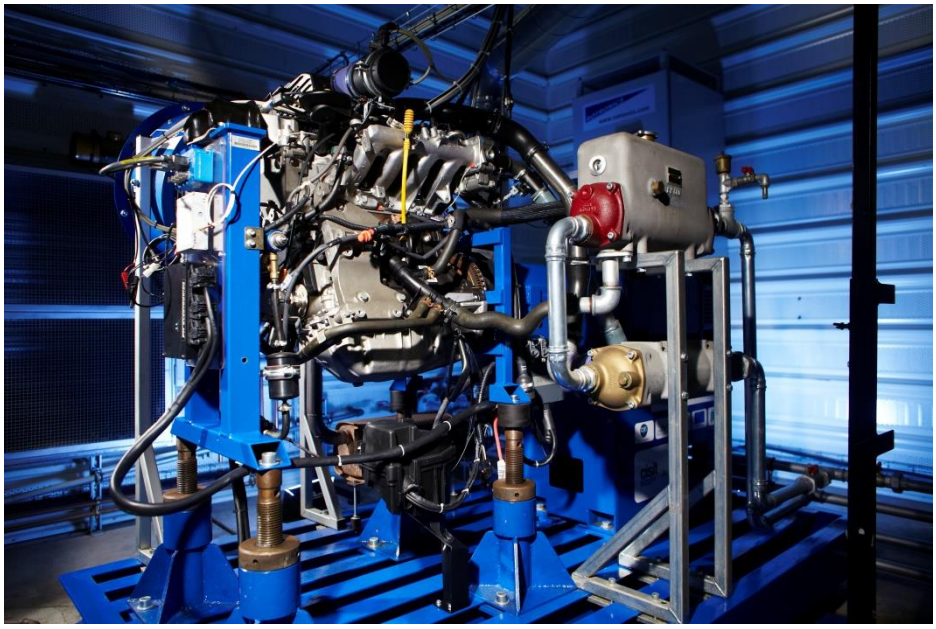

Fig. 8. Engine test bench of the LAMIH (UMR CNRS 8201), University of Valenciennes, France

Chapter 3 presents the methodology for the design of the idle speed controller. The control law is chosen and the Lyapunov direct method is then applied to study the stability of the closed-loop. LMI conditions are obtained and relaxed to be solved. Due to the complexity of the controller, an alternative controller is designed, ensuring the same performances but with a less complex structure that can be more easily handled by a commercial Electronic Control Unit (ECU). Simulations and experimental results are provided to show the feasibility of the proposed controller.

Chapter 4 presents the steps of the air-fuel ratio controller design. The transformation from a variable transport delay to a fixed delay is introduced and generalized. A linear controller is chosen and the Lyapunov direct method is again applied. LMI conditions are obtained for TS models with known delay on the input. Similarly to Chapter 3, simulation and experimental results highlight the efficiency of the proposed methodology.

Finally, a conclusion ends the thesis with a summary of the results analysis, discussions, limits and perspectives of the presented work.

CHAPTER I: Generalities about IC Engine

…and then I'm going to show these people what you don't want them to see.

Neo (K. Reeves) in *Matrix*

1. Why considering IC engine management as a research topic

1.1. Functioning of the engine

Ground transportation vehicles are using several kinds of fuel and engines to ensure their propulsion: Gasoline, Diesel, hybrid propulsion including electricity, hydrogen and so on, biofuels, etc... Among them, the gasoline engine is the most common (more than 50% in Europe) and is the one considered in this thesis. A global scheme of the functioning of the gasoline engine can be found in (Lauber et al., 2011) (Fig. 9).

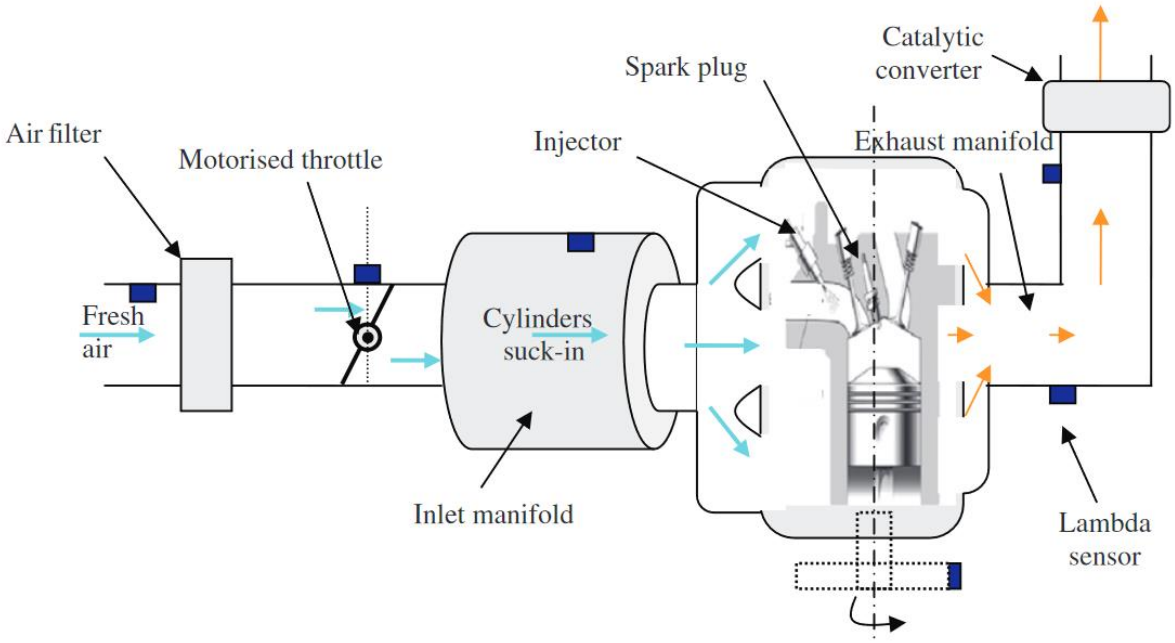

Fig. 9. Global scheme of the gasoline engine

The motorized throttle is connected to the gas pedal and it is responsible for bringing air inside the cylinders from the intake manifold. While the air is entering inside a cylinder, fuel is injected, creating the air-fuel mixture that is blended inside the cylinder. The spark plug generates the spark that ignites the mixture and creates the combustion, so the production of the torque via the piston. The burnt fuel and gas are then exhausted through the exhaust manifold to the catalytic converter, when they are chemically transformed to reduce the pollution.

The most common gasoline engines are composed of four cylinders that are following a cycle (the 4-stroke engine): Intake of air and fuel; Compression of the mixture and spark ignition; Expansion of the piston by the combustion and torque production; Exhaust of the gas and fuel that stay unburnt, as summarized in Fig. 10. Each cylinder changes his phase when a dead-center is reached. Two dead-centers have to be distinguished: Top-dead-center, when the piston is at the maximum of its linear displacement, and Low-dead-center, when it is at the minimum. Then, the change of phase occurs every 180 degrees of the crankshaft and all the cylinders complete the cycle in two turns of the engine (720 crankshaft degrees) (Fig. 11). This repetitive behavior makes the gasoline engine be considered as a cyclic or a periodic system as the definition given in (Bittanti and Colaneri, 2009).

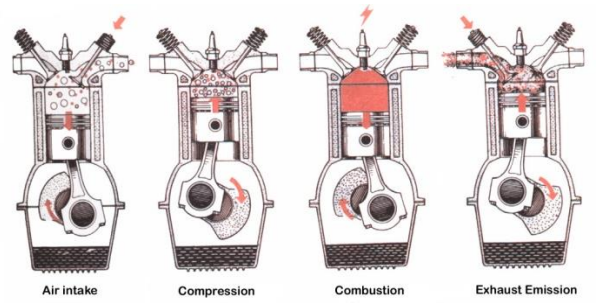

Fig. 10. Different cycles of a cylinder

Phase / Cylinders	C1	C2	C3	C4
P1 (0° to 180°)	I	C	H	E
P2 (180° to 360°)	C	E	I	H
P3 (360° to 540°)	E	H	C	I
P4 (540° to 720°)	H	I	E	C

I: Intake (1) C: Compression (2)

E: Expansion (3) H: Exhaust (4)

Fig. 11. Example of an engine phase configuration

The efficiency of the engine can be measured considering the torque generated for a given air-fuel mixture, the average consumption of fuel or the quantity of remaining gas after the combustion that are partially transformed by the catalytic converter and are released as pollutant gases.

1.2. Evaluation of the engines: Driving cycles

In order to evaluate the engine efficiency in term of fuel consumption and pollution reduction, trials are realized on roller test benches. The vehicles have to follow a speed reference given by a driving cycle which is used to represent several road driving conditions. The driving cycles are constantly improved, like the New European Driving Cycle (NEDC) that provides in 1970 an urban cycle composed of four similar schemes, and in 1990 an extra-urban cycle containing more acceleration-deceleration phases (Fig. 12). The last cycle that was built in 2015 by experts from all over the world, the Worldwide harmonized Light vehicles Test Procedure (WLTP) is considered as the most representative of the human behavior for cars (Fig. 13) (Pavlovic et al., 2016).

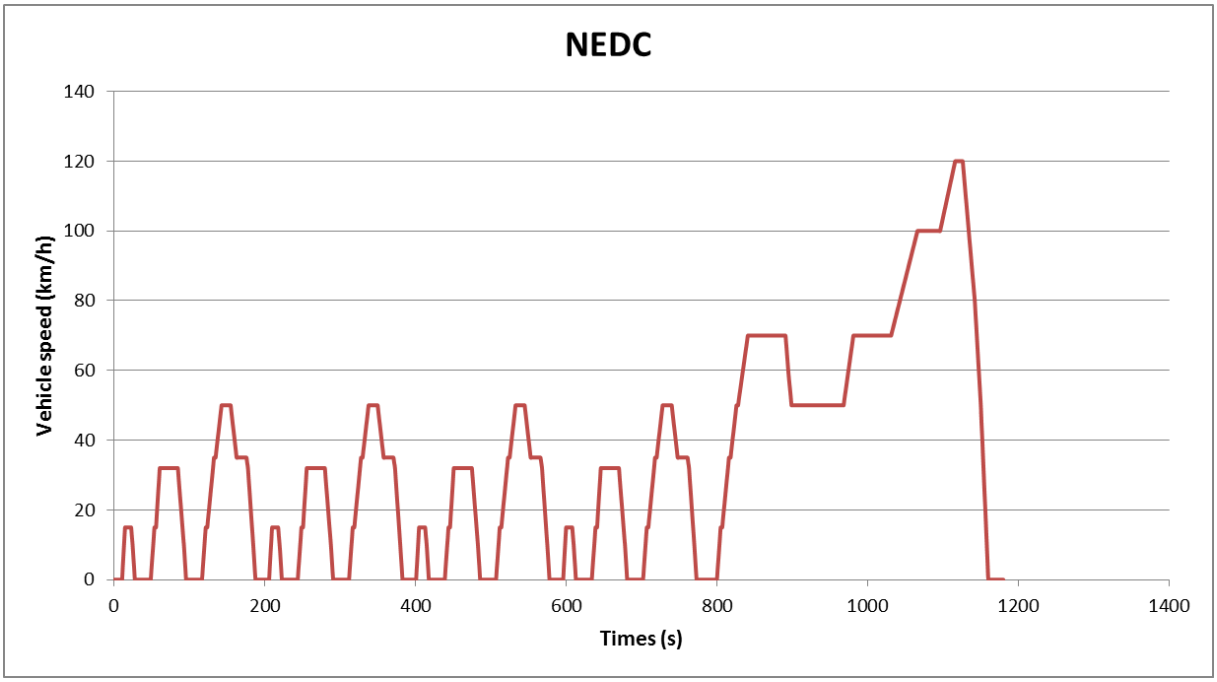

Fig. 12. The New European Driving Cycle

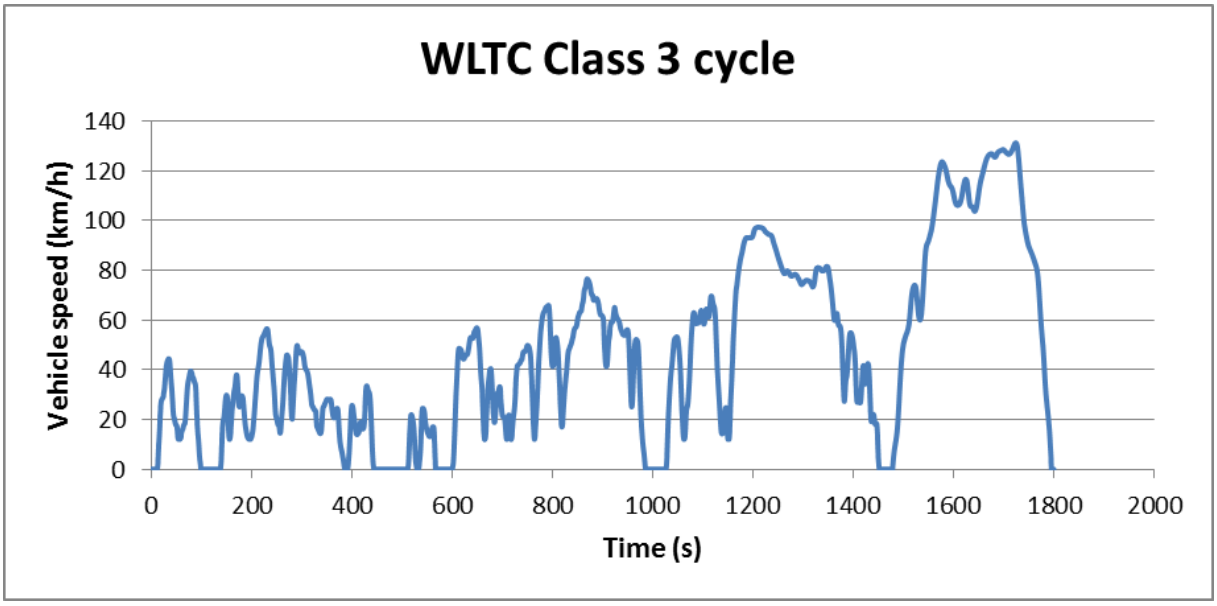

Fig. 13. The Worldwide harmonized Light vehicles Test Procedure for Class 3b vehicles (most common)

Governmental entities, such as the European Union, have increased the constraints about emissions of polluting gases on the car manufacturers through several norms, such as the European emissions standards (Euro I to Euro VI). However, until Euro III, the driving cycle used for the emissions tests is the NEDC, which is not the most representative. Indeed, brutal changes of speed and speed variance are directly linked to the emissions of pollutant gases (Nesamani et al., 2017). Since 2000, constraints imply cold start (around 30°) which is a critical phase for pollution. Moreover, differences in emissions and fuel consumption between driving cycles and real-world driving represent between 30% and 40% (Fontaras et al., 2017). Even if efforts have been done in the legislations to build less polluting cars, there is still room for improvement especially during transient operation.

Considering the worldwide concerns car engines represent and how constraints and tests are currently reinforced to reduce their impact on the planet and the humanity, several possibilities have been investigated to improve the efficiency of the engines: mechanical researchers focus their work on topics like reducing the frictional losses between the piston and the cylinder chamber (Rahmani et al., 2017), chemical researchers working on alternative fuels such as alcohol (Yusri et al., 2017), and so on… Our work remains in the context of electronic engine control which has received a growing interest from the automotive industry. The next part proposed to answer the question How is controlled a gasoline IC engine?

2. Spark ignition (SI) Engine control

2.1. Introduction to SI engine control

2.1.1. Main control inputs for standard SI engines

Electronic engine control has been considered since the engines are equipped with an Electronic Control Unit (ECU) containing algorithms to automatically control the mechanical actuators of the

engine. Among the most important actuators of the engine, a vast interest has been focused on controlling the motorized throttle, the injectors and the spark plugs. The control input for the motorized throttle is the desired angle for the butterfly valve. The injectors have two control inputs: The start of injection and the injection time. Then, knowing the fuel mass flow inside the injectors, it is possible to estimate the amount of fuel injected in the cylinders. Contrary to the throttle that acts on the global amount of air for all the cylinders, each cylinder has its own injector, allowing designing a customized control for every cylinder. For a four cylinder engine, the injectors have then eight control inputs, the start of injection and the injection time for each cylinder. Similarly to the injectors, there is one spark plug per cylinder. They are responsible for creating the spark that is igniting the air-fuel mixture. The control input of each spark plug is called the spark advance and it is measured in degrees before the Top-dead-center (degrees BTDC). It represents the moment the spark is generated during the Compression phase before the piston reaches its maximum position, the Top-Dead-Center. These are the main control elements of the standard engines, as presented in Fig. 14.

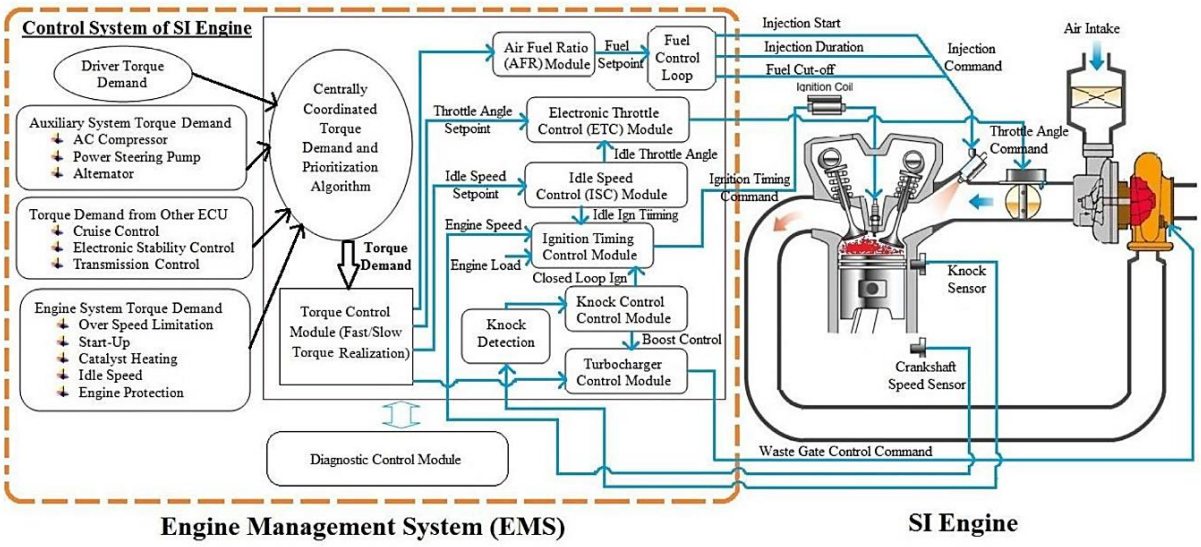

Fig. 14. Engine Control System architecture presented in (Ashok et al., 2016)

2.1.2. New technologies for engine control

In order to improve the standard engine efficiency, new technologies and actuators have been developed. The Exhaust Gas Recirculation (EGR) system reduces the production of NO_X by driving the exhaust unburnt gases to the intake manifold, passing through a thermic cooler (Thomasson, 2009; Wei et al., 2012). The EGR wastegate valve is then another control input for the engine system. More complex structures can be found, such as dual-loop EGR including a standard EGR loop and a turbocharged loop equipped with a Variable Geometry Turbocharger (VGT) as in (Daasch et al., 2016).

In order to enhance the control of the combustion inside the cylinders, some technologies have been investigated to control the amount of air inside each cylinder, such as it is done with the injectors for the fuel. This technology features Variable Valve Timing (VVT) and Variable Valve Lift (VVL) and provides a customized control of each intake and exhaust valve of each cylinder as depicted in Fig. 15 (Leroy and Chauvin, 2013; Xie et al., 2014).

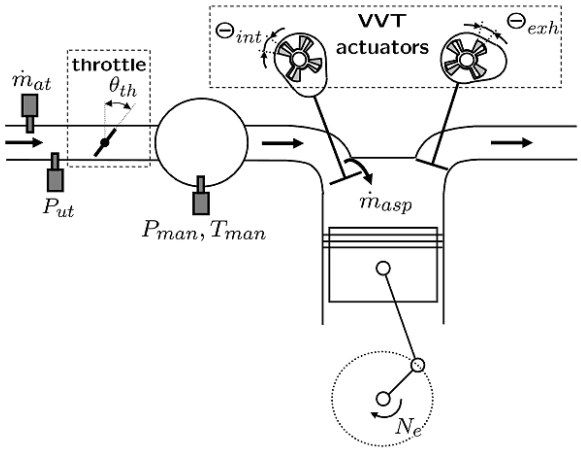

Fig. 15. Air-path with variable valve timing actuators as in (Leroy et al., 2008)

Considering the direction taken by both the research and the industry in the automotive sector on hybrid vehicles (Enang and Bannister, 2017) or biofuel combustion (Carbot-Rojas et al., 2017), the gasoline engine remains a constant and important part whose control has to be improved to optimize these combined architectures. How are the engines in commercial cars currently controlled?

2.2. Industrial control strategies

2.2.1. Position of the car manufacturers

Car industries have nowadays to face different pressures from the socio-technique business market, the globalization and the economic crisis. In addition, they received more and more constraints from the governments and legislative entities, so a real fight starts between them. A fight that is not always fair-played. The 18 September 2015, investigations revealed that the German car manufacturer Volkswagen had an algorithm to automatically detect emissions test conditions and to switch to 'ideal' control strategies where pollution reduction is considered in spite of power torque. The reports details that Volkswagen cars generate forty times more pollution in real-driving conditions than the results announced during the European emission tests. The insistence of the investigations reveals that other car manufacturers, like Audi, Seat, Renault or Porsche, have done similar procedures to "cheat" during the tests. More than the legal question it raises, the Volkswagen scandal was a disaster from an economic, ecologic and human health point of view (Oldenkamp et al., 2016).

Interviewed during the Paris' Automotive Show 2016, several representatives of the main automotive supplies (Dacia, Suzuki, Jeep, Alfa Romeo…) answered to the question "is this car polluting?" by "no, it does not pollute, it is conformed to the European norms". This summarizes well the current industrial philosophy: doing the minimum for their cars to be validated during the European emission tests. From the engine control point of view, if a very simple controller provides average performances but meets the norms constraints, it is acceptable.

In addition to this legal minimum design, an historical background has to be taken into account: because applied control theory is a "recent" science compared with mechanics or chemistry, it has received a growing interest in the automotive industries since last two decades. If they have no

problem about modelling the nonlinear behavior of the engine and the combustion inside a cylinder with the mechanical background they can rely on, the control of nonlinear periodic systems and the control theory tools such as Lyapunov functions are rarely explored by the car suppliers. Indeed, because of socio-techniques constraints, they prefer to have simple engine control strategies that can be understood and tuned along the manufacturing process of the engines.

2.2.2. Simple control strategies

2.2.2.1. Look-up tables

Among the simple strategies used by the car manufacturers, the most common is the look-up table (LUT). It consists on a table with several inputs and one output, constructed along operating points. It is built based on hours of engine tests, by setting the control inputs through a gridded space to reach the operating static points, see Fig. 16. Then, for the control, the maps are inverted to get the control inputs in function of measured values (speed, intake manifold pressure and so on). From a control aspect, it is usually used as open-loop control, mainly feedforward action. Instead of considering any complex nonlinear model, the nonlinearities can be 'manually' modelled along the points of the map to fit the behavior of the engine at a given moment.

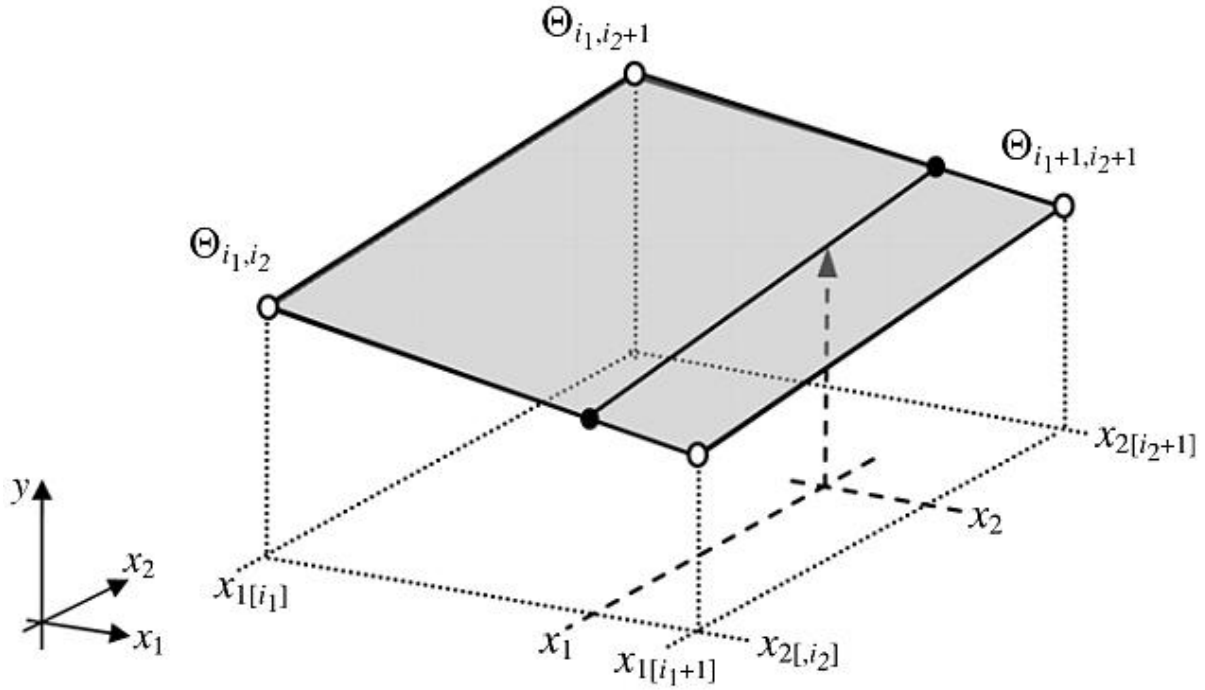

Fig. 16. 2-dimensions look-up table and interpolation as in (Peyton Jones and Muske, 2009)

This raises two main drawbacks: first, the LUT cannot ensure satisfying performance in transient phases. While the behavior of the engine is mastered on the operating points, when the engine is switching between two points, linearizing and interpolating are used to determine the control to apply to this highly nonlinear system, which highlights the problem of stability, see Fig. 17.

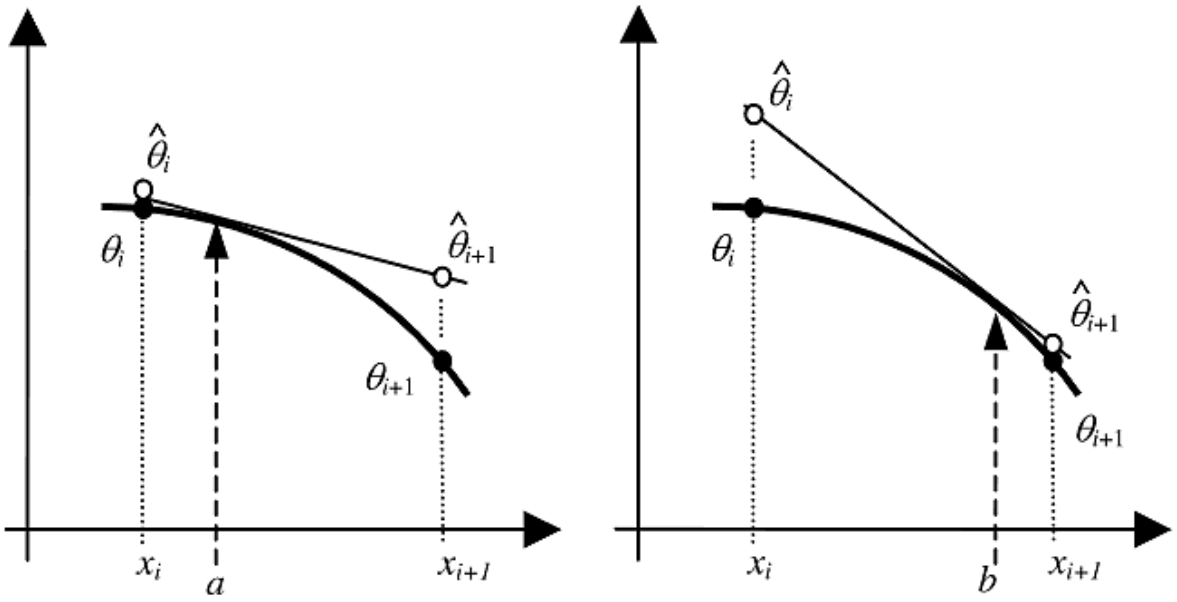

Fig. 17. Problem of interpolation of nonlinear systems as in (Peyton Jones and Muske, 2009)

The second one is that the physical changes that may occur on the engine (change of temperature, aging, …) are hardly taken into account by the maps, so by the generated commands. LUT depending on the engine temperature can be constructed, from the cold start to nominal hot conditions, however, this increases the number of hours needed to setup one engine (Peyton Jones and Muske, 2009). Several changes, such as mechanical aging or mechanical imperfections inside each cylinder, are impossible to be considered by static look-up tables. An adaptive algorithm could be included to change in real-time the look-up tables, but implementation of such algorithms is limited by the capacities of the industrial controllers, see Chapter 1, Section 5.1.2.1.

2.2.2.2. PID controllers

The PID controllers are the most common feedback controllers used in the industrial applications and are still considered in the research field (Liu et al., 2015). They are composed of three action terms: Proportional, Integral and Derivative, such as the control law is

$$u(t) = K_p e(t) + \frac{1}{T_i}\int e(t)dt + K_d \dot{e}(t) \tag{1.2.1}$$

Where $e(t) = y_{ref} - y(t)$ is the error between the output of the system and the considered reference the system has to track. Due to the presence of the integral term, the PID controller provides transient performances as well as reference tracking. For this ability to track references, PID controllers are used in numerous applications in engine control, such as the wastegate throttle control (Thomasson, 2009) or injector control for air-fuel ratio management (Ebrahimi et al., 2012). Moreover, thanks to this integral term, it is able to compensate any static error that may occur with aging. However, this integral term can be a problem in case of input saturation, a common case in real-world applications. If the command is saturated, the integral part will continue integrating the tracking error, making the control signal diverging. An anti-windup structure can be implemented to avoid this problem, as introduced in (Hanus, 1980). The structure is depicted in Fig. 18.

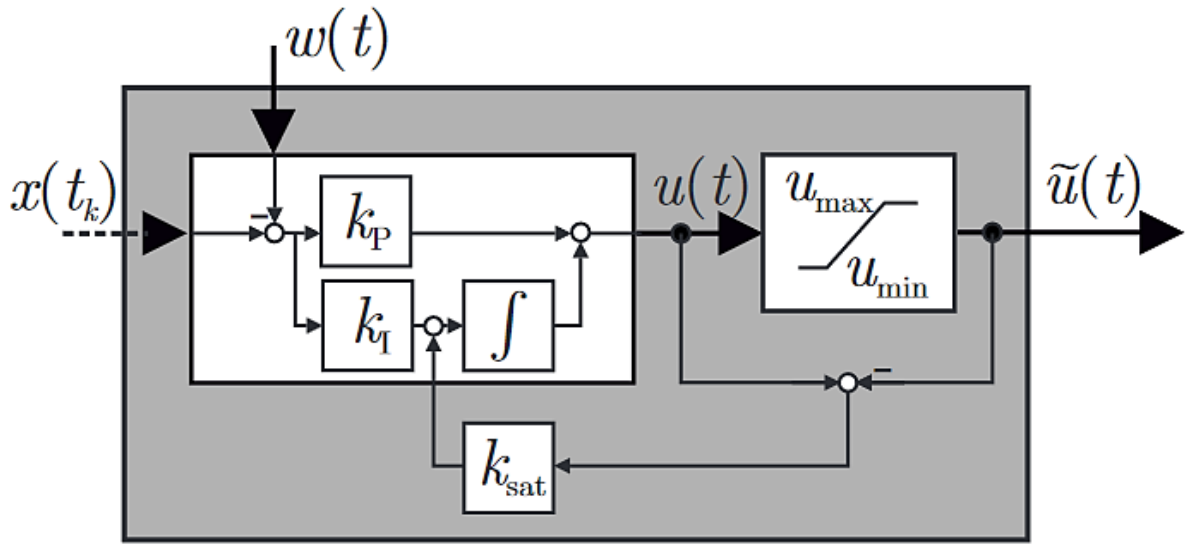

Fig. 18. Anti-windup structure for a PI controller presented in (Lehmann and Johansson, 2012)

A second problem that may appear is the derivative term. It is hard to implement and present a backoff behavior: when the measured output signals are saturated, it can cause similar problem as a saturated input for the integral term (Theorin and Hägglund, 2015).

Despite their performances, PID controllers present the main disadvantage of the tuning of the parameters. Normally, the PID belongs to the class of model-based controllers, where the gains are obtained through a stability analysis of the closed-loop. Because the engine is a highly complex and nonlinear system, three approaches exist: Tuning the PID parameters on a very simple linearized model, tuning the parameters empirically or design self-tuning adaptive PID (Däubler et al., 2007). Because the parameters are often hard to get by the analytical way, the stability of the closed-loop is rarely ensured. That is why PID controllers are mainly used to control linear parts of the engine, like the motorized throttle (Solyom and Eriksson, 2006). Some research has been done in improving the PID structure, for example with fuzzy logic (Premkumar and Manikandan, 2015), sliding mode (Tavakoli and Seifi, 2016) or fractional order PID (Shah and Agashe, 2016).

Improving the existing simple controllers to deal with nonlinear systems, or investigate new methodologies is the position of the automotive research community. Instead of passing the norms, automotive researchers work on optimizing the reduction of pollution and fuel consumption (Killingsworth et al., 2009; Waschl et al., 2014; Ji et al., 2016; Meng and Pan, 2016). Facing nonlinearities, the academic researchers have proposed to adapt control theories to the applicative world, like neural network control (Liu and Zhou, 2010) or model-based control (Eriksson and Nielsen, 2000), to control the three inputs of a standard engine: the motorized throttle, the fuel injection and the spark advance. The throttle is controlled in the special case of idle speed, where the driver does not apply any input. The spark advance is controlled to optimize the produced torque. The fuel injection is controlled to balance the air-fuel mixture. What can be controlled in an engine with these three inputs?

3. Idle Speed Control

3.1. Introduction to Idle Speed Control

Idle Speed Control (ISC) is a special case of the engine control. It occurs when the driver does not apply a direct input, so the motorized throttle needs to be automatically controlled to regulate the engine speed. The most common configuration is when no command is sent from the gas pedal, so the car is not moving and the engine is working at a constant idle speed. The situation occurs for example when a traffic light is red, or at the start of the engine, even if some technologies have been developed to face these issues (Shancita et al., 2014), like the stop-and-start technology alimented with electric battery (Ozdemir and Mugan, 2013) or hydrogen (Ji et al., 2016). Other situations can be in case of hybrid vehicles where the gasoline engine only works to reload the batteries like an electric generator (Zhang et al., 2016). In this case or in the other, the gasoline engine has no gear engaged and it does not need to produce any torque to satisfy driver demands or road profile, only to maintain a constant idle speed.

As a control point of view, ISC includes following a constant reference, the idle speed reference that should be as low as possible without staling. Indeed, by reducing the rotations per minute of the engine during the idle phases, the fuel consumption is also reduced (Guzzella and Onder, 2010). However, disturbances may occur during the idle speed, for example, a torque demand from the electric starter equipment when an electronic device (air-conditioning, etc…) is turned on (Ma et al., 2002). So the idle speed control module should include enough robustness to handle disturbance rejection. A summary of the idle speed control structure is given in Fig. 19.

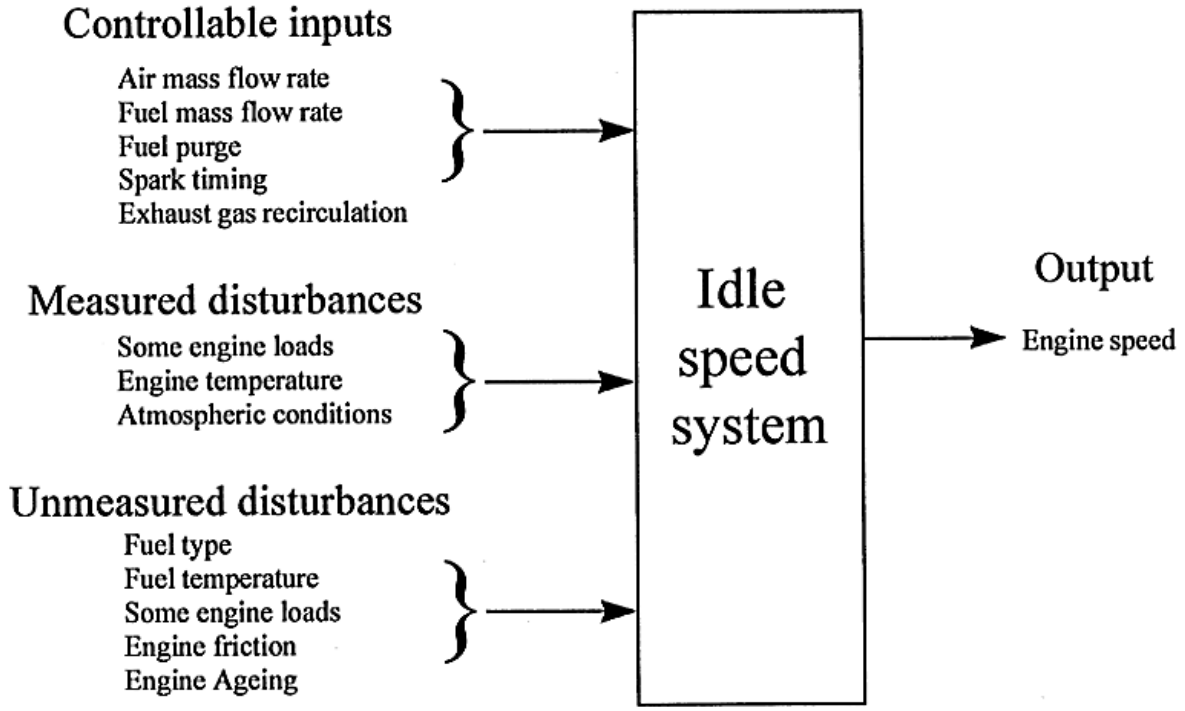

Fig. 19. Inputs, outputs and disturbances of idle speed control (Thornhill et al., 2000)

The control inputs involved in idle speed control are the throttle and the spark plugs. They are both involved in the torque production, so in the speed dynamics. In this configuration, the throttle

produces a slow-response torque whereas the spark plugs contribute with a fast-response but a small magnitude (so it can be considered as efficiency with respect to the torque) as in (Solyom and Eriksson, 2006). A common idle speed control strategy is then to set the spark plugs at non-optimal conditions, and to reach the optimal point when a disturbance occurs to quickly handle it while the throttle is controlled to reach again the idle speed reference. As a summary, two kinds of controller have to be designed: One for the throttle and one for the spark plugs customized for each cylinder. What are the existing strategies for controlling these elements?

3.2. Throttle control for idle speed regulation

3.2.1. Throttle control strategies

The control of the throttle in idle speed context has been hugely addressed in the literature (Hrovat and Sun, 1997; Thornhill et al., 2000; Ye, 2007; Ashok et al., 2016) through different methodologies. As previously detailed, the PID controllers, for their tracking ability and their easy application, have been commonly used for throttle control to regulate the speed at idle (Solyom and Eriksson, 2006). As the output to match the reference, PID ISC controllers use the engine speed or the produced torque. Indeed, it is common to use a torque structure to represent the engine, considering the torque reference, the torque produced by the air path and the contribution of the spark also as a torque (Bohn et al., 2006). However, the torque structure presents the main inconvenient that torques are not measured variables of the engine.

The adaptive controller theory has been investigated due to his flexibility. The control law is based on time-varying gains that are estimated and then adapted. The structure can be enhanced with disturbance rejection, anti-windup or extension to time-delay systems for the Adaptive Posicast Controller (APC) (Yildiz et al., 2011) (Fig. 20). The adaptive controller can be improved by combining the flatness-based theory and the fuzzy logic (Rigatos et al., 2014a).

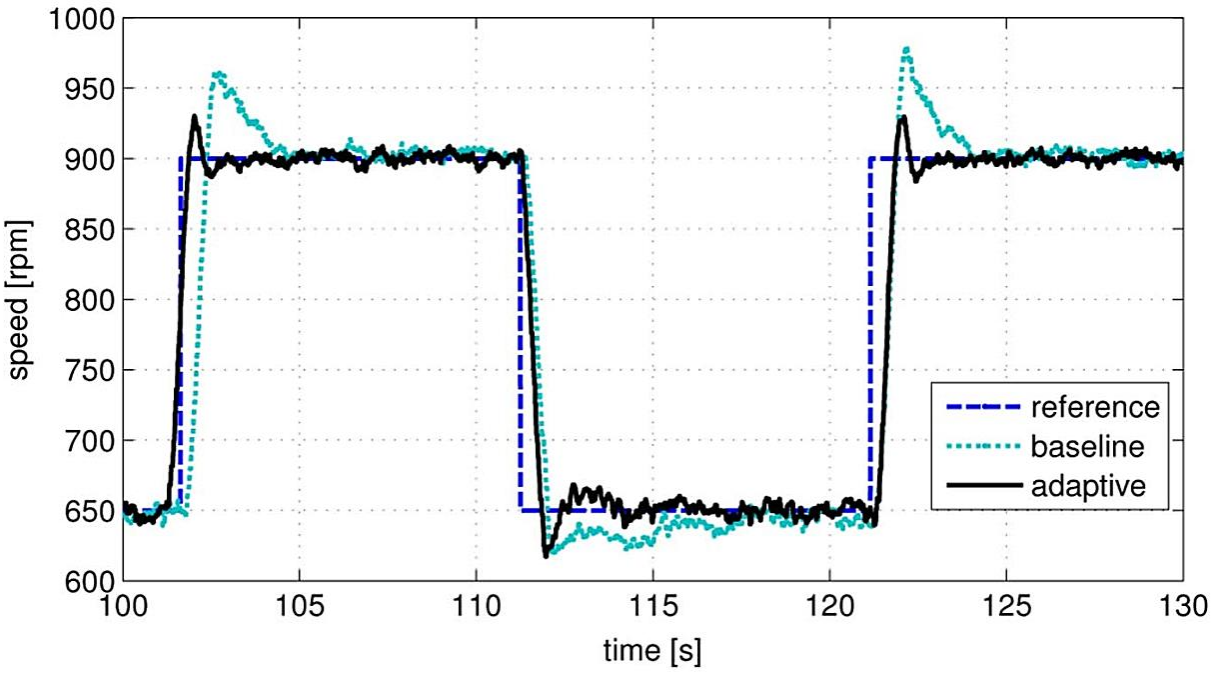

Fig. 20. Real-time results of the idle speed controlled by the Adaptive Posicast Controller designed in (Yildiz et al., 2011)

Fuzzy logic and fuzzy control have been used since last century to control the engine (Bortolet et al., 1997). Indeed, fuzzy control presents the advantage of being able to control a nonlinear system such as the internal combustion engine without the complex modelling part. These controllers are based on rules and expert-knowledge to control the throttle to reach the idle speed. The fuzzy logic has been used in complement to other strategies in a vast part of the engine control literature, for example for the air-fuel ratio (Ghaffari et al., 2008) or for diesel engine control (García-Nieto et al., 2009).

Contrary to the fuzzy logic, the model-based controllers have been hugely investigated in the literature since most of the equations of the air-path dynamic are known. Model Predictive Control (MPC) has received a growing interest in the automotive industry for its ability to solve optimization problems with specific constraints, like the ones engine manufacturers have been imposed (Hrovat et al., 2012). A Model Predictive idle speed controller has been developed in (Di Cairano et al., 2012) including throttle and spark advance control and facing disturbances (Fig. 21) and the particular case of the cold start. Specific improvements have been realized in the field of MPC to deal with nonlinear systems, and Nonlinear Model Predictive Controllers have been implemented in idle speed control (Xu et al., 2013). To solve the finite horizon problem in the Model Predictive Control, the optimization algorithm can be adapted to the case of idle speed control (Kang et al., 2014).

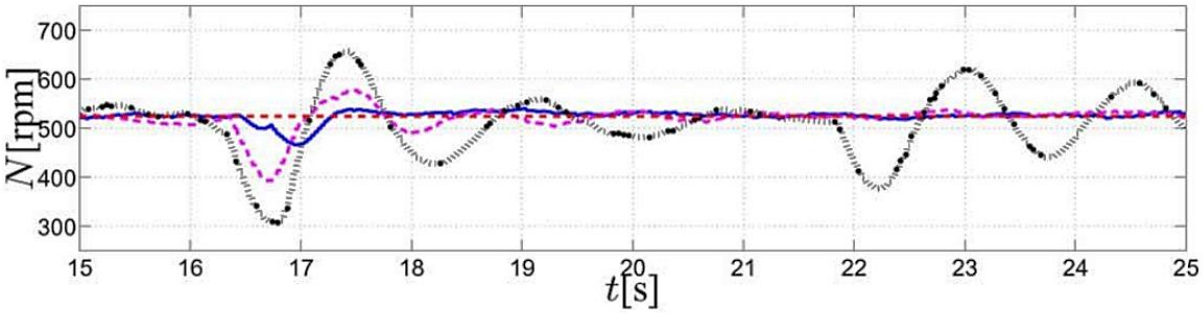

Fig. 21. Real-time results of the Model Predictive idle speed controller in (Di Cairano et al., 2012)

Model Predictive Controllers are based on a model to express a finite horizon problem to optimize in order to compensate the nonlinearities. However, model-based controllers need an accurate model and required enough computational power to be implemented. When a model is required, how are modelled the different elements of the air-path?

3.2.2. Control-oriented air-path models

Several control-oriented models of the air-path exist in the literature (Carbot-Rojas et al., 2017). The motorized throttle is the input of the model; it is in charge of injecting the air. The second part is the intake manifold whose pressure is a crucial element of the engine since it is related to the difference of the air mass flow entering through the throttle and the air mass flow leaving to the cylinders. The dynamics of the air flow going through the intake valve inside the cylinder is the third element. Then, when the air is inside the cylinder, by compression and combustion, it is responsible of the production of the torque. Considering the piston-crankshaft system, the linear displacement of the piston creates a rotation movement of the crankshaft, so a variation in the engine speed.

The throttle is a nonlinear system that can include backlash with hysteretic behavior and air fluid dynamics on the surface of the valve, see Fig. 22. Nonlinear controllers have been designed to handle the nonlinear hysteretic phenomenon such as in (Wang and Huang, 2013). However, some control-oriented models represent the throttle as a first-order model with a time constant to follow a given reference (the driver pedal or, in case of idle speed, the command generated by the controller).

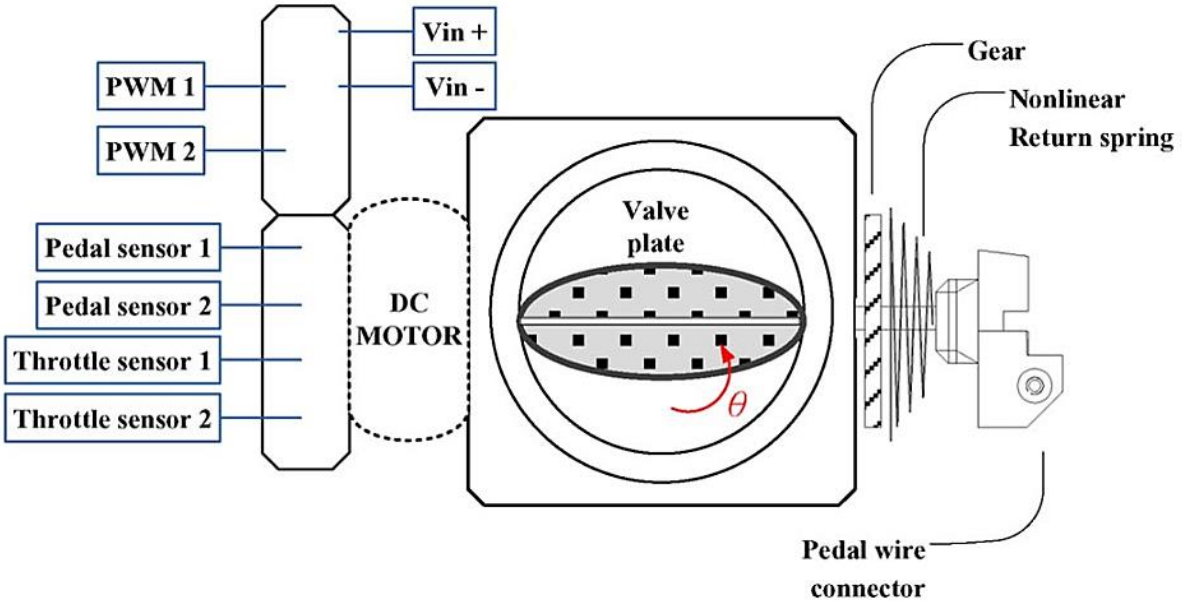

Fig. 22. Scheme of the different elements of the motorized throttle in (Wang and Huang, 2013)

As for the intake manifold pressure, since the gas propagation laws are known inside this element, it is traditionally directly modelled from the equation of the fluid mechanics (Kang et al., 2014). Moreover, even with new gas recirculation technologies such as the Variable Geometry Turbocharger (Daasch et al., 2016), the gas propagation equations inside the intake manifold are well known and established from the fluid mechanic physics, so a model of the intake manifold pressure is quite easy to derive and, because this element of the engine is equipped with several sensors (pressure, air mass flow), parameter estimation can be done in good conditions.

While the air enters in the cylinder, some phenomena can appear around the intake valve, such as scavenging or backflow. Because of the difference of pressure between the intake manifold and the inside of the cylinder, a part of the remained exhaust gases can leave the cylinder through the intake valve (backflow). The same phenomenon appears with the exhaust valve (scavenging). These phenomena can be modelled (Leroy and Chauvin, 2013) and compensate in the control law (Huber et al., 2015).

Similarly to the control part, the torque produced by one cylinder remains a problem in the engine modelling since it is not measured, making any identification process complicated. Some mechanical models detail the link between the amount of air inside a cylinder and the torque it generates, however, they are usually combustion models with finite elements modelling, so hard to use from a control point of view. Because the amount of air inside the cylinder is not measured, estimation through observer has been developed in the Takagi-Sugeno framework (Barbarisi et al., 2002; Kerkeni et al., 2010). Instead of considering the amount of air, other models describe the torque as a function of the pressure inside the cylinder (Kang et al., 2016), or as a function depending on the

intake manifold pressure (called Intake Pressure Control (Huber et al., 2015)). Since the pressure inside a cylinder is also not measured, observers have been developed to estimate it (Guardiola et al., 2017). The torque in control-oriented models is usually modelled through static maps (Xu et al., 2013; Ngo et al., 2014) that need to be calibrated using experimental engine test bench (Desheng et al., 2014). Some direct static approximations have been developed in the past (Connolly and Rizzoni, 1994; Ball et al., 2000), and they have been emphasized with model-based observers such as Kalman filters (Chauvin et al., 2004; Majecki et al., 2015), Hammerstein systems (Laila and Gruenbacher, 2016), sliding mode observers (Zhixiong et al., 2017) or angular observers (Losero et al., 2015).

Considering the produced torque, it is easy to obtain a model for the rotational dynamics of the crankshaft since it is a standard second law of Newton with rotational elements submitted to active torque (produced torque) and resistive torque (load torque, an external disturbance) (Wang et al., 2006; Balluchi et al., 2010).

In idle speed context, the speed is regulated using two inputs: The throttle is responsible for a long-term torque while the spark advance can produce a fast-response torque. As detailed in the literature review, several methodologies, such as fuzzy logic control, adaptive control, neural networks control, model-predictive control or Takagi-Sugeno control, have been applied to the throttle management. What are the challenges and the strategies involved in the spark advance control?

3.3. Spark advance control

3.3.1. Spark advance control challenges

The spark advance φ represents the moment where the spark ignites the mixture. It is expressed in relation with the crankshaft degree before the top-dead-center (degrees BTDC). Taking into account the dynamics of the chemical reactions, the combustion occurs and the torque is produced. Fig. 23 depicts the different steps of the torque production between the Compression and the Expansion phase.

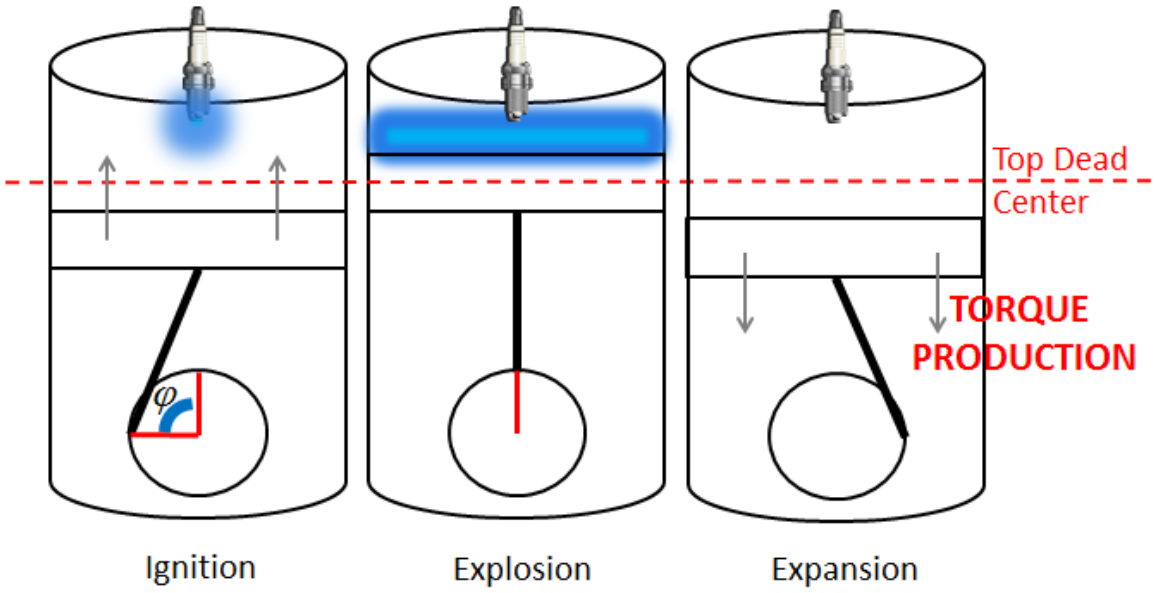

Fig. 23. Scheme of the spark advance along the engine phases

The challenge of spark advance control is that the torque produced by a cylinder is a nonlinear function of the spark advance that is barely unknown. Experimental mapping, nonlinear approximation, modelling the contribution of the spark is a real issue and again, since the torque is not measured, the identification process remains very hard. Considering the pressure inside a cylinder, which is directly linked to the combustion of the air-fuel mixture, it is possible to distinguish three cases (Fig. 24)

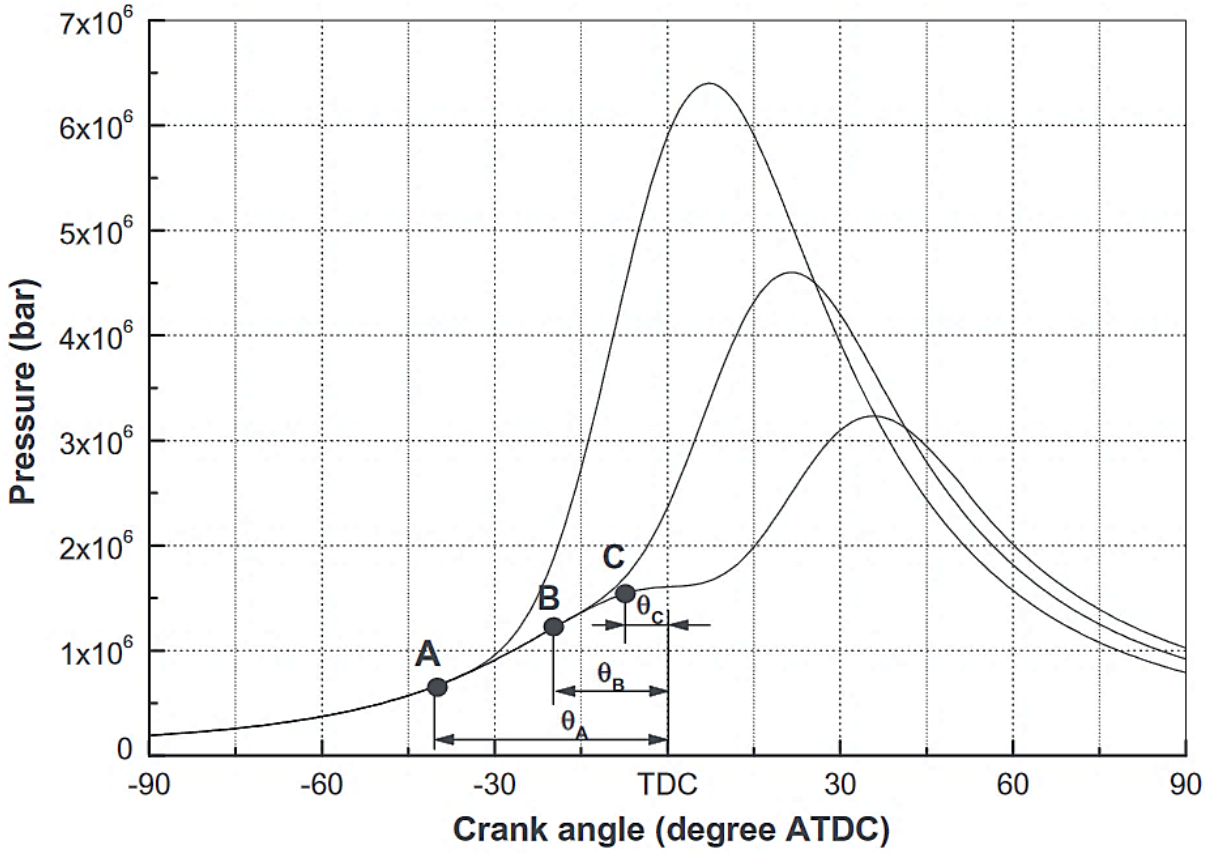

Fig. 24. Evolution of the in-cylinder pressure in function of the spark advance in (Saraswati et al., 2011)

If the spark is too late and too close to the Top-Dead-Center (Point C), then the piston will already have passed the TDC when the combustion occurs; then, all the distance done by the piston, thanks to the inertia, will be lost for the torque production. The spark should be set to the particular point (Point B) called optimal spark advance where the combustion starts exactly when the piston is at the TDC. However, because of the nonlinear behavior of the chemical combustion, it is hard to reach perfectly this point, and it can be dangerous: if the spark is too early, i.e. too far from the Top-Dead-Center (Point A), the chemical reaction can be disturbed (auto-ignition, (Misdariis et al., 2015)) and the combustion can occur before the piston reaches the TDC. The pressure is then increasing inside the combustion chamber of the cylinder and can cause the destruction of the engine in a very few time (Ceschini et al., 2017). This effect is called knocking, and it represents the main challenge of spark advance control. Each cylinder is equipped with a knocking sensor, and the current industrial strategies are to hugely decrease the spark advance (towards the TDC) when the knocking sensor detects some vibrations.

Another point of the spark advance control challenge is the customization of the control of each cylinder. Indeed, as they are all equipped with independent spark plugs, it is possible to design a specific spark advance control for each cylinder, taking into account their own particularities and behavior since it is known that they are not working the same way, depending on their position (Grizzle et al., 1991).

Spark advance control represents an important challenge for engine control, since it is highly nonlinear. The knocking effect can appear and destroy the engine. A cylinder-per-cylinder spark advance control should be designed since each cylinder has a different behavior and is equipped with independent technology. How are these complex problematics handled by the control strategies?

3.3.2. Spark advance control strategies

In idle speed control, the spark advance has an important role since it can influence the torque produced by a cylinder, so idle speed control is a combination of throttle control and spark advance control. While the engine industry mainly controls the spark advance in open-loop with static maps, researchers have explored different theories to design closed-loop controllers.

Since the contribution of the spark advance in the torque production is nonlinear and unknown, fuzzy logic has been considered to design spark advance controllers (Ghaffari and Shamekhi, 2005; Di et al., 2010; Saraswati et al., 2011). Using fuzzy logic and heuristic reasoning represent an advantage while no model is needed. A membership function structure can be implemented, with the different steps of the fuzzy control (fuzzyfication, inference rule-based model and defuzzyfication). Because they are based on knowledge, it is possible to use fuzzy logic to control individually the spark advance of each cylinder like in (Di et al., 2010).

As the knock effect has an important role in spark advance control, several studies in the literature focus their research on designing a spark advance control coupled with a knock detection algorithm. Based on the knock sensor information, the theory of probability is used to detect knocking and adjust in real time the spark advance to stay in an optimal area away from the knocking zone so the vibrations do not destroy the engine. The spark advance controller can be either based on likelihood and stochastic methods to identify statistical models (Peyton Jones et al., 2013; Thomasson et al., 2016; Peyton Jones et al., 2017) or extremum seeking algorithms (Shen et al., 2017).

While a part of the research has been done with a probabilistic approach, on the other hand, model-based controllers have been developed using different techniques for both modelling and controller design. Because of the lack of measures from the physical phenomenon inside the cylinder, observer-based control has been investigated. Considering the difference between the spark advance timing and the occurrence of the combustion as a delay, a spark advance controller has been designed using the theoretical background in nonlinear time-delay systems in (Bengea et al., 2004), observing the intake manifold pressure and the speed and controlling both the throttle and the global spark advance (i.e., one command for all the spark plugs). The observer-based method has also been used to estimate the current load torque the idle speed controller has to face, and to adapt the spark advance as depicted in Fig. 25 (Czarnigowski, 2010).

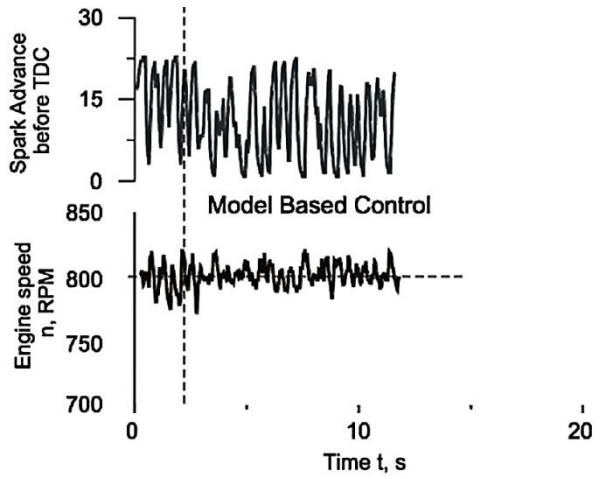

Fig. 25. Spark advance control for idle speed with occurrence of a load as in (Czarnigowski, 2010)

Spark advance control has also been designed on mathematical and/or physical models with structures allowing a controller design. By considering the idle speed control as a simple linearized transfer function, it is possible to use the classic feedback methodologies to design a L_∞ controller for the spark advance (Albertoni et al., 2005). Considering a torque structure, controllers can be developed for both the throttle and the global spark advance with their respective torque reference to follow (Bohn et al., 2006) (Fig. 26 and Fig. 27), even if the torques are not measured, making the identification process of the model difficult.

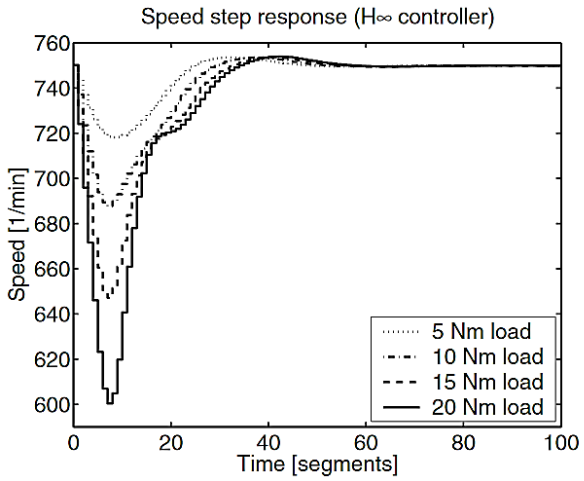

Fig. 26. Idle speed control for several load torques in (Bohn et al., 2006)

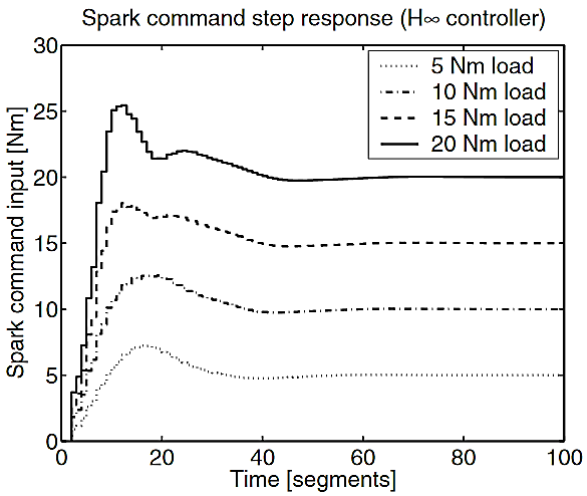

Fig. 27. Spark advance control for several load torques in (Bohn et al., 2006)

Similarly to the throttle control, Model Predictive Control has been investigated for spark advance control. Based on a model trying to reproduce the physical phenomenon occurring during an combustion inside the cylinder, the structure of the MPC has been improved to multi-input MPC to control both throttle and spark advance for idle speed control (Di Cairano et al., 2012). While MPC has been using a discrete-time model of the engine dynamics, a special class of model and associated controller, in the hybrid framework, considers continuous-time dynamics triggered by discrete events. Using an hybrid model for the engine, an hybrid controller is designed to control both throttle and spark advance in idle speed context (Balluchi et al., 2010) (Fig. 28, Fig. 29 and Fig. 30)

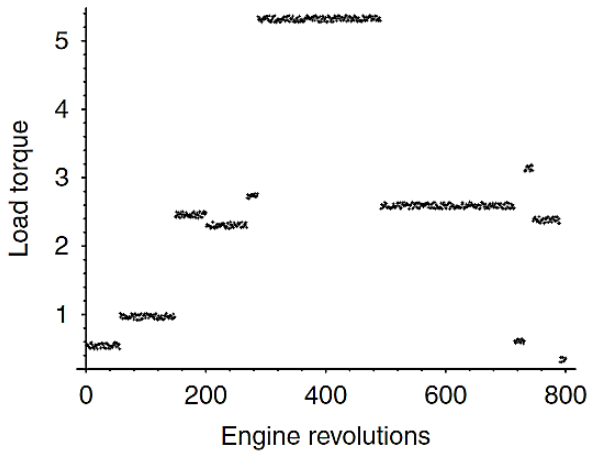

Fig. 28. Load torque considered for the simulation results in (Balluchi et al., 2010)

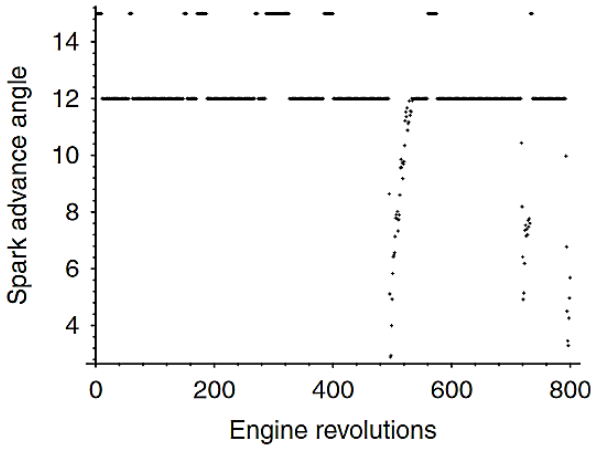

Fig. 29. Spark advance hybrid feedback controller in (Balluchi et al., 2010)

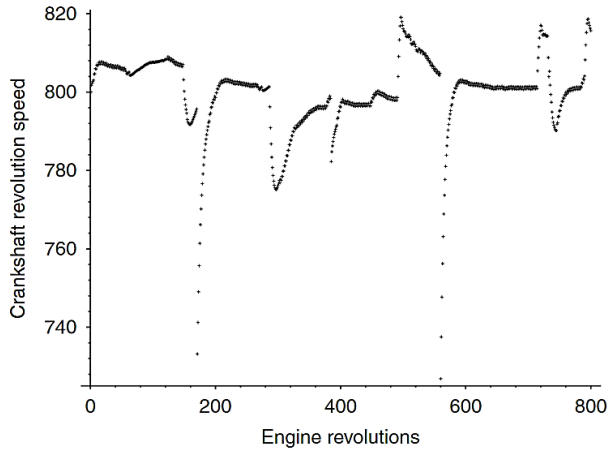

Fig. 30. Idle speed control to the reference $n = 800 rpm$ as in (Balluchi et al., 2010)

As one can see, the strategy of setting the spark advance to a non-optimal value and quickly reaching the optimal value for idle speed control is a strategy that provides robustness and disturbance rejection when a load torque occurs. The only disadvantage of model-based controllers is that they imply an identified model to rely on. Considering its nonlinear and uncertain behavior, how is the spark advance and its contribution to the torque modelled in the literature?

3.3.3. Spark advance models

In the case of the spark advance, it is particularly difficult to get an accurate model. Indeed, the relation between the spark advance, the cylinder pressure and the torque production is nonlinear and, because of the chaotic behavior of the combustion, hard to model.

The same modelling techniques have been applied for the spark advance, for instance, the static look-up tables have been used in addition to the torque structure in (Bohn et al., 2006). Since the torque is not measured, it is estimated through a combination of experimental maps, such as the one presented in Fig. 31 displaying the values of the difference between the minimum spark advance and the optimal spark advance, called relative spark advance. This look-up table makes the link with the speed and the air mass flow inside a cylinder, which is also not measured. Then, other look-up

tables can be defined, for example to express the contribution, or efficiency, of the spark advance in function of this difference of spark (Fig. 32).

$f_{\Delta\min}(N, m'_{cyl})$ [°]

1/min mg/seg	400	600	800	1000	1250	1500	2000
100	-41.5	-41	-40.5	-38	-40.5	-40	-38.5
150	-41.5	-44	-46	-44	-42.5	-38.5	-39.5
200	-38	-41.5	-43.5	-46.5	-43.5	-38.5	-42
250	-36	-39.5	-43	-45	-42	-38.5	-42
300	-34.5	-38.5	-41.5	-44	-42	-39.5	-41
350	-34.5	-37.5	-41	-43	-40	-37	-42
400	-34.5	-37.5	-40.5	-42	-41.5	-42.5	-41.5
450	-33.5	-37.5	-40	-42	-43.5	-44.5	-45.5
500	-33	-36	-38.5	-42.5	-44.5	-46	-46.5
550	-32.5	-35.5	-38	-42.5	-44.5	-46.5	-47

Fig. 31. LUT of the relative spark advance in function of the speed and the air mass flow inside the cylinder in (Bohn et al., 2006)

$f_{igneff}(\Delta\alpha)$

°	-49.9	-45.4	-42.4	-40.1	-37.9	-35.6	-33.8	-31.5
	0.008	0.06	0.12	0.2	0.27	0.35	0.42	0.52

°	-29.3	-26.3	-24	-20.6	-16.9	-11.6	-6.4	0
	0.61	0.7	0.76	0.82	0.88	0.94	0.98	1

Fig. 32. LUT of the efficiency or the contribution (second row) in function of the relative spark advance (first row, in degrees) in (Bohn et al., 2006)

As the global torque is a combination of the air inside the cylinder and the spark advance, more realistic look-up tables have been designed, considering the torque in function of measured values such as the manifold pressure and the spark advance, as depicted in Fig. 33.

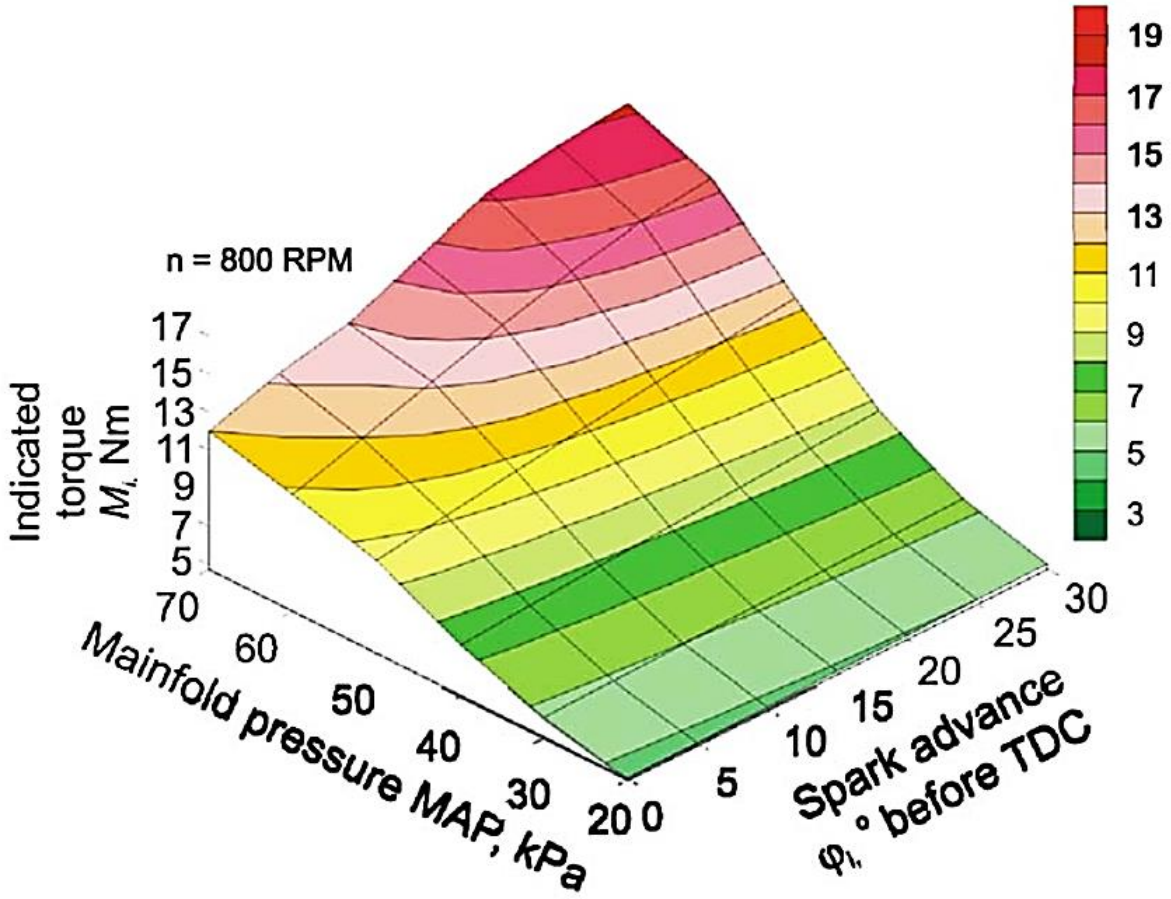

Fig. 33. Torque map in function of the manifold pressure and the spark advance at idle speed (Czarnigowski, 2010)

A famous experimental-based model for the torque contribution of the spark advance is called the bell-shape distribution model. Indeed, for a given amount of air, it is possible to express the engine torque in function of the spark advance, using sensors like torque meters. Fig. 34 illustrates the bell-shape model obtained with experimental results in (Eriksson, 1999). The MBT point (Maximum Brake Torque) represents the optimal torque the spark advance can generate, so the optimal spark advance point. As detailed previously in Fig. 24, by going closer to the Top-Dead-Center, the torque hugely decreases. However, by increasing the advance of the spark (going further from the TDC), knocking can appear, so this part should be avoided, that is why the bell-shape does not model ignition angles before 30 degrees BTDC.

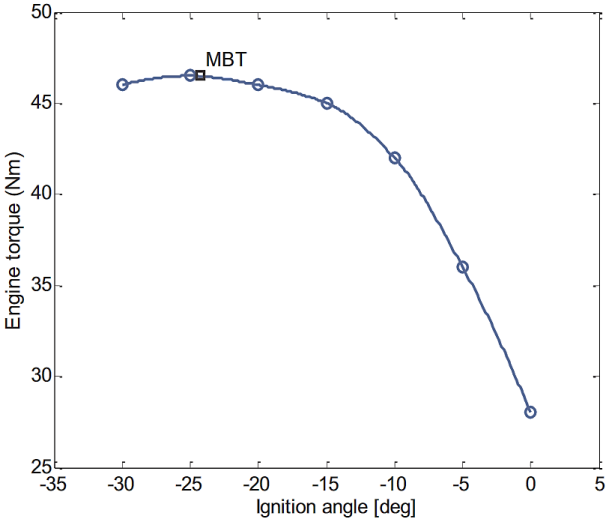

Fig. 34. Engine torque in function of the ignition angle (Peyton Jones et al., 2013)

Several approaches have been considered to obtain the bell-shape model without measuring the torque. One of them is to evaluate the efficiency through performances indicators such as the IMEP or the CA50, and pollution emissions. The IMEP (Indicated Mean Effective Pressure), sometimes associated with the BMEP (Brake Mean Effective Pressure) is a criterion to maximize in order to get the optimal pressure for the torque production of a cylinder. Fig. 35 presents the bell-shaped distribution of the IMEP in function of the spark advance, based on experimental data and interpolated.

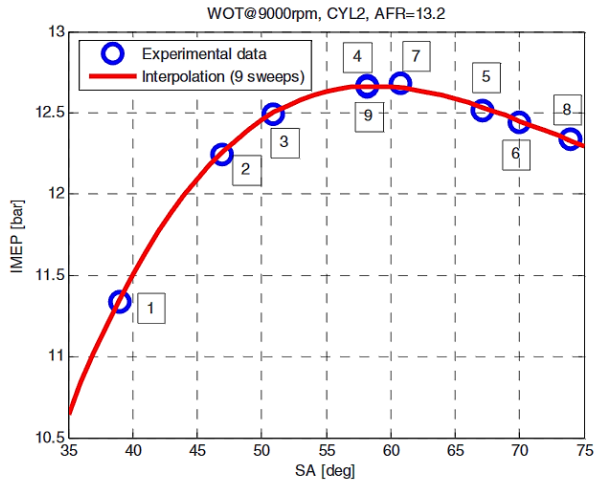

Fig. 35. Distribution of the IMEP in function of the spark advance in (Corti et al., 2014)

The CA50 or MFB50 (Mass Fraction Burnt) is the crank angle when 50% of the air-fuel mixture has been burnt during the combustion. It is known that this CA50 indicator is related to the spark advance (Gao et al., 2015). Thus, it is possible to express the CA50 in function of the spark advance in a similar bell-shaped distribution through maps, and then to express the thermal efficiency, so the spark advance efficiency, in function of the CA50 (Liu et al., 2017; Shen et al., 2017).

Another methodology to model the bell-shape distribution between the spark advance and the produced torque/the efficiency/the spark contribution, is to use mathematical functions. Indeed, this distribution can be approximated by a cosine function (Di Cairano et al., 2012) such as :

$$f_{spk}(t) = \cos\left(\varphi(t) - \varphi_{MBT}(t)\right)^{\xi} \tag{1.3.1}$$

With $f_{spk}(t)$ the contribution of the spark, $\varphi(t)$ the spark advance in degrees before TDC, $\varphi_{MBT}(t)$ the optimal spark advance depending on the current engine speed and ξ an engine parameter to identify. Other mathematical functions can be used, such as polynomial expressions. In (De Santis et al., 2006), the global torque produced by the engine is expressed as a polynomial expression depending on the intake manifold pressure and the spark advance. In the hybrid model of (Balluchi et al., 2010), the global torque is a product between the torque produced by the air path and the spark advance contribution, modelled by a third order polynomial expression (Fig. 36).

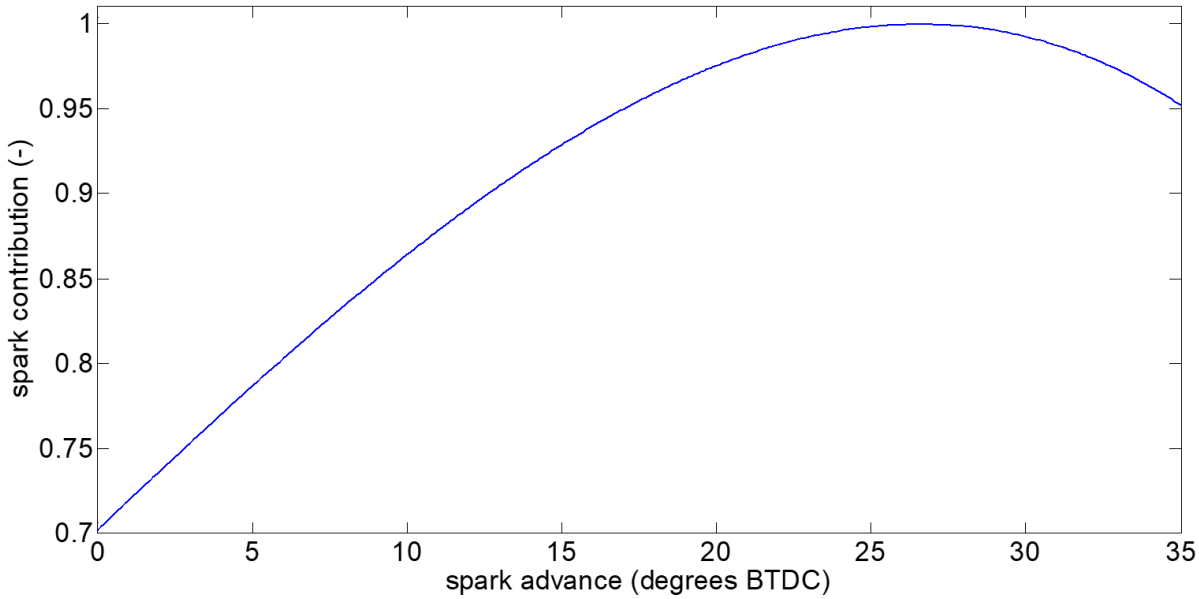

Fig. 36. Spark advance contribution with the Magneti Marelli engine of (Balluchi et al., 2010)

As it has been introduced among the literature review, idle speed control represents a challenge for the engine manufacturers because of the nonlinear behaviors involved in such a situation. The lack of measures, mainly in the phenomenon occurring inside the cylinder during the combustion, such as the pressure, the spark advance contribution or the torque production, makes the usual strategies of the industry engineers based on look-up tables inefficient. Since it implies reference tracking, disturbance rejection and multi-input multi-output control, idle speed control has received a growing interest from the control research community where it has been largely addressed. However, either for the throttle control or the spark advance control, the design of controllers uses the same techniques: Empirical or self-tuned PID controllers, adaptive structure, model-free controllers (based on fuzzy logic or neural networks) or model-based control. In both cases, the problematic is similar: how to control such a nonlinear system with a chemical combustion inside where no sensor can be added and uncertainties remain due to the explosive behavior? The control of the combustion through the control of the air and the spark advance has been vastly considered. On the three inputs implied in the engine control, the fuel injectors are involved in the control of the combustion and the

post-combustion phenomenon, mainly with the exhaust gases and their management via the three-ways catalyst. It is a crucial element since it is the only input able to deal with pollution and gas emissions. What are the challenges with fuel injection control and what strategies are used to reduce pollution emission to respect the legislations?

4. Air-Fuel Ratio control

4.1. Introduction to air-fuel ratio control

While the throttle and the spark advance are responsible for controlling the speed, so the consumption through the torque production, fuel injectors are the only elements that can deal with the pollution emission of the engine, through a value called air-fuel ratio. It represents the ratio $\lambda(t)$ between the quantity of the amount of air and the amount of fuel inside the cylinder before the combustion, such as:

$$\lambda(t) = \frac{m_{air}(t)}{m_{fuel}(t)} \tag{1.4.1}$$

A particular air-fuel ratio is called the stoichiometry, when fuel and air are in proportions such as $\lambda_s = 14.67$. For common interpretation, the air-fuel ratio is usually normalized such as:

$$\lambda(t) = \frac{m_{air}(t)}{\lambda_s \cdot m_{fuel}(t)} \tag{1.4.2}$$

During the combustion, the mixture is burnt according to the chemical kinetics including the air (O_2) and a generic type of gasoline $(C_xH_zO_z)$ (Bougrine et al., 2014):

$$C_xH_yO_z + \left(x + \frac{y}{4} - \frac{z}{2}\right)O_2 \rightarrow xCO_2 + \frac{y}{2}H_2O \tag{1.4.3}$$

Then, the chemical process transforms the chemical elements of the air-fuel burnt mixture (H,N,O,OH,NO) in post-flame gases $(CO_2,H_2O,O_2,N_2,H_2,CO)$. Emissions kinetic models have been subject to many research, from the last century (Bowman, 1975; Schuetzle et al., 1994) to most recent models (Valério et al., 2003; Bougrine et al., 2014; Demesoukas et al., 2015; Karvountzis-Kontakiotis and Ntziachristos, 2016). Considering this huge chemical literature, it is possible to describe the chemical processes operating in the post-combustion phase as seven reactions:

$$\begin{aligned} &OH \leftrightarrow 0.5O_2 + 0.5H_2 \\ &NO \leftrightarrow 0.5O_2 + 0.5N_2 \\ &H_2 + 0.5O_2 \leftrightarrow H_20 \\ &CO + 0.5O_2 \leftrightarrow CO_2 \\ &H \leftrightarrow 0.5H_2, O \leftrightarrow 0.5O_2, N \leftrightarrow 0.5N_2 \end{aligned} \tag{1.4.4}$$

So the air-fuel ratio is directly related to the post-flame pollutant emissions due to the chemical equilibrium of proportions: The more fuel you inject, the more post-flame gases you create.

At this point of the engine, several methodologies have been investigated to reduce the pollutant emissions, such as injecting water inside the cylinder after the combustion (Mingrui et al., 2017) or, from a mechanical point of view, changing the trajectory of the piston (Zhang and Sun, 2016).

Then, when the cylinder enters in the Exhaust phase, the exhaust valve opens and most of the gases leave the combustion chamber. A part of the post-flame gases stays there, being called Residual Gas Fraction (GFR). They include residual fuel, residual air and residual unburnt gases (Kumar and Shen, 2017). The exhaust gases of all the cylinders are evacuated to the exhaust manifold, joining and mixing at the confluence point, see Fig. 37.

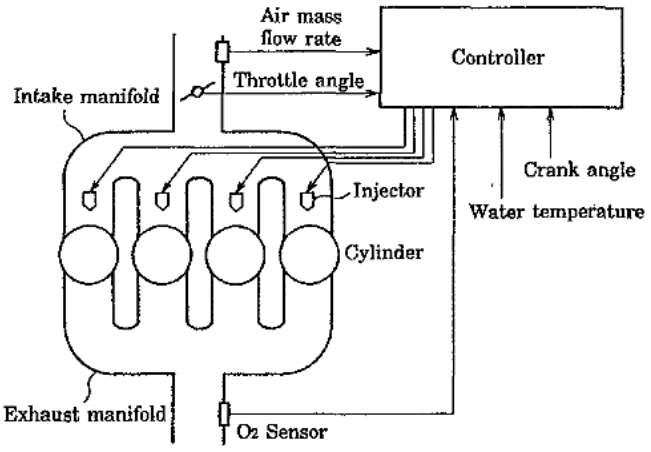

Fig. 37. Detail of the manifolds before and after the cylinders in (Takahashi and Sekozawa, 1995)

This is problematic since all the exhaust gases are mixed together at the confluence point, so it is difficult to determine which cylinder produced this quantity of pollutant gases. The exhaust gases reach then the lambda sensor, or UEGO sensor (Universal Exhaust Gas Oxygen). From the previously exposed problem of the gas confluence, the unicity of the oxygen sensor is one of the main challenges in air-fuel ratio control, since the sensor measures the air-fuel ratio of a mixture of burnt gases coming from all the cylinders. Moreover, the lack of redundancy of the sensor can be a problem in case of sensor failure (Dongliang et al., 2011).

As presented in the global scheme of the engine in Fig. 9, the UEGO sensor is followed by the Three-Ways Catalyst (TWC) or catalytic converter. This crucial element is dedicated to the reduction of the pollutant emissions by a chemical way (chemical conversion or transformation). It is connecting the engine cylinders and the tailpipe, and receives the post-flame gases in input, converts them and exhausts the transformed gases to the atmosphere, as presented in the Fig. 38.

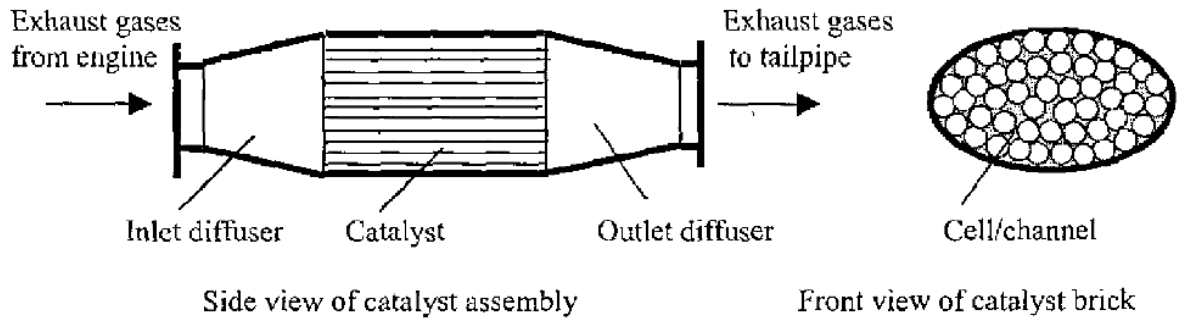

Fig. 38. Scheme of a catalyst device in (Shamim, 2004)

The chemical conversion is to transform harmful gases such as nitrogen oxides (NO_x), carbon monoxides (CO) and unburnt hydrocarbons (HC) into substances such as water (H_20), nitrogen (N_2) and carbon dioxide (CO_2) (Fig. 39) (Alkemade and Schumann, 2006; Kiwitz et al., 2012):

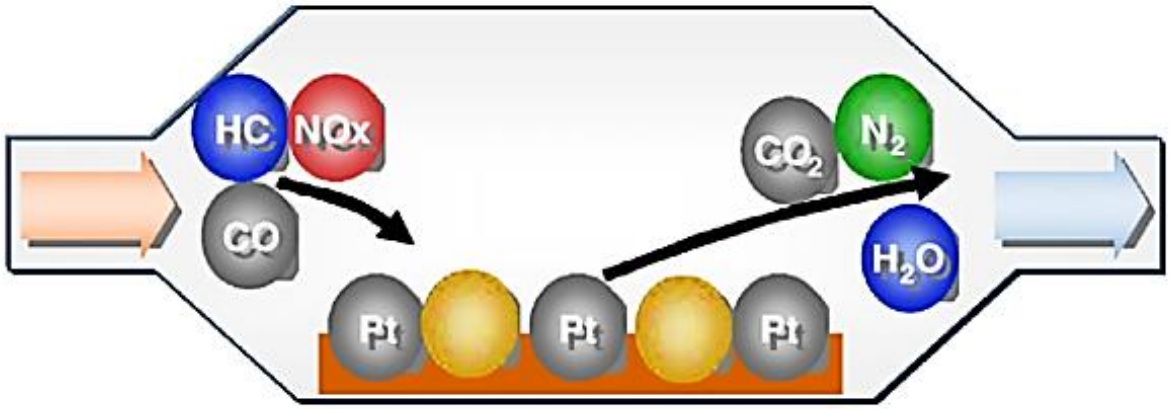

Fig. 39. Scheme of the chemical conversion inside a TWC in (Alkemade and Schumann, 2006)

$$\begin{aligned} 2NO_x &\rightarrow N_2 + xO_2 \\ 2CO + O_2 &\rightarrow 2CO_2 \\ C_xH_{2y} + \left(x + \frac{y}{2}\right)O_2 &\rightarrow xCO_2 + yH_2O \end{aligned} \tag{1.4.5}$$

As a crucial element of the pollution reduction process, the Three-Ways Catalyst has been modelled through several methodologies, such as empirical models (Balenovic and Backx, 2001) or different chemical and physical models, based on the gases dynamics, and depending on the elements involved in the transformation (Santos and Costa, 2009; Ling et al., 2012; Kumar et al., 2014; Sabatini et al., 2015; Bickel et al., 2017). The TWC has received constant improvements to better transform the post-flame gases and reduce the exhaust emissions, such as adding chemical elements to the catalyst conversion like gold (Ulrich et al., 2017). To solve the unicity of the UEGO sensor, another oxygen sensor can be added after the TWC to improve its functioning (Fiengo et al., 2005). Some prototypes of new TWC technologies have been developed to improve the conversion rate, transforming more molecules inside the exhaust gases, as presented in the chemical transformation efficiency of a prototype of TWC in Fig. 40 (Hasan et al., 2016a, 2016b)

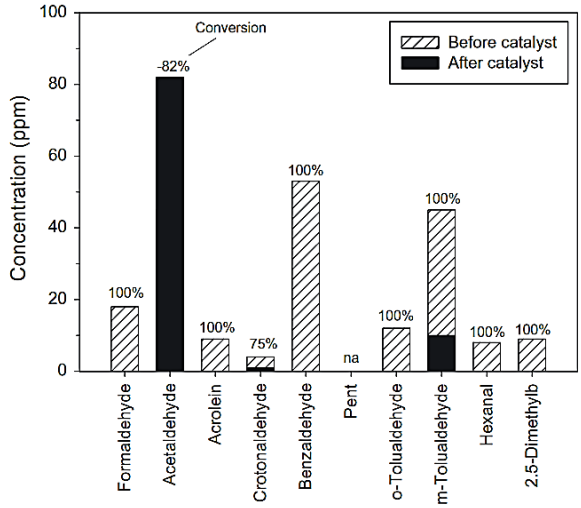

Fig. 40. Concentration of aldehydes in the exhaust gases, before and after the catalyst in the TWC prototype in (Hasan et al., 2016a)

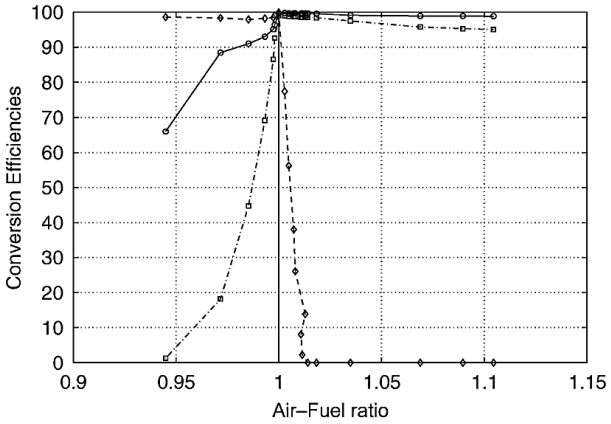

Fig. 41. Conversion rate of the TWC in function of the AFR (Fiengo et al., 2005)

However, the three-ways catalyst presents one main inconvenient: the efficiency of the chemical conversion is highly depending on the air-fuel ratio. Indeed, if the air-fuel mixture is lean ($\lambda(t) > 1$ so more air than fuel), the catalytic converter does not succeed to transform all the NO_x elements. In case of a rich air-fuel mixture, i.e., more fuel than air ($\lambda(t) < 1$), the carbon monoxide CO are badly converted. The optimal conversion efficiency of the three-ways catalyst is ensured when the air-fuel ratio is at the stoichiometry, i.e. $\lambda(t) = 1$, as summarized in Fig. 41.

Consequently, in order to optimize the functioning of the three-ways catalyst, so the reduction of the pollution, air and fuel have to be injected in stoichiometric proportions. This is the main challenge of air-fuel ratio control (Norimatsu and Isomura, 1981). While the amount of air is imposed as an external disturbance, either by a driver request or controlled by the idle speed controller, the air-fuel ratio control module has to regulate the amount of fuel to be injected so the air-fuel mixture ratio is at the stoichiometry point, ensuring an optimal conversion of the exhaust gases. As a control problem, the control input is the injector of each cylinder, by setting the start of injection (SOI) and the time of injection (TOI).

Air-fuel ratio control presents different problems. The main one is the delay between the injection of fuel inside the cylinder and the arrival of the post-flame gases to the UEGO sensor that is depending on the engine speed, so not constant. The other difficulty is to control each injector separately, in order to guarantee that the air-fuel ratio of all the cylinders is at the stoichiometry. This is due to the fact that the post-flame gases are mixed at the confluence point, and the UEGO sensor measures the air-fuel ratio of these mixed post-flame gases from all the cylinders. Because of the time-varying delay and the necessity to control individually each cylinder, air-fuel ratio control is an important challenge in engine control:

- Challenge#1: Maintaining the AFR at 1
- Challenge#2: Control of time-varying delayed systems
- Challenge#3: Individual control of each injector

What strategies have the researchers implemented to solve these problems and reduce the pollution of the commercial cars?

4.2. Control of the injectors

Because of the challenges of the air-fuel ratio control problem, it is mainly solved by static maps in the car industry, avoiding to deal with time-varying delay and by providing a global control signal for all the injectors.

Similarly to the idle speed control, because it implies reference tracking ($\lambda_{ref} = 1$) and disturbance rejection, the PI/PID structure has been explored. However, the time-varying delay remains a problem for integral-based controllers. Indeed, in case of a fixed or known delay, it is possible to compensate it with a Smith predictor. The standard Smith predictor can be used with a PID controller if the time-varying delay is mapped (Desheng et al., 2014), approximated (Ebrahimi et al., 2012) or considered as fixed (Jankovic and Magner, 2011), see Fig. 42. The Smith predictor structure can be improved to deal with time-varying delays (De Oliveira et al., 2017). Then, PID controllers can be designed (Kahveci and Jankovic, 2010; Kahveci et al., 2014b; Khajorntraidet et al., 2015). The PID controllers can hardly handle Challenge #2 (see Section 4.1) that is, control of time-varying delayed systems. Controlling each injector implies to design four PID controllers due to their SISO structure (He et al., 2008). The closed-loop system, including four controllers separately designed, may be unstable, so stability analysis methods have been investigated, for example with the Fourier analysis (Schick et al., 2011) or the spectral analysis (Cavina et al., 2010). The integral structure of the PID can be adapted with the lifting technique to handle Challenge #3 (Grizzle et al., 1991; Moraal et al., 1993).

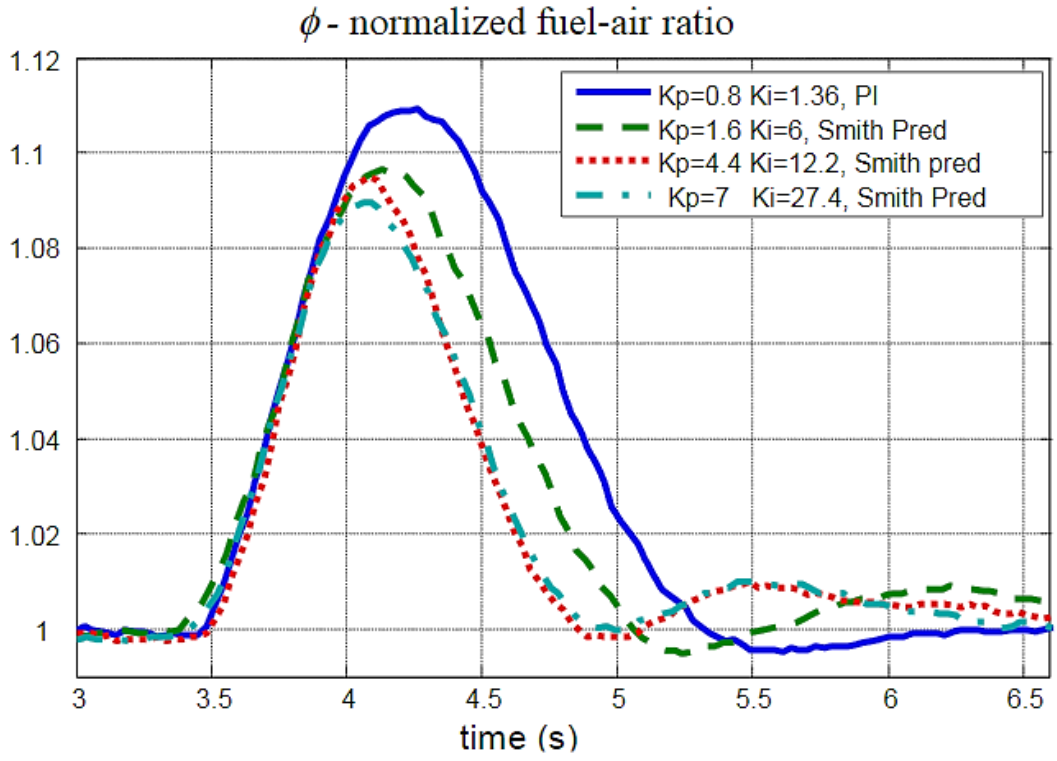

Fig. 42. Comparison between simple PI controller and PI with a Smith predictor structure, for different controller gains, in presence of a disturbance, in (Jankovic and Magner, 2011)

While facing nonlinear systems with particularities such as varying-time delay, two main approaches are considered: model-free or model-based control. Among the first category, the fuzzy logic has been considered for its performance superior to the PI or the maps-based control (Chamaillard and Perrier, 2001; Zhi-Xiang, 2016). The fuzzy logic has been combined to a lot of different control methodologies, such as the PID controller for the air-fuel ratio control (Jansri and Sooraksa, 2012).

Adaptive control has been investigated to create algorithms that can adapt to the challenges the air-fuel ratio control involve. Particularly, the Adaptive Posicast Controller (APC), specially designed for time-delay systems, has been considered in (Yildiz et al., 2010) where the delay is assumed to be fixed, see Fig. 43. Adaptive control can provide a solution to the SISO problem by considering more than one input, for example in (Khajorntraidet and Shen, 2016) where a controller is designed for the fuel injection and the spark advance in the special case of lean-burn conditions. Adaptive control can also be combined with other theory, for example, an adaptation fuzzy law can be designed for online parameter tuning for a PID controller (Ghaffari et al., 2008; Wang and Jiao, 2015). However, the adaptive control cannot handle time-varying delay so the adaptive algorithm is more used in complement of another controller design. The engine can be empirically modelled using grey-boxes, so a feedforward (Gerasimov et al., 2016) or a state feedback (Jiao and Shen, 2011) with an adaptation law can be designed, see Fig. 44 for the feedforward results. This concept of getting alternative models for the engine to design a state feedback has been investigated through the flatness theory in which the air-fuel ratio system can be represented as a linear one (Rigatos et al., 2014b).

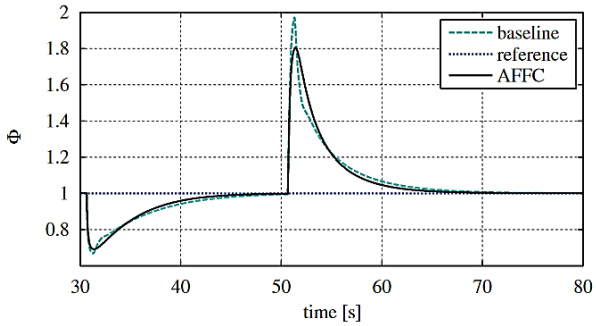

Fig. 43. Experiment results of air-fuel ratio (Φ) control by the Adaptive FeedForward Controller facing disturbance in (Yildiz et al., 2010)

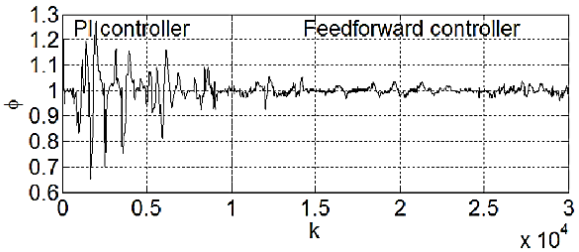

Fig. 44. Experiment results of air-fuel ratio (ϕ) control by the feedforward inverse adaptive controller in (Gerasimov et al., 2016)

In the same philosophy, the neural networks (NN) can represent the complexity of the engine through several layers without any physical modelling part and a neural network controller can be designed (Alippi et al., 2003; Arsie et al., 2007). Data fusion can be used from the different sensors of the engine to enhance the neural network construction and the NN data-driven controller (Jia et al., 2011; Gerasimov and Pshenichnikova, 2012). Similarly, neural networks methodology can be combined with fuzzy logic to improve the performances (Liu and Zhou, 2010).

By considering data-driven techniques, iterative control has been investigated for their ability to provide a controller without any kind of model, physical or empirical. Iterative controllers are based on optimization problem to minimize performance criterion and find parameters for a controller iteratively, considering an unknown system. Iterative-learning methodology has been used to design

air-fuel ratio controller (Hara et al., 2012) and reinforced with adaptive theory (Rupp et al., 2007) and switching control (Efimov et al., 2010) whose results are depicted Fig. 45.

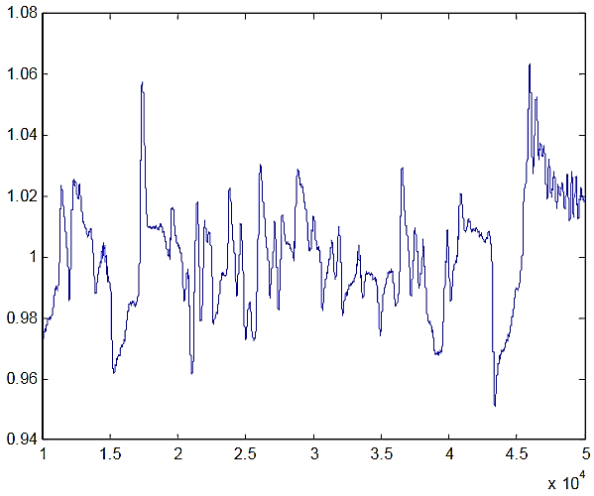

Fig. 45. Experimental results of the iterative switching controller developed in (Efimov et al., 2010)

The other approach for dealing with nonlinear systems is to design model-based controllers. Once a model is obtained, it can be written under the state-space representation. Then, classic state feedback can be designed (Chang et al., 1995; Andersson and Eriksson, 2005; Zhai and Yu, 2007). For nonlinear systems, the feedback controller can handle a linearizing property, as developed in (Guzzella et al., 1997). Another technique to deal with the nonlinear behavior of the system is to use the Lyapunov theory and the Lyapunov direct method to determine the gains of the controller that can stabilize the closed-loop system (Na et al., 2016). Moreover, it has been illustrated through comparison that a feedback controller has better performance than an adaptive PID for AFR control (Mallik and Aryan, 2015). The standard state feedback design can be enhanced by being combined with other methodologies such as adaptive law and robustness (Efimov et al., 2014) with a supervisory strategy for in-vehicle implementation, see Fig. 46 below.

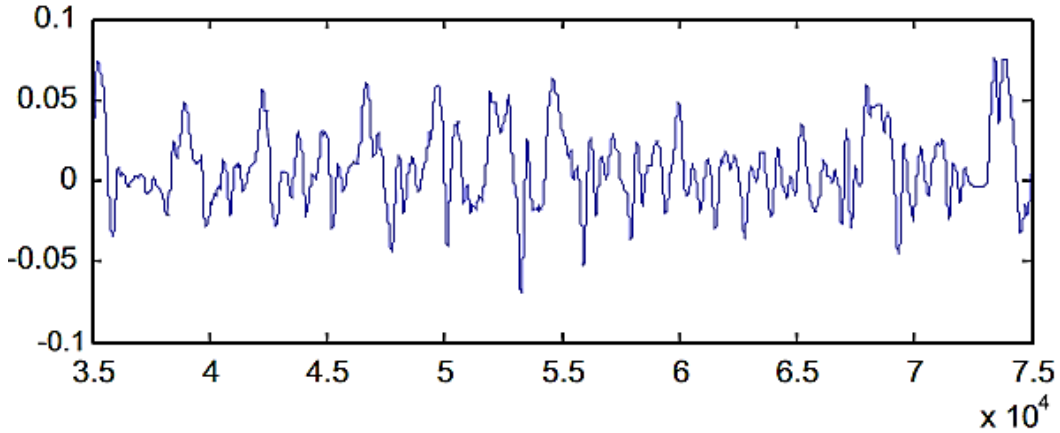

Fig. 46. Difference between the measured AFR and the reference AFR with the supervisory control obtained on a 5.3L vehicle in (Efimov et al., 2014)

Among the different developed methodologies, Model-Predictive Control has been applied to the air-fuel ratio control. Indeed, a controller based on a prediction algorithm, depending on value from the past and that is able to predict the future states of the system, is valuable in time-varying delays conditions. Once the model is obtained, the MPC can be designed for controlling the fuel injection (Wang et al., 2006; Polóni et al., 2007; Zhai et al., 2010; Shi et al., 2015) or for designing an individual controller for each fuel injector (Li and Shen, 2011). The Model-Predictive methodology can be improved with other techniques such as adaptive MPC (Abdi et al., 2011), neural networks-based design (Saraswati and Chand, 2010), nonlinear MPC (Wojnar et al., 2013) or data-driven MPC (Hu et al., 2014). For the MPC design, the delay can be either considered as fixed (Zhai and Yu, 2009) or compensated (Trimboli et al., 2009) as depicted in Fig. 47. The Model-Predictive structure can be generalized in a Generalized Predictive feedback controller (GPC) that can be applied to individually control each injector (Kumar and Shen, 2017), succeeding the challenge #3.

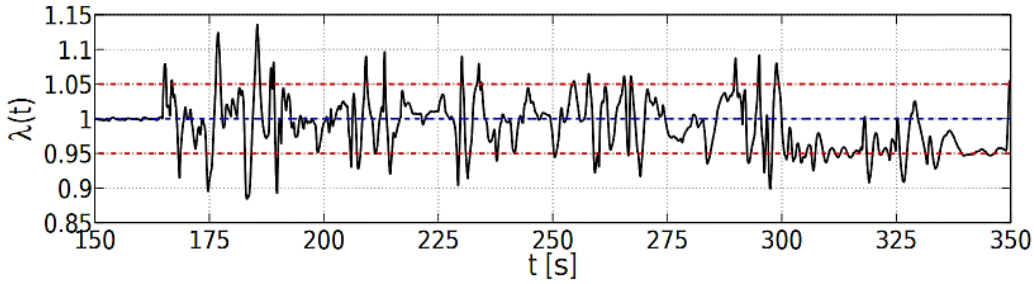

Fig. 47. AFR control with the MPC and delay compensation in (Trimboli et al., 2009)

Once the state-space representation of the system is obtained, it is clearly nonlinear in the case of an engine. A methodology, based on fuzzy logic and the sector nonlinearity approach, has been developed by Takagi and Sugeno (Takagi and Sugeno, 1985) to directly deal with nonlinearities. Indeed, this approach exactly represents the nonlinear system considered inside a domain of validity. Because of that, this approach has been considered to deal with such a nonlinear system the air-fuel ratio is. A fuzzy Takagi-Sugeno controller has been developed for controlling the global injection in (Lauber et al., 2007, 2011), taking into account the time-varying delay directly during the controller design methodology. Simulation results are presented in Fig. 48.

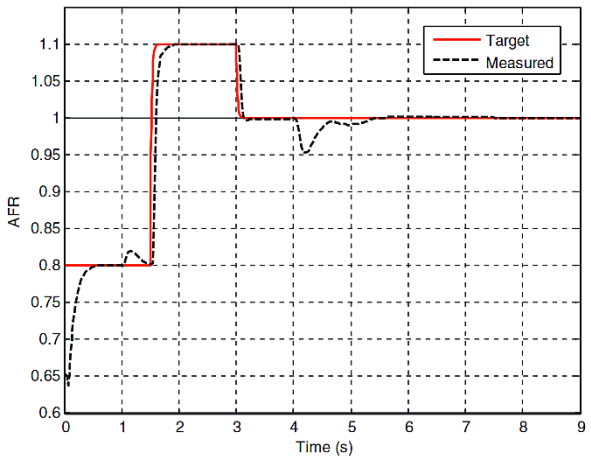

Fig. 48. Simulation results of the fuzzy Takagi-Sugeno AFR controller developed in (Lauber et al., 2011)

Either the classic state-feedback, the Model-Predictive Controller or the fuzzy Takagi-Sugeno state-feedback needs a model to rely on. The different elements involved in the air-fuel problem have been previously detailed, but how are they modelled in a control-oriented way? And how are the nonlinear aspect and the time-varying delay represented in the literature?

4.3. Control-oriented air-fuel ratio models

As presented in the challenges of the air-fuel ratio control, the system is composed of several elements. First, the fuel is injected by the injector through the fuel path. Then, it is mixed with the air inside the cylinder, before exploding when the spark plug ignites the mixture. This chemical mixture is transformed in post-flames gases that leave the cylinder to go to the exhaust manifold, where they reach the confluence point and they meet the exhaust gases from the other cylinders. Finally, they pass through the UEGO sensor where the air-fuel ratio is measured, giving feedback for the air-fuel ratio controller to maintain the air-fuel mixture in stoichiometry proportions during the combustion.

Similarly to the model for the idle speed control or the spark-advance control, maps and empirical methods have been investigated to represent the nonlinear behavior, neglecting the time-varying delay (Li and Shenton, 2010, 2012; Desheng et al., 2014), see Fig. 49.

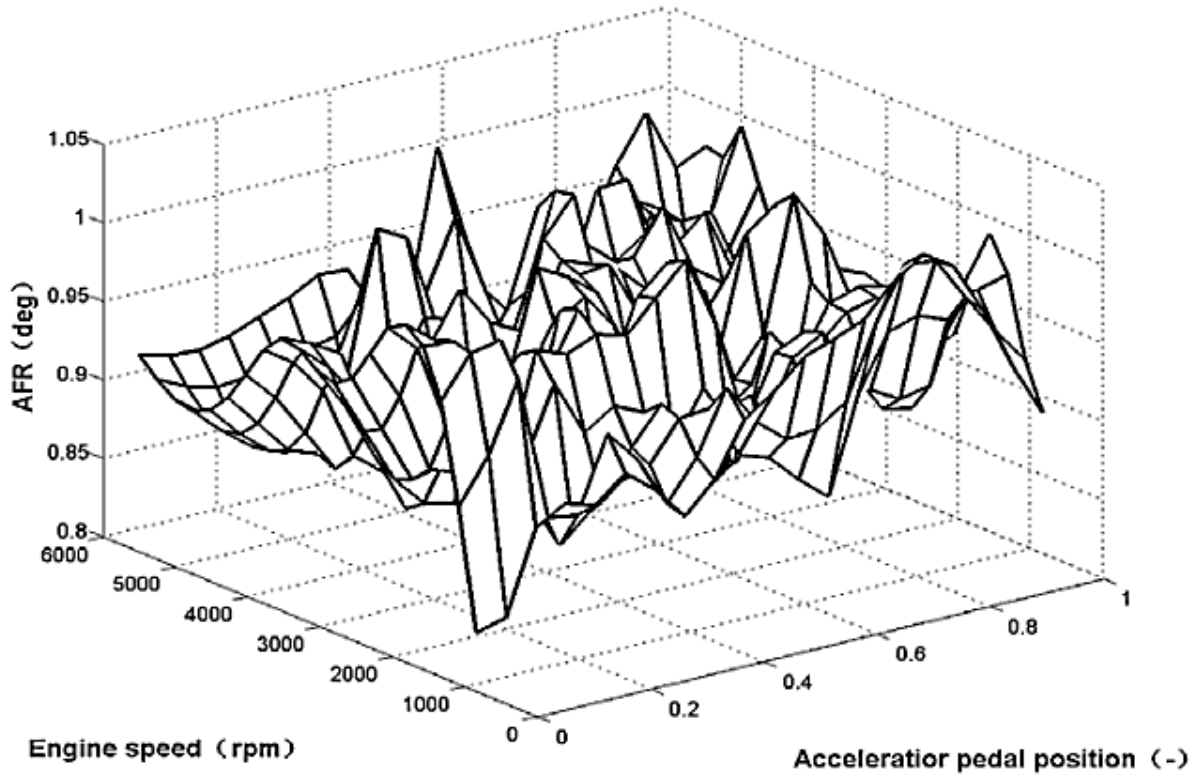

Fig. 49. Mapping of the air-fuel ratio in function of the engine speed and the pedal position in (Desheng et al., 2014)

In the same philosophy, black-box models have been developed to avoid describing the physical elements and considering only data-based models. One of the most used black-box model is the Neural Networks, such as the wavelet neural networks (Abdi et al., 2011) or an algorithm called the ARX or the NARX model (Neural network AutoRegressive model with External inputs). Because black-

box models rely on sensor data, the identification process is crucial (Arsie et al., 2006; Dickinson et al., 2009). Since they are based on algorithmic programing, they are very efficient combined with a Model-Predictive Controller (Polóni et al., 2007; Saraswati and Chand, 2010). Particular cases of black-box models have been investigated, for example, one generated through an impulse response of the system (Volterra model) combined with neural networks and controlled by a MPC (Shi et al., 2015, 201) or an algorithmic model based on chaotic time series and chaos optimization (Donghui et al., 2014; Donghui, 2016). The validation of the Volterra model is presented in Fig. 50 as an example.

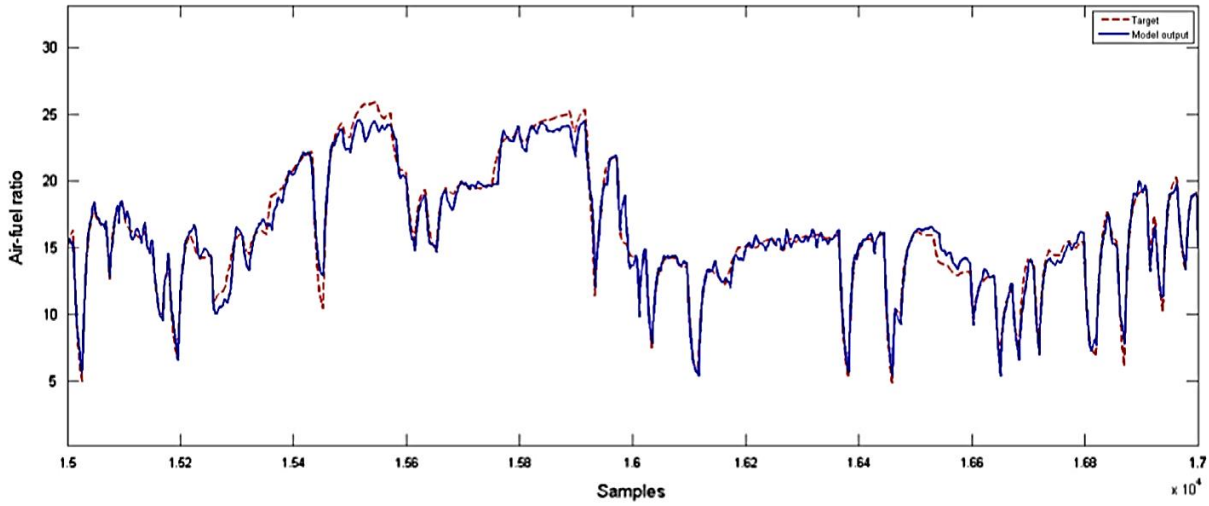

Fig. 50. Validation of the Volterra model for the non-normalized air-fuel ratio (1.4.1) in (Shi et al., 2015)

On the contrary of these experimental-based black-box models, another approach consists on directly modelling the behavior of the system. A first model has been developed based on transfer functions: it is a First-Order Plus Dead Time (FOPDT) model. The first order transfer function can model the dynamics of the UEGO sensor when the exhaust gases reach its location. The dead-time, or the delay, can be added using the exponential form of the Laplace domain. However, the limitations of transfer functions make it hard to model a nonlinear delayed system. The time-varying delay is either considered as fixed (Rupp et al., 2007) or approximated, for example with a Padé approximation of the first-order (Zope et al., 2009; Kahveci and Jankovic, 2010; Ebrahimi et al., 2012; Kahveci et al., 2014b, 2014a) or the second-order (Postma and Nagamune, 2012) to make the design of a model-based controller easier. The first-order Padé approximation for the time-varying delay is depicted in Fig. 51.

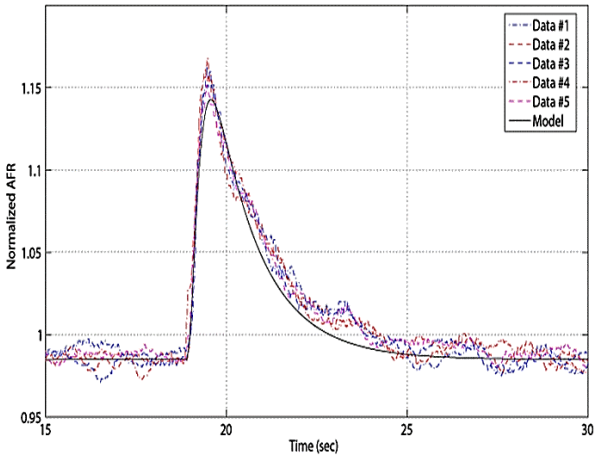

Fig. 51. First-order Padé approximation of the delay based on experimental data in (Kahveci and Jankovic, 2010)

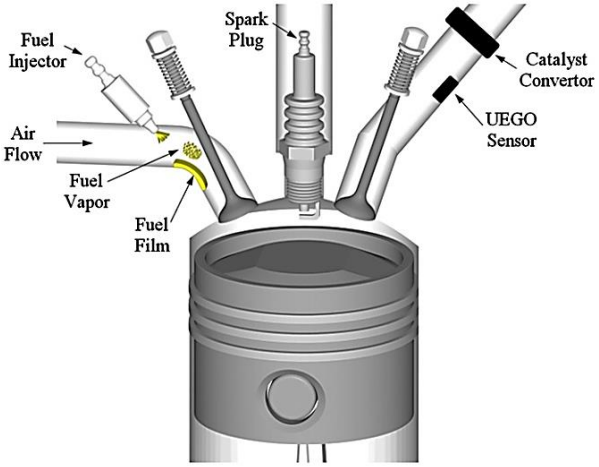

Fig. 52. Scheme of the different elements and phenomenon involved in the fuel path in (Ebrahimi et al., 2012)

The second model is called the Mean-Value Engine Model (MVEM). It is the most used in model-based engine control (Hendricks et al., 1996). It represents each element of the system separately, mainly based on the physics laws and can be identified using experimental sets of data from engine test benches (Gerasimov and Pshenichnikova, 2012). MVEM can be improved with neural networks methodology to represent the parts for which the laws of the physics are not known or too complex for controller design (Wang et al., 2006; Wang and Yu, 2008; Zhai and Yu, 2009, 200; Zhai et al., 2010).

Starting with the injectors and the fuel path, the dynamics of the injected fuel has been modelled taking into account different phenomenon such as the wall wetting or the fuel vapor, as represented in Fig. 52. The wall-wetting is a quantity of fuel that remains on the intake collector of a cylinder during the injection, while the fuel vapor is created due to the high pressure in the injector pipe (Lauber et al., 2011; Jansri and Sooraksa, 2012). The periodic behavior of the engine can be taken into account to model the global and individual fuel dynamics (Liu and Shen, 2012). Since the fuel is not responsible for the torque, a combustion model is not mandatory for the air-fuel ratio control; however, the thermal efficiency model can be written and the individual air-fuel ratio can consequently be obtained (Na et al., 2016).

Similarly to the intake manifold, the exhaust manifold is an easy element to model since it involves gases propagation which is a phenomenon described by physics laws (Kerkeni et al., 2008). The exhaust gases mixing at the confluence point can be modelled in function of their original cylinder using a periodic representation, such as in (Li and Shen, 2011; Liu et al., 2011). However, the crucial point of the intake manifold is the time-varying delay taken by the post-flame gases to reach the UEGO sensor.

Among the time-varying delays, two categories have to be distinguished: the variable time delay and the variable transport delay (Zhang and Yeddanapudi, 2012). While the first category is dedicated to delays whose variations are only dependent on the time, the second category – variable transport delays – include delays depending on time-varying variables or states of the system. In the case of the air-fuel ratio, the variable transport from the exhaust valve to the UEGO sensor has been modelled as a function of the measured variable of the engine. One is based on experimental results;

indeed, it has been observed that the variable transport delay is equal to one engine cycle, or two engines turns, so a model depending on the engine speed can be obtained (Jiao and Shen, 2011; Lauber et al., 2011; Wang and Jiao, 2015). Another model involves the air mass flow inside the cylinder (Mallik and Aryan, 2015). A more complex model can be obtained by combining a speed-dependent term and a flow-dependent one (Trimboli et al., 2009), see Fig. 53.

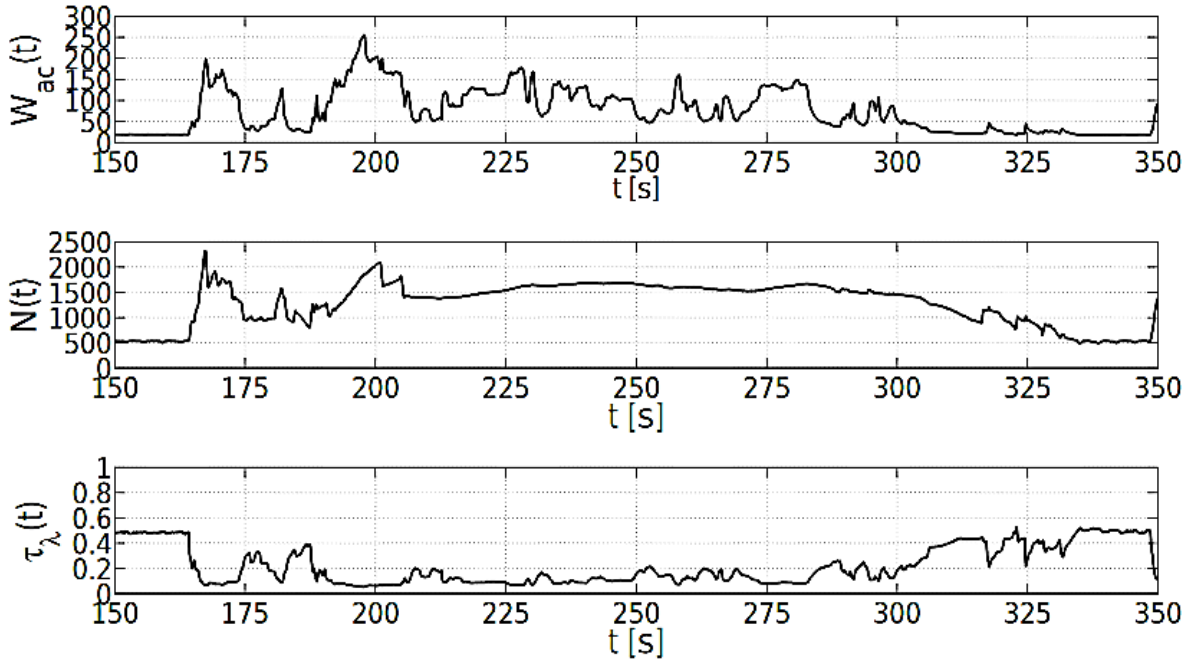

Fig. 53. Variable transport delay $\tau_\lambda(t)$ as a function of the engine speed $N(t)$ and the air mass flow $W_{ac}(t)$ in (Trimboli et al., 2009)

The UEGO sensor can be modelled as a first-order system with a small time constant. The Three-Ways Catalyst (TWC) can be modelled in a control-oriented way. The amount of oxygen stored inside the TWC can be obtained and taken into account in the design of the air-fuel ratio controller (Trimboli et al., 2009; Mallik and Aryan, 2015).

However, if the presented models allow the controllers to achieve the challenges #1 and #2, maintaining the air-fuel ratio to the stoichiometry and dealing with the time-varying delay respectively, the lack of measurements do not permit to individually control each fuel injector to achieve the challenge #3 as long as the individual air-fuel ratio is not measured. How does on obtain this crucial value that is not available with the sensors equipped in a commercial car engine?

The answer remains in the other part of the control theory: Observer design. The first observers involved in estimating individual air-fuel ratio were based on Kalman filters (Hendricks et al., 1996) or on nonlinear sliding mode techniques to estimate the heat released by the combustion, the air mass inside a cylinder so the individual AFR (Shiao and Moskwa, 1996). As for the air-fuel ratio control, observing the individual air-fuel ratio may need a model or not.

Model-free observers can be based for example on neural networks (Zhai and Yu, 2007) where they are used to estimate the air mass inside a cylinder, since it is not measured (contrary to the amount of fuel that can be deduced from the start of injection and the injection timing). Signal processing

and spectral analysis can allow estimating the individual air-fuel ratio so individual controllers (PI) can be designed in (Cavina et al., 2010).

On the contrary, model-based observers can be designed using the previously control-oriented models. The most common model-based observer is called the unknown input observer, and it has been used in order to estimate the individual air-fuel ratio (He et al., 2008; Na et al., 2016). Experimental results are depicted in Fig. 54 for a six-cylinders engine. The unknown input observer methodology can be converted to the specific fuzzy Takagi-Sugeno context (Kerkeni et al., 2008; Lauber et al., 2011). The time-varying delay can be either removed from the controller design using a high order sliding mode observer to directly estimate the AFR (Akram et al., 2013) or taken into account in the observer design to improve the estimation of individual air-fuel ratios (Wang and Liu, 2016), as illustrated in Fig. 55 with the second and the third cylinders.

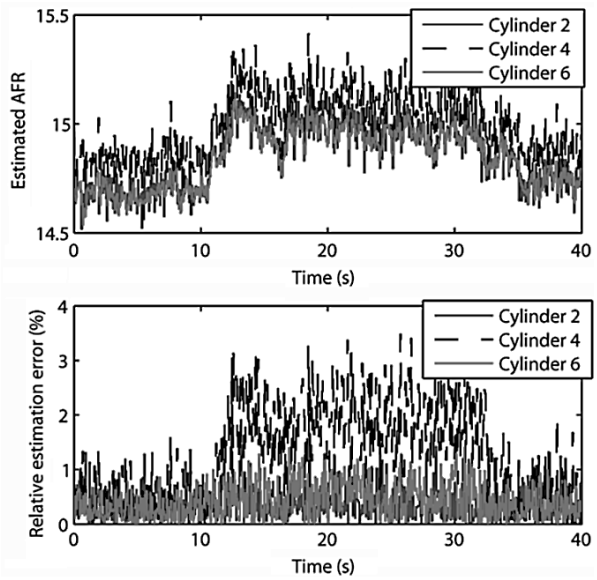

Fig. 54. Estimated individual AFR and estimation error of the unknown input observer developed in (He et al., 2008)

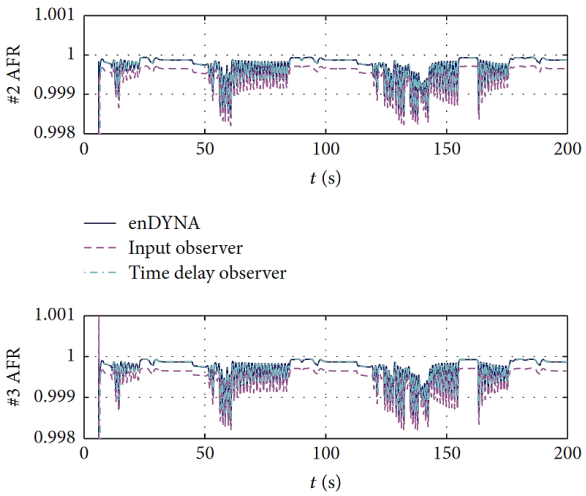

Fig. 55. Comparison of estimated individual AFR using an unknown input observer with and without integrating the time-varying delay in the design in (Wang and Liu, 2016)

The fuel injection is responsible for the balance of the air-fuel ratio inside the cylinder. If the mixture is in stoichiometric proportions, the three-ways catalyst has an optimal functioning and converts the post-flame gases into non-dangerous gases that are rejected in the atmosphere. Because it is crucial for the pollution control, injectors control has been hugely addressed in the literature. Several solutions have been investigated to face the different challenges of air-fuel ratio control, reference tracking, time-varying delay and individual control. Since challenge #1 is always achieved, if one uses an integral action to have reference tracking and disturbance rejection, the delay challenge is still a problem. The fact that the delay can be varying in function of the engine speed, it presents a difficulty for the controller design and, most of the time, it is either mapped, approximated or considered as fixed. Only a few studies are taking this variable transport delay into account during the controller design in spite of the performance a delay-dependent controller should offer. How can the time-varying delay be included directly into the controller design?

The individual control of each injector has been investigated, mainly through observer-controller structure, using different estimation techniques to get the individual air-fuel ratio without adding any new sensor. However, it is well known that the separation principle does not stand for nonlinear systems; so the observer and the controllers cannot be designed independently, and the stability analysis of the closed-loop should take into account both the observer and all the controllers (in case of multiple controllers). What could theoretical techniques be used to study the stability of an observer-controllers structure for nonlinear systems?

As it has been illustrated through the state of the art in air-fuel ratio control, the used methodologies are similar to the idle speed or the spark advance control: either model-free or model-based control, including neural networks and empirical/heuristic for the first one and model-predictive control for the second. In spite of their performances, these methods are still employed mainly in the academic world, while car industry prefers simple solutions. What are the limits of these advanced control methodologies? How to deal with the challenges that remain without a satisfying solution? What can trade-off be realized between theoretical demonstrations and applicative implementations?

5. Motivation and contribution

5.1. Motivation

5.1.1. Challenges

Nowadays, cars represent a crucial challenge for the society and the humanity since it involves economy, ecology, industry and health. In this context, it is essential to optimize the control of the engine. Among the different control inputs, the throttle and the spark advance are involved in the particular case of the idle speed, while the fuel injection controls the air-fuel ratio to reduce the pollution.

The challenges for controlling these elements are summarized in Table 1.

Table 1. Challenges of the engine control

Throttle control	Spark advance control	Fuel injection control
• Throttle #1: Reference tracking, disturbance rejection • Throttle #2: Nonlinear behavior • Throttle #3: Engine torque not measured	• Spark #1: Optimization but avoiding knocking • Spark #2: Nonlinear behavior • Spark #3: Individual control	• Fuel #1: Reference tracking, disturbance rejection • Fuel #2: Variable transport delay • Fuel #3: Individual control

As one can see, several challenges are common for the different control problematics (reference tracking and disturbance rejection, individual control, nonlinear behavior). The reference tracking challenge, for the throttle and the fuel control respectively, are always achieved, whatever the method considered, since almost all the controllers include an integral action to track constant references.

The nonlinear behavior still remains a big issue; indeed, most of the existing methods avoid the nonlinearities, by linearizing, mapping or approximating. Because the engine models are always nonlinear, model-free controllers have been explored and developed, in spite of the existence of methodologies to deal directly with the nonlinearities, such as the Takagi-Sugeno representation.

Similarly to the nonlinearities, the variable transport delay has been avoided by being either fixed, mapped, estimated or compensated. The presence of a time-varying delay on the input implies a trade-off: taking it into account during the controller design can increase performances but also the complexity of the control law. This remains an unsolved problem.

The unmeasured values problem has been partially solved with the use of observers in the case of air-fuel ratio, so individual control strategies have been designed, mainly by designing separately the observers and the controllers. However, the separation principle does not stand in the nonlinear context, and stability methods such as the direct Lyapunov method are rarely considered. In the case of the spark advance, the lack of models makes observer design complicated, so the individual control of the spark plugs is mainly based on empirical and model-free methods. What are the limits of the existing methodologies?

5.1.2. Limits of the existing methodologies

To face the different challenges of engine control, the researchers have adapted the theoretical methodologies to the application problem. The different solutions are summarized in Table 2

Table 2. Literature review of the methods applied in engine control

Model-free control	Model-based control
• Fuzzy logic control • Adaptive control • Neural Networks control • Stochastic/signal processing control • Iterative control	• PI/PID control • State-feedback control • Hybrid control • Model-Predictive Control • Fuzzy Takagi-Sugeno control

5.1.2.1. Model-free controllers

Model-free controllers have been applied to the different engine control problems for their ability to get performances without the complex engine modelling part. They can be considered as black-box methodologies, where the system to be controlled is obtained through identification algorithms from sensor signals, or as purely model-free like iterative control or fuzzy logic. They can be based on expert knowledge or complex algorithm programming. In the case of a highly nonlinear system such as the engine, this avoid directly dealing with the nonlinearities; however, the specific cases due to the nonlinear behavior have to be taken into account in the rules of the fuzzy logic or the algorithms of the iterative control. Then, it can be very costly for the embedded electronic control unit to run stochastic programs, for example in real-time.

In the case of neural networks, the identification/training phase can be long in order to get efficient controllers, while this mainly remains an experiment-based methodology, highly depending on the

considered engine. Indeed, the main inconvenient of these methodologies is the unicity of the proposed strategy. After the identification process, the black-box model is obtained for the currently used engine and, because they are not representing the different elements of the engine, adding a component such as a turbocharger implies to re-identify the all neural network for example. Moreover, this does not achieve the industry requirement to have a control structure that can be understood along the development chain. If the technician that makes the final adjustment of the engine wants to modify the specific value of the controller involved in the waste-gate control, the black-box-based control makes it difficult from a socio-technical point of view.

Another inconvenient of data-driven control strategies is the dependence relation between the control and the quality of the sensors. For signal processing or heuristic control, having bad quality or biased sensors can disturb the control signal and decrease the performances. While it is difficult to use it alone, the adaptive technique can be coupled with other control strategies to make them more flexible facing disturbances or lose of information from the sensors. However, considering a neural network with several layers to deal with all the particular situations of the engine, the designed algorithm control with a sensor signal treatment to get a high quality information and an adaptation law, it is impossible to implement a so complex control strategy in an embedded industrial controller with limited performances and where most of the memory is dedicated to safety supervision. If these model-free controllers can face the different control challenges, mainly by avoiding the difficulties and nonlinearities, they need a computation power that makes them costly to implement in real-time in a commercial ECU.

5.1.2.2. Model-based controllers

On the other hand, model-based controllers have the advantage of relying on a physical model representing each component of the whole system. Consequently, each subsystem can be identified separately, and adding a turbocharger to the engine does not change the controller structure. That is why the model-based controllers are able to solve the individual control challenge, while adding or removing injectors or spark plugs is not a problem and does not need a whole identification process to determine the new control law. Based on the model described as differential equations, the engine can be represented in the state-space. Because of the nonlinear behavior of the engine, the system is modelled using a nonlinear state-space representation where nonlinearities are in the system matrix and the input matrix.

While PID controllers and state feedback have been designed on simplified or linearized models, other techniques as hybrid control, Model-Predictive Control or fuzzy Takagi-Sugeno control can deal with the nonlinear behavior. In the hybrid theory, the nonlinearities can be expressed using a combination of continuous-time dynamics triggered with discrete-time events. Indeed, the hybrid model can efficiently translate the periodic aspect of the engine. Static state-feedback controllers can be designed for each continuous-time subsystem (low-level control) while a hybrid strategy can switch from one to another (high-level control). However, the nonlinearities may remain in the continuous-time dynamics after getting the hybrid model. Linearizing can help designing the state-feedback, but the nonlinear behavior is not taken into account. Moreover, embedding in a commercial ECU a feedback controller for each continuous-time dynamics, in addition to the global hybrid controller to commute, represents an important computational cost for the electronic control unit. Even if the theoretical contribution on hybrid controllers has stability analysis for the closed-

loop, the same limits that the PID and the standard state-feedback controllers are disadvantaging the hybrid controllers, in addition to the difficulty to embed such a complex control structure.

Model-Predictive Control (MPC) has efficient results due to their prediction algorithm. Indeed, based on a dynamical model, the controller calculates inside a prediction window the possible values for the future states, taking into account the past states. Using a large prediction window, the MPC is able to cope with the nonlinearities and change the control signal to handle them. However, computing the prediction window is a highly costly algorithm for an embedded controller with limited capacities. According to the performances of the used ECU, a trade-off has to be realized between the computational cost of the whole MPC algorithm and the size of the prediction window. Considering the industrial controllers equipped in commercial cars, the prediction window has to be reduced so importantly than the future states are approximately predicted and the nonlinear behavior is hardly handled. That is why, with the current capacities of the embedded ECU, Model-Predictive Control is very hard to compute, so to implement for real-time engine control.

The fuzzy Takagi-Sugeno (TS) methodology can provide an exact representation of the considered system inside a domain of validity. It consists on a collection of linear sub-models triggered with nonlinear functions called membership functions. A fuzzy TS controller can be designed, and the stability of the closed-loop system can be analyzed using the direct Lyapunov method. Usually, Linear Matrix Inequalities (LMI) conditions are obtained. However, one of the limits of this approach is the domain of validity in which a solution may not be found for the LMI problem. Then, in order to find a solution to the LMI problem and get the controller gains, the domain of validity has to be reduced and it may be so small than it is equivalent to linearize the system. Theoretical contributions in the domain of TS models, such as more complex Lyapunov functions or relaxations, can be used to reduce the conservativeness of the method and find solutions to the LMI problem without reducing the domain.

While increasing the complexity of the Lyapunov function and the relaxation of the matrix inequalities does not impact the computational cost of the ECU since it is offline operations, the complexity of the control law can be hard to implement in an embedded engine controller. Indeed, it has been proved than better performances can be obtained with more complex laws, for example including real-time matrix inversion (Guerra and Vermeiren, 2004) or by increasing the number of nonlinear functions that have to be calculated at each sample. Particularly, considering control laws including time-varying delays, the final controller can have an important computational cost, so it may not be suitable for the industry constraints. However, as a model-based state-feedback fuzzy controller, it can deal with individual control if the input vector includes the different controllable actuators.

For its ability to deal with nonlinear systems, since it represents a major challenge in engine control, a solution based on fuzzy TS controller is developed. How to reduce the computational cost of the complex fuzzy control laws while keeping the same performance? How does one deal with variable transport delays without having a too complex controller that cannot be computed by a commercial ECU?

5.2. Contribution

The engines are systems in constant change. Indeed, new technologies are designed to improve their function to reach the evolution of the emission regulations. A turbocharger or an Exhaust Gas Recirculation (EGR) can be added and an identification of the whole process may be needed every time for a black-box model; it is not suitable according to the time constraints of the car industry, that is why a model-based solution has been chosen.

For its ability to represent the periodic behavior of the engine and to model the nonlinear dynamics with polynomial equations, the hybrid model from (Balluchi et al., 2010) is considered. An adaptation is realized to convert the continuous/discrete hybrid model into a continuous-time periodic state-space representation. Then, the model is improved to catch all the nonlinear dynamics that the original model did not consider.

Contrary to the maps that take long tim to be built, the identification phase is very short for models. The different elements of the engine are identified separately to get the constant parameters. Adding a new element just implies to identify it. Moreover, a huge theoretical and practical background exist in the identification field, so even the parameters of the most nonlinear equations of the engine dynamics can be estimated with existing powerful tools. A nonlinear continuous-time periodic state-space representation with identified parameters is then obtained.

However, the electronic control unit can generate control signals only in discrete-time, so a conversion is needed. Transforming the model into a discrete-time domain involves a time-varying sampling period. This can be solved by considering a particular discrete-time domain, the crank-angle domain, whose sampling period is related to the angle of the crankshaft, so the engine speed. The model becomes a nonlinear periodic state-space representation in the crank-angle domain.

The unmeasured dynamics, such as the torque production inside the cylinder after the combustion, can be expressed through measured variables using the periodicity property. It is possible, by choosing an appropriate sampling period of the crank-angle domain, to traduce the periodic behavior into difference of samples. Then, the unmeasured dynamics can be expressed as function of measured variables from other periods or at different sampling instants.

The nonlinearities inside the model represent one of the most crucial challenges of engine control. Instead of linearizing or using maps to avoid dealing with the nonlinear aspect, the Takagi-Sugeno representation is used to directly deal with the nonlinearities. The model can then be transformed into a TS model in the crank-angle domain.

Another advantage of the TS models is the huge theoretical background in closed-loop stability analysis and control design. From the simplest linear state-feedback to complex controllers implying real-time matrix inversions and combination of nonlinear membership functions, fuzzy TS controllers can be designed to solve the challenges of the engine control.

In the case of idle speed control, the complexity of the system makes it impossible to find a satisfying domain where a linear controller or a fuzzy state-feedback controller can be obtained. There is a need to investigate more complex control laws, which implies an increase of the complexity and the computational cost. Particularly, controllers with real-time matrix inversions are among the most efficient TS controllers and they can provide a solution to the LMI problem. After computing the LMI conditions, the control gains are obtained to stabilize the closed-loop system of idle speed. However,

real-time matrix inversions are very costly for embedded ECU. That is why a solution has been developed to design alternative controllers that can provide the same performance as the complex ones but without the real-time matrix inversions. It results in a fuzzy state-feedback with combination of nonlinear membership functions, which is less costly for the ECU (depending on the size of the system).

Concerning the air-fuel ratio, the transformation to the crank-angle domain makes the delay fixed. This transformation is extended and generalized to every kind of variable transport delay. Because the delay is no longer time-varying, strategies for fixed delayed input system can be applied. By solving the challenge of time-varying delays, a simple linear controller can be designed using the Lyapunov direct method for the stability analysis of the closed-loop and by solving the LMI problem.

The contributions result in the design of two controllers for the engine control. The idle speed control is ensured by a multiple-sums fuzzy state-feedback controller. The state is augmented with an integral action, so challenge #1 of the throttle control (reference tracking and disturbance rejection) is ensured. Challenge #2 dealing with the nonlinear behavior is handled with the TS representation. The unknown engine torque discussed challenge #3 is described as a function of measured values expressed at different samples in the crank-angle domain. The air-fuel ratio control is realized by a linear state-feedback with an integral action, ensuring performances for the challenge #1 of the fuel injection control. The variable transport delay has been made fixed in the new crank-angle domain, allowing the design of simple controller for time-varying delayed systems. Because of the structure of the designed controllers, they are easy to implement in a commercial ECU and it represents a low-computational-cost solution. Table 3 summarizes the contributions of the thesis according to the different challenges introduced in Table 1, where the green color symbolizes an achieved challenge and the red one a challenge not taken into account in the thesis.

Table 3. Contribution to the engine control

Throttle control	Spark advance control	Fuel injection control
• Throttle #1: Reference tracking, disturbance rejection • Throttle #2: Nonlinear behavior • Throttle #3: Engine torque not measured	• Spark #1: Optimization but avoiding knocking • Spark #2: Nonlinear behavior • Spark #3: Individual control	• Fuel #1: Reference tracking, disturbance rejection • Fuel #2: Variable transport delay • Fuel #3: Individual control

This document presents the different steps of the applied methodology to systematically design fuzzy TS controllers in order to control the engine.

CHAPTER II: Control oriented models

Each world has its laws, you just have to discover them.

P. K. Dick, *Eye in the Sky*

1. Introduction

This chapter is dedicated to control-oriented engine models since a model-based controller has been chosen. In chapter 1, several models have been investigated. The chosen model is then presented and adapted to be suitable for advanced fuzzy TS controller design. The constant parameters of the model have been identified using identification algorithms with measured signals from the engine test bench located at the LAMIH, Valenciennes. The whole scheme of the gasoline engine model is depicted in Fig. 56 where the control inputs (in green) are denoted $u_{thr}(t)$, $u_{spk}(t)$ and $u_{inj}(t)$ for the throttle valve input and the spark advance input, respectively. The load torque $T_L(t)$ is expressed as an external disturbance (in red). The outputs of the system are the engine speed $n(t)$ and the air-fuel ratio $\lambda(t)$ (in blue).

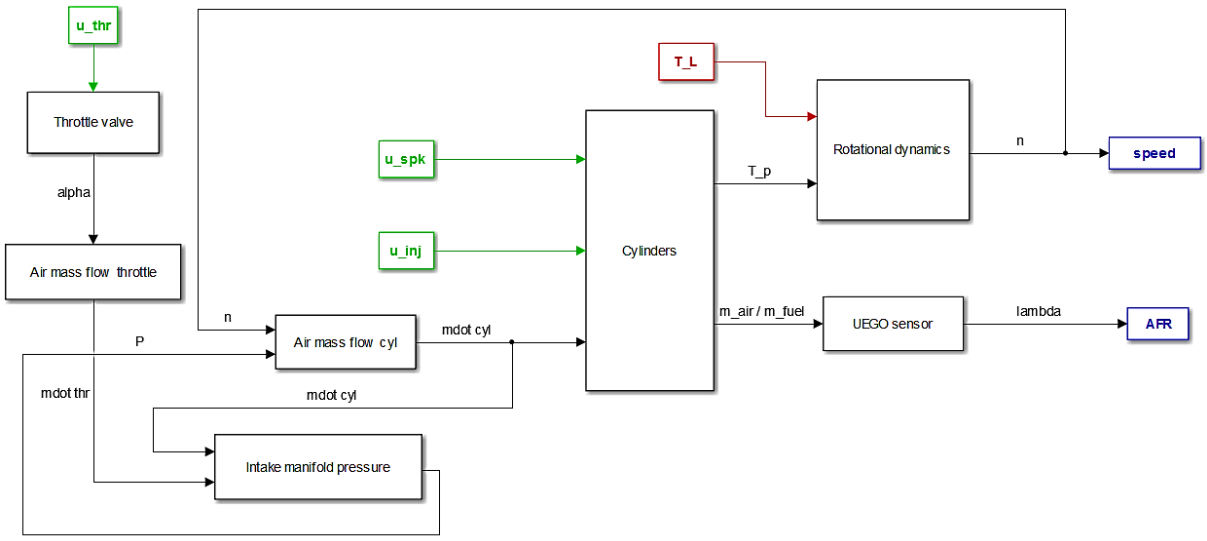

Fig. 56. Scheme of the engine model

2. Choice of the model

2.1. Hybrid model for idle speed

In order to design a model-based advanced fuzzy TS controller, a model is needed first. As expressed along the first chapter, the main critical point of the model for the idle speed control is the torque production with complex nonlinear dynamics. This problem can be dealt using the periodicity of the engine. This periodic behavior can be expressed through different theoretical methodologies. (Balluchi et al., 2010) has chosen to use the hybrid modelling for representing the engine.

A hybrid model is characterized by several continuous-time dynamics that are triggered according to discrete events. It can be seen as several continuous sub-models that are activated depending on events, in the case of the engine, crank angle events. The four phases can be represented and triggered every time the crankshaft reaches a Top-Dead Center. Particularly, the hybrid model has the advantage of being able to model the different steps accomplished by a cylinder, including the torque production. Hybrid models have the ability of representing the nonlinear behavior of a

system, through the continuous-time dynamics that may be nonlinear and through the switch between the different sub-models that can represent most of the particular functioning cases.

The air-path model for the idle speed is composed of several sub-models representing the different elements and phenomenon occurring in the engine. Fig. 57 presents the air-path model in the global structure in Fig. 56.

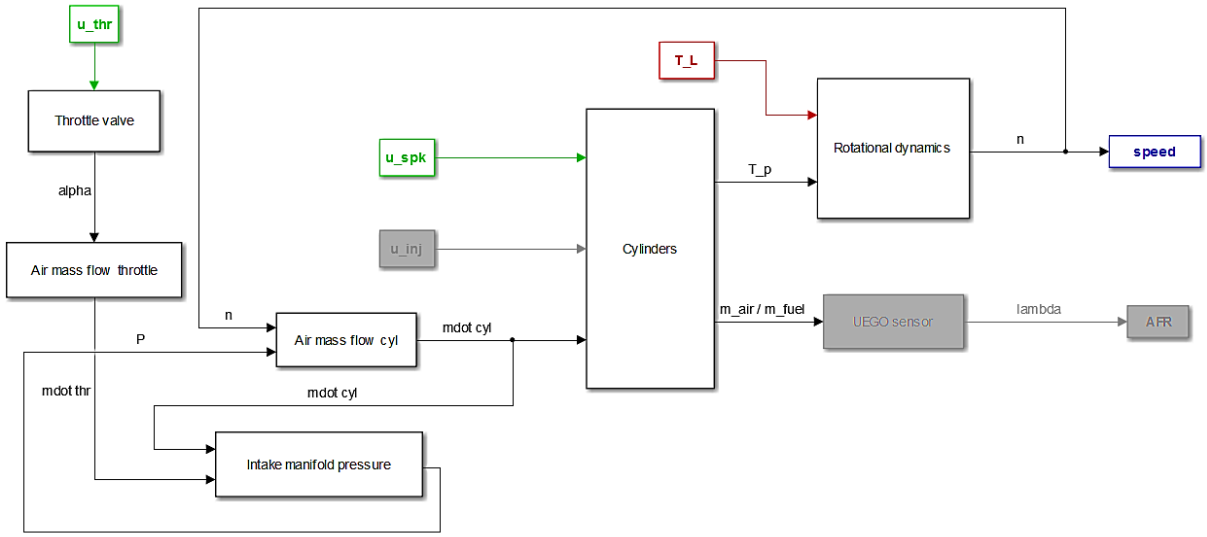

Fig. 57. Scheme of the idle speed model

The first organ of the idle speed model is the throttle valve. While it was mechanically connected in the past, it is now controlled via the ECU to improve performances during normal driving conditions and to maintain the engine at an idle speed during the idle phases. Instead of modelling the throttle has a nonlinear system with complex fluid dynamics, it is considered as a first-order system which reaches the reference in a certain response time τ_{thr} :

$$\dot{\alpha}(t) = -\frac{1}{\tau_{thr}}\left(\alpha(t) - u_{thr}(t)\right) \tag{2.2.1}$$

where $\alpha(t)$ is the position of the throttle in degrees and $u_{thr}(t)$ the command generated by the electronic control unit in degrees. The response time τ_{thr} (of seconds) is a constant parameter of the engine that needs to be identified. As an example, it has been identified in (Balluchi et al., 2010) with dataset from a Magneti Marelli engine and its value is $\tau_{thr} = 8.35 \times 10^{-2} s$. Through the throttle valve, the air enters then into the intake manifold.

The intake manifold is an element of the air-path equipped with a lot of sensors (air mass flow entering and leaving, pressure sensor…) and the law of the gases propagation is well known, so the intake manifold pressure is an organ easy to model and to identify. It is based on the physical phenomenon happening inside when an amount of air is injected by the throttle valve, while another amount of air leaves to the cylinders. This balance between the two air mass flows can be expressed as following:

$$\dot{P}(t) = \frac{RT}{V}\left(\dot{m}_{thr}(t) - \dot{m}_{cyl}(t)\right) \tag{2.2.2}$$

where $P(t)$ is the pressure inside the intake manifold in mbar, $\dot{m}_{thr}(t)$ and $\dot{m}_{cyl}(t)$ are the air mass flow entering and leaving the intake manifold respectively, expressed in kg/s. The engine parameters are described as R the perfect gases constant in appropriate unit, T the temperature of the air inside the intake manifold and V the plenum volume.

Since the two mass flows $\dot{m}_{thr}(t)$ and $\dot{m}_{cyl}(t)$ are highly nonlinear with hardly-modelled dynamics, they are approximated using polynomial equations depending of measured variables. By identifying the coefficients of the polynomials using datasets from an engine test bench, it is possible to get an accurate model based on a polynomial approximation. For example, the dynamics of the air mass flow passing through the throttle valve and entering the intake manifold can be approximated considering a polynomial expression depending on the throttle position:

$$\dot{m}_{thr}(t) = s_0 + s_1 \cdot \alpha(t) + s_2 \cdot \alpha(t)^2 \tag{2.2.3}$$

where the parameters $\{s_0, s_1, s_2\}$ are constant that need to be identified.

The air mass flow leaving the intake manifold to the cylinders depends on the difference of pressure between the intake manifold and the cylinders it aims to enter. Moreover, since the intake valves of the cylinders are actuated periodically, it is also depending on the engine speed. The polynomial expression can be constructed such that:

$$\dot{m}_{cyl}(t) = c_0 + c_1 \cdot P(t) + c_2 \cdot n(t) + c_3 \cdot P(t) \cdot n(t) \tag{2.2.4}$$

where $n(t)$ denotes the engine speed in rpm and $\{c_0, \ldots, c_3\}$ the constant parameters of the polynomial expression that have to be identified. Then, when the *i*-th cylinder is in the Intake phase, the air mass flow enters inside it.

It is well known that the torque production is depending on the air mass inside the cylinder and the spark advance. This part is crucial for the engine control, however, the torque is not a measured variable and the dynamics of its production are highly nonlinear, making the torque production one of the hardest elements to model. While this problem has been avoided by the use of static maps, the hybrid model of (Balluchi et al., 2010) proposes a set of polynomial expressions, depending on different configurations, to model the torque production. Hybrid models are often represented as chart diagrams with the different sub-models and their associated continuous-time dynamics, and the discrete-time events that make the transition between them, as depicted in Fig. 58.

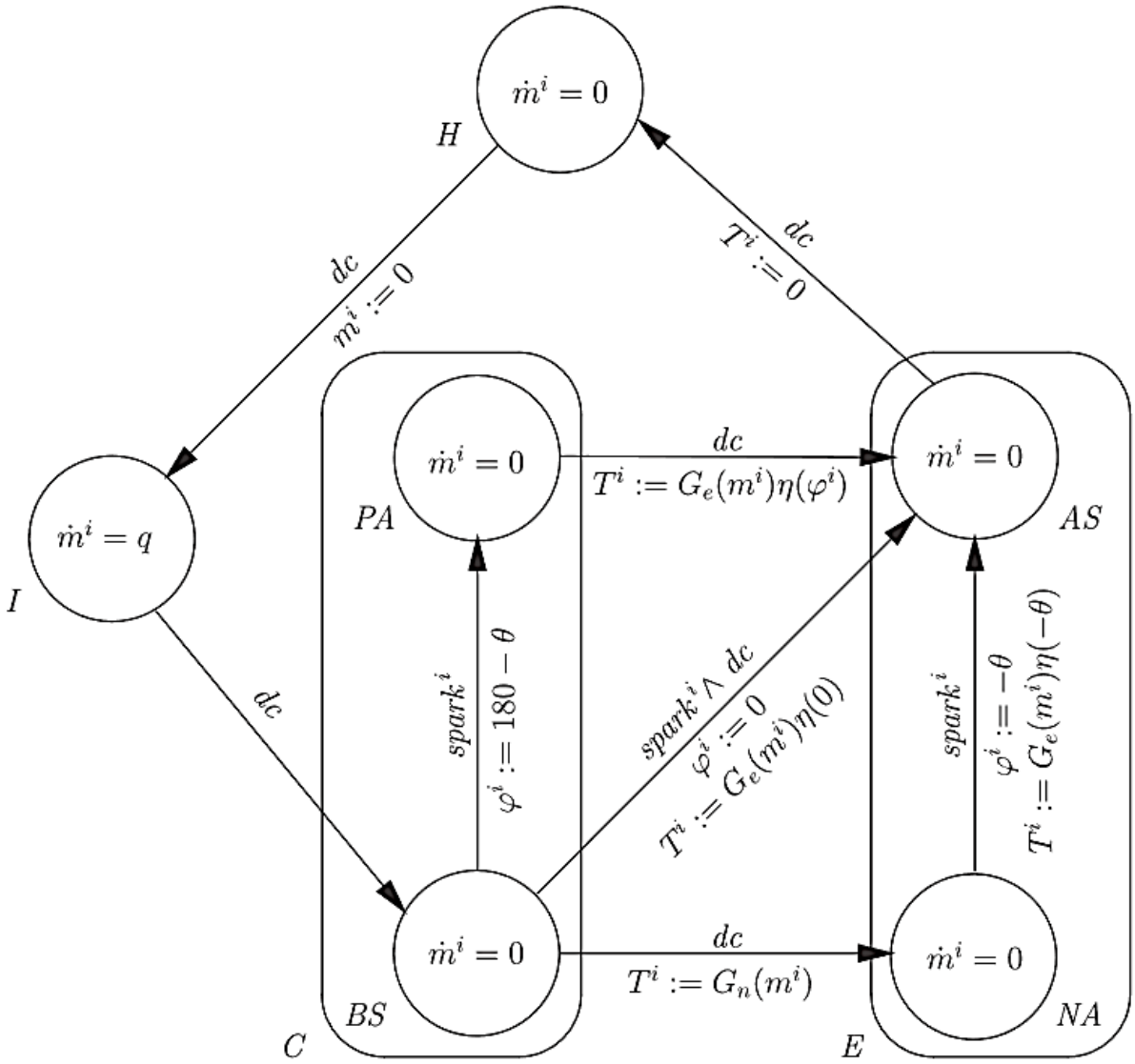

Fig. 58. Torque production represented as an hybrid model in (Balluchi et al., 2010)

The four phases of the engine are represented as “I” for the Intake, “C” for the Compression, “E” for the Expansion and “H” for the Exhaust. As one can see, the conditions to change from a phase to another one always contain the moment when a dead center “dc” is reached. During the Intake phase, the cylinder is filled with the air-fuel mixture. The air mass flow entering into the *i*-th cylinder $\dot{m}^i(t)$ is then equal to $\dot{m}_{cyl}(t)$ (where $\dot{m}_{cyl}(t)$ corresponds to q on the diagram). Then, after the Bottom-Dead-Center, the cylinder is in the Compression phase (Before-Spark phase, “BS”). The air no longer enters inside $(\dot{m}^i(t) = 0$ in the diagram). Then, two cases are possible: either the spark advance $\varphi^i(t)$ is positive (noted “PA”), so the spark ignites the air-fuel mixture during the Compression phase, or the spark advance is negative (spark retard, noted “NA”) and then the combustion occurs later in the Expansion phase. Thanks to the hybrid structure of the model, the two cases can be taken into account. A particular case is when the spark occurs exactly at the Top-Dead-Center (transition from “BS” to “AS”, After-Spark). When the spark ignites the mixture, the torque of the i-th cylinder $T^i(t)$ is produced (every transition going to “AS”) and it can be described as a product between two polynomial expressions, one depending on the air mass inside the cylinder

$G_e\left(m^i(t)\right)$ and the other one depending on the spark advance $\eta\left(\varphi^i(t)\right)$ (it can be considered as an efficiency since it is varying between 0 and 1):

$$\begin{cases} T^i(t) = G_e(t)\cdot\eta(t) \\ G_e(t) = h_0 + h_1\cdot m^i(t) + h_2\cdot m^i(t)^2 \\ \eta(t) = v_0 + v_1\cdot\varphi^i(t) + v_2\cdot\varphi^i(t)^2 + v_3\cdot\varphi^i(t)^3 \end{cases} \quad (2.2.5)$$

Then, the cylinder enters into the Exhaust phase, where no torque is produced anymore, and the amount of air is reset to zero before starting again the Intake phase. The total torque production can be calculated summing the torque produced by all the cylinders when they are in the Expansion phase:

$$T_P(t) = \sum_{i=1}^{n_{cyl}} T^i(t) \quad (2.2.6)$$

with n_{cyl} the number of cylinders, in our case, $n_{cyl} = 4$. The assumption is done in this model that only one cylinder at every moment is producing torque, i.e., cylinders are considered as ideally working and no effect such as backflow is taken into account. Then, the torque produced on the crankshaft influences the engine speed $n(t)$ according to the dynamical expression:

$$\dot{n}(t) = a_0\cdot n(t) + b_0\cdot\left(T_P(t) - T_L(t)\right) + e_0 \quad (2.2.7)$$

where $\{a_0, b_0, e_0\}$ are constants derived from the second law of Newton for rotational elements, i.e., they include engine mechanical parameters such as inertia. $T_L(t)$ is the load torque in Nm imposed to the engine; it can be for example a demand from the electric starter when an electronic device is turned on (the air conditioning for instance).

This completes the model for the idle speed control: indeed, the whole air-path is modelled, from the throttle command to the amount of air entering into the cylinders. Then, thanks to the hybrid representation developed in (Balluchi et al., 2010), the torque production is expressed as a polynomial function depending on the amount of air and on the spark advance. The global torque is then used in the rotational dynamics of the engine, making the link between the throttle command and the engine speed that can be controlled to the idle reference. Considering the literature background, what model can be used in the context of air-fuel ratio? Since the variable transport delay is challenging, how to model such a phenomenon?

2.2. Air-fuel ratio model

The model considered in the case of air-fuel ratio control is a Mean-Value Engine Model (MVEM) as the several ones developed in the literature and presented in the previous chapter. The MVEM represents a global model of the engine, i.e. the behavior of each cylinder is not represented, however, their effects are taken into account as mean values. As a beginning, this model allows designing a global controller common to all the cylinders. In order to achieve the challenge #2 of controlling each cylinder individually, another model should be adapted, for example using the hybrid behavior of the idle speed model detailed in (Balluchi et al., 2010).

While the idle speed mainly deals with pre-combustion gases, the air-fuel ratio concerns post-flame gases. However, instead of a complex model of the chemical reaction and the gases propagation, the air-fuel ratio can be expressed as a function depending on the amount of air and the amount of fuel inside a cylinder during the Expansion phase. Fig. 59 represents the engine components used in the air-fuel ratio model.

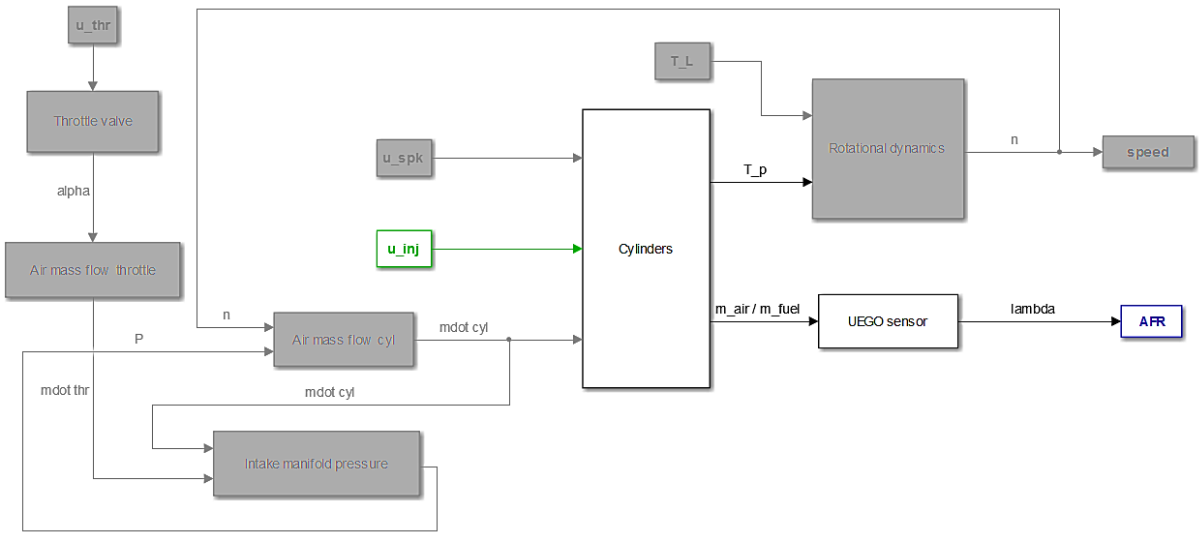

Fig. 59. Scheme of the air-fuel ratio model

Due to the location of the oxygen sensor, and since the air-fuel ratio occurs during the Expansion phase, it implies to deal with one challenging part of the air-fuel ratio: the variable transport delay. Thus it is very important to represent the variable transport delay in a proper way. Because the objective is to find a transformation where this variable transport delay becomes fixed, the chosen model represents the delay as two turns of the engine crankshaft (Lauber et al., 2011). Then, it can be expressed as a function of the crank angles (two turns, so $\theta_{fix} = 720$ crankshaft degrees) and the rotational velocity $\dot{\theta}(t)$ such as:

$$\delta(t) = \frac{\theta_{fix}}{\dot{\theta}(t)} \tag{2.2.8}$$

Then, considering that $\dot{\theta}(t) = 6 \cdot n(t)$, the final expression of the variable transport delay is:

$$\delta(t) = \frac{\theta_{fix}}{6 \cdot n(t)} \tag{2.2.9}$$

So the air-fuel ratio measured at the instant t depends on the air mass and the fuel mass inside the cylinder at the instant $t - \delta(t)$. Then, considering a first-order plus dead time (FOPDT) dynamics for the UEGO sensor, it results the following air-fuel ratio model adapter from (Lauber et al., 2011):

$$\dot{\lambda}(t) = \frac{1}{\tau_\lambda}\left(\frac{1}{\lambda_s} \times \frac{m_{air}\left(t-\delta(t)\right)}{K_{inj}\left(t_{inj}\left(t-\delta(t)\right)-t_0\right)} - \lambda(t)\right) \tag{2.2.10}$$

where $\lambda(t)$ stands for the normalized air-fuel ratio thanks to the stoichiometric coefficient $\lambda_s = 14.67$ as considered in the equation (1.4.2). $m_{air}(t)$ represents the amount of air, while the amount of fuel is not expressed using the complex model of the fuel dynamics but with a simplified expression considering the product between the injection timing $t_{inj}(t)$ in microseconds and an engine parameter K_{inj} depending on the injector actuators. t_0 stands for the dead-time of injection and τ_λ the response time of the UEGO sensor. Both K_{inj} , t_0 and τ_λ have to be identified.

Thanks to the model described in equation (2.2.10), it is possible to control the air-fuel ratio by commanding the global injection timing. Indeed, the structure of the model generates a unique control law applied to all the injectors without considering individual behaviors. This constitutes one limit of the developed approach that is not able to deal with the Challenge #3 of individual injector control. The air-mass inside the cylinder is considered as an external disturbance (whose value is depending on the idle speed control module). Because they are working independently, the two control problems can be separated based on the two detailed models. However, these models present several inconvenient that have to be considered before designing the controllers.

The hybrid model used in the idle speed control context for modelling the torque generation has the advantage of depicting the nonlinear complexity of the combustion, however, since the torque is not measured, identifying the model can be challenging. Moreover, a hybrid controller can be designed based on such a model but this control structure is very costly for the embedded ECU and does not solve the problem of the nonlinearities in the system. The choice of the control structure is to consider a fuzzy Takagi-Sugeno controller for its ability to deal with the nonlinear behavior of the model. However, in order to design such a controller, the hybrid model needs to be transformed into a state-space representation. How to convert this periodic continuous/discrete model into a state-space system where a controller can be easily designed?

3. Model transformations

3.1. State-space representation

3.1.1. Idle speed model

In order to design a fuzzy Takagi-Sugeno controller, i.e. an advanced fuzzy state-feedback, the idle speed model (denoted by the sub-index a_α) has to be expressed as a state-space representation. It has to be then converted from this hybrid model. The continuous-time dynamics triggered with discrete-time events can be seen as a switched system, however, since the discrete-time events are depending on the crankshaft angle, the periodic representation can be considered such as:

$$\dot{x}_\alpha(t) = A_\alpha^p \cdot x_\alpha(t) + B_\alpha^p \cdot u_\alpha(t) \tag{2.3.1}$$

where $x_\alpha(t)$ is the state vector of size $n_x \times 1$ with n_x the number of states, $u_\alpha(t)$ the input vector of size $n_u \times 1$ with n_u the number of control inputs, A_α^p state matrices depending on the period p

and of size $n_x \times n_x$ and B_α^p the input matrices of size $n_x \times n_u$. The period p is included in the set $\{1,2,3,4\}$ where $p=1$ represents the first cylinder in the Intake phase, according to the periodic behavior of the engine, see Fig. 10 and Fig. 11.

First, let us consider the throttle dynamics expressed in (2.2.1). The state vector is composed of the throttle position $\alpha(t)$ as first state, i.e. $x_1(t)=\alpha(t)$ while the throttle reference $u_{thr}(t)$ is the first component of the input vector $u_\alpha(t)$. Similarly, equations (2.2.2) to (2.2.4) can be considered to build the state vector such as $x_2(t)=P(t)$, $x_3(t)=\dot{m}_{thr}(t)$ and $x_4(t)=\dot{m}_{cyl}(t)$. However, the air mass flows can be replaced by their polynomial expressions in order to reduce the number of states.

Let us now transform the torque production part. Since the torque generated by one cylinder is depending on the air mass inside it, four states (one per cylinder) can be added such as $x_5(t)=m^1(t)$ until $x_8(t)=m^4(t)$. Through these four states and the periodic aspect, the hybrid model for torque generation has to be transformed. For example, let us consider the first cylinder. During the Intake phase, i.e. $p=1$, the time-derivative of the air mass inside the cylinder is equal to the air mass flow leaving the intake manifold, so $\dot{x}_5^1(t)=x_4(t)$. Then, during the Compression and the Expansion phases, the air mass is maintained, i.e. $\dot{x}_5^2(t)=0$ and $\dot{x}_5^3(t)=0$. This state is then reseted during the Exhaust phase to represent the post-flame gases leaving the cylinder, so $\dot{x}_5^4(t)=-\dot{m}_M$ with the convenient saturation $\dot{m}_M$, so that the state is ensured to be equal to zero at the end of the engine cycle. The same scheme can be used for the other cylinders in order to construct the state matrices A^p.

Since the model is simplified so that only one cylinder is producing torque and not the others, it is possible to directly model the total torque production, so $x_9(t)=T_P(t)$. As mentioned before, in the hybrid model of (Balluchi et al., 2010), it is calculated when a cylinder is in the Expansion phase and it is expressed as the product of two polynomial expressions, one depending on the air mass inside the cylinder $G_e(t)$ and the other one, $\eta(t)$ depending on the spark advance $\varphi^i(t)$. For model simplification, only the positive spark advance ('PS' in the hybrid model of (Balluchi et al., 2010) in Fig. 58) is considered. The spark advance of each cylinder then belongs to the input vector $u_\alpha(t)$. However, because a product is involved, two possible models can be done: It is either considering the air-dependent function as a nonlinearity in the input matrices B_α^p multiplying the spark advance command. In that case, the problem is that the nonlinearity, depending on the air mass inside the cylinder, is not composed of measured variables, making the use of nonlinear tools (such as the Takagi-Sugeno framework) difficult. Otherwise, the spark contribution $\eta(t)$ can be considered as a nonlinearity multiplying the torque produced by the amount of air $G_e(t)$ in the A^p matrices. Since the spark advance is known and measured, this option is the most convenient, however, the spark advance is then no longer a control input of the matrices B_α^p. In order to realize a spark advance control in the future, observers should be designed for estimating air mass inside the cylinders, and then taken into account during the design of fuzzy Takagi-Sugeno controllers with unmeasured nonlinearities, see for example (Guerra et al., 2006, 2012a; Blandeau et al., 2017). In order to design

an idle speed controller, the spark advance contribution is considered as a nonlinearity multiplying the torque produced by the air, so it does not appear in the B_α^p matrices.

Then, with the total torque produced by all the cylinders as $x_9(t)$, it can be related to the engine speed $n(t)$ through equation (2.2.7). This completes the periodic state-space representation (2.3.1) with the column state vector described as below:

$$x_\alpha(t)=\left[\alpha(t) \quad P(t) \quad \dot{m}_{thr}(t) \quad \dot{m}_{cyl}(t) \quad m^1(t) \quad \cdots \quad m^4(t) \quad T_P(t) \quad n(t)\right]^T \tag{2.3.2}$$

With the following state matrices depending on the period p :

$$A_\alpha^1=\begin{bmatrix} -\frac{1}{\tau_{thr}} & 0 & 0 & 0 & 0 & 0 & 0 & 0 & 0 & 0 \\ 0 & 0 & \frac{RT}{V} & -\frac{RT}{V} & 0 & 0 & 0 & 0 & 0 & 0 \\ NL_1(t) & 0 & 0 & 0 & 0 & 0 & 0 & 0 & 0 & 0 \\ 0 & NL_2(t) & 0 & 0 & 0 & 0 & 0 & 0 & 0 & 0 \\ 0 & 0 & 0 & 1 & 0 & 0 & 0 & 0 & 0 & 0 \\ 0 & 0 & 0 & 0 & 0 & 0 & 0 & 0 & 0 & 0 \\ 0 & 0 & 0 & 0 & 0 & 0 & -\dot{m}_M & 0 & 0 & 0 \\ 0 & 0 & 0 & 0 & 0 & 0 & 0 & 0 & 0 & 0 \\ 0 & 0 & 0 & 0 & 0 & 0 & 0 & NL_3(t) & 0 & 0 \\ 0 & 0 & 0 & 0 & 0 & 0 & 0 & 0 & NL_4(t) & 0 \end{bmatrix} \tag{2.3.3}$$

$$A_\alpha^2=\begin{bmatrix} -\frac{1}{\tau_{thr}} & 0 & 0 & 0 & 0 & 0 & 0 & 0 & 0 & 0 \\ 0 & 0 & \frac{RT}{V} & -\frac{RT}{V} & 0 & 0 & 0 & 0 & 0 & 0 \\ NL_1(t) & 0 & 0 & 0 & 0 & 0 & 0 & 0 & 0 & 0 \\ 0 & NL_2(t) & 0 & 0 & 0 & 0 & 0 & 0 & 0 & 0 \\ 0 & 0 & 0 & 0 & 0 & 0 & 0 & 0 & 0 & 0 \\ 0 & 0 & 0 & 0 & 0 & 0 & 0 & 0 & 0 & 0 \\ 0 & 0 & 0 & 1 & 0 & 0 & 0 & 0 & 0 & 0 \\ 0 & 0 & 0 & 0 & 0 & 0 & 0 & -\dot{m}_M & 0 & 0 \\ 0 & 0 & 0 & 0 & 0 & NL_3(t) & 0 & 0 & 0 & 0 \\ 0 & 0 & 0 & 0 & 0 & 0 & 0 & 0 & NL_4(t) & 0 \end{bmatrix} \tag{2.3.4}$$

$$A_\alpha^3 = \begin{bmatrix} -\frac{1}{\tau_{thr}} & 0 & 0 & 0 & 0 & 0 & 0 & 0 & 0 & 0 \\ 0 & 0 & \frac{RT}{V} & -\frac{RT}{V} & 0 & 0 & 0 & 0 & 0 & 0 \\ NL_1(t) & 0 & 0 & 0 & 0 & 0 & 0 & 0 & 0 & 0 \\ 0 & NL_2(t) & 0 & 0 & 0 & 0 & 0 & 0 & 0 & 0 \\ 0 & 0 & 0 & 0 & 0 & 0 & 0 & 0 & 0 & 0 \\ 0 & 0 & 0 & 0 & 0 & -\dot{m}_M & 0 & 0 & 0 & 0 \\ 0 & 0 & 0 & 0 & 0 & 0 & 0 & 0 & 0 & 0 \\ 0 & 0 & 0 & 1 & 0 & 0 & 0 & 0 & 0 & 0 \\ 0 & 0 & 0 & 0 & NL_3(t) & 0 & 0 & 0 & 0 & 0 \\ 0 & 0 & 0 & 0 & 0 & 0 & 0 & 0 & NL_4(t) & 0 \end{bmatrix} \tag{2.3.5}$$

$$A_\alpha^4 = \begin{bmatrix} -\frac{1}{\tau_{thr}} & 0 & 0 & 0 & 0 & 0 & 0 & 0 & 0 & 0 \\ 0 & 0 & \frac{RT}{V} & -\frac{RT}{V} & 0 & 0 & 0 & 0 & 0 & 0 \\ NL_1(t) & 0 & 0 & 0 & 0 & 0 & 0 & 0 & 0 & 0 \\ 0 & NL_2(t) & 0 & 0 & 0 & 0 & 0 & 0 & 0 & 0 \\ 0 & 0 & 0 & 0 & -\dot{m}_M & 0 & 0 & 0 & 0 & 0 \\ 0 & 0 & 0 & 1 & 0 & 0 & 0 & 0 & 0 & 0 \\ 0 & 0 & 0 & 0 & 0 & 0 & 0 & 0 & 0 & 0 \\ 0 & 0 & 0 & 0 & 0 & 0 & 0 & 0 & 0 & 0 \\ 0 & 0 & 0 & 0 & 0 & 0 & NL_3(t) & 0 & 0 & 0 \\ 0 & 0 & 0 & 0 & 0 & 0 & 0 & 0 & NL_4(t) & 0 \end{bmatrix} \tag{2.3.6}$$

Where the first nonlinearity $NL_1(t)$ is depending on the throttle position $\alpha(t)$ according to the equation (2.2.3), the second nonlinearity $NL_2(t)$ is depending on the pressure $P(t)$ and the engine speed $n(t)$ in function of the equation (2.2.4), the third nonlinearity $NL_3(t)$ is the calculation of the torque depending on the amount of air inside the cylinder in the Expansion phase and the spark advance, as a combination of the expressions of $G_e(t)$ and $\eta(t)$ in equation (2.2.5). Finally, the fourth nonlinearity represents the expression of the rotational dynamics of the engine crankshaft expressed in (2.2.7). The input vector is then 1×1 with only the throttle command $u_{thr}(t)$ and the input matrices not depending on the period, such that:

$$B_\alpha^1 = B_\alpha^2 = B_\alpha^3 = B_\alpha^4 = \begin{bmatrix} \frac{1}{\tau_{thr}} & 0 & 0 & 0 & 0 & 0 & 0 & 0 & 0 & 0 \end{bmatrix}^T \tag{2.3.7}$$

3.1.2. Air-fuel ratio model

Since it is already in a suitable form, the state-space model of the air-fuel ratio control problem (denoted a_λ) can be obtained directly as a delayed-input system such that:

$$\dot{x}_\lambda(t) = A_\lambda \cdot x_\lambda(t) + B_\lambda \cdot u_\lambda\left(t-\delta(t)\right) \tag{2.3.8}$$

where the state is the normalized air-fuel ratio $x_\lambda(t) = \lambda(t)$, the state matrix $A_\lambda = -\frac{1}{\tau_\lambda}$, the delayed input such as $u_\lambda\left(t-\delta(t)\right) = \frac{1}{t_{inj}\left(t-\delta(t)\right) - t_0}$ where $t_{inj}(t)$ is the injection timing and $\delta(t)$ the variable transport delay implied by the exhaust manifold and the sensor location. Then, the input matrix is $B_\lambda = \frac{m_{air}\left(t-\delta(t)\right)}{\lambda_s K_{inj}}$. The main difficulty remains in the term $m_{air}\left(t-\delta(t)\right)$ which creates a non-measured nonlinearity with a time-varying delay in the input matrix.

3.2. Crank-angle domain

Now that the model has been written in a continuous-time state-space representation, it is in a suitable form to design a controller. However, since the electronic control unit (ECU) is running in discrete-time, the model-based controller should be working in discrete-time. Moreover, the cylinders of the engine are equipped with several sensors. For example, in the commercial engine of the test bench in the LAMIH, a sensor measures when the piston reaches a dead-center, i.e. when the crankshaft turns about 180 degrees. Another sensor is providing a pulse signal every six crankshaft degrees. Then, a particular discrete-time domain whose sampling period is depending on the crank angle may be considered. This crank-angle domain has been developed in the past (Hazell and Flower, 1971; Powell et al., 1987) and its use has been validated for engine control context (Yurkovich and Simpson, 1997).

This domain is based on the crankshaft angle $\theta(t)$. The first step to convert the continuous-time state-space representation into a crank-angle discrete-time model is to express the time derivate of the state vector in function of the crankshaft angle, such that:

$$\dot{x}(t) = \frac{dx(t)}{dt} = \frac{dx(t)}{d\theta(t)} \times \frac{d\theta(t)}{dt} = \frac{dx(t)}{d\theta(t)} \times \dot{\theta}(t) \tag{2.3.9}$$

In the case of the engine rotations, the time derivative of the crank angle $\dot{\theta}(t)$ can be expressed in function of the engine speed $n(t)$ in rpm such that $\dot{\theta}(t) = 6 \cdot n(t)$. Then, the derivative of the state $x(t)$ in function of $\theta(t)$ is:

$$\frac{dx(t)}{d\theta(t)} = \frac{\dot{x}(t)}{6 \cdot n(t)} \tag{2.3.10}$$

In order to convert the state-space from the continuous-time domain to the crank-angle domain, the transformation of Euler is used according to the crankshaft angle $\theta(t)$, such that:

$$\frac{x^\theta(k+1) - x^\theta(k)}{T_s^\theta} \simeq \frac{dx(t)}{d\theta(t)} \tag{2.3.11}$$

where $x^{\theta}(k)$ stands for the state vector expressed in the crank angle $\theta(t)$ domain at the k sample and T_s^{θ} the sampling period in crankshaft degrees, chosen to be small enough that no information is lost during the translation, i.e. the Euler's transformation is ideal. Concerning the engine application, and taking into account the sensor equipment of the engine test bench, the choice of the sampling period is made such that $T_s^{\theta} = 180°$, i.e. the model in the crank-angle domain is triggered whenever e dead center is reached. By combining (2.3.10) and (2.3.11), the conversion formula from a continuous-time state-space representation to the crank-angle domain defines the next sample of the discrete-time state vector $x^{\theta}(k+1)$ such that:

$$x^{\theta}(k+1) = x^{\theta}(k) + \frac{T_s^{\theta}}{6 \cdot n(k)} \frac{dx(k)}{dt} \tag{2.3.12}$$

Considering the equation (2.3.12), the state-space models (2.3.1) and (2.3.8) can be expressed in the crank-angle domain:

$$\begin{cases} x_{\alpha}^{\theta}(k+1) = A_{\alpha}^{\theta,p} \cdot x_{\alpha}^{\theta}(k) + B_{\alpha}^{\theta,p} \cdot u_{\alpha}^{\theta}(k) \\ x_{\lambda}^{\theta}(k+1) = A_{\lambda}^{\theta} \cdot x_{\lambda}^{\theta}(k) + B_{\lambda}^{\theta} \cdot u_{\lambda}^{\theta}\left(k - \Upsilon\left(\delta(k)\right)\right) \end{cases} \tag{2.3.13}$$

where $x_{\alpha}^{\theta}(k)$ and $x_{\lambda}^{\theta}(k)$ are respectively the state vectors of the idle speed control and the air-fuel ratio control expressed in the domain depending on the crankshaft angle $\theta(t)$. $\Upsilon\left(\delta(k)\right)$ is the function converting the variable transport delay $\delta(t)$ in the crank-angle domain; this function is detailed in Section 4 dedicated to the air-fuel ratio control.

The hybrid model of (Balluchi et al., 2010) considered for the idle speed control has been converted into a periodic state-space representation. The hybrid dynamics (combination of continuous-time dynamics triggered with discrete-time events) that represents the periodic behavior of the engine has been translated into the state and input matrices that are periodically variable. The model for the air-fuel ratio control has been written in the state-space form, so two continuous-time models have been obtained.

By considering the sensors equipping the commercial engines, mainly those inside the cylinders sending pulse signals according to crankshaft degrees, it is possible to write these two models in a suitable discrete-time domain depending on the crank angle. Based on the Euler's transformation in the crank angle domain, these models have been converted into this particular discrete-time domain whose sampling period is depending on the crankshaft degrees.

However, these new angular models are not ready yet for being used in controller design. As presented in Section 1, the main disadvantage of model-based controllers is the need of an accurate identification of the model parameters. Among the state vector, the torque produced by the cylinders is not measured, making the identification process difficult. A solution could be to implement an unknown input observer; however, computing model-based observers in real-time is costly for engine control units (ECU). Considering that the model is triggered in the crank angle

domain, would it be possible to express the unknown dynamics, such as the torque production, in function of measured values at different samples k ?

4. Model reduction for control

The air-fuel ratio model is already in a suitable form for controller design, so the constant parameters just need to be identified. Concerning the engine model for the idle speed control, several problems arise: the state vector is composed of 10 states, but thanks to the relations between the states, it is possible to reduce the size of the state vector, so the computational cost of the control law. Moreover, some dynamics, such as the torque production, are composed of non-measured values, so they have to be expressed in function of known values.

4.1. Pressure model

The dynamics of the intake manifold pressure in the crank-angle domain $P(k+1)$ is depending on the air mass flows leaving the throttle ($\dot{m}_{thr}(k)$) and entering into the cylinders ($\dot{m}_{cyl}(k)$). The dynamics of these air mass flows are modelled as polynomial expressions depending on the throttle position $\alpha(k)$ for $\dot{m}_{thr}(k+1)$ and the pressure $P(k)$ and the engine speed $n(k)$ for $\dot{m}_{cyl}(k+1)$. Then, it is possible to express the pressure dynamics $P(k+1)$ in function of $\alpha(k)$, $P(k)$ and $n(k)$, such that:

$$P(k+1)=P(k)+\frac{RTT_s^{\theta}}{6Vn(k)}\left(s_0+s_1\alpha(k)+s_2\alpha(k)^2-c_0-c_1P(k)-c_2n(k)-c_3P(k)n(k)\right) \tag{2.4.1}$$

The size of the state vector is reduced to 8 with:

$$x_{\alpha}^{\theta}(k)=\left[\alpha(k) \quad P(k) \quad m^1(k) \quad \cdots \quad m^4(k) \quad T_P(k) \quad n(k)\right]^T \tag{2.4.2}$$

4.2. Torque production model

As mentioned, the problem of the torque production dynamics is the lack of measures to identify the model of the produced torque, which depends on the air mass inside the cylinder according to equation (2.2.5). Since implementing an unknown input observer would be costly for the embedded controller, a solution has to be found using model transformations to express the torque production in function of measured values (Laurain et al., 2016a).

Considering one cylinder, the torque is produced during the Expansion phase. The torque is calculated as a product between a function depending on the air mass and a function depending on the spark, see equation (2.2.5). The amount of air during the Expansion phase is related to the air mass flow that was entering in the cylinder during the Intake phase. Then, the torque production during the Expansion phase could be expressed using values of the previous Intake phase. Since the model is triggered according to crank angle events, by considering a sampling period $T_s^{\theta}=180°$, the sample index k represents the current engine cycle while the sample $k-1$ represents the previous engine cycle. For example, the amount of air inside a cylinder is constant between the Expansion

phase (when the torque is produced) and the Compression phase. Considering the current engine cycle as the Expansion phase for the index k, it stands:

$$m_{air}(k) = m_{air}(k-1) \tag{2.4.3}$$

The amount of air inside the cylinder during the Compression phase is related to the air mass flow entering the cylinder during the Intake phase as depicted in Fig. 60.

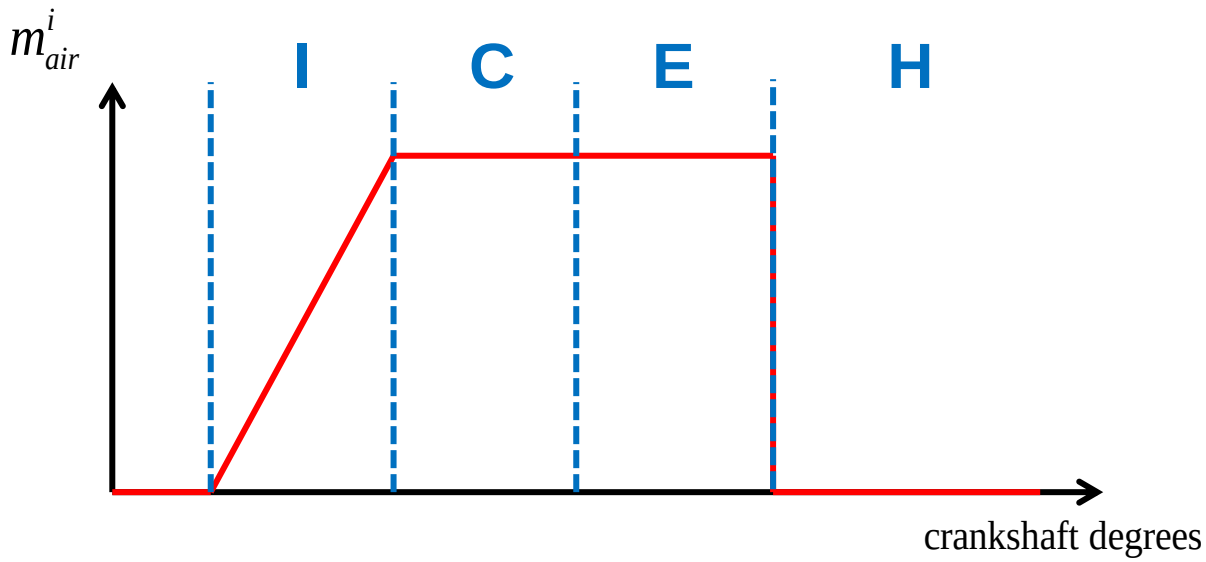

Fig. 60. Scheme of the air mass inside the i-th cylinder

Then, the air mass inside the cylinder at the end of the Intake phase can be expressed by the air mass flow and the duration of the Intake phase. This time is depending on the engine speed at that moment, such that:

$$m_{air}(k-2) = \dot{m}_{air}(k-2) \times \frac{60}{2 \cdot n(k-2)} \tag{2.4.4}$$

Thanks to this expression of the air mass inside the cylinder, it is possible to express the torque production in function of known values:

$$\begin{cases} T^{i}(k) = G_e(k) \cdot \eta(k) \\ G_e(k) = h_0 + \dfrac{30 h_1 \dot{m}_{air}(k-2)}{n(k-2)} + \dfrac{900 h_2 \dot{m}_{air}(k-2)^2}{n(k-2)^2} \\ \eta(k) = v_0 + v_1 \cdot \varphi^{i}(k) + v_2 \cdot \varphi^{i}(k)^2 + v_3 \cdot \varphi^{i}(k)^3 \end{cases} \tag{2.4.5}$$

Since the spark advance control is not considered in the design of the idle speed controller, the model is simplified by considering that the spark advance should be controlled to its optimal value such that $\eta(k) = 1$. Then, the torque production is only depending on the air path. It can be replaced in the engine speed dynamics so it only depends on measured values:

$$n(k+1)=n(k)+\frac{T_s^\theta}{6n(k)}\left(a_0 n(k)+b_0\left(T_P(k)-T_L(k)\right)+e_0\right) \tag{2.4.6}$$

For simplification purpose and since the idle speed controller has to be robust enough to handle external disturbances, the load torque $T_L(k)$ is removed from the design, assuming that it is known and measured since it is a torque demand from the starter after turning on an electronic device. Moreover, the torque production is considered equal to zero when there is no air inside the cylinder, so $h_0=1$. By combining (2.4.5) and (2.4.6) and considering all the assumptions, it stands:

$$n(k+1)=n(k)+\frac{T_s^\theta}{6n(k)}\left(a_0 n(k)+\frac{30h_1b_0\dot{m}_{air}(k-2)}{n(k-2)}+\frac{900h_2b_0\dot{m}_{air}(k-2)^2}{n(k-2)^2}+e_0\right) \tag{2.4.7}$$

For identification purpose, a change of variables is realized to avoid the product of constant parameters, so the final equation of the rotational dynamics of the engine is:

$$n(k+1)=n(k)+\frac{T_s^\theta}{6n(k)}\left(a_0 n(k)+\frac{30a_1\dot{m}_{air}(k-2)}{n(k-2)}+\frac{900a_2\dot{m}_{air}(k-2)^2}{n(k-2)^2}+e_0\right) \tag{2.4.8}$$

where $T_s^\theta=180$ crankshaft degrees so the index $k-2$ denotes two engine cycles before the considered k cycle. The air mass flow $\dot{m}_{air}(k-2)$ can be replaced by its expression according to equation (2.2.4) so the engine speed dynamics only depends on the engine speed and the pressure.

Considering the equation (2.4.8) making the connection between the engine speed and the air mass flow, it is possible to reduce the state vector as:

$$x_\alpha^\theta(k)=\left[n(k)^T \quad n(k-1)^T \quad n(k-2)^T \quad P(k-2)^T \quad \alpha(k-2)^T\right]^T \tag{2.4.9}$$

As one can see, by fixing the sampling period in function of the engine cycle, i.e. $T_s^\theta=180$, the model is no longer periodic since the torque production at the k moment is expressed through measured values during the $k-2$ phase. From a collection of 4 matrices of size 10×10, the state-space representation is now composed of a 5 states vector where the periodic behavior of the engine is integrated in the difference of samples in the crank angle domain. The full model can now be identified:

$$x_\alpha^\theta(k+1)=A_\alpha^\theta\cdot x_\alpha^\theta(k)+B_\alpha^\theta\cdot u_\alpha^\theta(k) \tag{2.4.10}$$

with $A_\alpha^\theta=\begin{bmatrix}1&0&0&NL_1(k)&0\\1&0&0&0&0\\0&1&0&0&0\\0&0&0&1+NL_2(k)&NL_3(k)\\0&0&0&0&-NL_4(k)\end{bmatrix}$ and $B_\alpha^\theta=\begin{bmatrix}0\\0\\0\\0\\NL_4(k)\end{bmatrix}$, where the nonlinearities are fully measured and stand for:

$$\begin{cases} NL_1(k) = \dfrac{T_s^\theta}{6P(k-2)n(k)}\left(a_0 n(k) + \dfrac{30a_1\dot{m}_{air}(k-2)}{n(k-2)} + \dfrac{900a_2\dot{m}_{air}(k-2)^2}{n(k-2)^2} + e_0\right) \\ NL_2(k) = \dfrac{-RTT_s^\theta}{6VP(k-2)n(k-2)}\left(-c_0 - c_1 P(k-2) - c_2 n(k-2) - c_3 P(k-2)n(k-2)\right) \\ NL_3(k) = \dfrac{RTT_s^\theta}{6V\alpha(k-2)n(k-2)}\left(s_0 + s_1\alpha(k-2) + s_2\alpha(k-2)^2\right) \\ NL_4(k) = \dfrac{T_s^\theta}{6\tau_{thr}n(k-2)} \end{cases} \quad (2.4.11)$$

5. Model identification

If the polynomial expressions used in the model of (Balluchi et al., 2010) can easily represent the nonlinear behavior of the engine, however they present the disadvantage of increasing the number of constant parameters that need to be identified. Engine model identification and validation have been in a spotlight during the last decade in the applied research domain. An ideal procedure for engine calibration has been developed in (Isermann and Sequenz, 2016). Optimization algorithms for parameters identification have been designed, such as data-driven methods (Haghani et al., 2016), extremum seeking (Tan et al., 2016) and horizon D-optimization approach (Toyoda and Shen, 2017).

For the identification of the models, datasets are used. These data come from the engine test bench located at the LAMIH (UMR CNRS 8201) in Valenciennes, France presented in Fig. 8. The test bed is composed of a D4FT 1.2L Renault engine working with gasoline. As already mentioned, it is equipped with the same sensors as a commercial car. The only exception is the programmable engine control unit (ECU) that is unlocked to allow implementing the controllers using a Matlab/Simulink interface and realized by the French company FH Electronics.

5.1. Idle speed model

In spite of the background in engine calibration recent research, classical methodologies (simplex, gradient descent, nonlinear least squares…) are used to perform the identification of the unknown parameters since the algorithms are already implemented in the Design Optimization toolbox of Simulink. A first dataset is considered with an idle speed reference set to $n_{ref} = 900rpm$ and the engine working at usual hot temperature $T > 75°C$. After convergence of several algorithms, the results of the identification process are presented in Fig. 61, where the blue solid line represents the measured data while the green dotted line depicts the simulation result with the identified constant parameters.

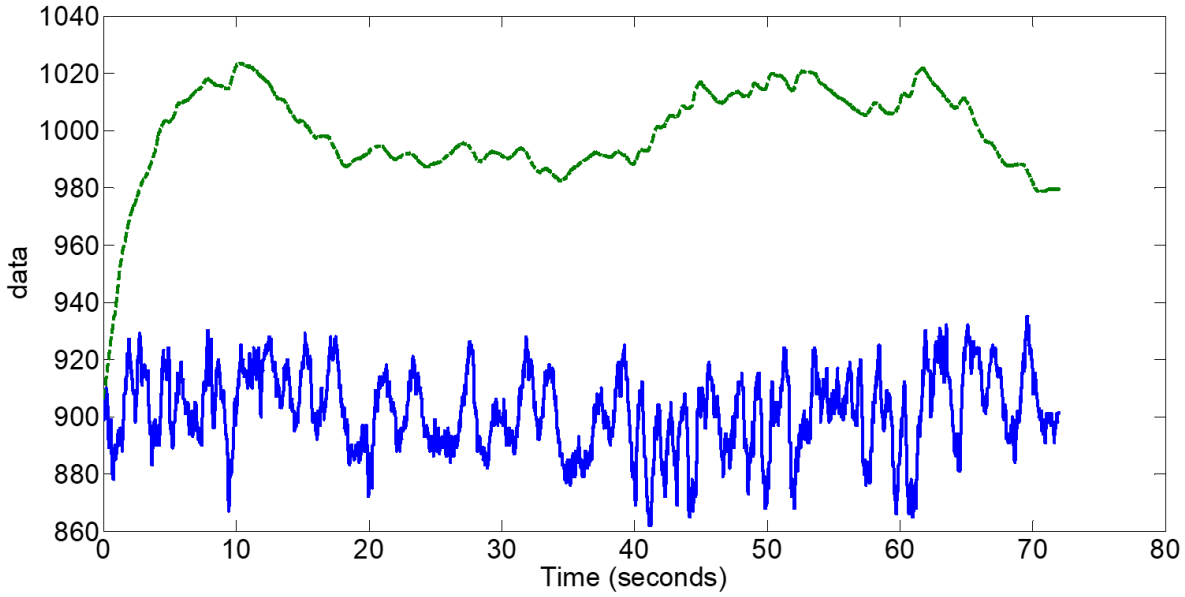

Fig. 61. Results of the first identification of the idle speed model

As one can see, the model is not able to catch all the dynamics of the engine test bench, so it needs to be improved.

5.1.1. Model improvements

A first improvement that can be realized is to replace the air mass flow $\dot{m}_{air}(k)$ by the throttle position $\alpha(k)$. Indeed, for a considered dataset and due to the nonlinear dynamics it involves, the air mass flow is measured with some noise that cannot be neglected. Then, changing it by the measure of the throttle position, whose sensor is more accurate, can reduce the noise. Fig. 62 and Fig. 63 present the measured values of the air mass flow and the throttle position for a considered dataset.

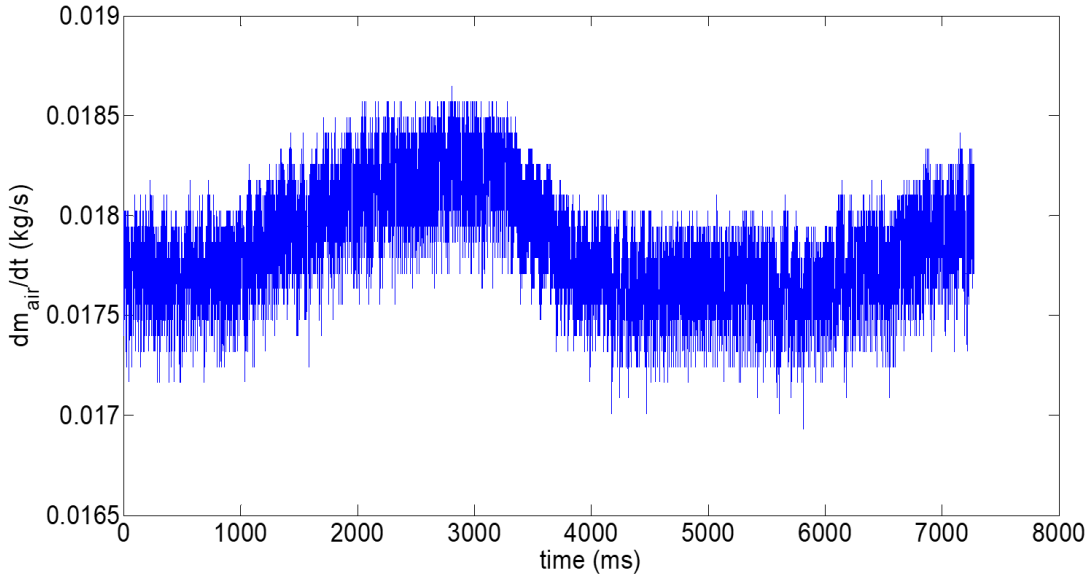

Fig. 62. Measure of the air mass flow from the engine test bench

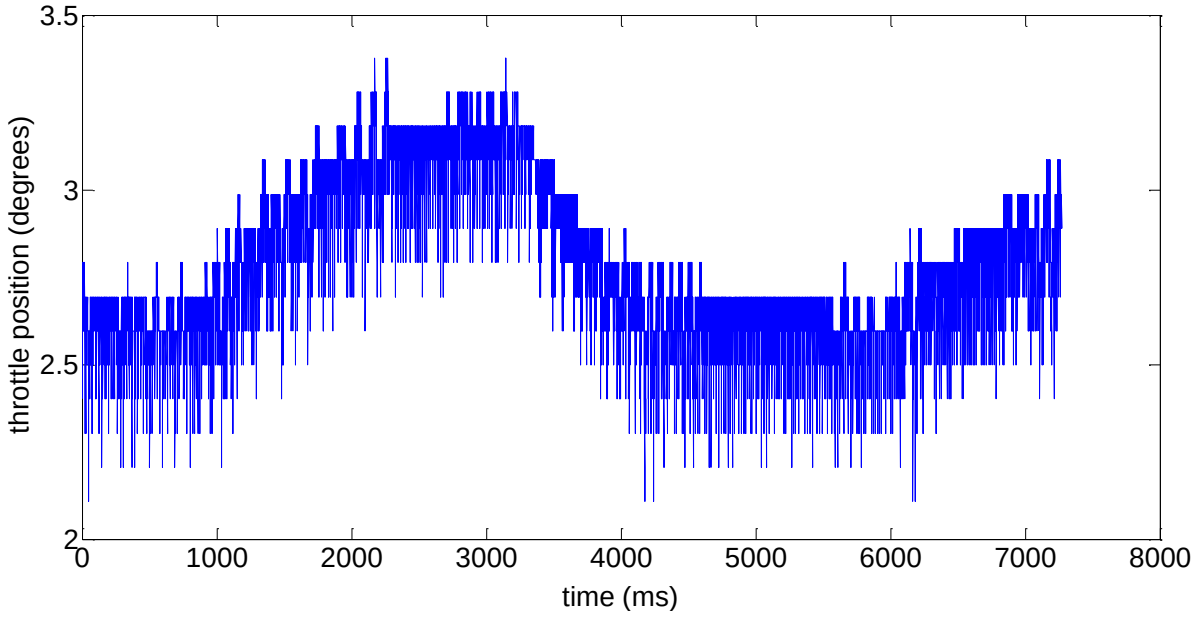

Fig. 63. Measure of the throttle position from the engine test bench

As one can see, the throttle position sensor is less noisy than the measurement of the air mass flow going through the intake manifold pressure, i.e. the amplitude of the variations around the mean value is less important in the Fig. 63. Moreover, in addition to the improvement of the measures, replacing the air mass flow by the throttle position can also reduce the number of states, since the pressure of the intake manifold is no longer necessary. Equation (2.4.8) is then changed to:

$$n(k+1)=n(k)+\frac{T_s^{\theta}}{6n(k)}\left(a_0 n(k)+\frac{30a_1\alpha(k-2)}{n(k-2)}+\frac{900a_2\alpha(k-2)^2}{n(k-2)^2}+e_0\right) \tag{2.5.1}$$

and the new state vector:

$$x_{\alpha}^{\theta}(k)=\left[n(k)\quad n(k-1)\quad n(k-2)\quad \alpha(k-2)\right]^T \tag{2.5.2}$$

However, this is not sufficient to get better results during the identification process. After investigating the datasets, it appears that the current implemented controllers (air-fuel ratio controller, spark advance controller) make the identification difficult. Indeed, these controllers are based on maps and they do not provide satisfying performances (air-fuel ratio far from the stoichiometric proportions, spark advance far from the optimal). Even if the two problems of air-fuel ratio control and idle speed control can be separately addressed, the connection between them needs to be taken into account during the identification process. First, the assumption that $\eta(k)=1$ for the spark advance needs to be reconsidered, so the product between the air and the spark should appear in the model, such that equation (2.5.1) becomes:

$$n(k+1)=n(k)+\frac{T_s^{\theta}}{6n(k)}\left(a_0 n(k)+a_1\cdot\phi(k-2)+a_2\cdot\phi(k-2)^2+e_0\right) \tag{2.5.3}$$

with $\phi(k)=\frac{30\cdot\alpha(k)\cdot\varphi(k)}{n(k)}$. Based on the recorded datasets from the engine test bench, the air-fuel ratio $\lambda(k)$ divides the produced torque during the Intake phase (moment where the fuel is injected in the cylinder), such that equation (2.5.3) becomes:

$$n(k+1)=n(k)+\frac{T_s^{\theta}}{6n(k)}\left(a_0 n(k)+\frac{a_1\cdot\phi(k-2)}{\lambda(k-2)}+\frac{a_2\cdot\phi(k-2)^2}{\lambda(k-2)}+e_0\right) \tag{2.5.4}$$

5.1.2. Identification and Validation

Now that the model has been improved, the constant parameters $\{\tau_{thr},a_0,a_1,a_2,e_0\}$ can be identified with the Parameter Estimation function of Simulink, considering an engine dataset with the speed around the idle speed reference with small amplitude variations, as displayed in Fig. 64.

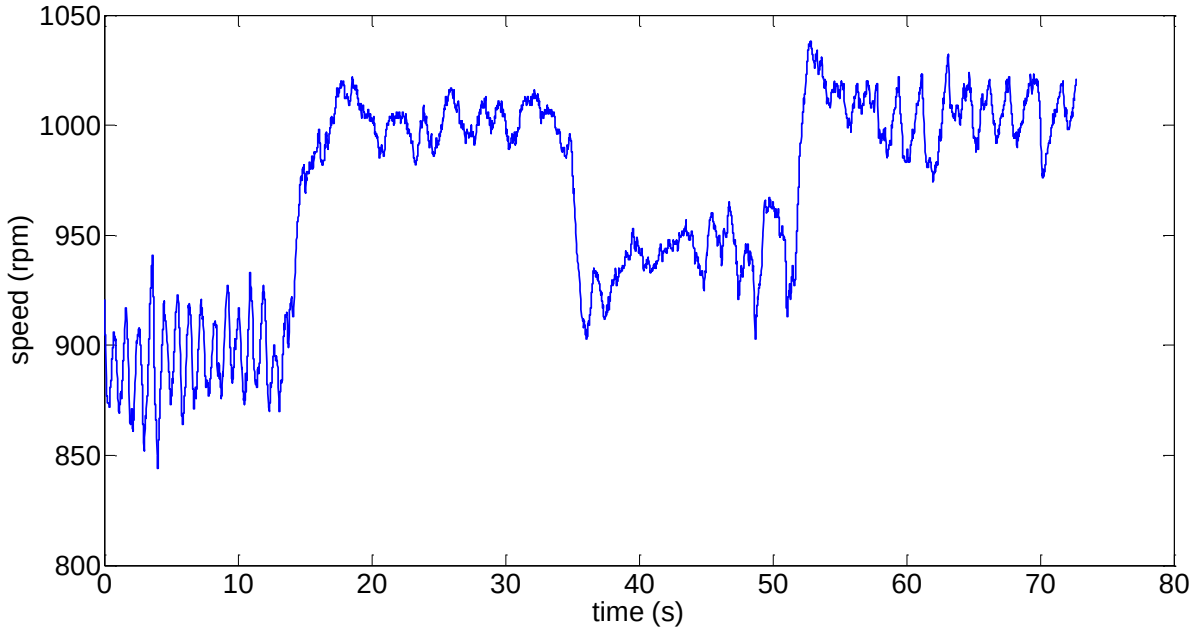

Fig. 64. Engine dataset used for the identification of the throttle model

The constant time of the throttle valve is obtained such that:

$$\tau_{thr}=0.021815 \tag{2.5.5}$$

Fig. 65 depicts the results of the identification process. As one can see, the simulated first-order model fits the experimental data.

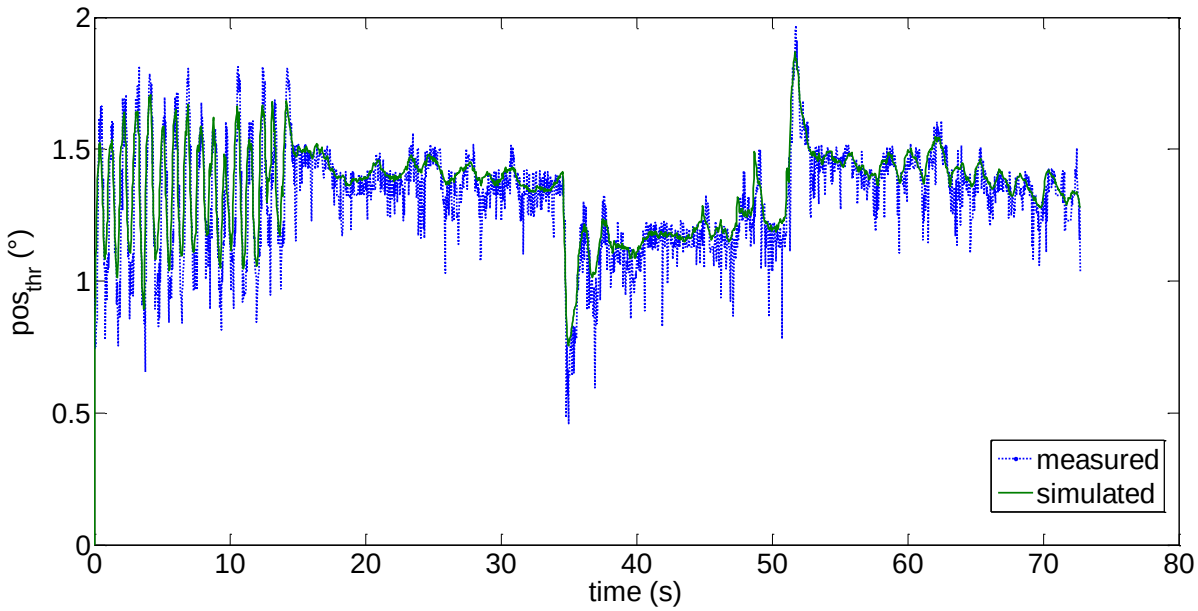

Fig. 65. Result of the identification process of the throttle position

Even if idle speed control is the main objective, the validation of the throttle model (2.2.1) is realized with an engine dataset with a changing speed in order to catch the transient dynamics, see Fig. 66. As one can see on Fig. 67, the model of the throttle (solid green) even fits the measured data (dotted blue) with a varying engine speed.

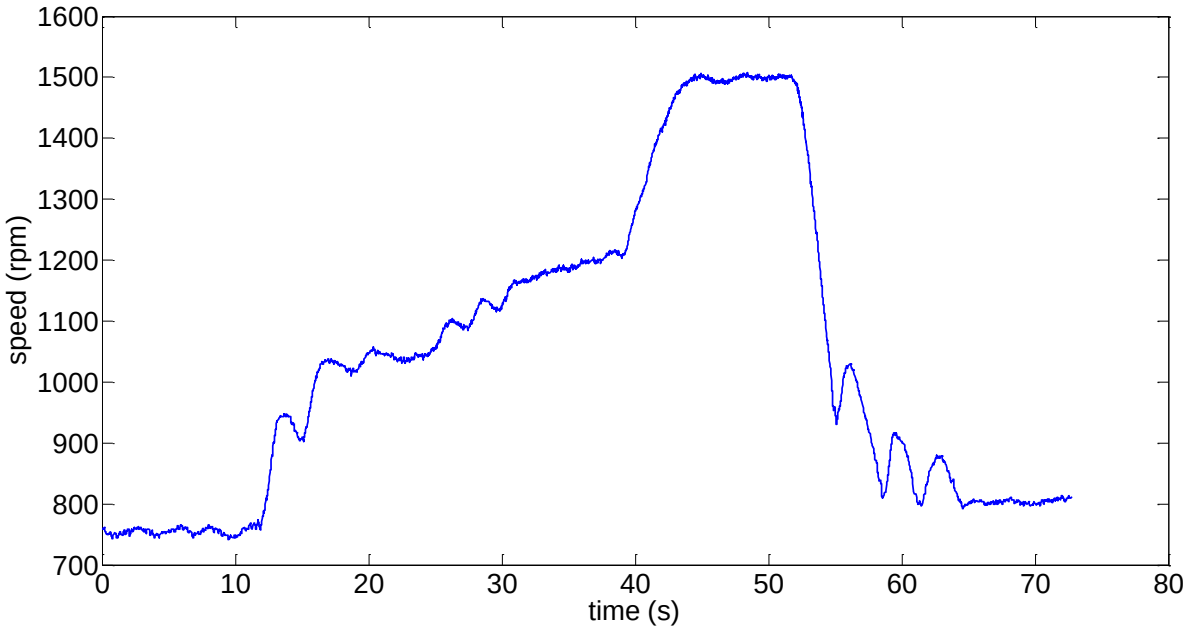

Fig. 66. Measured engine speed used for the validation of the throttle model

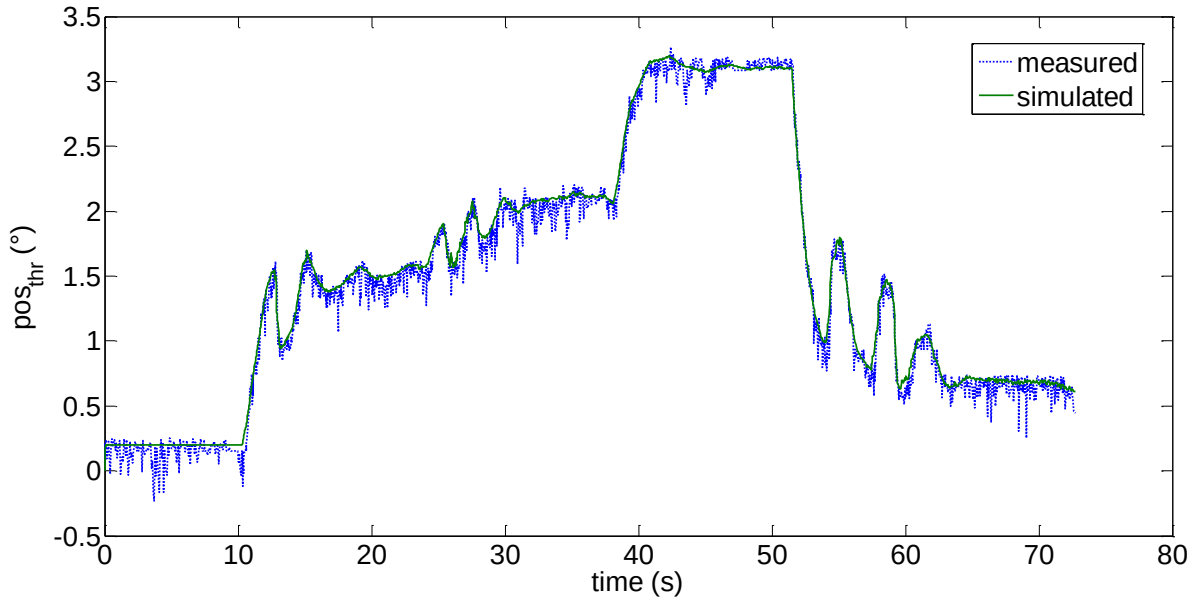

Fig. 67. Validation of the throttle model with a variable speed

Similarly, the rotational dynamics (2.5.4) has been identified with an engine dataset whose engine speed is variable in order to catch the transient behavior $\left(900rpm < n(t) < 3100rpm\right)$. Fig. 68 presents the results of the identification process, where the model in dotted green line fits with the measured data in solid blue line from the engine test bench.

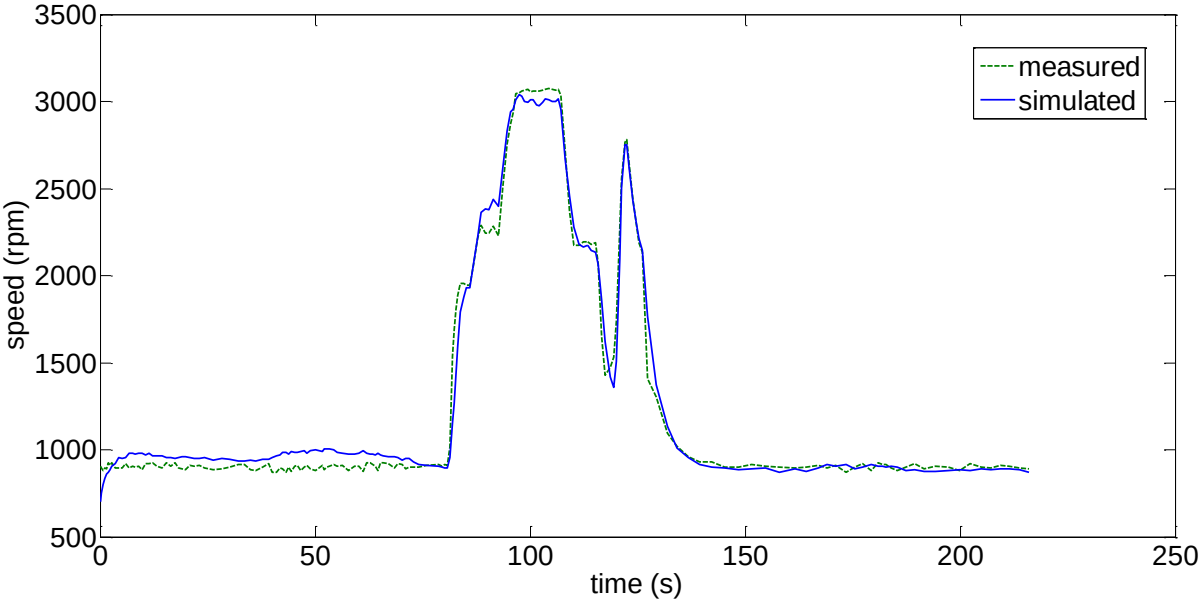

Fig. 68. Identification of the rotational dynamics model with variable engine speed

The parameters of the rotational dynamics model are identified such that:

$$\begin{aligned} a_0 &= -0.3432 \quad e_0 = 281.9019 \\ a_1 &= 39.9705 \quad a_2 = 340.9411 \end{aligned} \tag{2.5.6}$$

A validation using another engine dataset can be realized. Fig. 69 depicts the output of the model in blue solid line compared with the measured speed in dotted green. As one can see, even at idle speed, an identification error appears between the measured and the simulated signal. However, since the idle speed controller includes an integral action to solve the Challenge #1 of idle speed control (reference tracking and external disturbance rejection), the parametric uncertainties should be compensated by the integral action.

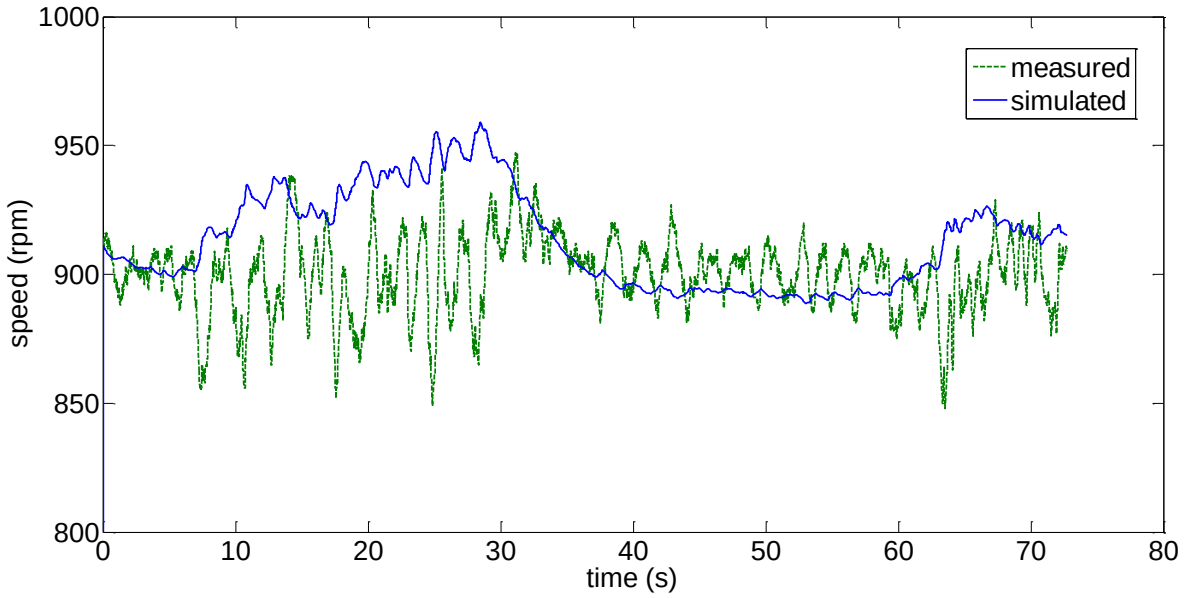

Fig. 69. Validation of the rotational dynamics model

Now that the model for idle speed control described by equations (2.2.1) and (2.5.4) has been identified and validated, see constant parameters (2.5.5), the model for air-fuel ratio control can be studied and identified.

5.2. Air-fuel ratio model

The air-fuel ratio model in the crank-angle domain includes three constant parameters that need to be identified: the injectors gain K_{inj}, the injectors dead-time t_0 and the sensor response time τ_λ, such that:

$$\lambda^\theta(k+1)=\lambda^\theta(k)+\frac{T_s^\theta}{6n(k)\tau_\lambda}\left(\frac{1}{\lambda_s}\times\frac{m_{air}\left(k-\Upsilon(\delta(k))\right)}{K_{inj}\left(t_{inj}\left(k-\Upsilon(\delta(k))\right)-t_0\right)}-\lambda(k)\right) \tag{2.5.7}$$

As already mentioned in the Introduction section, the main challenge for air-fuel ratio control is the time-varying delay $\delta(t)$. Since this delay is depending on the inverse of the speed, see equation (2.2.9), the delay is more important when the engine speed is low. That is why the air-fuel ratio control is first considered during the idle speed phase. One could say that the speed should be constant during the idle speed. However, staying close to the reference is highly depending on the implemented strategy, and for controllers with bad performances such as ones based on maps, the accuracy of the reference tracking may make the engine speed varying, even in idle speed context, as

depicted in Fig. 70 with the measured air-fuel ratio from the engine test bench with the current implemented map-based controller.

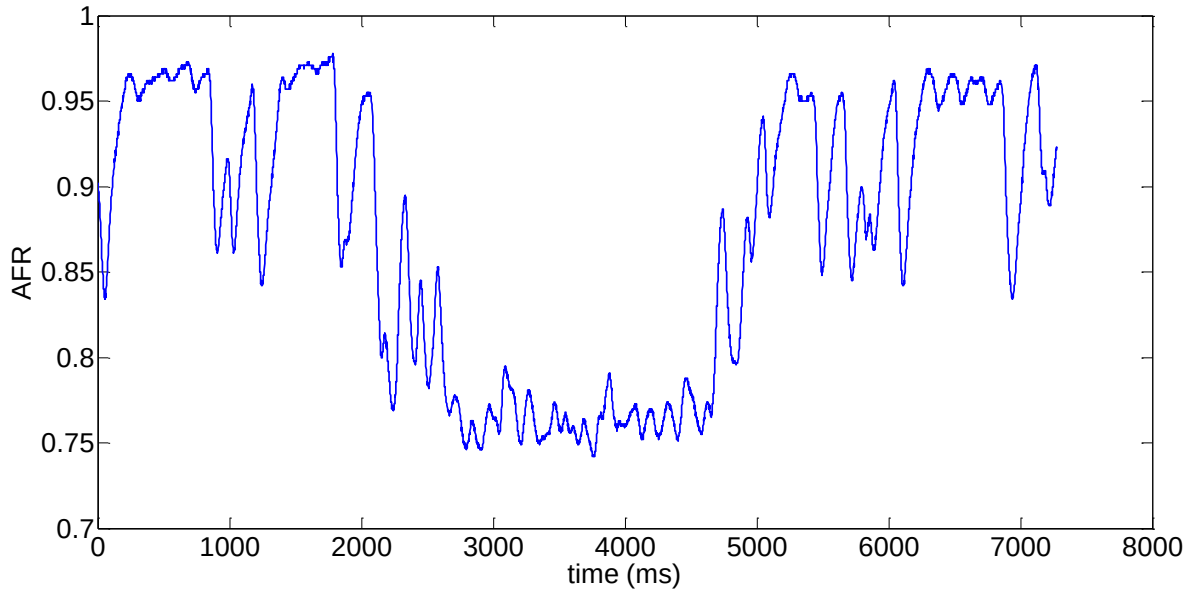

Fig. 70. Measured air-fuel ratio with the map-based idle speed controller

Moreover, due to the presence of external disturbances that may occur, the speed is frequently changing, so a static strategy cannot be considered. That is why identifying the crank-angle model (2.2.10) does not provide any good results since it does not depend on the engine speed.

5.2.1. Model improvements

The engine speed needs to be included in the air-fuel ratio model. After several trials, the engine speed was introduced through two polynomial expressions of second-order K_1 and K_2, such that:

$$\lambda^{\theta}(k+1)=\lambda^{\theta}(k)+\frac{T_s^{\theta}}{6n(k)\tau_{\lambda}}\left(\frac{K_1(n(k))}{\lambda_s K_{inj}}\times\frac{m_{air}(t-\Upsilon(\delta(k)))}{(t_{inj}(t-\Upsilon(\delta(k)))-t_0)}-K_2(n(k))\cdot\lambda(k)\right) \tag{2.5.8}$$

with $K_1(k)=b_0+b_1\cdot n(k)+b_2\cdot n(k)^2$ and $K_2(k)=c_0+c_1\cdot n(k)+c_2\cdot n(k)^2$

5.2.2. Identification and Validation

If using gains with polynomial expressions can catch the transient dynamics, it also increases the number of constant parameters to be identified. For a simple first-order plus dead time model as described in (2.5.8), 9 parameters have to be identified: $\{\tau_{\lambda},K_{inj},t_0,b_0,\ldots,b_2,c_0,\ldots,c_2\}$. Using the algorithms of the Design Optimization toolbox of Simulink, they have been identified with the following values:

$$\begin{array}{lll}\tau_{\lambda}=5.0519 & K_{inj}=0.2968 & t_0=-0.0028\\ b_0=-0.5291 & b_1=0.0029 & b_2=1.2509\cdot10^{-6}\\ c_0=-0.3104 & c_1=0.0018 & c_2=1.7733\cdot10^{-6}\end{array} \tag{2.5.9}$$

The model parameters (2.5.9) have been identified with an engine dataset whose conditions are idle speed $n(t) \simeq 900 rpm$ and hot temperature $T > 70°C$. As depicted in Fig. 71, the model (green) is only valid at idle speed conditions, even if the current implemented strategy (blue) has poor open-loop performances.

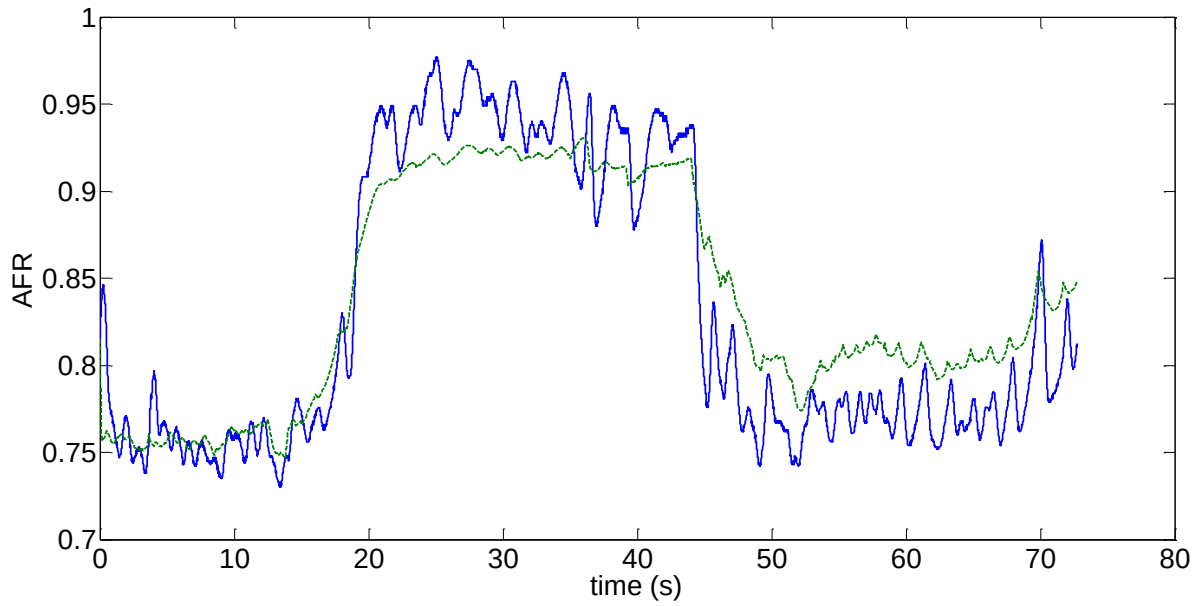

Fig. 71. Identification of the air-fuel ratio model at idle speed conditions

Since the model includes gains with polynomial expressions depending on the engine speed, it can handle the speed variations that appear in idle speed context. Moreover, thanks to these gains, the model (green) also fits the measured data (blue) with changing engine speed around nominal conditions $n(t) = 2000 rpm$, as presented in Fig. 72.

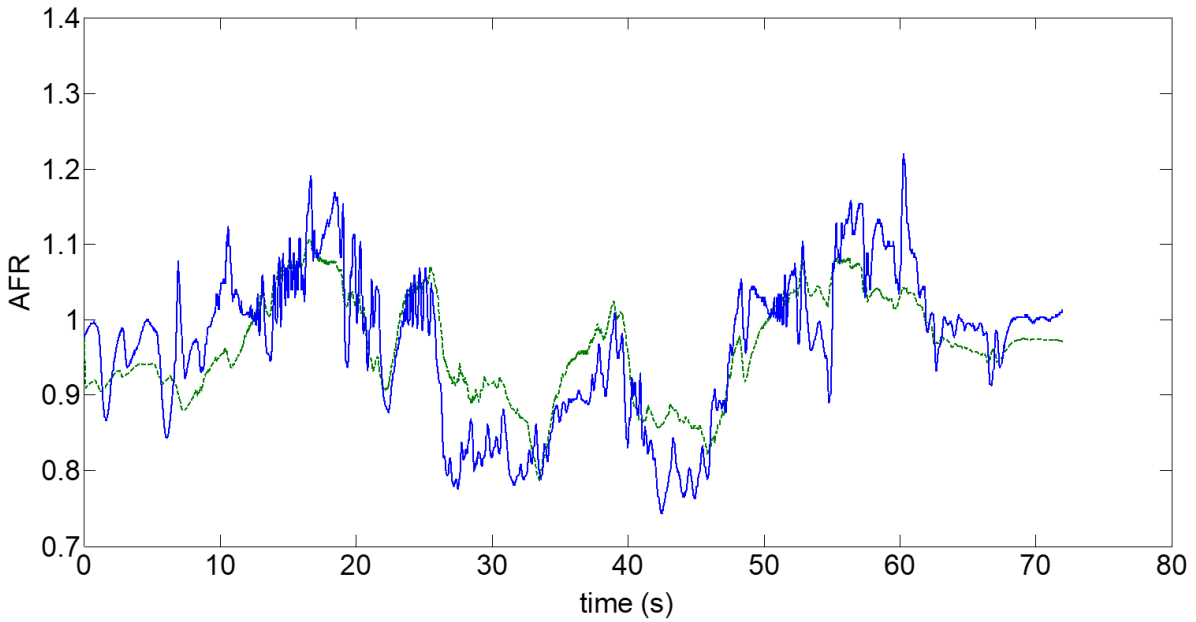

Fig. 72. Validation of the air-fuel ratio model in hot temperature and variable speed conditions

The model is now valid even if the engine speed varies as long as the engine temperature is hot. However, cold engine conditions are challenging since the chemistry of the combustion and the three-ways catalyst behavior is dependent on the temperature. That is why cold start engine control has been in a spotlight in the research community since the last decade (Manzie et al., 2009; Zhang et al., 2010; Keynejad and Manzie, 2011; Mozaffari and Azad, 2015). Fig. 73 presents the results of the air-fuel ratio model (green) validation with an engine dataset (blue) at idle speed and low temperature conditions $T \approx 30°C$. As one can see, the speed-dependent gains are not able to fit the measured data and an error occurs.

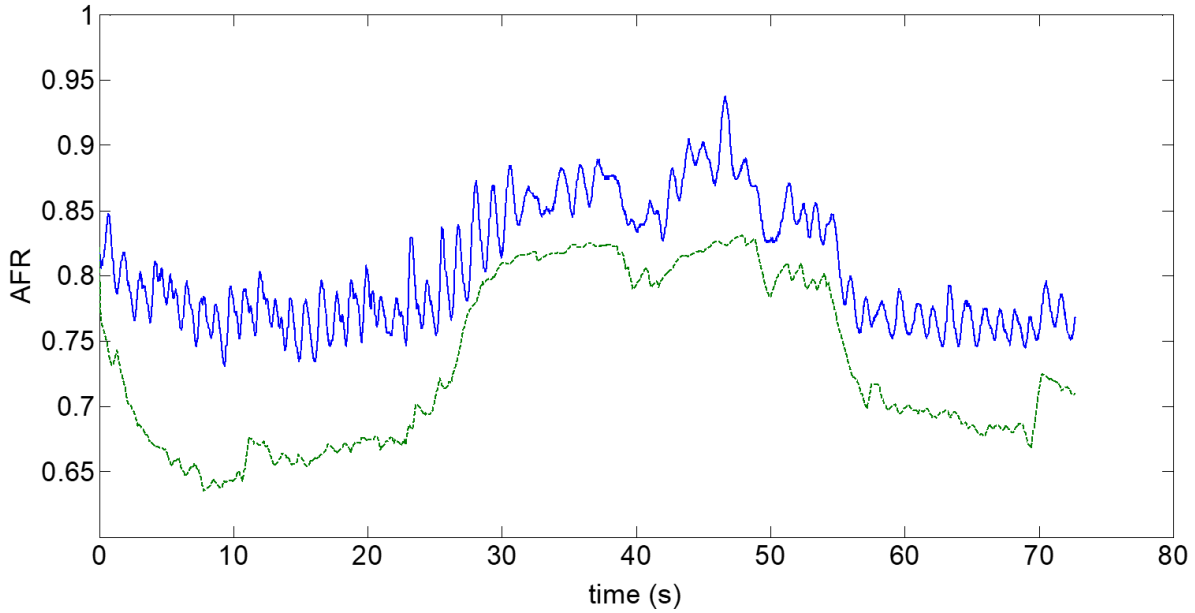

Fig. 73. Validation of the air-fuel ratio model at idle speed and cold conditions

Since cold start engine control is a very specific problem, it should be handled by another control module so it is not addressed here. That is why the model used for the air-fuel ratio controller design is the one described by equation (2.5.8) with the constant parameters (2.5.9).

The two models have been identified for idle speed control and air-fuel ratio control respectively, i.e. the constant parameters that are only depending on the engine equipment (response time of actuators and sensors for example) are now known. In order to fit the measured data, the models have been improved, mainly by including other measured values such as the engine speed, the air-fuel ratio and the spark advance. They can either be included directly or through gains with polynomial expressions. Since the output of the two models are matching the measured data from the engine bench sensors, they are accurate enough so model-based controllers can be designed.

However, by improving the models, nonlinearities have also been created in addition to the existing ones. The main challenge of engine control, i.e. dealing with such a complex and nonlinear system, still remains. In the past, nonlinearities have been deleted by linearizing, approximated by mapping or skipped by heuristic methodologies, but better performance should be obtained by taking into the nonlinearities during the controller design. How to obtain an exact representation of the nonlinear

system instead of linearizing or approximating with maps? How to deal with complex systems by including the nonlinear behavior in the design of the model-based controllers?

6. Dealing with nonlinearities

The main difficulty in engine control is to deal with nonlinearities. Indeed, once one decides to design a model-based controller, most of the engine models include nonlinearities. Moreover, using the transformation in the crank-angle domain (2.3.12) always implies at least one nonlinear term due to:

$$NL(k) = \frac{T_s^{\theta}}{6 \cdot n(k)} \tag{2.6.1}$$

whose variation is presented in Fig. 74.

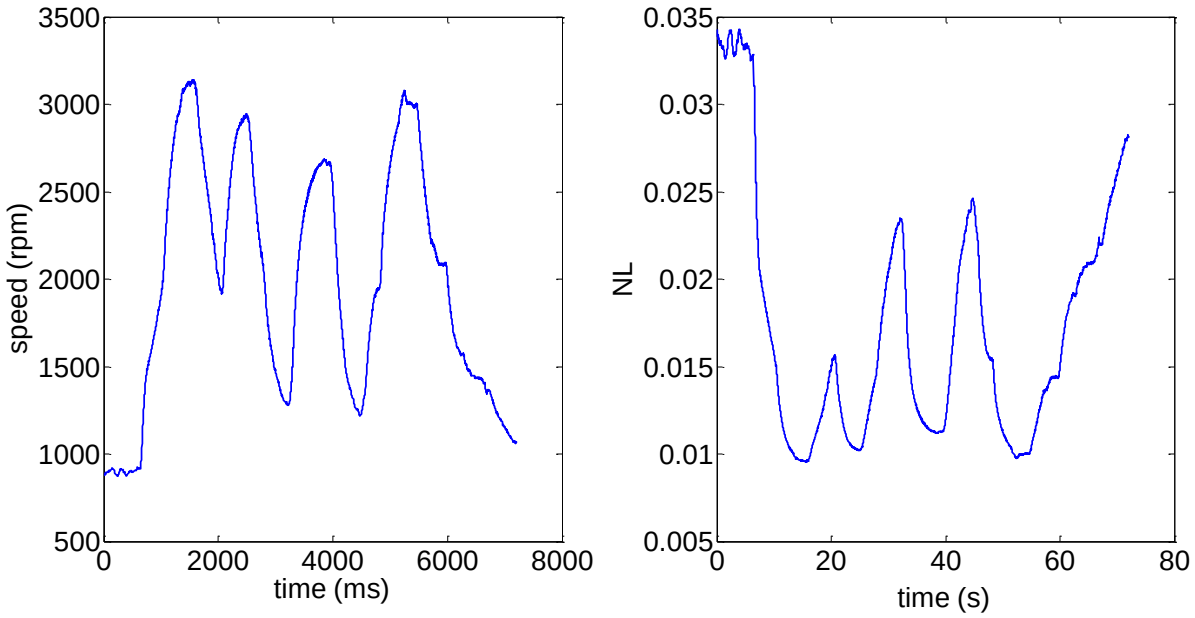

Fig. 74. Variation of the nonlinear term $NL(k)$ in function of the engine speed $n(k)$

That is why there is a need for theoretical tools that allows dealing with the nonlinearities instead of removing them with linearization or approximating them with static look-up tables.

6.1. General introduction to the Takagi-Sugeno representation

Among the available tools to deal with nonlinear systems, the choice has been made to use the Takagi-Sugeno modelling (TS) (Takagi and Sugeno, 1985). Indeed, TS models have the advantage of exactly representing the considered nonlinear system in a certain domain of validity. This domain of validity is a polytope whose vertices are composed of linear subsystems (based on the sector nonlinearity approach). Inside this domain, the nonlinear system is exactly represented by a combination of several linear subsystems triggered together with nonlinear functions called membership functions. These functions are coming from the fuzzy logic.

6.2. Application to the engine model

An example based on the engine model, considering nonlinear terms (2.6.1), illustrates the different steps of the methodology from the nonlinear system to the Takagi-Sugeno fuzzy model definition.

6.2.1. Methodology illustration

As mentioned, the engine models contain nonlinearities, moreover, the crank-angle domain transformation involves the nonlinear term (2.6.1). Considering as an example the throttle dynamics (2.2.1) written in the crank-angle domain:

$$\alpha^{\theta}(k+1)=\alpha^{\theta}(k)+\frac{T_s^{\theta}}{6\cdot n^{\theta}(k)}\left(\frac{u_{thr}^{\theta}(k)-\alpha^{\theta}(k)}{\tau_{thr}}\right) \tag{2.6.2}$$

with the sampling period previously defined as $T_s^{\theta}=180$. Notice that even with a simple first-order system like the throttle valve, the crank-angle transformation makes it nonlinear. The nonlinear state-space representation can be obtained as a quasi-LPV system:

$$x_{ex}^{\theta}(k+1)=A_{ex}^{\theta}(k)\cdot x_{ex}^{\theta}(k)+B_{ex}^{\theta}(k)\cdot u_{ex}^{\theta}(k) \tag{2.6.3}$$

where the sub-index x_{ex} stands for "example", $x_{ex}^{\theta}(k)=\alpha^{\theta}(k)$, $u_{ex}^{\theta}(k)=u_{thr}^{\theta}(k)$, $A_{ex}^{\theta}(k)=1-\frac{T_s^{\theta}}{6\cdot\tau_{thr}\cdot n^{\theta}(k)}=1-\frac{1}{\tau_{thr}}NL(k)$ and $B_{ex}^{\theta}=\frac{T_s^{\theta}}{6\cdot n^{\theta}(k)}=\frac{1}{\tau_{thr}}NL(k)$.

- First step: Defining the domain of validity

The first step of the methodology to get the TS model is to define the polytope, i.e. the domain of validity in which the TS model exactly represents the nonlinear system (2.6.2). As an application to the engine, the vertices of the polytope are related to physical and mechanical bounds of the system. For example, since the nonlinearity is depending on the engine speed $n(k)$, it is possible to define bounds in the idle speed context, such as $n(k)\in\left[n^m,n^M\right]$ where $n^m=600rpm$ and $n^M=1200rpm$. According to equation (2.6.1), the domain of validity can be created such that:

$$NL(k)\in\left[NL^m,NL^M\right] \tag{2.6.4}$$

where $NL^m=\frac{T_s^{\theta}}{6\cdot n^M(k)}=0.025$ and $NL^M=0.05$.

- Second step: Defining the collection of linear subsystems

As mentioned, the idea behind the TS modelling is to represent the nonlinear system (2.6.3) as a combination of several linear subsystems whose number r is related to the number of nonlinearities n_{NL} such that $r=2^{n_{NL}}$. In the considered example, since only one nonlinear term appears, 2 linear subsystems have to be defined such that:

$$\begin{cases} x_{ex}^{\theta}(k+1)=A_1^{\theta}\cdot x_{ex}^{\theta}(k)+B_1^{\theta}\cdot u_{ex}^{\theta}(k) \\ x_{ex}^{\theta}(k+1)=A_2^{\theta}\cdot x_{ex}^{\theta}(k)+B_2^{\theta}\cdot u_{ex}^{\theta}(k) \end{cases} \tag{2.6.5}$$

where the collection of subsystems is defined depending on the identified constant parameter τ_{thr} from (2.5.5) as:

$$\begin{cases} A_1^\theta = 1 - \dfrac{1}{\tau_{thr}} NL^m = -0.146; \quad B_1^\theta = \dfrac{1}{\tau_{thr}} NL^m = 1.146 \\ A_2^\theta = 1 - \dfrac{1}{\tau_{thr}} NL^M = -1.292; \quad B_2^\theta = \dfrac{1}{\tau_{thr}} NL^M = 2.292 \end{cases} \tag{2.6.6}$$

- Third step: Defining the membership functions

Now that the linear local models have been obtained, the membership functions $h_i\left(z(k)\right)$ need to be defined, where $z(k)$ is the premise variables vector, i.e., the vector containing the nonlinearities; in the considered example, since the presented system contains only one nonlinearity, $z(k) = NL(k)$. As already mentioned in section 3.1.1, this premise vector should be fully measured, even though some recent researches have been focusing on unmeasured nonlinearities. Based on this premise vector, it is possible to define the normalize premise functions $\omega_i(k)$ such that:

$$\begin{cases} \omega_1(k) = \dfrac{NL^M - NL(k)}{NL^M - NL^m} = \dfrac{0.05 - NL(k)}{0.025} \\ \omega_2(k) = 1 - \omega_1(k) \end{cases} \tag{2.6.7}$$

In this case with one nonlinear term, the membership functions $h_i\left(z(k)\right)$ are defined such that:

$$h_i\left(z(k)\right) = \omega_i(k), \; i \in \{1,2\} \tag{2.6.8}$$

These functions have the property of convex sums, i.e. $h_i\left(z(k)\right) > 0$ and $\sum_{i=1}^{2} h_i\left(z(k)\right) = 1$.

- Fourth step: Defining the Takagi-Sugeno model

Once the membership functions have been defined, the Takagi-Sugeno model is obtained by combining the linear local models with the nonlinear membership functions, such that:

$$x_{ex}^\theta(k+1) = \sum_{i=1}^{r} h_i\left(z(k)\right)\left(A_i^\theta \cdot x_{ex}^\theta(k) + B_i^\theta \cdot u_{ex}^\theta(k)\right) \tag{2.6.9}$$

- Notation

For simplification of the notation, the fuzzy matrix $\sum_{i=1}^{r} h_i\left(z(k)\right) A_i^\theta$ is written A_z^θ. Similarly, let us define B_z^θ such that the TS model (2.6.9) can be written:

$$x_{ex}^\theta(k+1) = A_z^\theta \cdot x_{ex}^\theta(k) + B_z^\theta \cdot u_{ex}^\theta(k) \tag{2.6.10}$$

6.2.2. Methodology validation

The Takagi-Sugeno model (2.6.10) is an exact representation of the considered nonlinear system (2.6.3). In order to validate the model, let us consider an engine dataset in idle speed conditions such as the engine speed is varying as depicted in Fig. 75. Fig. 76 displays the value taken by the nonlinear term $NL(k)$ and the membership functions $h_1(k)$ and $h_2(k)$. As one can see, the engine speed stays inside the domain of validity, i.e. $n(k) \in [600rpm, 1200rpm]$ and the sum of the membership functions is equal to 1.

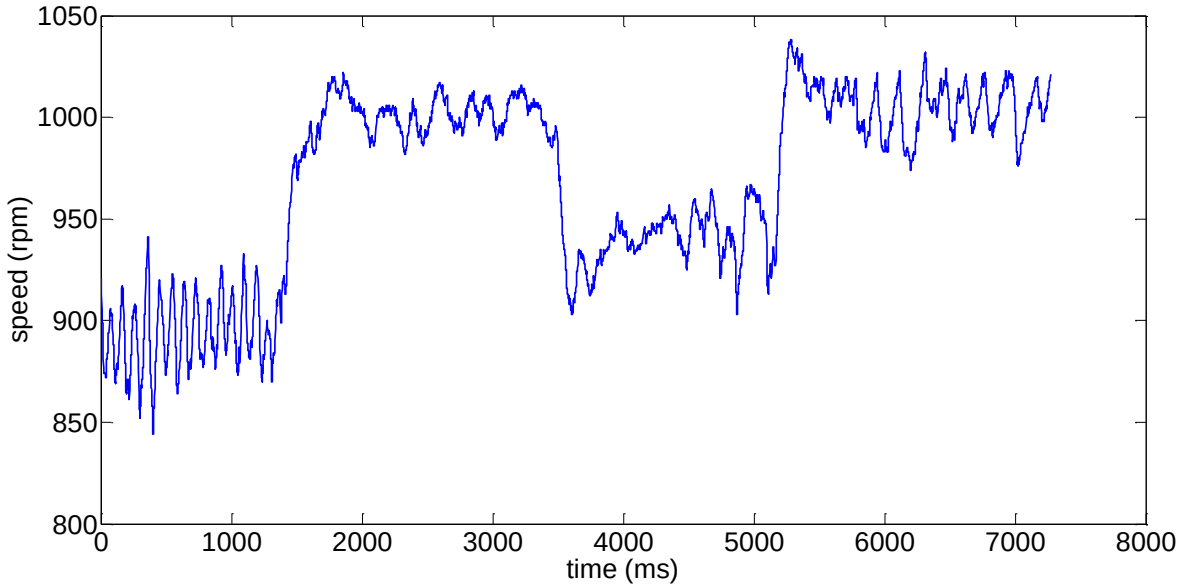

Fig. 75. Variations of the engine speed in the considered dataset from the test bench

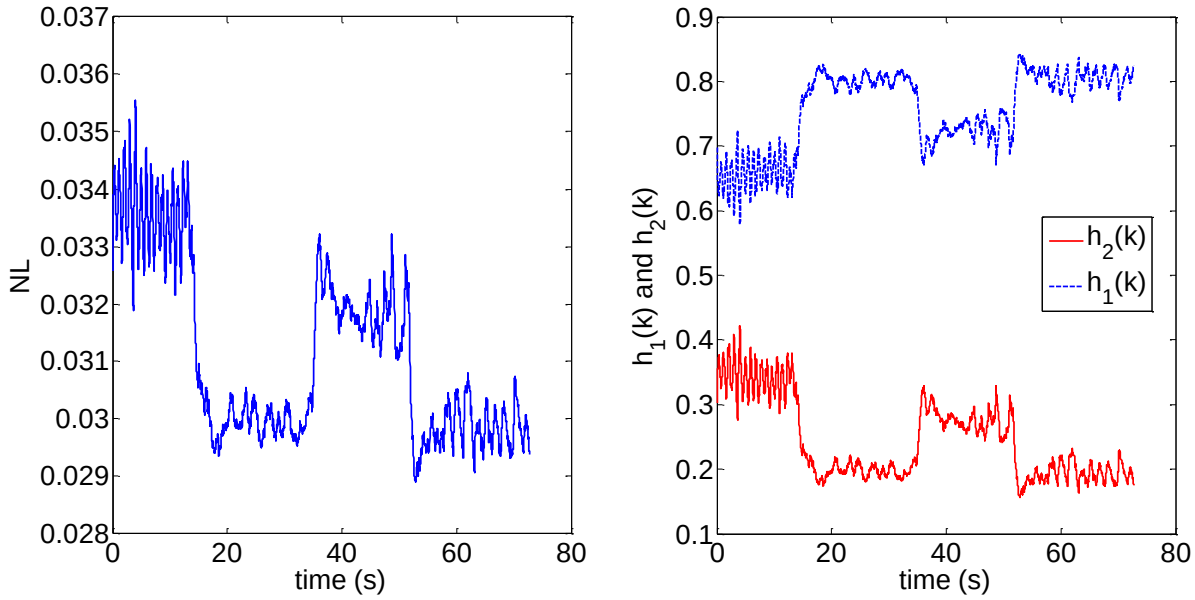

Fig. 76. Variations of the nonlinear term $NL(k)$ and the membership functions $h_i(z(k))$

The validation of the exactitude of the Takagi-Sugeno model of the throttle valve is presented in Fig. 77. The measured throttle position from the engine dataset recorded on the engine test bench is depicted in blue line (1). The output of the continuous-time model from equation (2.2.1) is depicted

in red line (2). The output of the throttle valve model described in the crank-angle domain is depicted in green line (3). The output of the TS model for the throttle valve (2.6.10) is depicted in magenta line (4). As one can see, (4) provides an exact representation of (3). The differences that may appear between (1), (2) and (4) are due to the parameter identification errors, see previous section 5.

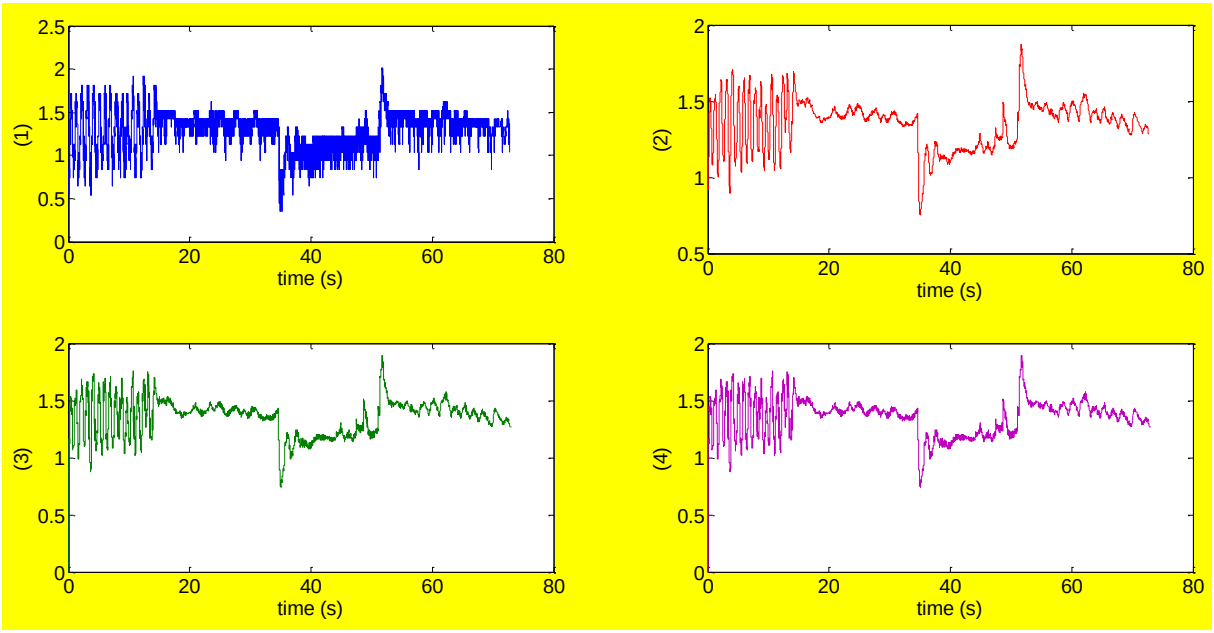

Fig. 77. (1) the throttle position in degrees from the engine dataset (blue); (2) the throttle position in degrees from the continuous model (red); (3) the throttle position in degrees from the crank-angle model (green); (4) the throttle position in degrees from the TS model (magenta)

6.2.3. Takagi-Sugeno engine models

The methodology developed with the example of the throttle valve model can be extended to the whole engine model, including the rotational dynamics and the air-fuel ratio model. Then, two TS models can be obtained from (2.3.13) in two particular domains Ω_α and Ω_λ such that:

$$\Omega_\alpha : \begin{cases} n(k) \in [750,1200] \\ \alpha(k) \in [1,15] \\ \varphi(k) \in [4,28] \\ \lambda(k) \in [0.7,1.2] \end{cases} \qquad \Omega_\lambda : \begin{cases} n(k) \in [660,3500] \\ \dot{m}_{air}(k) \in [0.0139,0.0278] \end{cases} \tag{2.6.11}$$

Then, the TS engine models can be written as:

$$\begin{cases} x_\alpha^\theta(k+1) = A_{\alpha,z}^\theta \cdot x_\alpha^\theta(k) + B_z^\theta \cdot u_\alpha^\theta(k) \\ x_\lambda^\theta(k+1) = A_{\lambda,z}^\theta \cdot x_\lambda^\theta(k) + B_{\lambda,z}^\theta \cdot u_\lambda^\theta\left(k - \Upsilon\left(\delta(k)\right)\right) \end{cases} \tag{2.6.12}$$

Where $x_\alpha^\theta(k) = \left[n(k) \quad n(k-1) \quad n(k-2) \quad \alpha(k-2) \right]^T$, $x_\lambda^\theta(k) = \lambda^\theta(k)$ and $\left\{ A_{\alpha,z}^\theta, B_{\alpha,z}^\theta, A_{\lambda,z}^\theta, B_{\lambda,z}^\theta \right\}$ stand for fuzzy matrices such as the definition of the notation (2.6.10). Considering the idle speed model, the TS exact representation stands in the domain (2.6.11) for:

$$A_{\alpha,z}^{\theta}=\begin{bmatrix} 1+a_0\cdot NL_3(k) & 0 & 0 & NL_1(k) \\ 1 & 0 & 0 & 0 \\ 0 & 1 & 0 & 0 \\ 0 & 0 & 0 & 1-\dfrac{NL_2(k)}{\tau_{thr}} \end{bmatrix}; B_{\alpha,z}^{\theta}=\begin{bmatrix} 0 \\ 0 \\ 0 \\ \dfrac{NL_2(k)}{\tau_{thr}} \end{bmatrix} \tag{2.6.13}$$

with the following nonlinearities:

$$\begin{cases} NL_1(k)=\dfrac{T_s^{\theta}}{6\cdot\alpha(k-2)\cdot n(k)}\left(\dfrac{a_1\cdot\phi(k-2)}{\lambda(k-2)}+\dfrac{a_2\cdot\phi(k-2)^2}{\lambda(k-2)}+e_0\right) \\ \phi(k)=\dfrac{30\cdot\alpha(k)\cdot\varphi(k)}{n(k)} \\ NL_2(k)=\dfrac{T_s^{\theta}}{6\cdot n(k-2)} \\ NL_3(k)=\dfrac{T_s^{\theta}}{6\cdot n(k)} \end{cases} \tag{2.6.14}$$

For the air-fuel ratio model (2.5.8), it is exactly represented by the following TS model in the domain (2.6.11):

$$A_{\lambda,z}^{\theta}=1-NL_4(k); B_{\lambda,z}^{\theta}=NL_5(k) \tag{2.6.15}$$

With the following nonlinearities:

$$\begin{cases} NL_4(k)=\dfrac{T_s^{\theta}\cdot K_2(k)}{6\cdot\tau_{\lambda}\cdot n(k)} \\ NL_5(k)=\dfrac{T_s^{\theta}\cdot K_1(k)\cdot\dot{m}_{air}(k)}{6\cdot\tau_{\lambda}\cdot\lambda_s\cdot K_{inj}\cdot n(k)} \end{cases} \tag{2.6.16}$$

Since the models developed for engine control contain nonlinearities, an approach taking into account the nonlinearities instead of removing them has been considered. Thanks to the sector nonlinearity approach, it is possible to obtain an exact TS representation for the two challenges of the engine control: idle speed control and air-fuel ratio control. This modelling process represents a nonlinear system by a combination of linear sub-systems weighted by membership functions in a polytope called domain of validity.

In term of TS fuzzy controller design, it allows extending the methodologies from the linear domain (state feedback and so on) to the fuzzy TS domain by taking into account the membership functions. Advanced control laws can be obtain by increasing the number of membership functions or by adding the inverse of fuzzy matrices (Guerra and Vermeiren, 2004). Due to the presence of these nonlinear membership functions along the controller design, how to obtain the gains of the controller? Moreover, the membership functions are computed in real-time and used in the controller, how to ensure the stability of the closed-loop system with a TS fuzzy controller? In the

particular case of the reference tracking in the engine, how to design a controller with an integral action? The first address problem is the idle speed control, what kind of fuzzy controller should be designed to control the throttle valve in order to regulate the engine speed with the challenges it implies?

CHAPTER III: Idle speed control

Every day, we change the world, but to change the world in a way that means anything, that takes more time than most people have. It never happens all at once. It's slow. It's methodical. It's exhausting.

Elliot (R. Malek) in *Mr.Robot (Season 1)*

1. Introduction

This chapter is dedicated to idle speed controller design. For their ability to represent each component of the engine separately, model-based controllers have been chosen. So a model for the idle speed has been developed, based on the hybrid dynamics of (Balluchi et al., 2010). It has been converted in a domain whose sampling period is depending on the crankshaft angle. The model has been reduced to be more suitable for the design of the controller. It stands a discrete state-space representation expressed in the crank-angle domain with four states and one control input, the throttle valve degrees $u_{thr}(k)$, such that:

$$x_\alpha^\theta(k+1) = A_{\alpha,z}^\theta \cdot x_\alpha^\theta(k) + B_z^\theta \cdot u_\alpha^\theta(k) \tag{3.1.1}$$

where $x_\alpha^\theta(k) = \left[n(k) \quad n(k-1) \quad n(k-2) \quad \alpha(k-2) \right]^T$ and

$$A_{\alpha,z}^\theta = \begin{bmatrix} 1+a_0 \cdot NL_3(k) & 0 & 0 & NL_1(k) \\ 1 & 0 & 0 & 0 \\ 0 & 1 & 0 & 0 \\ 0 & 0 & 0 & 1-\dfrac{NL_2(k)}{\tau_{thr}} \end{bmatrix}; B_{\alpha,z}^\theta = \begin{bmatrix} 0 \\ 0 \\ 0 \\ \dfrac{NL_2(k)}{\tau_{thr}} \end{bmatrix}$$

where

$$\begin{cases} NL_1(k) = \dfrac{T_s^\theta}{6 \cdot \alpha(k-2) \cdot n(k)} \left(\dfrac{a_1 \cdot \phi(k-2)}{\lambda(k-2)} + \dfrac{a_2 \cdot \phi(k-2)^2}{\lambda(k-2)} + e_0 \right) \\ \phi(k) = \dfrac{30 \cdot \alpha(k) \cdot \varphi(k)}{n(k)} \\ NL_2(k) = \dfrac{T_s^\theta}{6 \cdot n(k-2)}, NL_3(k) = \dfrac{T_s^\theta}{6 \cdot n(k)} \end{cases}$$

The nonlinearities remaining in the model has been dealt with the Takagi-Sugeno representation. As introduced, this methodology based on the sector nonlinearity approach can provide an exact model of the nonlinear system. Moreover, the idle speed controller can be designed based on the Takagi-Sugeno fuzzy tools.

Then, the originality of the proposed idle speed controller is, based on the model, triggered according to the sampling period T_s^θ considered as every 180 crankshaft degrees. It has the advantage of reducing the number of computation compared with fixed-time strategies. However, in case of low speed (as in idle context), the discrete control law will be applied with an important inter-sample time.

As mentioned, the idle speed controller has to follow the speed reference, so it has to include an integral action. Moreover, this action should be efficient enough to reject external disturbances that may occur when an electronic device is turned on and a torque is demanded from the starter.

Takagi-Sugeno (TS) fuzzy controller can handle these challenges for idle speed by including in their structure an integral action in addition to the membership functions to deal with the nonlinear behavior. How can the membership functions be included in the control design and how to prove the stability of the closed-loop system? Moreover, computing a fuzzy control law can be costly for the embedded control unit in the case of a model so much nonlinear that simple fuzzy controllers are not able to stabilize the closed-loop systems. What kind of fuzzy controllers can be considered for the complex problem of idle speed control? Since advanced and complex TS fuzzy controllers have to be investigated, they can be very costly for the embedded control unit, that is why an alternative controller is developed. How to ensure that this alternative controller has the same performance than the advanced TS controller but reducing the computational cost of the control law?

2. Introduction to the TS fuzzy controllers

2.1. PDC controllers

The idea behind Takagi-Sugeno (TS) fuzzy control is to use the tools available in linear control theory in the vertices of the polytope, i.e. the local linear sub-models, and to improve the control law by including the membership functions. Let us consider first the simplest controller in linear state space stabilization, the linear state feedback:

$$u(k) = -K \cdot x(k) \tag{3.2.1}$$

This control law is described in discrete-time, however, k can represent a sample in crank angle if such a domain is considered. Then, the state feedback can be improved to a TS fuzzy controller, the Parallel Distributed Compensation or PDC controller (Wang et al., 1996), by including the membership functions $h_i(z(k))$ where $z(k)$ stands for the premise vector as already defined in Chapter 2 Section 6. The PDC controller has been introduced by (Wang et al., 1996) and it is described as:

$$u(k) = -\sum_{i=1}^{r} h_i(z(k)) K_i \cdot x(k) \tag{3.2.2}$$

Or, considering the notation previously defined,

$$u(k) = -K_z \cdot x(k) \tag{3.2.3}$$

Then remains the question of how to get the gains K_i (composed of r matrices). Contrary to the linear state feedback where pole placement can be easily used, it does not work anymore in nonlinear context since the stability of each local model is not sufficient to guarantee the stability of the whole closed-loop system.

2.2. Stabilization and Lyapunov method

Instead of the traditional linear stability criteria (Routh/Nyquist for example), a more general technique to study the stability of a dynamical closed-loop system, linear or nonlinear, can be considered. One of them is the Lyapunov direct method, developed at the beginning of the twentieth century.

A dynamical system is stable in the sense of Lyapunov if there exists a function that verifies being decreasing. Then, it can be seen as an energy function and its decrease ensures that the system converges to a stable state. An example of a Lyapunov function $V(k)$ is the quadratic one, defined as:

$$V(k) = x(k)^T \cdot P \cdot x(k) \tag{3.2.4}$$

where $x(k)$ is the state vector of the state-space representation and P a symmetric definite positive the Lyapunov matrix of the same size of the state matrices A_i. Note that the Lyapunov function can be more complex (non-quadratic Lyapunov functions), for example, as presented in (Guerra and Vermeiren, 2004), a Lyapunov matrix depending on the membership function, i.e. $V(k) = x(k)^T \cdot P_z \cdot x(k)$. Then, the decrease of the Lyapunov function $V(k)$ in the special discrete-time domain depending on the crankshaft angle is defined as:

$$\Delta V = V(k+1) - V(k) < 0 \tag{3.2.5}$$

By replacing the terms in equation (3.2.5) by the expression of the Lyapunov function (3.2.4), $x(k+1)$ appears and can be replaced by its expression according to the state-space description $A_z x(k) + B_z u(k)$, introducing in the stability analysis the system with matrices A_z and B_z.

The difference between $V(k)$ and $V(k+1)$, separated by one sample in crank-angle domain according to $T_s^\theta = 180$. The equations can be rewritten such that equation (3.2.5) stands for:

$$X^T Q X < 0 \tag{3.2.6}$$

and the state-space representation (3.1.1) can be written:

$$RX = 0 \tag{3.2.7}$$

Then, it is possible to apply the Finsler lemma (De Oliveira and Skelton, 2001). Then, (3.2.5) is verified if there exist a matrix M such as:

$$MR + (*) + Q < 0 \tag{3.2.8}$$

From this inequality and depending on the choice of the matrix M, the goal is then to formulate as a Linear Matrix Inequality (LMI) problem as defined in (Boyd et al., 1994). To this aim, the membership functions must be removed from the conditions by using for example relaxations, such as (Tanaka et al., 1998; Tuan et al., 2001). The LMI problem can be treated by solvers like LMI Toolbox of Matlab. The gains of the controller that ensure the stability of the closed-loop system can be obtained.

Remark (Source of conservativeness): Several sources of conservativeness appear during the design of TS fuzzy controllers. The first one concerns the choice of the Takagi-Sugeno model, because it is not unique, different LMI problems can be obtained with different domain of solutions. From the application point of view, a small domain of validity means that the controller can only stabilize the engine in a very small range of engine speed, and a torque demand from the starter too large can make the system leave the domain of validity, so the stability of the closed-loop system is not ensured anymore. Note that the system can be stable outside of the domain of validity, but it is not proved with the chosen Lyapunov function.

The second source of conservativeness is the choice of the candidate Lyapunov function. The most commonly used is the quadratic Lyapunov function (Wang et al., 1996). As already mentioned, if the problem is unfeasible with this kind of function more complex one can be defined such as non-quadratic one, as studied in (Guerra and Vermeiren, 2004).

The third source of conservativeness relies on the relaxations to remove the membership functions in order to obtain the LMI conditions. During this transformation, sufficient conditions are derived from necessary and sufficient one. Several relaxations exit in the literature from obvious one (Tanaka and Sano, 1994) to more complex (Mozelli et al., 2009) with the possibility to add slack variables (Teixeira et al., 2003).

The last source of conservativeness is the choice of the controller structure. Instead of the PDC controller (3.2.3), it is possible to introduce the membership functions in the control law with several combinations, called non-PDC controllers. They can obtain better performance. One of the possible combination is to increase the number of membership functions (multi-sums fuzzy matrices):

$$u(k) = -K_{zz\ldots z} \cdot x(k) \tag{3.2.9}$$

Another option, among others, is to invert a fuzzy matrix, as introduced in (Guerra and Vermeiren, 2004):

$$u(k) = -K_z \cdot H_z^{-1} \cdot x(k) \tag{3.2.10}$$

This controller with fuzzy matrix inverse (CFMI) has been largely used in the control theory, for relaxing the conditions obtained in (Guerra and Vermeiren, 2004) in both continuous and discrete time domains (Ding et al., 2006; Guerra et al., 2012a; Lendek et al., 2015). The CFMI has been implemented for stabilization of a continuous-time system in (Lam and Leung, 2007) or as an output feedback in (Bouarar et al., 2009). The impact of noise on a PDC and non-PDC has been studied in (Chang et al., 2012). By increasing the number of gains, more relaxed results can be obtained while solving the LMI problem, as proved in (Xie et al., 2013). However, the use of a real-time matrix inversion could be costly for an embedded computer.

Considering an embedded ECU, a controller design procedure would be to develop LMI conditions first for a PDC controller, and if the domain of solutions is not satisfying, considering a non-PDC controller. In the case of the idle speed controller design, the domain of validity of the TS model is a crucial point since we want to reject external disturbances that may increase or decrease the engine speed, so the domain has to be large enough to contain these several cases. If the PDC controller

does not provide satisfying results, a non-PDC controller should be considered, even if the complexity of the controller structure implies an increase of the computational cost. Now that the model for the idle speed controller is defined in Section 2 and the TS fuzzy control law structure has been introduced, a TS fuzzy idle speed controller can be designed.

3. Application to the idle speed control

3.1. Complexity and uncertainties

The complexity of a control law stands for the number of basic operations realized at every sampling period. By basic operations, one must understand addition and multiplication. Since the Electronic Control Unit has limited performance, it is crucial to assess the computational cost of the control laws. Table 4 presents some examples of complex operations that may be involved in the controllers based on basic operations. M stands for any square matrix of size n_M, N for a matrix of size $n_N \times 1$, x represents a vector such as the state vector, of size $1 \times n_M$, s is a scalar and r is the number of local models

Table 4. Examples of complex operations combining several basic operations

$s \cdot M$	$C = n \cdot n$
$M \cdot x$	$C = \left(n + \left(n-1\right)\right) \cdot n$
$M \cdot N$	$C = \left(n + \left(n-1\right)\right) \cdot n \cdot n$
$M_z = \sum_{i=1}^{r} h_i\left(k\right) \cdot M_i$	$C = r \cdot n \cdot n + r - 1$
M_{zz}	$C = r \cdot r \cdot \left(n \cdot n + 1\right) + r \cdot r - 1$
$M_{z\ldots z}, \quad \vartheta sums$	$C = r^{\vartheta} \cdot \left(n^2 + \left(\vartheta - 1\right)\right) + r^{\vartheta} - 1$

According to the definition of the PDC controller (3.2.3), it is composed of a combination of linear gains triggered with the same membership functions as the TS model. The complexity of the PDC control law can be calculated in function of the mathematical operations involved. Based on Table 4, the complexity is equal to:

$$C_{PDC} = r \cdot {n_M}^2 + r - 1 + 2 \cdot {n_M}^2 + n_M\left(n_M - 1\right) \tag{3.3.1}$$

where r stands for the number of local models (8 for the idle speed model) and n_M the size of the state matrix (4 with the considered model). The complexity of the control law, 179 operations, can be minimized by either reducing the length of the state vector such as presented in Section 2 or reducing the number of local models. Indeed, the TS model (3.1.1) is composed of three nonlinearities. However, $NL_2\left(k\right)$ and $NL_3\left(k\right)$ are very similar since the only difference is the sampling period at which the engine speed $n\left(k\right)$ is considered:

$$NL_2(k)=\frac{T_s^\theta}{6\cdot n(k-2)},\quad NL_3(k)=\frac{T_s^\theta}{6\cdot n(k)} \tag{3.3.2}$$

Then, a possibility to limit the number of local models is to express both nonlinearities $NL_3(k)$ and $NL_2(k)$ in the same way introducing an uncertainty Δ such as:

$$n(k)=\frac{1}{1+\Delta}n(k-2) \tag{3.3.3}$$

where the uncertainty Δ is bounded by Δ_M such that $|\Delta|<\Delta_M$. The model (3.1.1) can be written as:

$$x_\alpha^\theta(k+1)=\sum_{i=1}^{r}h_i(k)\left(\left(A_{\alpha,i}^\theta+\Delta A_i\right)x_\alpha^\theta+B_iu_\alpha^\theta\right) \tag{3.3.4}$$

where the state and input matrices are:

$$A_{\alpha,z}^\theta=\begin{bmatrix}1+a_0\cdot NL_2(k) & 0 & 0 & NL_1(k)\\ 0 & 1 & 0 & 0\\ 0 & 0 & 1 & 0\\ 0 & 0 & 0 & 1-\dfrac{NL_2(k)}{\tau_{thr}}\end{bmatrix};B_{\alpha,z}^\theta=\begin{bmatrix}0\\0\\0\\\dfrac{NL_2(k)}{\tau_{thr}}\end{bmatrix} \tag{3.3.5}$$

and the fuzzy matrix of uncertainties stands for:

$$\sum_{i=1}^{r}h_i(k)\Delta A_i=\sum_{i=1}^{r}h_i(k)Ha_i\partial(k)E_a \tag{3.3.6}$$

The bound of the uncertainty appears in the E_a matrix: $E_a=\begin{bmatrix}\Delta_M & 0 & 0 & 0\end{bmatrix}$ while the nonlinearity is included in the fuzzy matrix Ha_z such that $\sum_{i=1}^{r}h_i(k)Ha_i=\begin{bmatrix}a_0NL_2(k) & 0 & 0 & 0\end{bmatrix}^T$. The varying term $\partial(k)$ represents the uncertainty and verifies the following property: $\partial(k)^T\partial(k)\le I$.

Then, thanks to the uncertainty description, the number of nonlinearities can be reduced from 3 to 2, reducing the number of local models from 8 to 4, so the complexity of the PDC control law (from 179 to 111 operations).

3.2. Integral action

In order to achieve the challenge of set-point tracking and external disturbance rejection, an integral action needs is designed. The error $e_\alpha^\theta(k)$ is defined such that:

$$e_\alpha^\theta(k)=y_{\alpha,ref}-y_\alpha^\theta(k)=y_{\alpha,ref}-C_\alpha^\theta\cdot x_\alpha^\theta(k) \tag{3.3.7}$$

With $C_\alpha^\theta = \frac{T_s^\theta}{6 \cdot n(k)} \cdot [1 \quad 0 \quad 0 \quad 0]$. The state vector can be augmented as $\bar{x}_\alpha^\theta(k) = \begin{bmatrix} x_\alpha^\theta(k) \\ e_\alpha^\theta(k) \end{bmatrix}$. The notation $\bar{a}$ denotes an augmented state or an augmented matrix for the rest of the manuscript. Then, the new fuzzy state and input matrices can be defined as:

$$\bar{A}_{\alpha,z}^\theta = \begin{bmatrix} A_{\alpha,z}^\theta & 0 \\ -C_\alpha^\theta & 1 \end{bmatrix}, \Delta\bar{A}_z = \begin{bmatrix} \Delta A_z & 0 \\ 0 & 0 \end{bmatrix}, \bar{B}_{\alpha,z}^\theta = \begin{bmatrix} B_{\alpha,z}^\theta \\ 0 \end{bmatrix} \tag{3.3.8}$$

State feedback controllers, either fuzzy or not, can be designed using the new augmented state vector $\bar{x}_\alpha^\theta(k)$.

3.3. Fuzzy controllers

3.3.1. PDC controller

Considering a PDC controller, i.e. a fuzzy state feedback such as the one described in (3.2.3) with the corresponding indexes, it is possible to use the direct Lyapunov method to study the stability of the whole closed-loop system. The choice of the candidate Lyapunov function is a non-quadratic such as defined in (Guerra and Vermeiren, 2004) so the domain is larger than the one obtained using a quadratic function:

$$V_\alpha(k) = \bar{x}_\alpha^\theta(k)^T \cdot P_z \cdot \bar{x}_\alpha^\theta(k) \tag{3.3.9}$$

where P_z stands for the fuzzy matrix, i.e. $\sum_{i=1}^{r} h_i(k) P_i$. The direct Lyapunov method for discrete-time systems can be applied, so the Lyapunov function has to decrease between two samples, i.e.

$$\Delta V_\alpha = V_\alpha(k+1) - V_\alpha(k) < 0 \tag{3.3.10}$$

In order to apply the Finsler's lemma as presented in (3.2.8), $\Delta V_\alpha < 0$ can be written:

$$\begin{bmatrix} \bar{x}_\alpha^\theta(k) \\ \bar{x}_\alpha^\theta(k+1) \end{bmatrix}^T \begin{bmatrix} -P_z & 0 \\ 0 & P_{z+} \end{bmatrix} \begin{bmatrix} \bar{x}_\alpha^\theta(k) \\ \bar{x}_\alpha^\theta(k+1) \end{bmatrix} < 0 \tag{3.3.11}$$

where the notation P_{z+} denotes $\sum_{i=1}^{r} h_i(k+1) P_i$. Then, the closed-loop system stands for:

$$\bar{x}_\alpha^\theta(k+1) = \left(\bar{A}_{\alpha,z}^\theta + \Delta\bar{A}_z\right) \cdot \bar{x}_\alpha^\theta(k) - \bar{B}_{\alpha,z}^\theta \cdot F_{\alpha,z}^\theta \cdot \bar{x}_\alpha^\theta(k) \tag{3.3.12}$$

where $\bar{A}_{\alpha,z}^\theta$, $\Delta\bar{A}_z$ and $\bar{B}_{\alpha,z}^\theta$ are the augmented matrices described in (3.3.8). Equation (3.3.12) can be written:

$$\begin{bmatrix} \bar{A}_{\alpha,z}^\theta + \Delta\bar{A}_z - \bar{B}_{\alpha,z}^\theta \cdot F_{\alpha,z}^\theta & -I \end{bmatrix} \begin{bmatrix} \bar{x}_\alpha^\theta(k) \\ \bar{x}_\alpha^\theta(k+1) \end{bmatrix} = 0 \tag{3.3.13}$$

Using the Finsler's lemma (3.2.8), the inequality (3.3.10) is verified if there exists a matrix M such that:

$$M\cdot\left[\bar{A}_{\alpha,z}^{\theta}+\Delta\bar{A}_z-\bar{B}_{\alpha,z}^{\theta}\cdot F_{\alpha,z}^{\theta}\quad -I\right]+(*)+\begin{bmatrix}-P_z & 0\\ 0 & P_{z+}\end{bmatrix}<0 \tag{3.3.14}$$

Where $(*)$ in the matrices stands for the symmetric term and in equalities or inequalities stands for the symmetric matrix of the left-side term. By fixing $M=\begin{bmatrix}0\\ I\end{bmatrix}$, inequality (3.3.14) can be written:

$$\begin{bmatrix}-P_z & (*)\\ \bar{A}_{\alpha,z}^{\theta}+\Delta\bar{A}_z-\bar{B}_{\alpha,z}^{\theta}\cdot F_{\alpha,z}^{\theta} & P_{z+}-2\cdot I\end{bmatrix}<0 \tag{3.3.15}$$

In order to deal with the uncertain matrix $\Delta\bar{A}_z$, an upper bound can be obtained using the following lemma:

Lemma 1: Considering two matrices W and Y with appropriate sizes, the following inequality stands for any matrix $Q=Q^T>0$:

$$W\cdot Y^T+Y\cdot W^T\le W\cdot Q\cdot W^T+Y\cdot Q^{-1}\cdot Y^T \tag{3.3.16}$$

For the proof, the interested reader can refer to (Wang et al., 1992). It stands:

$$\begin{bmatrix}0 & (*)\\ \Delta\bar{A}_z & 0\end{bmatrix}\le\begin{bmatrix}\mu^{-1}\cdot E_a^T\cdot E_a & 0\\ 0 & \mu\cdot Ha_z\cdot Ha_z^T\end{bmatrix} \tag{3.3.17}$$

where Combining (3.3.15) and (3.3.17), the matrix inequality (3.3.15) becomes:

$$\begin{bmatrix}-P_z+\mu^{-1}\cdot E_a^T\cdot E_a & (*)\\ \bar{A}_{\alpha,z}^{\theta}-\bar{B}_{\alpha,z}^{\theta}\cdot F_{\alpha,z}^{\theta} & P_{z+}-2\cdot I+\mu\cdot Ha_z\cdot Ha_z^T\end{bmatrix}<0 \tag{3.3.18}$$

Using a Schur complement, inequality (3.3.18) becomes:

$$\begin{bmatrix}-P_z & (*) & (*)\\ E_a & -\mu\cdot I & (*)\\ \bar{A}_{\alpha,z}^{\theta}-\bar{B}_{\alpha,z}^{\theta}\cdot F_{\alpha,z}^{\theta} & 0 & P_{z+}-2\cdot I+\mu\cdot Ha_z\cdot Ha_z^T\end{bmatrix}<0 \tag{3.3.19}$$

As already mentioned, $P_z=\sum_{i=1}^{r}h_i(k)P_i$ so the membership functions are still in the inequality. In order to make (3.3.19) a Linear Matrix Inequality (LMI) as defined in (Boyd et al., 1994), these membership functions have to be removed using relaxation conditions. Among the existing methods, the relaxation of Tuan in (Tuan et al., 2001) does not imply the use of other variables, so the complexity of the conditions for obtaining the controller gains does not increase. For the rest of the manuscript, the relaxation of Tuan is used to get LMI conditions that are solved using LMI Toolbox of Matlab software:

Relaxation of Tuan (Tuan et al., 2001): Considering the system including the uncertainties (3.3.4) and the integral action (3.3.8), considering the PDC controller $u(k) = -F_z \cdot x(k)$, the closed-loop system is stable if there exist a scalar μ and matrices M_2, K_i and positive matrices P_i such that:

$$\begin{cases} \Gamma_{ii}^k < 0, \quad \forall i,k \in \{1,...r\}^2 \\ \frac{2}{r-1} \cdot \Gamma_{ii}^k + \Gamma_{ij}^k + \Gamma_{ji}^k < 0, \quad \forall i,j,k \in \{1,...r\}^3, i \neq j \end{cases} \tag{3.3.20}$$

With the quantity defined as:

$$\Gamma_{ij}^k = \begin{bmatrix} -P_i & (*) & (*) \\ E_a & -\mu \cdot I & (*) \\ \bar{A}_{\alpha,i}^{\theta} - \bar{B}_{\alpha,i}^{\theta} \cdot F_{\alpha,j}^{\theta} & 0 & P_k - 2 \cdot I + \mu \cdot Ha_i \cdot Ha_j^T \end{bmatrix} \tag{3.3.21}$$

In these LMI conditions, the system matrices are known, i.e. the domain of validity of the TS model is fixed to compute $\bar{A}_{\alpha,i}^{\theta}$ and $\bar{B}_{\alpha,i}^{\theta}$. However, due to the complexity of the system, the LMI problem is unfeasible whatever the considered domain of validity, i.e. it is impossible to find controller gains that are able to stabilize the closed-loop system for a domain that is already too small for the application. For example, the problem is unfeasible considering variables inside the following domain of validity:

$$\begin{matrix} n(k) \in [700,800] & \alpha(k) \in [1,2] \\ \varphi(k) \in [2,3] & \lambda(k) \in [0.95,1.05] \end{matrix} \tag{3.3.22}$$

As a reminder, those variables are the ones involving in the nonlinearities of the system (3.1.1) and stand for $n(k)$ as the engine speed in rpm, $\alpha(k)$ as the throttle angle in degrees, $\varphi(k)$ as the spark advance angle in degrees before TDC and $\lambda(k)$ as the air-fuel ratio. As one can see, this domain is very restrictive considering the application, and still the LMI problem is unfeasible. As detailed in the remark concerning the source of conservativeness, it is possible to find more relaxed conditions by either changing the TS model so the control law, the Lyapunov function or the relaxation. Improvements could be obtained with a more complex Lyapunov function or a more efficient relaxation, however, the choice is done to change the control law for a more complex one. The PDC controller cannot stabilize such a complex system as the idle speed model.

3.3.2. Non-PDC controller

Among the non-PDC controller, the one involving a matrix inversion as developed in (Guerra and Vermeiren, 2004) and presented in (3.2.10) is considered:

$$u_{\alpha}^{\theta}(k) = -F_{\alpha,z}^{\theta} \cdot \left(H_{\alpha,z}^{\theta}\right)^{-1} \cdot \bar{x}_{\alpha}^{\theta}(k) \tag{3.3.23}$$

As presented in the literature, the controller with fuzzy matrix inversion (CFMI) provides valuable performance in spite of the real-time matrix inversion that increases the computational cost which can be a problem for an embedded engine control unit. The procedure to obtain LMI conditions can be adapted from (Lendek et al., 2015). Considering the delayed non-quadratic Lyapunov function:

$$V_\alpha(k) = \bar{x}_\alpha^\theta(k)^T \cdot P_{z-}^{-1} \cdot \bar{x}_\alpha^\theta(k) \tag{3.3.24}$$

The difference $\Delta V_\alpha(k) = V_\alpha(k+1) - V_\alpha(k)$ is written as in equation (3.3.10) to apply the Finsler's lemma. The closed-loop system is then written:

$$\left[\bar{A}_{\alpha,z}^\theta + \Delta\bar{A}_z - \bar{B}_{\alpha,z}^\theta \cdot F_{\alpha,z}^\theta \cdot \left(H_{\alpha,z}^\theta\right)^{-1} \quad -I\right]\begin{bmatrix}\bar{x}_\alpha^\theta(k)\\ \bar{x}_\alpha^\theta(k+1)\end{bmatrix} = 0 \tag{3.3.25}$$

The Finsler lemma is applied with the matrix $M = \begin{bmatrix}0\\ P_z^{-1}\end{bmatrix}$:

$$\mathrm{M} = \begin{bmatrix} -P_{z-}^{-1} & (*) \\ P_z^{-1} \cdot \left(\bar{A}_{\alpha,z}^\theta + \Delta\bar{A}_z - \bar{B}_{\alpha,z}^\theta \cdot F_{\alpha,z}^\theta \cdot \left(H_{\alpha,z}^\theta\right)^{-1}\right) & -P_z^{-1} \end{bmatrix} < 0 \tag{3.3.26}$$

and a congruence transformation, i.e. multiplying M from inequality (3.3.26) such that $\Psi^T \cdot \mathrm{M} \cdot \Psi < 0$ with the Ψ matrix defined as:

$$\Psi = \begin{bmatrix} H_z & 0 \\ 0 & P_z \end{bmatrix} \tag{3.3.27}$$

Then, it stands that $\Delta V_\alpha(k) < 0$ is verified if:

$$\begin{bmatrix} -\left(H_{\alpha,z}^\theta\right)^T \cdot P_{z-}^{-1} \cdot H_{\alpha,z}^\theta & (*) \\ \left(\bar{A}_{\alpha,z}^\theta + \Delta\bar{A}_z\right) \cdot H_{\alpha,z}^\theta - \bar{B}_{\alpha,z}^\theta \cdot F_{\alpha,z}^\theta & -P_z \end{bmatrix} < 0 \tag{3.3.28}$$

The uncertainties are managed such that presented in equation (3.3.17) and, similarly to the PDC design, Schur complements are used to avoid product of unknown terms. Inequality (3.3.28) becomes:

$$\begin{bmatrix} -\left(H_{\alpha,z}^\theta\right)^T - H_{\alpha,z}^\theta + P_{z-} & (*) & (*) \\ E_a \cdot H_{\alpha,z}^\theta & -\mu I & (*) \\ \bar{A}_{\alpha,z}^\theta \cdot H_{\alpha,z}^\theta - \bar{B}_{\alpha,z}^\theta \cdot F_{\alpha,z}^\theta & 0 & -P_z + \mu \cdot Ha_z \cdot Ha_z^T \end{bmatrix} < 0 \tag{3.3.29}$$

Then, the closed-loop system is stable considering the relaxation of Tuan (3.3.20) with the following quantity:

$$\Gamma_{ij}^k = \begin{bmatrix} -\left(H_{\alpha,j}^\theta\right)^T - H_{\alpha,j}^\theta + P_k & (*) & (*) \\ E_a \cdot H_{\alpha,j}^\theta & -\mu I & (*) \\ \bar{A}_{\alpha,i}^\theta \cdot H_{\alpha,j}^\theta - \bar{B}_{\alpha,i}^\theta \cdot F_{\alpha,j}^\theta & 0 & -P_j + \mu \cdot Ha_i \cdot Ha_j^T \end{bmatrix} \tag{3.3.30}$$

This LMI problem is feasible, i.e. controller gains can be found to stabilize the closed-loop system considering the domain of validity:

$$\begin{matrix} n(k)\in[600,1100] & \alpha(k)\in[0.5,5] \\ \varphi(k)\in[2,10] & \lambda(k)\in[0.8,1.2] \end{matrix} \tag{3.3.31}$$

As one can see, this domain of validity allows the speed varying around the reference value $n_{ref} = 800rpm$. Such variations can occur in presence of external disturbances. A decay-rate can be added to the conditions to accelerate the convergence of the Lyapunov function, such that:

$$\Delta V_\alpha(k) < -\beta^2 \cdot V_\alpha(k) \tag{3.3.32}$$

The normalized decay rate $\bar{\beta} = 1+\beta^2$ is defined such that $\bar{\beta}\in[0,1]$ and the new LMI conditions are obtained considering the quantity adapted from (3.3.30):

$$\Gamma_{ij}^k = \begin{bmatrix} -\bar{\beta}\cdot\left(H_{\alpha,j}^\theta\right)^T - \bar{\beta}\cdot H_{\alpha,j}^\theta + \bar{\beta}\cdot P_k & (*) & (*) \\ E_a \cdot H_{\alpha,j}^\theta & -\mu I & (*) \\ \bar{A}_{\alpha,i}^\theta \cdot H_{\alpha,j}^\theta - \bar{B}_{\alpha,i}^\theta \cdot F_{\alpha,j}^\theta & 0 & -P_j + \mu \cdot Ha_i \cdot Ha_j^T \end{bmatrix} \tag{3.3.33}$$

One can notice that the previous conditions (3.3.30) are obtained with $\bar{\beta} = 1$.

Due to the complexity of the idle speed TS model, modifications have been done to reduce the number of nonlinearities by adding uncertainties. An integral action has been included to track a reference and to reject external disturbances. Still, the simple form of a PDC controller is not able to stabilize the closed-loop system using the direct Lyapunov method with a non-quadratic function. Among the TS fuzzy controllers, a non-PDC has been considered. By adding the inversion of a fuzzy matrix, i.e. a combination of membership functions and local matrices, better performance are obtained and the LMI problem becomes feasible in a proper domain of validity. However, the matrix inversion can be hard to compute for an embedded ECU. What kind of controller can be designed to be a valuable alternative to the controller with the fuzzy matrix inversion, i.e. how to find an alternative controller ensuring the same performance but with less computational cost?

4. Alternative controller design

4.1. Matrix inversion problem

As already mentioned, the main inconvenient of the non-PDC controller involving a matrix inversion is that this operation is realized in real-time, i.e. at each sample time the control law is computed. For a limited embedded ECU such as the industrial ones, it can be costly to compute, considering that more than 70% of the internal memory is already dedicated to safety algorithms. The computational cost (or the complexity) of a considered controller can be estimated considering the number of basic operations (addition, subtraction, multiplication, division) realized in real-time. Concerning only the operation of matrix inversion, it involves several basic operations, as detailed in (Bunch and Hopcroft, 1974). Among the algorithms used to invert a matrix, the Strassen's algorithm is a good trade-off between complexity and rapidity. The number of operations involved in such an algorithm has been determined in (Bailey et al., 1991):

$$C\left(M^{-1}\right)=5.64\cdot n_M^{\log_2 7} \tag{3.4.1}$$

Where M stands for the matrix to invert and n_M its size. As one can see, the computational cost is depending on the size of the inverted matrix, as depicted in Fig. 78.

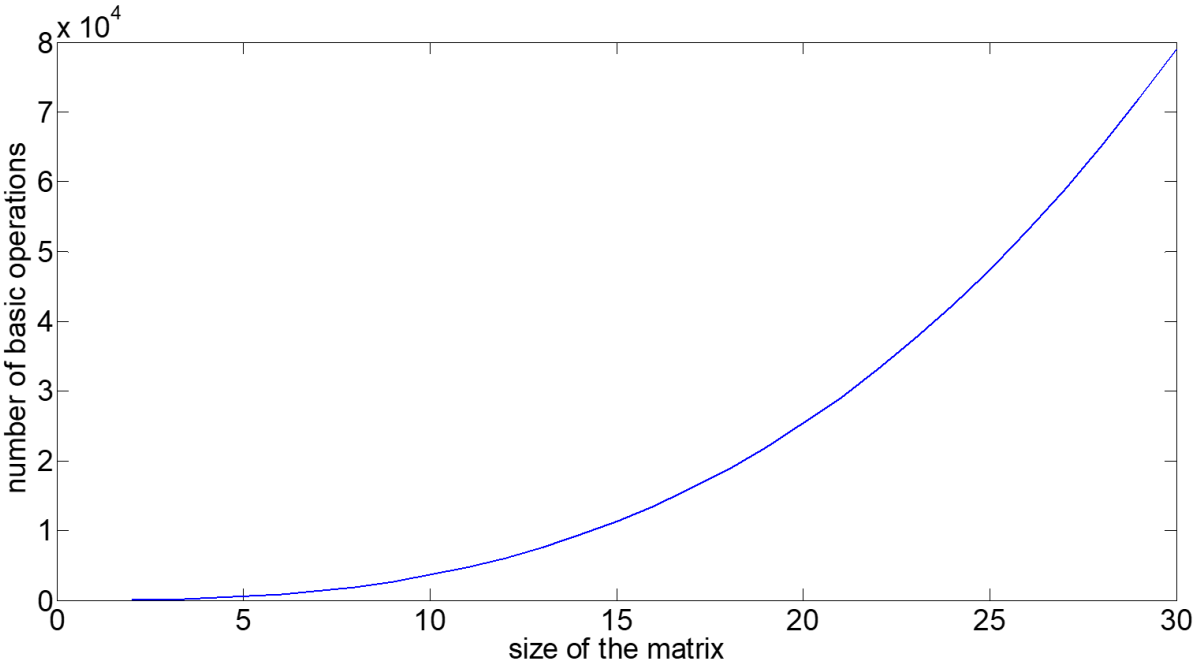

Fig. 78. Evolution of the complexity in function of the size of the matrix

Even if the size of the considered inverted matrix H_z^{-1} is equal to $n_H=5$, it still involves 517 basic operations only for the real-time inversion of a matrix. The complexity of the whole CFMI can be calculated using the Table 4:

$$C_{CFMI}=2\cdot\left(r\cdot n^2+r-1\right)+5.64\cdot n^{\log_2 7}+n^2\cdot\left(2\cdot n-1\right)+3\cdot n^2-n \tag{3.4.2}$$

As a matter of comparison, considering five states and two nonlinearities, the complexity of the PDC controller (which does not provide a solution to the LMI problem) is equal to 173 basic operations while the CFMI involves 1018 operations. This clearly states the complexity and the computational cost of the use of an advance TS fuzzy controller like the CFMI.

Not only the number of operations has to be considered when dealing with embedded applications, but also the numerical stability of the proposed algorithm for the matrix inversion. Several studies in the field of mathematics, for instance the work of (Bailey et al., 1991; Croz and Higham, 1992; Higham, 1992), highlight the fact that the most efficient and the fastest methods for matrix inversion, such as the Strassen's algorithm, may be numerically unstable and that is another reason why the matrix inversion should be avoided for real-time implementation.

Additionally, among the operations needed for the matrix inversion, there are some divisions. It has been demonstrated in the literature that the division operation is hardly computed by an embedded device: Indeed, it depends on the performance of the electronic control unit that are different from a laptop. In the work of (Shirazi et al., 1995), they detailed the difference between the basic operations

realized on several formats (16 and 18 bits). Moreover, computing floating-point operations generates errors due to rounding parts as presented in the paper of (Wilkinson, 1960) from a mathematical point of view and the work of (Goldberg, 1991) from the field of computer science. The propagation of the error implied in floating-point operations is more important for the division as it has been detailed in (Hillesland and Lastra, 2004).

For those reasons, the CFMI is a controller performant but hard to compute for an embedded ECU. Before considering any implementation in an engine test bench, an alternative controller has to be found which can provide similar performance but avoiding the real-time matrix inversion. A method has been developed using a multiple sums fuzzy matrix (Laurain et al., 2016b, 2017a).

4.2. Multiple sums fuzzy controller

The first developed approach to design an alternative controller to the CFMI is based on multiple sums fuzzy matrices. The methodology is composed of three steps: computing the gains of the non-PDC controller, finding the fuzzy matrices to approximate the inverted matrices H_z^{-1} and the second step is to apply the direct Lyapunov method to verify the stability of the closed-loop system.

4.2.1. Equivalency

The main idea behind this first approach is to approximate the non-PDC controller (3.3.23) by an alternative controller implying a multiple sums fuzzy matrix $G_{z..z}$. Considering the CFMI structure, the matrix F_z is obtained while solving the LMI conditions with the quantity (3.3.33) (3.5.3), so it can be removed from the alternative controller design, such that the control law of the CFMI (3.3.23) can be written:

$$u_\alpha^\theta(k) = -F_{\alpha,z}^\theta \cdot u_H^\theta(k) \tag{3.4.3}$$

With

$$u_H^\theta(k) = \left(H_{\alpha,z}^\theta\right)^{-1} \cdot \bar{x}_\alpha^\theta(k) \tag{3.4.4}$$

Then, the alternative controller has to provide the same performance as $u_H^\theta(k)$ but avoiding the inversion of weighted matrices $\left(H_{\alpha,z}^\theta\right)^{-1}$. For example, the structure of the alternative controller (CATS controller ; Counterpart for Advanced Takagi-Sugeno controller) is defined for a two-sums fuzzy matrix:

$$\tilde{u}_\alpha^\theta(k) = G_{\alpha,zz}^\theta \cdot \bar{x}_\alpha^\theta(k) \tag{3.4.5}$$

Where $G_{\alpha,zz}^\theta = \sum_{i=1}^{r}\sum_{j=1}^{r} G_{\alpha,ij}^\theta$ and the final implemented controller stands for:

$$u_\alpha^\theta(k) = -F_{\alpha,z}^\theta \cdot \tilde{u}_H^\theta(k) \tag{3.4.6}$$

In order to determine the accuracy of the approximation, an equivalence criterion γ is defined such that the two-sums CATS controller (3.4.5) is equivalent to (3.4.4), i.e. $u_H^\theta(k) \approx \tilde{u}_\alpha^\theta(k)$:

$$\left(\left(H_{\alpha,z}^{\theta}\right)^{-1}-G_{\alpha,zz}^{\theta}\right)^{T}\left(\left(H_{\alpha,z}^{\theta}\right)^{-1}-G_{\alpha,zz}^{\theta}\right)<\gamma I \tag{3.4.7}$$

After some matrix transformations, (3.4.7) becomes:

$$\left(I-\left(H_{\alpha,z}^{\theta}\right)^{T}\cdot\left(G_{\alpha,zz}^{\theta}\right)^{T}\right)\left(I-H_{\alpha,z}^{\theta}\cdot G_{\alpha,zz}^{\theta}\right)-\gamma\cdot\left(H_{\alpha,z}^{\theta}\right)^{T}\cdot H_{\alpha,z}^{\theta}<0 \tag{3.4.8}$$

A Schur complement allows writing inequality (3.4.8) in a matrix inequality form:

$$\Gamma_{zzz}=\begin{bmatrix}-\gamma\cdot\left(H_{\alpha,z}^{\theta}\right)^{T}\cdot H_{\alpha,z}^{\theta} & (*)\\ I-H_{\alpha,z}^{\theta}\cdot G_{\alpha,zz}^{\theta} & -I\end{bmatrix}<0 \tag{3.4.9}$$

Where $H_{\alpha,z}^{\theta}$ is already known from the CFMI design (3.5.3), γ is the equivalence criterion to be minimized in order to get a better approximation and $G_{\alpha,zz}^{\theta}$ the matrix gains of the alternative controller CATS.

4.2.2. Membership set

As one can see, the membership functions are still involved in the design. Relaxations could be applied to remove membership functions $h_i\left(z(k)\right)$, for example by taking into account the vertices and some cross-terms like in stability analysis. However, because the goal is to minimize the scalar parameter γ, in order to improve the accuracy of the approximation, more information about the membership functions have to be included. The idea of introducing the membership functions directly during the controller design process instead of relaxations has been highlighted in some works in the literature such as the paper (Meda-Campaña et al., 2015) about fuzzy controllability.

To this end, the premise variables $z_i(k)$ are defined as the i-th component of the vector $z(k)$ and the associated normalized premise functions $\omega_i(k)$ such that:

$$\omega_i(k)=\frac{z_i(k)-z_{i\min}}{z_{i\max}-z_{i\min}} \tag{3.4.10}$$

Where $z_{i\min}$ and $z_{i\max}$ are respectively the minimum and the maximum of the variables $z_i(k)$.

Remark (Premise functions): This definition generalizes the example given in Chapter 2, see equation (2.6.7)

Then, the $\omega_i(k)$ are gridded chosen among a set of values Ω_i with a chosen step λ_i: $\Omega_i=\{0,\lambda_i,2\lambda_i,...,1\}$. The set of values of the membership function E can be defined considering all the admissible combination of $\omega_i\in\Omega_i$, $i\in\{1,...,n_z\}$ according to a certain step $\lambda_z=\prod_{i=1}^{n_z}\lambda_i$ where n_z stands for the number of premise variables.

With this gridding methodology, we can consider different steps in each interpolation region and then easily cope with the physics of the real system considered. A hypothesis is that the more information one adds, i.e. the more values the set E contains, more accurate the approximation is.

This methodology to include the membership functions in the controller design can be applied to the inequality (3.4.9), such that the approximation of the CFMI by the CATS controller is ensured according to an equivalence criterion $\sqrt{\gamma}$ if the following constraints are verified:

$$\begin{gathered}\forall \alpha_1 \in \mathrm{E},\ldots,\forall \alpha_i \in \mathrm{E}\backslash\left\{1+\lambda_z-\sum_{p=1}^{i-1}\alpha_p,\ldots,1\right\},\ldots,\forall \alpha_r = 1-\sum_{i=1}^{r-1}\alpha_i, \\ \sum_{i=1}^{r}\sum_{j=1}^{r}\sum_{k=1}^{r}\alpha_i\alpha_j\alpha_k\Gamma_{ijk}<0\end{gathered} \tag{3.4.11}$$

Where α_i stands for the value taken by the membership functions inside the membership set $\mathrm{E}=0:0.25:1$ ($\lambda_z=0.25$) and the quantity Γ_{ijk} adapted from (3.4.9):

$$\Gamma_{ijk}=\begin{bmatrix}-\gamma\cdot\left(H_{\alpha,j}^{\theta}\right)^{T}\cdot H_{\alpha,i}^{\theta} & (*)\\ I-H_{\alpha,i}^{\theta}\cdot G_{\alpha,jk}^{\theta} & -I\end{bmatrix} \tag{3.4.12}$$

By solving the inequality (3.4.11), the gains of the CATS controller are obtained according to a given accuracy. Solving inequalities (3.4.11) only ensures that the CATS controller is approximating with the the CFMI controller. The stability of the whole closed-loop system with the CATS controller has to be verified using the direct Lyapunov method.

4.2.3. Lyapunov matrices

In order to verify the stability of the whole closed-loop system where the CATS controller (3.4.6) is applied on the system (3.3.8), the direct Lyapunov method is applied. The closed-loop system can be written:

$$\bar{x}_{\alpha}^{\theta}(k+1)=\left(\bar{A}_{\alpha,z}^{\theta}+\Delta\bar{A}_z\right)\cdot\bar{x}_{\alpha}^{\theta}(k)-\bar{B}_{\alpha,z}^{\theta}\cdot F_{\alpha,z}^{\theta}\cdot G_{\alpha,zz}^{\theta}\cdot\bar{x}_{\alpha}^{\theta}(k) \tag{3.4.13}$$

The candidate Lyapunov function is a non-quadratic one such as introduced in (Guerra and Vermeiren, 2004):

$$V_{\alpha}^{alt}(k)=\bar{x}_{\alpha}^{\theta}(k)^{T}\cdot\left(G_{\alpha,zz}^{\theta}\right)^{T}\cdot P_z\cdot G_{\alpha,zz}^{\theta}\cdot\bar{x}_{\alpha}^{\theta}(k) \tag{3.4.14}$$

Where P_i are positive definite Lyapunov matrices. The methodology is divided into two steps: First, finding the Lyapunov matrices P_i and next, verifying the stability of the whole closed-loop system knowing all the elements. The application of the direct Lyapunov method states that:

$$V_{\alpha}^{alt}(k+1)-V_{\alpha}^{alt}(k)<0 \tag{3.4.15}$$

Where $V_\alpha^{alt}(k+1)$ can be replaced by its expression according to the definition of the Lyapunov function (3.4.14) and the closed-loop system (3.4.13). Inequality (3.4.15) becomes:

$$-\Phi_{zzzzz}+\left(\bar{A}_{\alpha,z}^{\theta}+\Delta\bar{A}_z-\bar{B}_{\alpha,z}^{\theta}\cdot F_{\alpha,z}^{\theta}\cdot G_{\alpha,zz}^{\theta}\right)^T\Phi_{z+z+z+z+z+}\left(\bar{A}_{\alpha,z}^{\theta}+\Delta\bar{A}_z-\bar{B}_{\alpha,z}^{\theta}\cdot F_{\alpha,z}^{\theta}\cdot G_{\alpha,zz}^{\theta}\right)<0 \tag{3.4.16}$$

With $\Phi_{zzzzz}=\left(G_{\alpha,zz}^{\theta}\right)^T\cdot P_z\cdot G_{\alpha,zz}^{\theta}$. Using a Schur complement, (3.4.16) can be transformed into a matrix inequality:

$$\Gamma_{zzzzz}^{z+z+z+}=\begin{bmatrix}-\left(G_{\alpha,zz}^{\theta}\right)^T\cdot P_z\cdot G_{\alpha,zz}^{\theta} & (*)\\ P_{z+}\cdot G_{\alpha,z+z+}^{\theta}\cdot\left(\bar{A}_{\alpha,z}^{\theta}+\Delta\bar{A}_z-\bar{B}_{\alpha,z}^{\theta}\cdot F_{\alpha,z}^{\theta}\cdot G_{\alpha,zz}^{\theta}\right) & -P_{z+}\end{bmatrix}<0 \tag{3.4.17}$$

In order to deal with the uncertainties $\Delta\bar{A}_z$, the same technique is used, as presented along equations (3.3.17). The inequality (3.4.17) can be modified to make the uncertainty criterion μ appear according to the **Lemma 1** given in page 99:

$$\Gamma_{zzzzz}^{z+z+z+}=\begin{bmatrix}-\left(G_{\alpha,zz}^{\theta}\right)^T\cdot P_z\cdot G_{\alpha,zz}^{\theta} & (*) & (*)\\ P_{z+}\cdot G_{\alpha,z+z+}^{\theta}\cdot E_a & -\mu I & (*)\\ P_{z+}\cdot G_{\alpha,z+z+}^{\theta}\cdot\left(\bar{A}_{\alpha,z}^{\theta}+\Delta\bar{A}_z-\bar{B}_{\alpha,z}^{\theta}\cdot F_{\alpha,z}^{\theta}\cdot G_{\alpha,zz}^{\theta}\right) & 0 & -P_{z+}+\mu\cdot Ha_z\cdot Ha_z^T\end{bmatrix}<0 \tag{3.4.18}$$

As one can see, the membership functions $h_i(k)$ are still involved in the inequality (3.4.18). In order to obtain a LMI, one can use a relaxation to remove the nonlinear functions, but the same methodology considering the membership functions inside a membership set is used, for the same reasons (i.e. including more information in the resolution of the inequality). This new membership set E_V can be different from the one used along the resolution of the LMI problem (3.4.11). For example, let us consider the membership functions taking their values inside a membership set $\mathrm{E}_V=\{0,0.2,0.4,0.6,0.8,1\}$, i.e. $\lambda_z=0.2$, the Lyapunov matrices P_i are obtained if the following conditions are verified :

$$\begin{aligned}&\forall\alpha_1\in\mathrm{E},\ldots,\forall\alpha_i\in\mathrm{E}\backslash\left\{1+\lambda_z-\sum_{p=1}^{i-1}\alpha_p,\ldots,1\right\},\ldots,\forall\alpha_r=1-\sum_{i=1}^{r-1}\alpha_i,\\ &\forall\alpha_1^+\in\mathrm{E},\ldots,\forall\alpha_i^+\in\mathrm{E}\backslash\left\{1+\lambda_z-\sum_{p=1}^{i-1}\alpha_p^+,\ldots,1\right\},\ldots,\forall\alpha_r^+=1-\sum_{i=1}^{r-1}\alpha_i^+,\\ &\sum_{i=1}^{r}\sum_{j=1}^{r}\sum_{l=1}^{r}\sum_{m=1}^{r}\sum_{p=1}^{r}\sum_{q=1}^{r}\sum_{s=1}^{r}\sum_{t=1}^{r}\alpha_i\alpha_j\alpha_l\alpha_m\alpha_p\alpha_q^+\alpha_s^+\alpha_t^+\Gamma_{ijlmp}^{qst}<0\end{aligned} \tag{3.4.19}$$

With the quantity Γ_{ijlmp}^{qst} defined as:

$$\Gamma_{ijlmp}^{qst}=\begin{bmatrix}-\left(G_{\alpha,lm}^{\theta}\right)^T\cdot P_p\cdot G_{\alpha,lm}^{\theta} & (*) & (*)\\ P_q\cdot G_{\alpha,st}^{\theta}\cdot E_a & -\mu I & (*)\\ P_q\cdot G_{\alpha,st}^{\theta}\cdot\left(\bar{A}_{\alpha,i}^{\theta}-\bar{B}_{\alpha,i}^{\theta}\cdot F_{\alpha,j}^{\theta}\cdot G_{\alpha,lm}^{\theta}\right) & 0 & -P_q+\mu\cdot Ha_i\cdot Ha_j^T\end{bmatrix} \tag{3.4.20}$$

Remark (Stability analysis): Solving (3.4.19) does not ensure the stability of the closed-loop system, a last step is then required to prove $\Gamma_{zzzzzz+z+z+} < 0$. This problem clearly belongs to multi-dimensional fuzzy summations (MDFS) domain that has been explored in the literature. So, at that step any relaxation can be applied, for instance, Proposition 1 in (Sala and Ariño, 2007) allow removing the weighted terms and gives conditions only involving the terms (3.4.20). As all the matrices involved in the problem are known the LMI conditions lead to check only the eigenvalues of each inequality.

Remark (RATS observer) (Laurain et al., 2016d): Since the problem is dual, a similar methodology can be applied to obtain an alternative observer for the TS models:

$$\begin{cases} \hat{x}(k+1) = A_z \hat{x}(k) + B_z u(k) + S_z^{-1} K_z \left(y(k) - \hat{y}(k) \right) \\ \hat{y}(k) = C_z \hat{x}(k) \end{cases} \tag{3.4.21}$$

The alternative observer, the RATS observer (for Replica for an Advanced Takagi-Sugeno observer) is also based on multi-sums fuzzy matrix, such that:

$$\begin{cases} \hat{x}(k+1) = A_z \hat{x}(k) + B_z u(k) + R_{zz} K_z \left(y(k) - \hat{y}(k) \right) \\ \hat{y}(k) = C_z \hat{x}(k) \end{cases} \tag{3.4.22}$$

where R_{zz} is the RATS gain that is computed following the same methodology, i.e. by solving a matrix inequality similar to (3.4.9).

Remark (ECLATS controller) (Laurain et al., 2016c): Another methodology has been developed to provide an alternative controller to the CFMI. The design of the ECLATS controller (for Estimation-based Control Law for Approximating Takagi-Sugeno controller) relies on an observer that estimates the value of $\left(H_{\alpha,z}^{\theta} \right)^{-1} \cdot \bar{x}_{\alpha}^{\theta}(k)$. However, after calculating the complexity, the real-time estimation of the observer makes the ECLATS controller have more basic operations than the CFMI and the CATS controller. For the particular cases where the CFMI is less costly than the CATS, i.e. for TS systems with an important number of nonlinearities, the ECLATS controller remains a good trade-off between complexity and numerical stability while it does not involve any division.

5. Idle speed controller

5.1. Advanced fuzzy controller design

5.1.1. Controller gains

In order to maintain the engine speed at a constant reference value, an idle speed controller has been designed. Due to the nonlinearities of the model, the Takagi-Sugeno representation has been used. For reducing the number of nonlinearities, some uncertainties have been introduced into the design. In order to provide a good tracking of the reference and external disturbance rejection, an integral action has been added to the state vector. A first fuzzy controller has been developed, the PDC controller:

$$u_{\alpha}^{\theta}(k) = -K_{\alpha,z}^{\theta} \cdot \bar{x}_{\alpha}^{\theta}(k) \tag{3.5.1}$$

Considering the complexity of the model, the LMI conditions have been found unfeasible whatever the chosen domain of validity. So an advanced fuzzy controller has to be considered. Among the non-PDC controllers that have been developed in the literature, the one in (Guerra and Vermeiren, 2004) provides good performance but involves a matrix inversion in real-time. This Controller with Fuzzy Matrix Inversion (CFMI) has been designed solving LMI conditions:

$$u_\alpha^\theta(k) = -F_{\alpha,z}^\theta \cdot \left(H_{\alpha,z}^\theta\right)^{-1} \cdot \bar{x}_\alpha^\theta(k) \tag{3.5.2}$$

inside the domain of validity (3.3.31), the decay-rate can be fixed to $\bar{\beta} = 0.985$. The following controller gains are obtained:

$$\begin{aligned}
F_{\alpha,1}^\theta &= \begin{bmatrix} 10.9634 & 3.5426 & 0.0004 & -0.2717 & -0.3631 \end{bmatrix} \\
F_{\alpha,2}^\theta &= \begin{bmatrix} 4.5557 & 2.1253 & 0.0091 & -0.0125 & -0.1175 \end{bmatrix} \\
F_{\alpha,3}^\theta &= \begin{bmatrix} 11.9615 & 3.8461 & -0.1037 & -0.5210 & -0.4334 \end{bmatrix} \\
F_{\alpha,4}^\theta &= \begin{bmatrix} 6.8281 & 2.5726 & -0.0037 & -0.2856 & -0.1963 \end{bmatrix} \\
H_{\alpha,1}^\theta &= 10^3 \cdot \begin{bmatrix} 0.4738 & 0.1807 & -0.0026 & -0.0040 & 0.2311 \\ 0.3326 & 0.9274 & -0.0058 & -0.0037 & 0.1905 \\ 0.2810 & 0.5053 & 1.1676 & -0.0059 & 0.1754 \\ -0.0125 & -0.0036 & 0 & 0.0009 & 0.0003 \\ 0.2246 & 0.1063 & -0.0015 & 0.0010 & 0.4236 \end{bmatrix} \\
H_{\alpha,2}^\theta &= 10^3 \cdot \begin{bmatrix} 0.4930 & 0.2121 & -0.0007 & -0.0135 & 0.2332 \\ 0.2117 & 0.7995 & 0.0059 & -0.0037 & 0.2062 \\ 0.2699 & 0.3950 & 1.1381 & -0.0053 & 0.1829 \\ -0.0101 & -0.0031 & 0.0001 & 0.0007 & 0.0003 \\ 0.1276 & 0.1009 & 0.0017 & 0.0027 & 0.4264 \end{bmatrix} \\
H_{\alpha,3}^\theta &= 10^3 \cdot \begin{bmatrix} 0.4681 & 0.1866 & -0.0051 & -0.0024 & 0.2241 \\ 0.3362 & 0.9523 & -0.0072 & -0.0035 & 0.1810 \\ 0.2845 & 0.5259 & 1.1733 & -0.0061 & 0.1738 \\ -0.0131 & -0.0038 & 0.0001 & 0.0010 & 0.0004 \\ 0.2247 & 0.1098 & -0.0018 & 0.0010 & 0.4197 \end{bmatrix} \\
H_{\alpha,4}^\theta &= 10^3 \cdot \begin{bmatrix} 0.5041 & 0.2183 & -0.0001 & -0.0134 & 0.2278 \\ 0.2091 & 0.7995 & 0.0059 & -0.0035 & 0.1999 \\ 0.2691 & 0.3949 & 1.1379 & -0.0053 & 0.1827 \\ -0.0115 & -0.0034 & 0.0001 & 0.0007 & 0.0003 \\ 0.1269 & 0.1037 & 0.0018 & 0.0026 & 0.4226 \end{bmatrix}
\end{aligned} \tag{3.5.3}$$

5.1.2. Simulation results

Simulation results are then presented to validate the idle speed controller, first in a simulation framework before any implementation for experiments. The nonlinear model has been programmed with Matlab/Simulink, and the controller is designed. In order to make the simulation more 'realistic' and to avoid adding a noise to the signals, the simulation model is fed with measured values from the engine test bench located at the University of Valenciennes, France. This means that the model receives real values with sensor noise for some inputs such as the air-fuel ratio or the spark advance,

as presented in Fig. 79 and Fig. 80. The first simulation assesses the reference tracking of Challenge #1 of the idle speed control problem. The reference is set to several values of idle speed. Fig. 81 presents both the reference and the output of the model. As one can see, the idle speed controller succeeds in tracking the reference due to the presence of the integral action inside its structure. Considering the highly nonlinear behavior of the model, the response time of the closed-loop system is satisfying (2 seconds) for experiments. The response time could be improved by decreasing the decay-rate and getting higher gains, however, as a classical control trade-off, fastening the controller creates more oscillations due to the sensor noise. Fig. 82 presents the command generated every 180 crankshaft degrees by the idle speed controller.

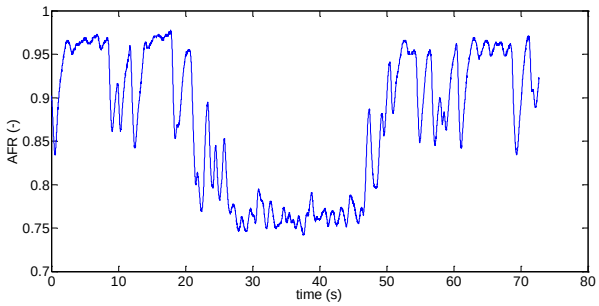

Fig. 79. Measured air-fuel ratio considered for the simulation

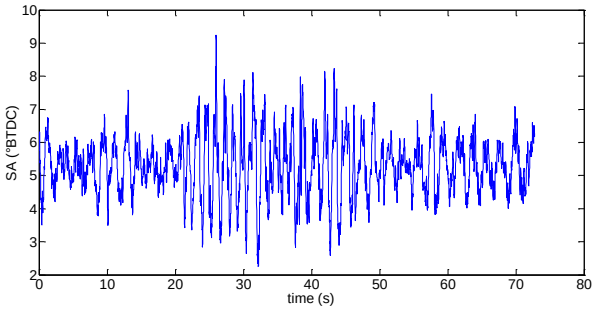

Fig. 80. Measured spark advance considered for the simulation, in degrees before top-dead center

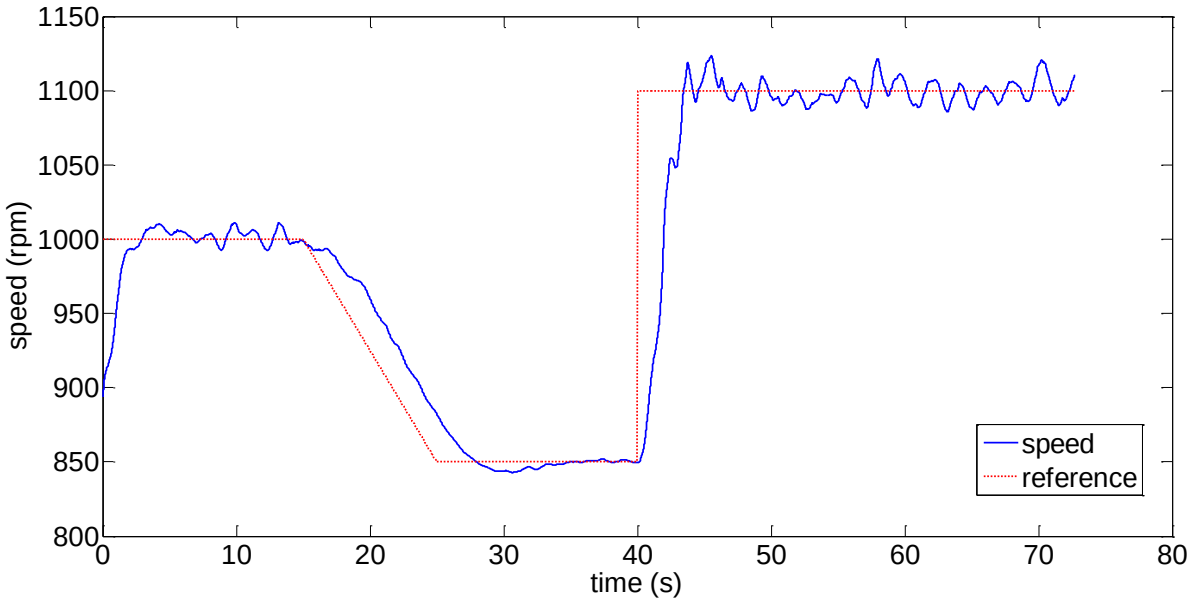

Fig. 81. Idle speed reference tracking

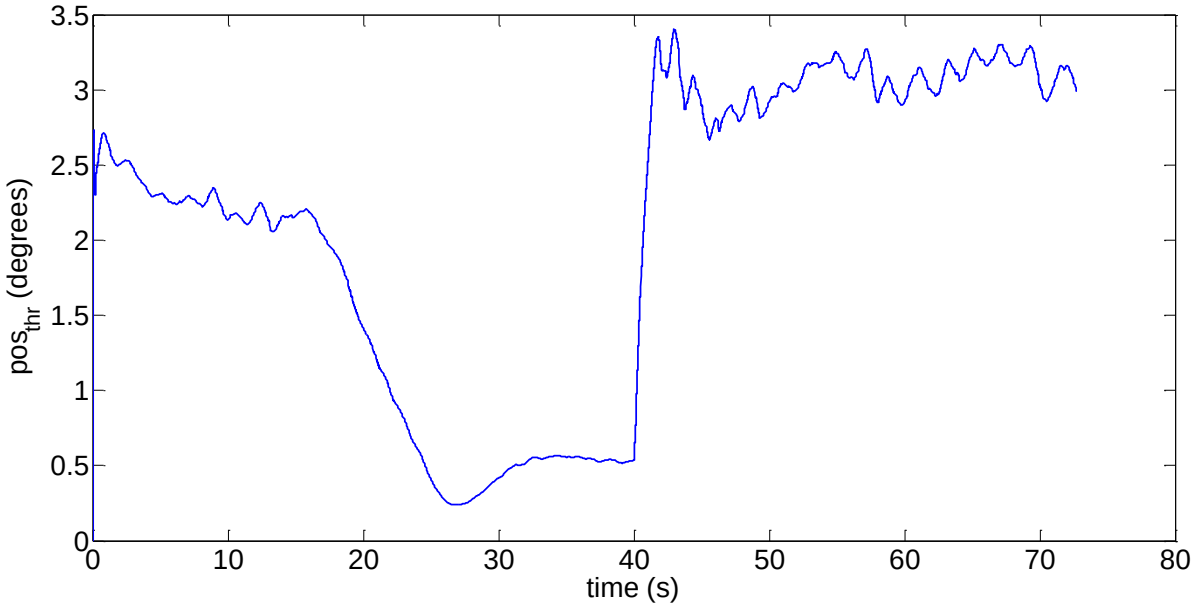

Fig. 82. Command generated by the idle speed controller for reference tracking

Now that the idle speed controller validates the reference tracking of the Challenge #1, a second simulation can be realized to assess the external disturbance rejection. The idle speed reference is set to $n_{ref} = 900rpm$ and a disturbance is created as presented in Fig. 83. It impacts the model as a load torque, see equation (2.2.7). This load torque has not been taken into account during the controller design, and no feedforward is designed to compensate the disturbance; only the integral action has to reject the external disturbance. The simulation is fed with the same measured air-fuel ratio and spark advance as presented in Fig. 79 and Fig. 80. Fig. 84 presents the output of the rotational dynamics model controlled by the idle speed controller triggered every 180 crankshaft degrees, depicted in Fig. 85.

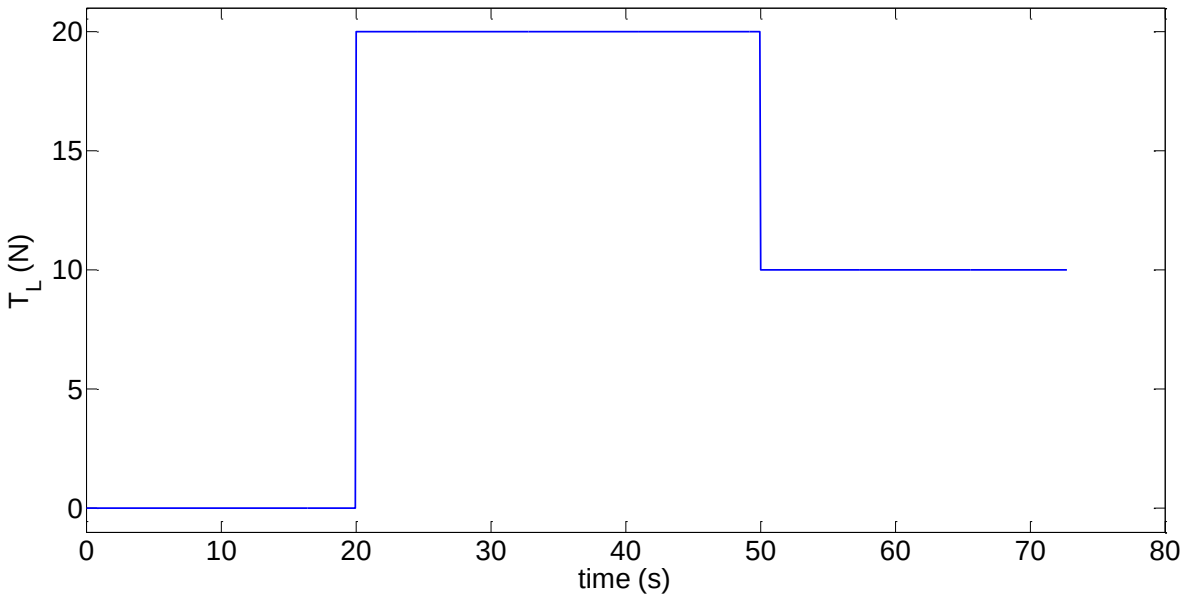

Fig. 83. Load torque simulated for the disturbance rejection

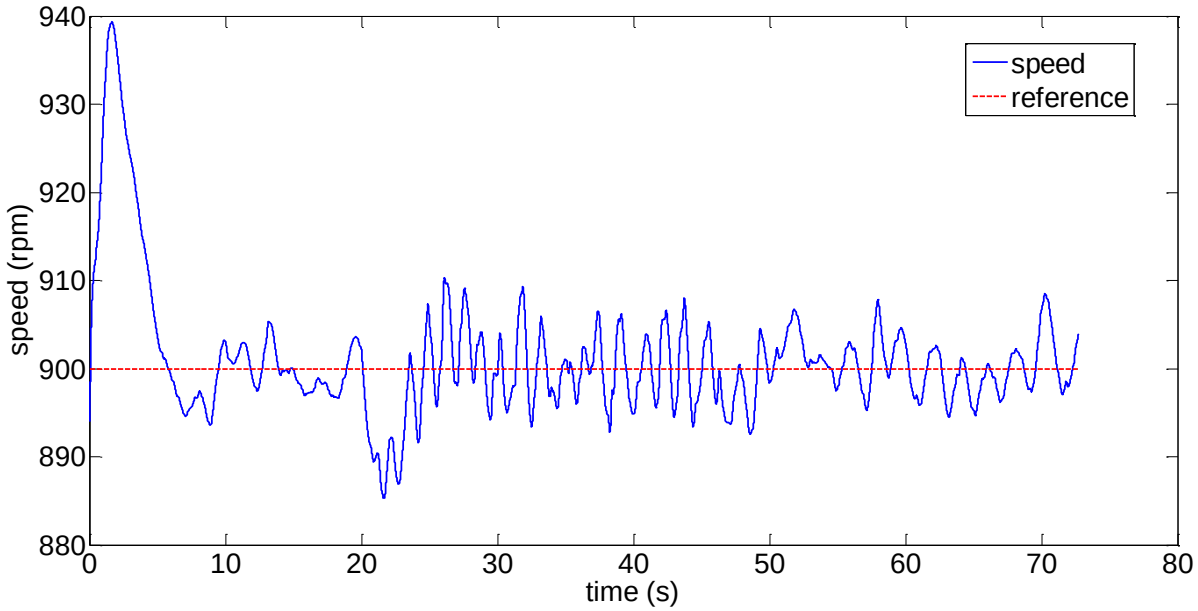

Fig. 84. Simulation result of idle speed control in presence of external disturbance

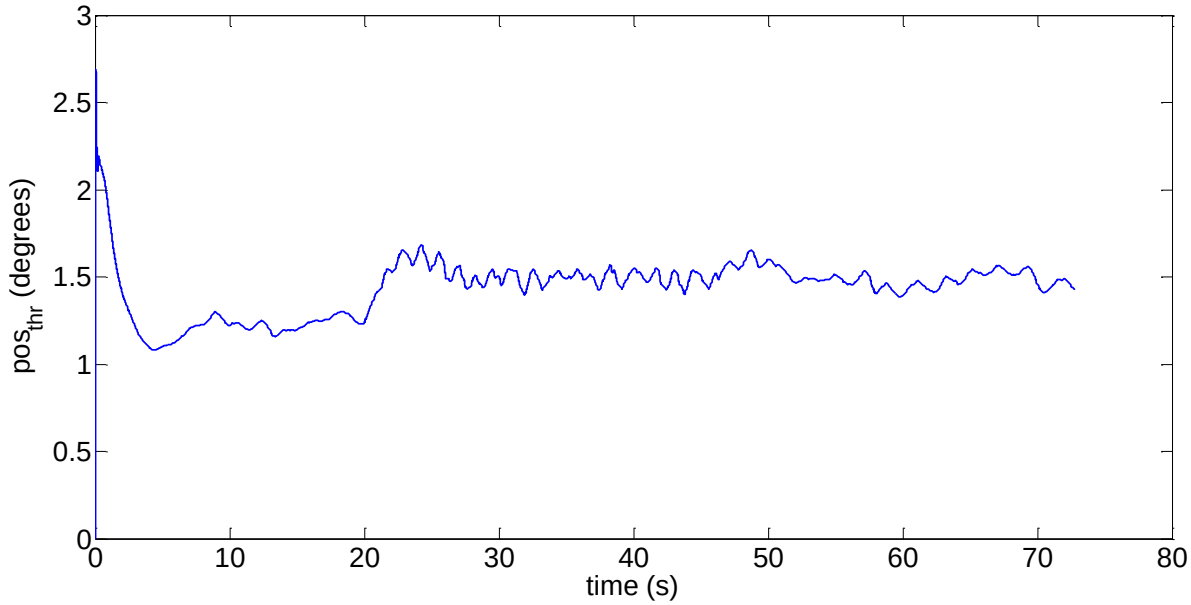

Fig. 85. Command generated by the idle speed controller to reject disturbances

As one can see, the idle speed controller that includes a fuzzy matrix inversion in its structure succeeds in rejecting external disturbances. Considering a load torque of 20 Nm, the speed is only decreasing by 10 rpm. When the value of the load torque is setting to 10 Nm, i.e. the disturbance impact is reducing, the speed seems not to be affected with the controller performance. The main inconvenient of the presented controller is the matrix inversion that is calculated at each sample time of the embedded control unit. Indeed, for an ECU with limited capacities such as the ones used in the automotive industries, it can be costly to compute such an operation. An alternative controller has been designed to get similar performances but avoiding any matrix inversion.

5.2. Alternative controller design

5.2.1. Controller gains

The alternative controller, the CATS controller (for Couterpart for Advanced Takagi-Sugeno controller), is based on a multiple sums fuzzy matrix. The one developed for the idle speed is composed of a two-sums matrix such that:

$$u_{\alpha}^{\theta}(k) = -F_{\alpha,z}^{\theta} \cdot G_{\alpha,zz}^{\theta} \cdot \bar{x}_{\alpha}^{\theta}(k) \tag{3.5.4}$$

Using the Lyapunov direct method and LMI conditions, the CATS controller is ensured to approximate the CFMI controller with a given accuracy. Moreover, the stability of the new closed-loop including the system and the CATS controller is verified, so the gains of the CATS controller can be implemented in the Electronic Control Unit of the engine test bench for real-time experiments. Considering the CFMI controller developed for the idle speed problem in (3.5.3), the equivalence criterion can be minimized to:

$$\gamma = 0.0014 \tag{3.5.5}$$

The gains of the alternative CATS controller are then obtained, 16 matrices 5-by-5: (3.5.6)

$$G_{\alpha,1,1} = \begin{bmatrix} 0.0037 & -0.0005 & 0 & 0.0177 & -0.0019 \\ -0.0008 & 0.0012 & 0 & 0.0021 & -0.0002 \\ 0 & -0.0004 & 0.0009 & 0.0034 & -0.0001 \\ 0.0478 & -0.0013 & 0.0001 & 1.3220 & -0.0266 \\ -0.0019 & -0.0001 & 0 & -0.0125 & 0.0034 \end{bmatrix}$$

$$G_{\alpha,1,2} = 10^{5} \cdot \begin{bmatrix} 0.0058 & 0 & 0.0002 & -1.3951 & 0.0014 \\ -0.0001 & 0 & 0 & -0.0099 & 0 \\ 0.0001 & 0 & 0 & -0.0144 & 0 \\ 0.0389 & 0.0023 & -0.0018 & 3.4160 & 0.0087 \\ -0.0001 & 0 & 0 & 0.0012 & -0.0001 \end{bmatrix}$$

$$G_{\alpha,1,3} = 10^{4} \cdot \begin{bmatrix} -0.0030 & 0.0007 & 0.0004 & 0.0305 & -0.0023 \\ -0.0001 & 0 & 0 & -0.0021 & -0.0003 \\ -0.0009 & -0.0001 & 0 & 0.0084 & -0.0004 \\ -0.1218 & 0.0038 & -0.0090 & -1.2075 & -0.0245 \\ 0.0001 & 0.0001 & 0 & 0.0013 & -0.0001 \end{bmatrix}$$

$$G_{\alpha,1,4} = 10^{3} \cdot \begin{bmatrix} 0.0111 & 0.0007 & 0.0009 & -0.0748 & -0.0003 \\ -0.0005 & 0 & 0.0001 & -0.0371 & -0.0011 \\ -0.0023 & 0 & 0.0001 & 0.0482 & -0.0018 \\ -0.5224 & -0.0184 & 0.0130 & -2.5025 & -1.0952 \\ 0.0014 & 0.0001 & -0.0002 & -0.0025 & 0.0023 \end{bmatrix}$$

$$G_{\alpha,2,1} = 10^5 \cdot \begin{bmatrix} -0.0058 & 0 & -0.0002 & 1.3951 & -0.0014 \\ 0.0001 & 0 & 0 & 0.0099 & 0 \\ -0.0001 & 0 & 0 & 0.0144 & 0 \\ -0.0389 & -0.0023 & 0.0018 & -3.4160 & -0.0087 \\ 0.0001 & 0 & 0 & -0.0012 & 0.0001 \end{bmatrix}$$

$$G_{\alpha,2,2} = \begin{bmatrix} 0.0055 & -0.0006 & 0 & 0.1205 & -0.0028 \\ -0.0005 & 0.0014 & 0 & -0.0017 & -0.0004 \\ -0.0004 & -0.0003 & 0.0009 & -0.0029 & 0 \\ 0.0838 & -0.0031 & -0.0001 & 3.4145 & -0.0464 \\ -0.0020 & -0.0001 & 0 & -0.0574 & 0.0036 \end{bmatrix} ..$$

$$G_{\alpha,2,3} = \begin{bmatrix} -3.6980 & -0.2177 & -0.2951 & 24.9865 & 0.0862 \\ 0.1801 & 0.0073 & -0.0239 & 12.3747 & 0.3584 \\ 0.7808 & -0.0045 & -0.0428 & -16.0547 & 0.6025 \\ 174.2067 & 6.1142 & -4.3460 & 836.1347 & 365.0212 \\ -0.4691 & -0.0404 & 0.0570 & 0.8062 & -0.7775 \end{bmatrix}$$

$$G_{\alpha,2,4} = 10^3 \begin{bmatrix} -0.2188 & -0.0034 & 0.0015 & -0.6504 & -0.0647 \\ 0.0061 & 0 & 0 & 0.0465 & -0.0009 \\ 0.0120 & 0.0001 & -0.0001 & -0.0749 & -0.0055 \\ -1.2249 & 0.0397 & 0.0245 & -3.5886 & -0.5791 \\ 0.0009 & 0 & -0.0001 & 0.0210 & 0.0001 \end{bmatrix}$$

$$G_{\alpha,3,1} = 10^4 \begin{bmatrix} 0.0030 & -0.0007 & -0.0004 & -0.0305 & 0.0023 \\ 0.0001 & 0 & 0 & 0.0021 & 0.0003 \\ 0.0009 & 0.0001 & 0 & -0.0084 & 0.0004 \\ 0.1218 & -0.0038 & 0.0090 & 1.2078 & 0.0245 \\ -0.0001 & -0.0001 & 0 & -0.0013 & 0.0001 \end{bmatrix}$$

$$G_{\alpha,3,2} = \begin{bmatrix} -3.6979 & -0.2175 & -0.2951 & 24.9805 & 0.0860 \\ 0.1802 & 0.0073 & -0.0239 & 12.3743 & 0.3584 \\ 0.7807 & -0.0046 & -0.0428 & -16.0537 & 0.6025 \\ 174.2077 & 6.1153 & -4.3450 & 836.0966 & 365.0208 \\ -0.4692 & -0.0404 & 0.0570 & 0.8063 & -0.7755 \end{bmatrix}$$

$$G_{\alpha,3,3} = \begin{bmatrix} 0.0035 & -0.0005 & 0 & 0.0100 & -0.0017 \\ -0.0007 & 0.0012 & 0 & 0.0027 & -0.0001 \\ 0 & -0.0004 & 0.0008 & 0.0036 & -0.0002 \\ 0.0445 & -0.0014 & 0 & 1.1574 & -0.0242 \\ -0.0018 & -0.0001 & 0 & -0.0083 & 0.0034 \end{bmatrix}$$

$$G_{\alpha,3,4} = 10^4 \cdot \begin{bmatrix} -0.0093 & 0.0003 & 0.0004 & -0.0238 & -0.0055 \\ -0.0005 & 0 & 0 & -0.0064 & 0.0002 \\ 0.0004 & 0 & 0 & 0.0073 & -0.0007 \\ -0.2625 & -0.0134 & 0.0014 & 1.3933 & 0.0420 \\ 0.0001 & 0 & 0 & -0.0013 & 0.0003 \end{bmatrix}$$

$$G_{\alpha,4,1} = \begin{bmatrix} -3.6982 & -0.2175 & -0.2951 & 24.9799 & 0.0862 \\ 0.1802 & 0.0073 & -0.0239 & 12.3743 & 0.3584 \\ 0.7808 & -0.0046 & -0.0428 & -16.0538 & 0.6025 \\ 174.2056 & 6.1145 & -4.3456 & 836.0973 & 365.0218 \\ -0.4692 & -0.0404 & 0.0570 & 0.8063 & -0.7775 \end{bmatrix}$$

$$G_{\alpha,4,2} = 10^3 \cdot \begin{bmatrix} 0.2188 & 0.0034 & -0.0015 & 0.6506 & 0.0647 \\ -0.0061 & 0 & 0 & -0.0465 & 0.0009 \\ -0.0120 & -0.0001 & 0.0001 & 0.0749 & 0.0055 \\ 1.2251 & -0.0397 & -0.0245 & 3.5949 & 0.5790 \\ -0.0009 & 0 & 0.0001 & -0.0211 & -0.0001 \end{bmatrix}$$

$$G_{\alpha,4,3} = 10^4 \cdot \begin{bmatrix} 0.0093 & -0.0003 & -0.0004 & 0.0238 & 0.0055 \\ 0.0005 & 0 & 0 & 0.0064 & -0.0002 \\ -0.0004 & 0 & 0 & -0.0073 & 0.0007 \\ 0.2625 & 0.0134 & -0.0014 & -1.3930 & -0.0420 \\ -0.0001 & 0 & 0 & 0.0013 & -0.0003 \end{bmatrix}$$

$$G_{\alpha,4,4} = \begin{bmatrix} 0.0052 & -0.0007 & 0 & 0.0998 & -0.0026 \\ -0.0005 & 0.0014 & 0 & -0.0015 & -0.0004 \\ -0.0004 & -0.0003 & 0.0009 & -0.0017 & 0 \\ 0.0799 & -0.0035 & -0.0002 & 2.9373 & -0.0436 \\ -0.0019 & -0.0001 & 0 & -0.0479 & 0.0035 \end{bmatrix}$$

Now that the controller gains have been obtained, the controller behavior and the closed-loop system need to be tested and validated through simulations before any real implementation. The first point is to assess the accuracy of the equivalence between the non-PDC controller and the alternative CATS controller that has been designed. The same scenario of disturbance rejection (Fig. 83 to Fig. 85) is considered, and the two controllers are implemented in parallel for comparison

purpose. Fig. 86 illustrates the efficiency of the equivalence between the designed CATS controller (3.5.4) and the non-PDC controller (3.5.2). As one can see, with an accuracy around 10^{-3}, see equation (3.5.5), the CATS controller approximates the performance of the non-PDC controller, even in transient phases, with less than 4% of error. This validates the use of the CATS controller instead of the non-PDC controller for real experiments. There is no need to test the CATS controller in simulation since the performance of both controllers is similar and the non-PDC controller has already been validated through simulations in the previous section.

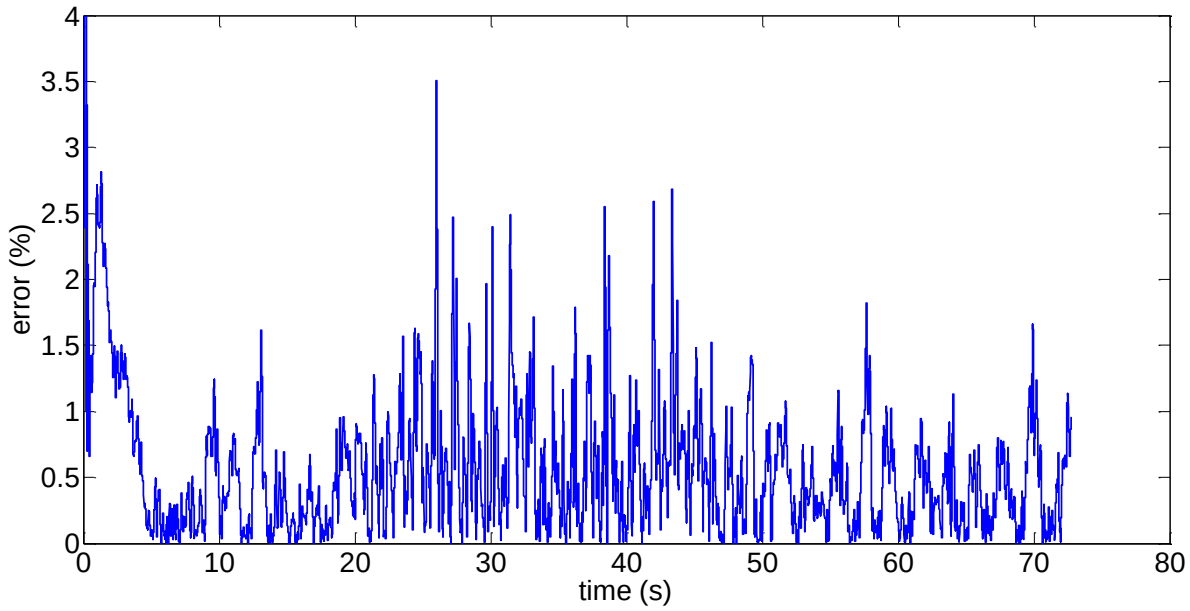

Fig. 86. Error between the non-PDC and the CATS controller, in percent

5.2.2. Experimental results

Experiments are realized on the engine test bench of the University of Valenciennes. The 16 gains of the CATS controller are embedded in the Electronic Control Unit and a switch is designed to detect idle speed conditions, i.e. driver pedal at zero position, and normal driving conditions, i.e. driver pedal at non-zero position.

A first scenario is designed to assess the reference tracking of the CATS controller on a real engine. The reference for the idle speed controller is set to $n_{ref} = \{900, 1000, 950, 1000\}$. The experimental results are given in Fig. 87 and Fig. 88, representing the measured engine speed and the command generated every 180 crankshaft degrees (but recorded every 10 ms, sampling time of the ECU) respectively. As one can see, the controller is able to handle varying references and stabilizes the engine speed around the desired reference with less than 50 rpm of error. Now that the integral action can handle the reference tracking of Challenge #1 of the idle speed control, the controller can be tested in disturbance rejection conditions.

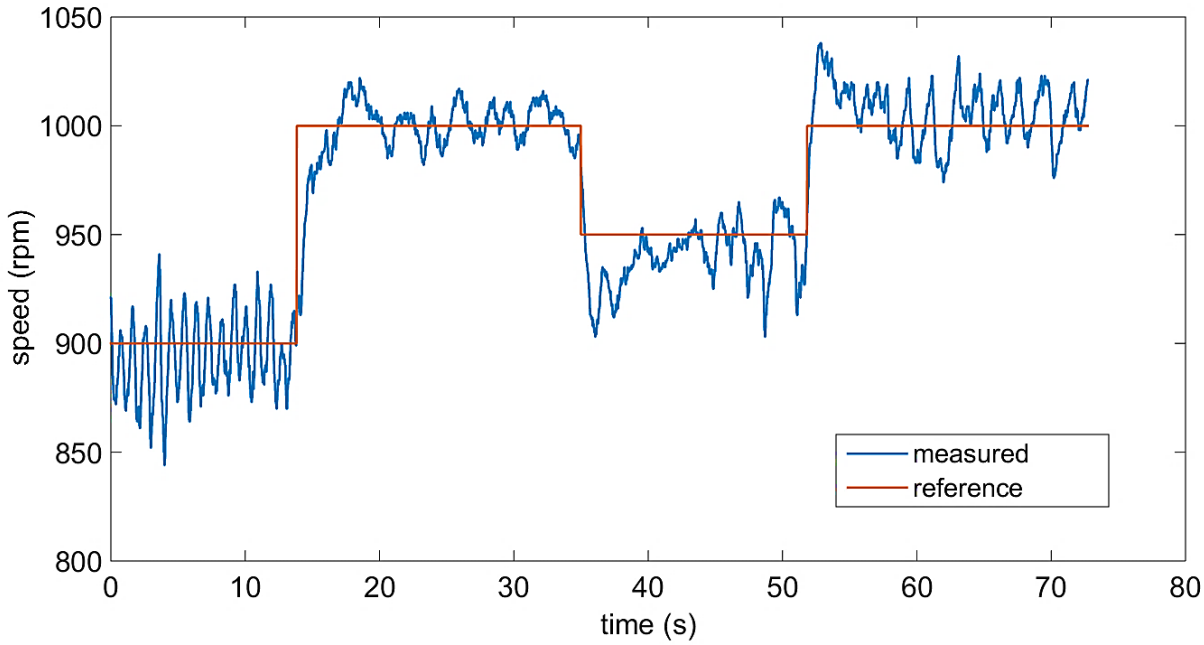

Fig. 87. Idle speed tracking varying references

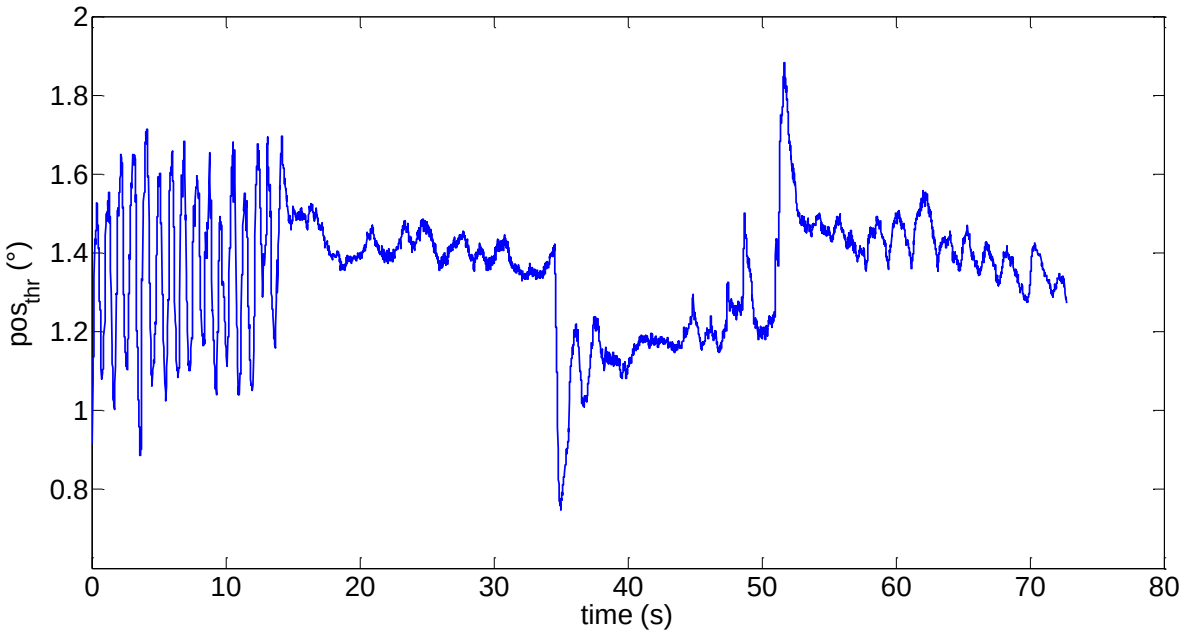

Fig. 88. Command generated by the idle speed controller to track the reference

A second scenario is realized considering external disturbances. These disturbances can be applied on the real engine by using the electric brake of the engine test bench. A ramp disturbance is applied at $t = 12s$ and released at $t = 45s$, creating a load torque from 5 Nm to 15 Nm. Fig. 89 and Fig. 90 present the engine speed and the command signal of the controller respectively. As one can see, the integral action increases the value of the command to reject the disturbance, however, since the load torque is maintained, the controller continues to integrate until the brake is finally released, creating a peak of 100 rpm of error. The engine speed comes back to a satisfying zone around the reference

value in less than 3 seconds $n_{ref} \pm 15rpm$. This validates the controller for handling the Challenge #1 of idle speed.

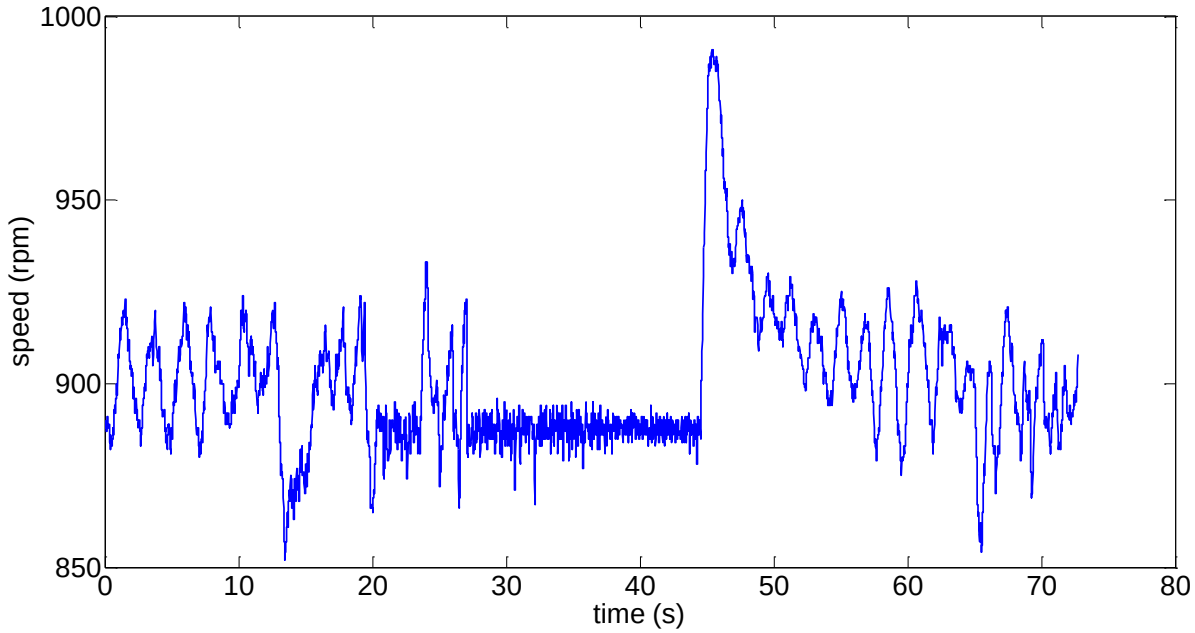

Fig. 89. Idle speed control in presence of external disturbances

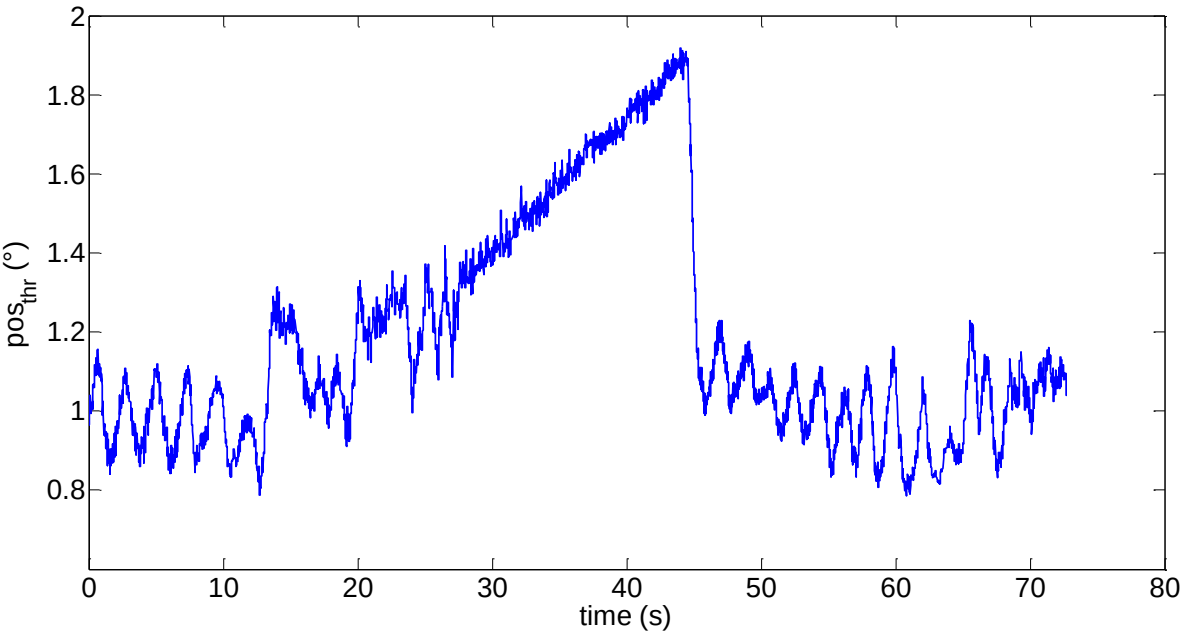

Fig. 90. Command generated by the idle speed controller to face disturbances

The third scenario focuses on other kind of disturbances that may occur while the engine is running at idle speed. For example, a strong input of the driver pedal can quickly increase the engine speed until 3200 rpm before being released (at $t = 15s$). Then, at $t = 57s$, a fault on the first injector appears (injection disabled). The engine is then running on 3 cylinders. Fig. 91 depicts the engine speed. As one can see, the switch between the idle speed controller and the driver pedal needs improvements since the integral action is still running while the engine speed is around 3000 rpm.

Then, when the pedal is released, the command signal was decreasing due to the integral action. It takes time to recover from this kind of disturbance. However, thanks to the anti-windup structure, when the command signal reaches the saturation bound, the integral action is maintained to the saturated value. Moreover, as one can see on the zoom in Fig. 92, the idle speed controller succeeds in tracking the reference value $n_{ref} = 900rpm$ even if a cylinder is disabled by a fault on an injector. Detecting faults on the injectors is explored in the section dedicated to the perspectives of this work. Fig. 93 presents the command generated by the idle speed controller to handle these kind of particular disturbances and faults.

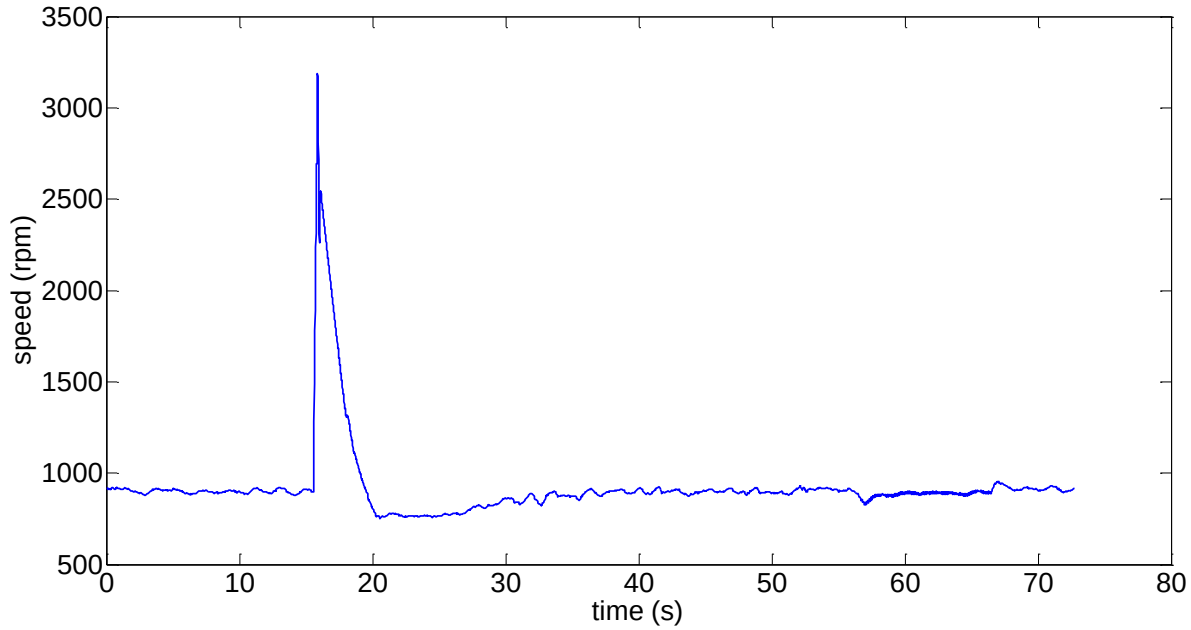

Fig. 91. Engine speed recovering from disturbances and faults

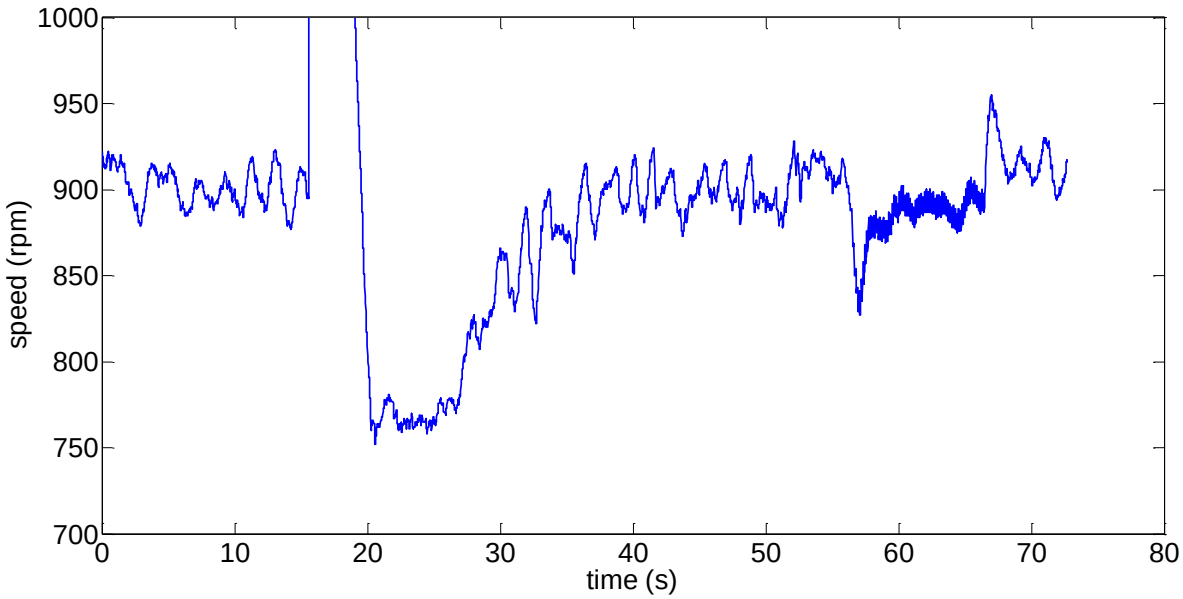

Fig. 92. Zoom of the engine speed in an idle speed frame

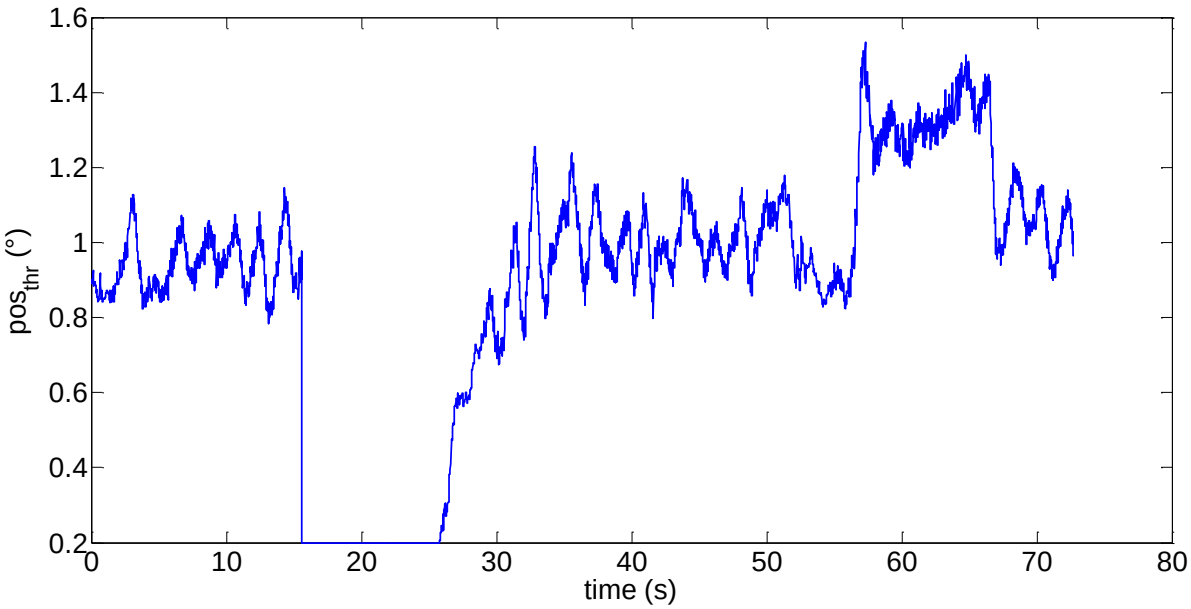

Fig. 93. Command generated by the idle speed controller to handle disturbances and faults

As one can see on this third scenario, the idle speed controller is able to handle a fault on the fuel injection system if one injector is disabled. After investigating the oscillating behavior of the engine speed controlled by the idle speed controller, see for example the experimental results in Fig. 94, it appears that the air-fuel ratio controller, based on static empirical maps, does not provide satisfying performance in controlling the fuel injection to maintain the air-fuel ratio around the stoichiometric value of $\lambda_{ref} = 1$, see the measured air-fuel ratio in Fig. 95. Since the air-fuel ratio is involved in the idle speed model, so in the controller structure, the oscillating behavior of the air-fuel ratio controlled by static maps can explain the oscillations appearing in the engine speed signal even if the idle speed controller implies an integral action.

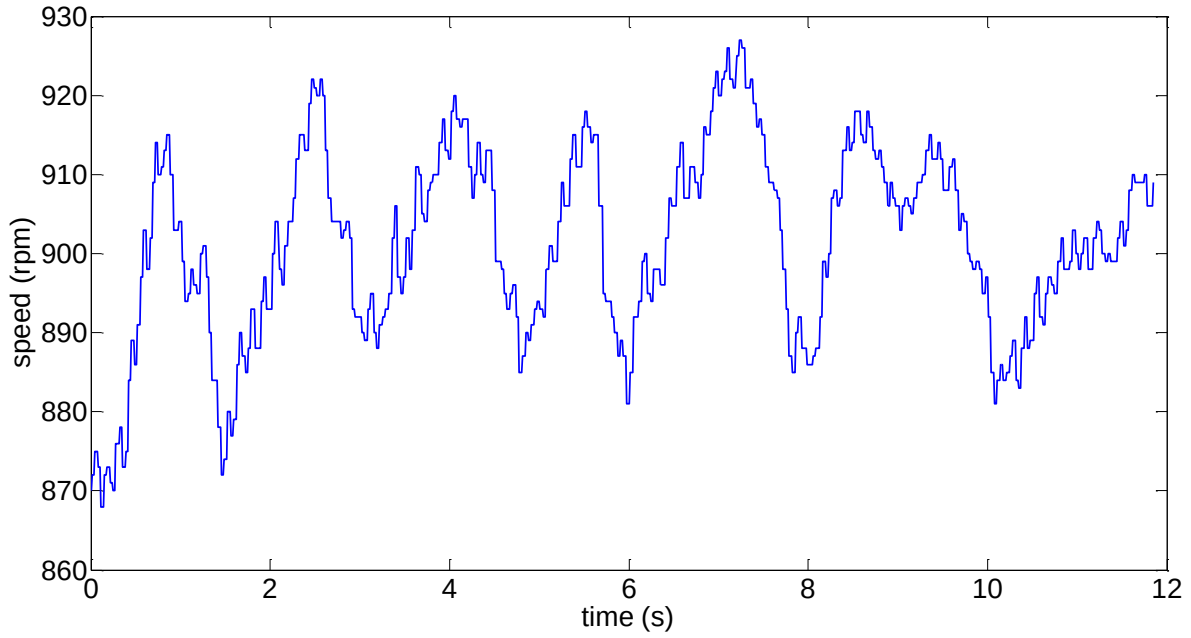

Fig. 94. Idle speed control with maps-based air-fuel ratio control

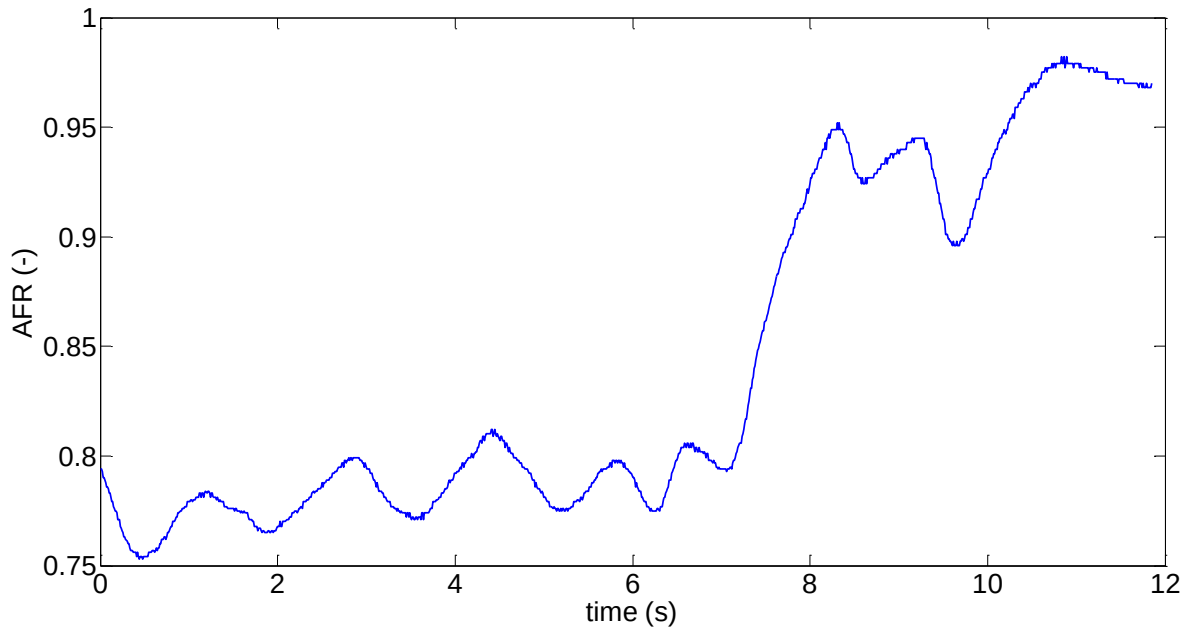

Fig. 95. Air-fuel ratio controlled by static empirical maps

A systematic methodology has been developed to answer the different challenges of idle speed control: Reference tracking, external disturbance rejection, dealing with the nonlinear behavior and unmeasured values such as the engine torque. Due to the complexity of the chosen model which involves the spark advance, an advanced controller has been investigated: a non-PDC controller. However, the structure of the controller involves a real-time matrix inversion. Keeping in mind that the implementation in industrial-like ECUs is the heart of the considered problem, an alternative controller has been proposed. The Lyapunov method has been applied to ensure that the closed-loop system with this new controller is also stable. Both simulation and experimental results have highlighted the efficiency of the proposed controller. It has been illustrated that idle speed control is a complex problem that implies the use of advanced controllers from the field of theory, and their complex structure needs to be adapted for real-time implementation. However, the results could be improved by addressing the problem of air-fuel ratio and fuel injection control, illustrating the problem of interdependency between the control loops. Since the air-fuel ratio model involves time-varying delays and nonlinearities, what kind of fuzzy controller has to be developed to maintain the air-fuel ratio in stoichiometric proportions, i.e. $\lambda_{ref} = 1$?

CHAPTER IV – Air-fuel ratio control

We depended on technology to wash our poisoned nations clean.

T. Karevik (Ayreon) in '*Planet Y Is Alive!*' from *The Source*

1. Air-fuel ratio control

This chapter is dedicated to the design of an air-fuel ratio controller. As already mentioned in the Chapter 1, the air-fuel ratio control is subject to three different challenges: reference tracking and disturbance rejection, variable transport delay and individual control of the injectors. Similarly to the design of the idle speed controller, an integral action can be included to achieve good performances in reference tracking and disturbance rejection. The originality of this chapter is to introduce a new methodology to deal with systems subject to variable transport delay on the input signal. As stated in the Chapter 1, this remains an unsolved problem. As a reminder, this transport delay is variable since it depends on the engine speed $n(k)$:

$$\delta(k) = \frac{\theta_{fix}}{6 \cdot n(k)} \tag{4.1.1}$$

where the fixed part of the delay stands for two engine turns, i.e. $\theta_{fix} = 720$. Fig. 96 and Fig. 97 are depicting the engine speed from the sensor on the engine test bench and the variation of the variable transport delay according to its expression (4.1.1). As one can see, the delay is time-varying and highly changing in normal driving conditions. Moreover, it is more important at the idle speed since it is depending on the inverse of the speed.

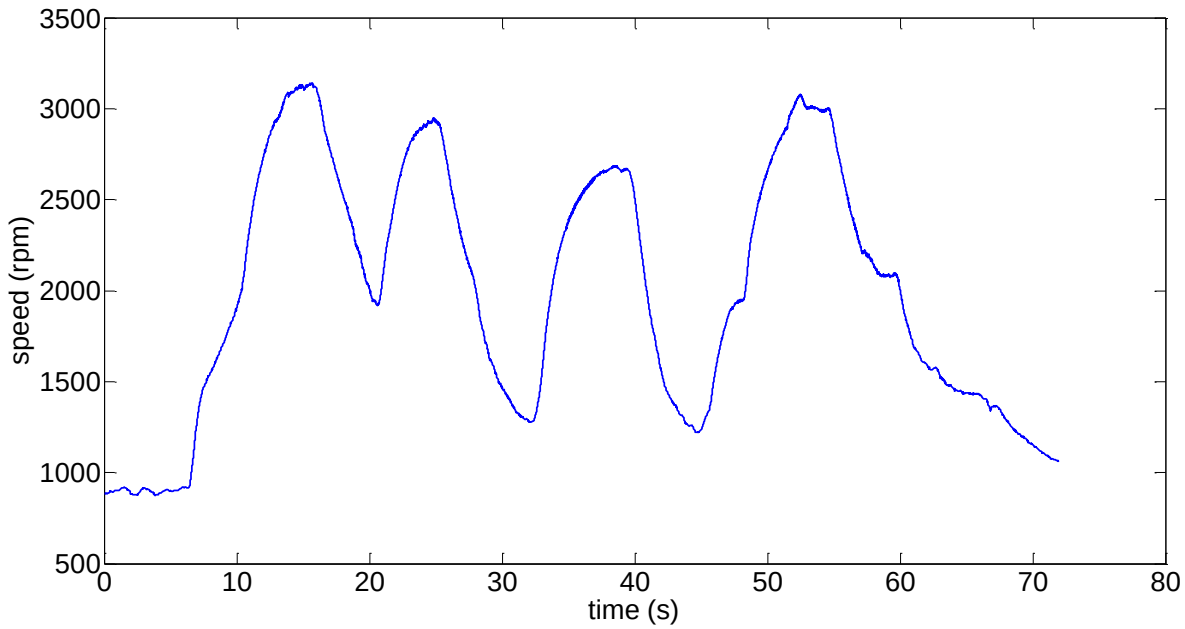

Fig. 96. Engine speed from a dataset collected on the engine test bench

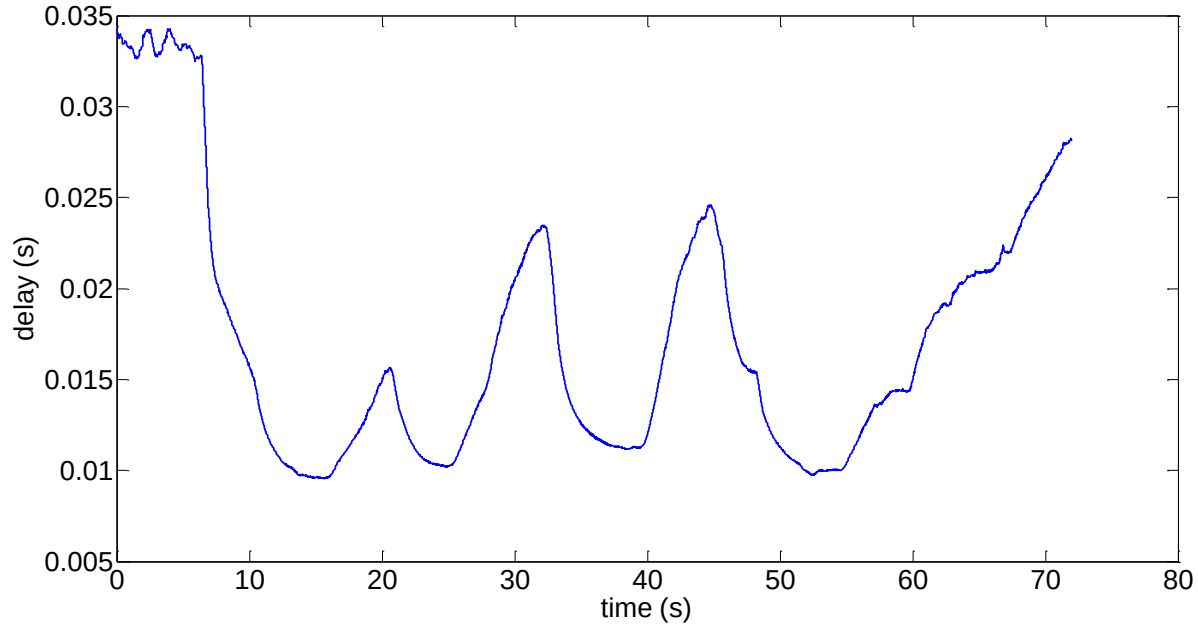

Fig. 97. Variation of the variable transport delay

A model-based controller has been chosen, even if the developed models include nonlinearities and variable delays since the proposed method allows dealing with both of them. A Mean-Value Engine Model (MVEM) has been detailed along Chapter 2, Section 5.2. This model has been converted into the crank-angle domain. It has been modified to include specific engine dynamics such that polynomial gains depending on the speed. Finally, it has been identified.

At the end, the model on which the controller can rely on is expressed as:

$$\lambda^{\theta}(k+1)=\lambda^{\theta}(k)+\frac{T_s^{\theta}}{6\cdot n(k)\cdot\tau_{\lambda}}\left(\frac{K_1(n(k))}{\lambda_s\cdot K_{inj}}\times\frac{m_{air}\left(k-\Upsilon(\delta(k))\right)}{\left(t_{inj}\left(k-\Upsilon(\delta(k))\right)-t_0\right)}-K_2(n(k))\cdot\lambda^{\theta}(k)\right) \quad (4.1.2)$$

With $K_1(k)=b_0+b_1\cdot n(k)+b_2\cdot n(k)^2$, $K_2(k)=c_0+c_1\cdot n(k)+c_2\cdot n(k)^2$ and the constant parameters that have been identified. This chapter details the function $\Upsilon(\bullet)$ which makes the variable transport delay $\delta(k)$ constant in the crank-angle domain. How the crank-angle domain can make a variable delay constant? Is this function $\Upsilon(\bullet)$ only existing in the crank-angle domain, or can it be generalized to any kind of variable transport delay?

The nonlinear behavior of the air-fuel ratio $\lambda^{\theta}(k)$ can be managed using the Takagi-Sugeno representation, as presented in Chapter 2. It stands that an exact TS representation can be obtained from (4.1.2):

$$x_{\lambda}^{\theta}(k+1)=A_{\lambda,z}^{\theta}\cdot x_{\lambda}^{\theta}(k)+B_{\lambda,z}^{\theta}\cdot u_{\lambda}^{\theta}\left(k-\Upsilon(\delta(k))\right) \quad (4.1.3)$$

Where the state and input matrices are:

$$A_{\lambda,z}^{\theta} = 1 - NL_4(k);\ B_{\lambda,z}^{\theta} = NL_5(k) \tag{4.1.4}$$

With the nonlinearities:

$$\begin{cases} NL_4(k) = \dfrac{T_s^{\theta} \cdot K_2(k)}{6 \cdot \tau_{\lambda} \cdot n(k)} \\ NL_5(k) = \dfrac{T_s^{\theta} \cdot K_1(k) \cdot \dot{m}_{air}\left(k - \Upsilon\left(\delta(k)\right)\right)}{6 \cdot \tau_{\lambda} \cdot \lambda_s \cdot K_{inj} \cdot n(k)} \end{cases} \tag{4.1.5}$$

Similarly to the methodology detailed in Chapter 3, since the model is under a Takagi-Sugeno form, fuzzy controllers can be developed. Even if the variable transport delay $\delta(k)$ becomes constant in the crank-angle domain thanks to the function $\Upsilon(\bullet)$, the input signal is still delayed. What is the impact of a constant delay in the design of a fuzzy controller? Is the complexity of the system too important so a PDC controller is not working, like the idle speed problem, and a non-PDC should be considered? Or is a linear state feedback enough once the state has been augmented with an integral action, and the gains obtained solving a LMI problem?

2. Variable transport delay

The air-fuel ratio system is subject to variable transport delay. Indeed, this delay is called transport delay since it is related to the location of a remoted sensor compared with the measured phenomenon where the input acts. Because it is dependent on the dynamics of the considered system, it is then variable or time-varying according to a certain variable. Concerning the air-fuel ratio system, the delay exists due to the location of the lambda sensor in the exhaust manifold while the air-fuel mixture is created inside the cylinder. It is commonly introduced in the literature as:

$$\delta(t) = \frac{\theta_{fix}}{\dot{\theta}(t)} \tag{4.2.1}$$

and is expressed in seconds. As a general point of view, $\theta(t)$ represents the variable whose delay is dependent. In the case of the air-fuel ratio, it stands for the crank angle and $\dot{\theta}(t)$ for the angular velocity. Then, the crank-angle domain transformation is proposed in Chapter 2. However, considering any system subject to variable transport delay, it is possible to find a transformation into a new domain, depending on $\theta(t)$. Even if it has been mainly used in engine control, the crank-angle domain transformation can be generalized and extended to any kind of domain, such as the meter domain (for example considering the conveyor belt problem) or the liter domain (considering the pipe flow problem). The following method is written as a generalized methodology that can be applied to any kind of system subject to variable transport delay (Laurain et al., 2017b).

The advantage for delayed systems to be transformed into such domains is that, since these domains are depending on the same variable as the variable transport delay, then this one becomes constant thanks to the function $\Upsilon(\bullet)$ introduced in (4.1.2). This function has to convert the time-varying delay $\delta(t)$ expressed in seconds into the new θ-domain, i.e. the crank-angle domain for the considered application, where it is expressed in the θ-unit. In order to respect the coherence of the units, it stands:

$$\Upsilon\left(\delta(t)\right) = \dot{\theta}(t) \cdot \delta(t) \tag{4.2.2}$$

Then, the variable transport delay can be fixed by considering an adequate sampling period T_s^θ (which is not in time but in θ-units, i.e. in crankshaft angles) such that the delay in the discrete domain is expressed as:

$$k - \Upsilon(\delta) = k - \mu_\delta \cdot T_s^\theta \tag{4.2.3}$$

where μ_δ is a constant integer chosen such that the delay is now expressed in number of samples according to the sampling period T_s^θ. Since they are connected in equation (4.2.3), the two variables T_s^θ and μ_δ can be obtained by fixing one and getting the other one:

$$T_s^\theta = \frac{\dot{\theta}(k) \cdot \delta(k)}{\mu_\delta} \leftrightarrow \mu_\delta = \frac{\dot{\theta}(k) \cdot \delta(k)}{T_s^\theta} \tag{4.2.4}$$

Taking into account that, considering the IC engine, $\theta_{fix} = 720$ crankshaft degrees and the sampling period has already been chosen according to the sensors equipment as $T_s^\theta = 180$ crankshaft degrees, the value of the constant delay expressed as a difference of samples can be obtained:

$$\mu_\delta = \frac{\dot{\theta}(k) \cdot \delta(k)}{T_s^\theta} = \frac{\theta_{fix}}{T_s^\theta} = 4 \tag{4.2.5}$$

Remark (Sampling period): In real-world applications, as the IC engine, the choice of the sampling period is usually constrained by the sensors equipment so that the constant delay cannot take any value (since it has to be an integer, the sampling period is also a multiple of the fixed part of the variable transport delay θ_{fix})

Now that the variable transport delay $\delta(t)$ has become constant in the crank-angle domain, the final air-fuel model can be written as:

$$\lambda^\theta(k+1) = \lambda^\theta(k) + \frac{T_s^\theta}{6 \cdot n(k) \cdot \tau_\lambda} \left(\frac{K_1\left(n(k)\right) \cdot m_{air}(k-4)}{\lambda_s \cdot K_{inj}\left(t_{inj}(k-4) - t_0\right)} - K_2\left(n(k)\right) \cdot \lambda^\theta(k) \right) \tag{4.2.6}$$

and its Takagi-Sugeno representation:

$$x_\lambda^\theta(k+1) = A_{\lambda,z}^\theta \cdot x_\lambda^\theta(k) + B_{\lambda,z}^\theta \cdot u_\lambda^\theta(k-4) \tag{4.2.7}$$

Where the state and input matrices are:

$$A_{\lambda,z}^{\theta} = 1 - NL_4(k);\ B_{\lambda,z}^{\theta} = NL_5(k) \tag{4.2.8}$$

With the nonlinearities:

$$\begin{cases} NL_4(k) = \dfrac{T_s^{\theta} \cdot K_2(k)}{6 \cdot \tau_{\lambda} \cdot n(k)} \\ NL_5(k) = \dfrac{T_s^{\theta} \cdot K_1(k) \cdot \dot{m}_{air}(k-4)}{6 \cdot \tau_{\lambda} \cdot \lambda_s \cdot K_{inj} \cdot n(k)} \end{cases} \tag{4.2.9}$$

Now that the delay is constant, the system is written as a delayed-input TS model. How to deal with constant delay on the input signal? What kind of fuzzy controller can be designed?

3. Controller design

3.1. Delayed input system

The air-fuel ratio, when the delay is considered, appears to be a system with time-varying delay on the control input signal. If the delay is constant, several methods exist to deal with it. In the frequency domain, it can be managed using a Smith predictor. Smith predictors have been adapted to the case of variable delays in (De Oliveira et al., 2017). In the state space in presence of constant delays, known or not, the developed methodologies are based on Lyapunov-Krasovskii as well as Lyapunov-Razumikhin theory, getting LMI conditions for stability, as presented in (Souza et al., 2001; Fridman et al., 2008; Fridman and Dambrine, 2009; Fridman, 2014). In the case of TS models subject to delays, several methodologies have been developed, mainly by including the delay inside the Lyapunov function to get delay-dependent LMI conditions (Yoneyama, 2007; Souza et al., 2009a, 2009b, 2014; Al-Hadithi et al., 2015; Bourahala et al., 2016; Lian et al., 2017; Wang and Liu, 2017; Xu et al., 2017)

However, most of the time, the delay is time-varying and unknown, which leads to conservative stability conditions and complex control laws. It is then a problem for both theoretical contributions (Dambrine and Richard, 1993; Zheng et al., 2015) and real-time applications (Blandeau et al., 2016).

In the considered application, thanks to the transformation to the crank-angle domain, the variable transport delay $\delta(t)$ becomes constant and equal to an integer $\mu_{\delta} = 4$ as a difference of sample according to the sampling period T_s^{θ}. This allows including the constant delay directly into the controller design, so the conditions are easier to verify and the control law can be simple. The first proposed method is to include the delay in the Lyapunov candidate function.

3.2. Delay-in-the-Lyapunov-function controller

The considered system of the air-fuel ratio problem has been written under the form of a TS fuzzy model with constant and known delayed input, see equation (4.2.7). Since it is known and constant, the delay can be included into the design of the controller, for example inside the candidate

Lyapunov function used to ensure the stability of the closed-loop system applying the Lyapunov direct method.

In order to get a simple controller that can be implemented in an industrial application, i.e. that can be embedded in an industrial ECU and tunable for engine technicians, let us consider a linear state-feedback controller:

$$u_\lambda^\theta(k) = -F_\lambda^\theta \cdot x_\lambda^\theta(k) \tag{4.3.1}$$

where F_λ^θ is the controller gain. Then, the whole closed-loop system can be obtained by replacing (4.3.1) into the TS fuzzy model (4.2.7):

$$x_\lambda^\theta(k+1) = A_{\lambda,z}^\theta \cdot x_\lambda^\theta(k) - B_{\lambda,z}^\theta \cdot F_\lambda^\theta \cdot x_\lambda^\theta(k-4) \tag{4.3.2}$$

In order to apply the Finsler's lemma already presented in Chapter 3, equation (3.2.8), equation (4.3.2) is written:

$$\begin{bmatrix} A_{\lambda,z}^\theta & -I & -B_{\lambda,z}^\theta \cdot F_\lambda^\theta \end{bmatrix} \begin{bmatrix} x_\lambda^\theta(k) \\ x_\lambda^\theta(k+1) \\ x_\lambda^\theta(k-4) \end{bmatrix} = 0 \tag{4.3.3}$$

Similarly to the design of the idle speed controller, the Lyapunov direct method can be used to ensure the stability of the closed-loop system, so a Lyapunov candidate function is defined. This function has to be decreasing such that:

$$V_\lambda(k+1) - V_\lambda(k) < 0 \tag{4.3.4}$$

with $V_\lambda(k)$ the Lyapunov function. As mentioned, the advantage of having a constant and known delay is that it can be taken into account during the design of the controller. The first methodology aims to introduce the constant delay in the Lyapunov candidate function such that:

$$V_\lambda(k) = x_\lambda^\theta(k)^T \cdot P_\lambda \cdot x_\lambda^\theta(k) + \sum_{i=k-\mu_\delta}^{k-1} x_\lambda^\theta(i)^T \cdot Q_\lambda \cdot x_\lambda^\theta(i) \tag{4.3.5}$$

In order to apply the Finsler's lemma, the inequality (4.3.4) can be written considering equation (4.3.5):

$$\begin{bmatrix} x_\lambda^\theta(k) \\ x_\lambda^\theta(k+1) \\ x_\lambda^\theta(k-4) \end{bmatrix}^T \begin{bmatrix} -P_\lambda + Q_\lambda & 0 & 0 \\ 0 & P_\lambda & 0 \\ 0 & 0 & -Q_\lambda \end{bmatrix} \begin{bmatrix} x_\lambda^\theta(k) \\ x_\lambda^\theta(k+1) \\ x_\lambda^\theta(k-4) \end{bmatrix} < 0 \tag{4.3.6}$$

Then, the Finsler's lemma previously detailed can be applied. It stands:

$$M \cdot \begin{bmatrix} A_{\lambda,z}^\theta & -I & -B_{\lambda,z}^\theta \cdot F_\lambda^\theta \end{bmatrix} + (*) + \begin{bmatrix} -P_\lambda + Q_\lambda & 0 & 0 \\ 0 & P_\lambda & 0 \\ 0 & 0 & -Q_\lambda \end{bmatrix} < 0 \tag{4.3.7}$$

with $M = \begin{bmatrix} 0 \\ M_{2zz}^{-1} \\ M_3^{-1} \end{bmatrix}$. Equation (4.3.7) can be written as a nonlinear matrix inequality:

$$\begin{bmatrix} -P_\lambda + Q_\lambda & (*) & (*) \\ M_{2zz}^{-1} \cdot A_{\lambda,z}^{\theta} & -M_{2zz}^{-1} - M_{2zz}^{-T} + P_\lambda & (*) \\ M_3^{-1} \cdot A_{\lambda,z}^{\theta} & -M_3^{-1} - F_\lambda^{\theta,T} \cdot B_{\lambda,z}^{\theta,T} \cdot M_{2zz}^{-T} & -M_3^{-1} \cdot B_{\lambda,z}^{\theta} \cdot F_\lambda^{\theta} + (*) - Q_\lambda \end{bmatrix} < 0 \tag{4.3.8}$$

The product terms can be managed considering matrix transformations such as a congruence with $diag(X, M_{2zz}, M_3)$ where $X = P_\lambda^{-1}$, Schur complements and changes of variables $F_\lambda \cdot Q_\lambda^{-1} = W$ such that the inequality (4.3.8) is equivalent to:

$$\begin{bmatrix} -X & (*) & (*) & (*) & (*) \\ X & -Q_\lambda^{-1} & (*) & (*) & (*) \\ A_{\lambda,z}^{\theta} \cdot X & 0 & -M_{2zz} - M_{2zz}^{T} & (*) & (*) \\ 0 & 0 & M_{2zz}^{T} & -X & (*) \\ A_{\lambda,z}^{\theta} \cdot X & 0 & -W^T \cdot B_{\lambda,z}^{\theta,T} - M_{2zz}^{T} & 0 & -B_{\lambda,z}^{\theta} \cdot W + (*) - Q_\lambda^{-1} \end{bmatrix} < 0 \tag{4.3.9}$$

LMI conditions can be obtained from the inequality (4.3.9) by removing the membership functions using the relaxation of Tuan as already presented in equation (3.3.20) considering the following quantity:

$$\Upsilon_{ij} = \begin{bmatrix} -X & (*) & (*) & (*) & (*) \\ X & -Q_\lambda^{-1} & (*) & (*) & (*) \\ A_{\lambda,i}^{\theta} \cdot X & 0 & -M_{2ij} - M_{2ji}^{T} & (*) & (*) \\ 0 & 0 & M_{2ji}^{T} & -X & (*) \\ A_{\lambda,i}^{\theta} \cdot X & 0 & -W^T \cdot B_{\lambda,i}^{\theta,T} - M_{2ji}^{T} & 0 & -B_{\lambda,i}^{\theta} \cdot W + (*) - Q_\lambda^{-1} \end{bmatrix} \tag{4.3.10}$$

Remark (Decay-rate): A decay-rate β can be added to accelerate the convergence of the Lyapunov function, such that the relaxation of Tuan can be applied on the new quantity:

$$\Upsilon_{ij} = \begin{bmatrix} -\beta \cdot X & (*) & (*) & (*) & (*) \\ X & -Q_\lambda^{-1} & (*) & (*) & (*) \\ A_{\lambda,i}^{\theta} \cdot X & 0 & -M_{2ij} - M_{2ji}^{T} & (*) & (*) \\ 0 & 0 & M_{2ji}^{T} & -X & (*) \\ A_{\lambda,i}^{\theta} \cdot X & 0 & -W^T \cdot B_{\lambda,i}^{\theta,T} - M_{2ji}^{T} & 0 & -B_{\lambda,i}^{\theta} \cdot W + (*) - Q_\lambda^{-1} \end{bmatrix} \tag{4.3.11}$$

Remark (PDC controller): Less conservative results can be obtained by considering a PDC controller, i.e. including the membership functions in the controller gain: $u_\lambda^{\theta}(k) = -F_{\lambda,z}^{\theta} \cdot x_\lambda^{\theta}(k)$. However, the delay directly impacts the membership functions when the closed-loop system is written. Equation (4.3.2) becomes:

$$x_\lambda^{\theta}(k+1) = A_{\lambda,z}^{\theta} \cdot x_\lambda^{\theta}(k) - B_{\lambda,z}^{\theta} \cdot F_{\lambda,z-4}^{\theta} \cdot x_\lambda^{\theta}(k-4) \tag{4.3.12}$$

where $F_{\lambda,z-4}^{\theta}$ stands for $\sum_{i=1}^{r} h_i\left(k-4\right)\cdot F_{\lambda,i}^{\theta}$. The obtained LMI conditions are similar to the ones with the quantity (4.3.10), however, since $F_{\lambda,z-4}^{\theta}$ appears, the relaxation of Tuan cannot be used to remove the membership functions and the matrix inequality has to be verified for every i and j in $\{1,\ldots,r\}$.

3.3. Reference tracking

The first challenge of the air-fuel ratio control is the reference tracking. In addition, maintaining a constant reference also implies external disturbance rejection. Like in PI controller design, one of the methodologies to realize a reference tracking is to augment the state vector by including an integral action, as it has been presented for the idle speed control. The state vector dedicated to the air-fuel ratio problem can similarly be augmented: $\bar{x}_{\lambda}^{\theta}\left(k\right)=\begin{bmatrix} x_{\lambda}^{\theta}\left(k\right) \\ e_{\lambda}^{\theta}\left(k\right) \end{bmatrix}$ where $e_{\lambda}^{\theta}\left(k\right)$ stands for the error between the reference and the current state, i.e. $e_{\lambda}^{\theta}\left(k\right)=\lambda_{ref}-\lambda^{\theta}\left(k\right)$. The new system can be written:

$$\bar{A}_{\lambda,z}^{\theta}=\begin{bmatrix} A_{\lambda,z}^{\theta} & 0 \\ -C_{\lambda,z}^{\theta} & 1 \end{bmatrix}, \bar{B}_{\lambda,z}^{\theta}=\begin{bmatrix} B_{\lambda,z}^{\theta} \\ 0 \end{bmatrix} \tag{4.3.13}$$

with $C_{\lambda}^{\theta}=\frac{T_s^{\theta}}{6\cdot n\left(k\right)}$ and the corresponding fuzzy matrix $C_{\lambda,z}^{\theta}$. However, by considering these new matrices (4.3.13), the LMI conditions associated with the quantity (4.3.10) are unfeasible no matter the chosen domain of validity. This is due to the inclusion of the delay inside the Lyapunov function. In order to achieve the Challenge #1 and to obtain a static gain such as the static state reaches the reference value, a term is added to the control law. It is adapted from the linear state-feedback design method presented in (Khalil, 1996) and transformed into the TS fuzzy framework as in (Lauber et al., 2003):

$$u_{\lambda}^{\theta}\left(k\right)=-F_{\lambda}^{\theta}\cdot\bar{x}_{\lambda}^{\theta}\left(k\right)+v_{\lambda}\left(k\right) \tag{4.3.14}$$

with:

$$v_{\lambda}\left(k\right)=\frac{\lambda_{ref}}{\left(I-A_{\lambda,z}^{\theta}+B_{\lambda,z}^{\theta}\cdot F_{\lambda}^{\theta}\right)^{-1}\cdot B_{\lambda,z}^{\theta}} \tag{4.3.15}$$

If this new term allows reaching the reference value, it is only valuable in static phases. The air-fuel ratio controller should obtain performances also in the transient phases since the engine is working in these dynamic phases in normal driving conditions.

Then, there is a need for less conservative conditions. Including the delay in the Lyapunov function is too restrictive and does not provide any feasible solution to the LMI problem while adding an integral action. According to the different sources of conservativeness already presented, in order to get

more flexible conditions, changes can be operated in: the TS model, the control law, the Lyapunov function or the relaxation. The hypothesis is made that including the delay directly in the state vector, i.e. obtaining a new TS model, should provide less conservative conditions since it will become a standard problem with a linear state-feedback and a quadratic Lyapunov function addressed in (Guerra and Vermeiren, 2004).

3.4. Delay-in-the-state controller

This second methodology proposes including the delay directly inside the state vector since it is known and constant in the crank-angle domain. Let us consider the state-space Takagi-Sugeno representation with the augmented state including the integral action for reference tracking:

$$\bar{x}_\lambda^\theta(k+1) = \bar{A}_{\lambda,z}^\theta \cdot \bar{x}_\lambda^\theta(k) + \bar{B}_{\lambda,z}^\theta \cdot u_\lambda^\theta(k-4) \tag{4.3.16}$$

Now, let us introduce the new control inputs $\{v_1(k),\ldots,v_4(k)\}$ such that equation (4.3.16) can be written:

$$\begin{cases} \bar{x}_\lambda^\theta(k+1) = \bar{A}_{\lambda,z}^\theta \cdot \bar{x}_\lambda^\theta(k) + \bar{B}_{\lambda,z}^\theta \cdot v_1(k) \\ v_1(k+1) = v_2(k) = u_\lambda^\theta(k-3) \\ \vdots \\ v_4(k+1) = u_\lambda^\theta(k) \end{cases} \tag{4.3.17}$$

Remark (Generalization): Note that this design methodology can be applied to any system with known and constant delay:

$$\begin{cases} x^\theta(k+1) = A_z x^\theta(k) + B_z v_1(k) \\ v_1(k+1) = v_2(k) = u^\theta\left(k-\left(\left(\mu_\delta-1\right)\right)\right) \\ \vdots \\ v_{\mu_\delta}(k+1) = u^\theta(k) \end{cases} \tag{4.3.18}$$

Since the transformation to the new θ domain can be generalized and applied to any system subject to variable transport delay, i.e. it is always possible to find a θ domain where the delay becomes known and constant, then the controller design methodology proposed in this chapter can be generalized to any constant transport delay μ_δ.

Since the controller is triggered whenever a dead center is reached, i.e. $T_s^\theta = 180$, then the delay is equal to 4 samples, so the state vector has to be augmented such that equation (4.3.17) is written:

$$\breve{x}_\lambda^\theta(k+1) = \breve{A}_{\lambda,z}^\theta \cdot \breve{x}_\lambda^\theta(k) + \breve{B}_{\lambda,z}^\theta \cdot u_\lambda^\theta(k) \tag{4.3.19}$$

with the new state vector:

$$\breve{x}_\lambda^\theta(k)^T = \left[\bar{x}_\lambda^\theta(k)^T \quad u_\lambda^\theta(k-4)^T \quad u_\lambda^\theta(k-3)^T \quad u_\lambda^\theta(k-2)^T \quad u_\lambda^\theta(k-1)^T \quad e_\lambda^\theta(k)^T\right]^T \tag{4.3.20}$$

and the matrices of the system:

$$\breve{A}_{\lambda,z}^{\theta}=\begin{bmatrix} A_{\lambda,z}^{\theta} & B_{\lambda,z}^{\theta} & 0 & 0 & 0 & 0 & 0 \\ 0 & 0 & 1 & 0 & 0 & 0 & 0 \\ 0 & 0 & 0 & 1 & 0 & 0 & 0 \\ 0 & 0 & 0 & 0 & 1 & 0 & 0 \\ 0 & 0 & 0 & 0 & 0 & 1 & 0 \\ 0 & 0 & 0 & 0 & 0 & 0 & 0 \\ -C_{\lambda,z}^{\theta} & 0 & 0 & 0 & 0 & 0 & 1 \end{bmatrix},\quad \breve{B}_{\lambda,z}^{\theta}=\begin{bmatrix} 0 \\ 0 \\ 0 \\ 0 \\ 0 \\ 1 \\ 0 \end{bmatrix} \tag{4.3.21}$$

3.4.1. Linear state-feedback

Considering the same linear state-feedback controller (4.3.1), the closed-loop system stands for:

$$\breve{x}_{\lambda}^{\theta}\left(k+1\right)=\breve{A}_{\lambda,z}^{\theta}\cdot\breve{x}_{\lambda}^{\theta}\left(k\right)-\breve{B}_{\lambda,z}^{\theta}\cdot F_{\lambda}^{\theta}\cdot\breve{x}_{\lambda}^{\theta}\left(k\right) \tag{4.3.22}$$

where F_{λ}^{θ} is the controller matrix gain of appropriate size 1×7.

Then, the LMI conditions can be easily obtained to ensure the stability of the whole closed-loop system (4.3.22) from (Guerra and Vermeiren, 2004) since the delay is no longer applied to the control input. The Lyapunov direct method is used to guarantee the stability considering a quadratic Lyapunov function such that:

$$V_{\lambda}\left(k\right)=\breve{x}_{\lambda}^{\theta}\left(k\right)^{T}\cdot P_{\lambda}\cdot\breve{x}_{\lambda}^{\theta}\left(k\right) \tag{4.3.23}$$

Then, matrix inequalities can be obtained. Since they imply only one product of membership functions, the relaxation of Tuan is not mandatory. The stability is ensured if the following quantity:

$$\Upsilon_{i}=\begin{bmatrix} X & \left(*\right) \\ \breve{A}_{\lambda,i}^{\theta}\cdot X-\breve{B}_{\lambda,i}^{\theta}\cdot F_{\lambda}^{\theta} & X \end{bmatrix} \tag{4.3.24}$$

verifies $\Upsilon_{i}>0,\quad\forall i\in\left\{1,\ldots,r\right\}$ where $X=P_{\lambda}^{-1}$.

Remark (Decay rate): A decay-rate can be added to accelerate the convergence of the Lyapunov function, such that the new quantity that has to verify $\Upsilon_{i}>0,\quad\forall i\in\left\{1,\ldots,r\right\}$ stands for:

$$\Upsilon_{i}=\begin{bmatrix} \beta\cdot X & \left(*\right) \\ \breve{A}_{\lambda,i}^{\theta}\cdot X-\breve{B}_{\lambda,i}^{\theta}\cdot F_{\lambda}^{\theta} & X \end{bmatrix} \tag{4.3.25}$$

3.4.2. PDC controller

Instead of a linear state-feedback, which is easy to implement (only one gain) but can be more conservative, a PDC controller can be designed taking into account the membership functions of the Takagi-Sugeno model (4.3.19):

$$u_\lambda^\theta(k) = -F_{\lambda,z}^\theta \cdot \breve{x}_\lambda^\theta(k) \tag{4.3.26}$$

Then, the new closed-loop system considering the control law (4.3.26) and the system (4.3.19) stands for:

$$\breve{x}_\lambda^\theta(k+1) = A_{\lambda,z}^\theta \cdot \breve{x}_\lambda^\theta(k) - B_{\lambda,z}^\theta \cdot F_{\lambda,z}^\theta \cdot \breve{x}_\lambda^\theta(k) \tag{4.3.27}$$

The same quadratic Lyapunov function $V_\lambda(k) = \breve{x}_\lambda^\theta(k)^T \cdot P_\lambda \cdot \breve{x}_\lambda^\theta(k)$ as in (4.3.23) is considered in order to apply the direct Lyapunov method. By replacing $\breve{x}_\lambda^\theta(k+1)$ by its value in (4.3.27), $\Delta V_\lambda < 0 \leftrightarrow V_\lambda(k+1) - V_\lambda(k) < 0$ can be written:

$$\left(A_{\lambda,z}^\theta - B_{\lambda,z}^\theta \cdot F_{\lambda,z}^\theta\right)^T \cdot P_\lambda \cdot \left(A_{\lambda,z}^\theta - B_{\lambda,z}^\theta \cdot F_{\lambda,z}^\theta\right) - P_\lambda < 0 \tag{4.3.28}$$

Remark (non-quadratic Lyapunov function): Instead of a quadratic Lyapunov function, a non-quadratic Lyapunov function such that:

$$V_\lambda(k) = \breve{x}_\lambda^\theta(k)^T \cdot P_{\lambda,z} \cdot \breve{x}_\lambda^\theta(k) \tag{4.3.29}$$

can be used since the development of LMI conditions are known from (Guerra and Vermeiren, 2004). However, the objective is to validate the systematic methodology for designing an air-fuel ratio controller, not to obtain the least conservative conditions.

In order to transform the inequality (4.3.28) into a matrix inequality, the Schur complement is applied:

$$\begin{bmatrix} -P_\lambda & (*) \\ A_{\lambda,z}^\theta - B_{\lambda,z}^\theta \cdot F_{\lambda,z}^\theta & -P_\lambda^{-1} \end{bmatrix} < 0 \tag{4.3.30}$$

Finally, a congruence with $diag\left(P_\lambda^{-1}, I\right)$ and the following changes of variable $X = P_\lambda^{-1}$ and $G_z = F_{\lambda,z}^\theta \cdot X$ lead to:

$$\begin{bmatrix} -X & (*) \\ A_{\lambda,z}^\theta \cdot X - B_{\lambda,z}^\theta \cdot G_z & -X \end{bmatrix} < 0 \tag{4.3.31}$$

Since it involves a double-product of membership functions (term $B_{\lambda,z}^\theta \cdot G_z$), the relaxation of Tuan can be used to get less conservative results than verifying the inequality $\forall i, j \in \{1, \ldots, r\}$, considering the quantity:

$$\Upsilon_{ij} = \begin{bmatrix} -X & (*) \\ A_{\lambda,i}^{\theta} \cdot X - B_{\lambda,i}^{\theta} \cdot G_j & -X \end{bmatrix} \tag{4.3.32}$$

Remark (non-PDC controller): A trade-off between performance and complexity has to be realized since a non-PDC controller can be used. As already mentioned in Chapter 3, Section 4.1, the use of non-PDC controllers embedded in an industrial ECU can be costly from a computational point of view.

4. Air-fuel ratio controller

The air-fuel ratio problem was concerned by several challenges, including the reference tracking, the external disturbance rejection, the nonlinear behavior and the variable transport delay.

In the proposed Mean-Value Engine Model, the fact that the air-fuel ratio is measured at the location of the UEGO sensor is represented by a variable transport delay. This delay is time-varying since it is dependent on the engine speed, according to equation (4.1.1). However, the transformation of the continuous-time domain model to a domain depending on the crankshaft angle offers the possibility to make the variable transport delay constant (and known). Indeed, since the delay expression is related to the engine speed, by going to a domain whose sampling value T_s^{θ} is expressed in crank angles, the delay becomes a difference of samples according to T_s^{θ}, see equations (4.2.3) to (4.2.5). This transformation can be extended to any kind of variable transport delay so the methodology can be applied for other systems than the engine control. However, due to the crank-angle domain transformation, one nonlinearity always appears. In order to manage the nonlinear behavior of the crank-angle model, the Takagi-Sugeno representation is used.

4.1. First methodology

4.1.1. Controller gains

Once the variable transport delay is constant and known, a linear controller can be designed. A first methodology that has been investigated is to consider the delay as part of the Lyapunov function for applying the direct Lyapunov method in order to ensure the stability of the whole closed-loop system. Thanks to such a methodology, LMI conditions (4.3.25) can be obtained. The decay-rate is fixed to $\beta = 0.98$ and the gain of the linear controller (4.3.1) is obtained by solving the LMI conditions:

$$F = -0.2973 \tag{4.4.1}$$

Inside the following domain of validity:

$$n(k) \in [700, 3500] \quad \dot{m}_{air}(k) \in [0.0139, 0.0278] \tag{4.4.2}$$

4.1.2. Simulation results

A simulation is then realized. The controller is triggered every 180 crankshaft degrees according to an engine speed measured on the engine test bench. The controller is applied on the continuous-time

model (2.3.8). Both the model and the controller are fed with the air mass flow collected on the engine test bench, so there is no need to add artificial noise to recreate experimental conditions. A first simulation is realized with an idle speed dataset. Fig. 98 presents the engine speed signal chosen to feed the model and the controller. Fig. 99 depicts the results of the simulation with the air-fuel ratio of the model controlled by the linear state-feedback (4.3.1) with the gain (4.4.1). Fig. 100 presents the command generated by the controller triggered every 180 crankshaft degrees and applied to all the injectors.

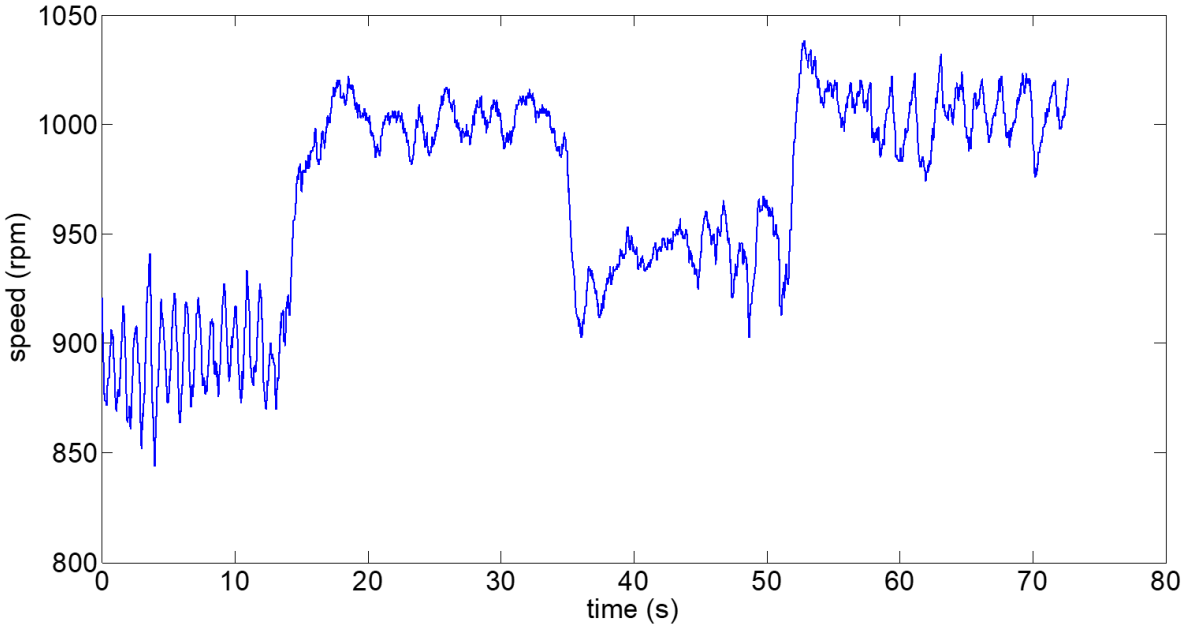

Fig. 98. Engine speed signal from the engine test bench dataset : idle speed conditions

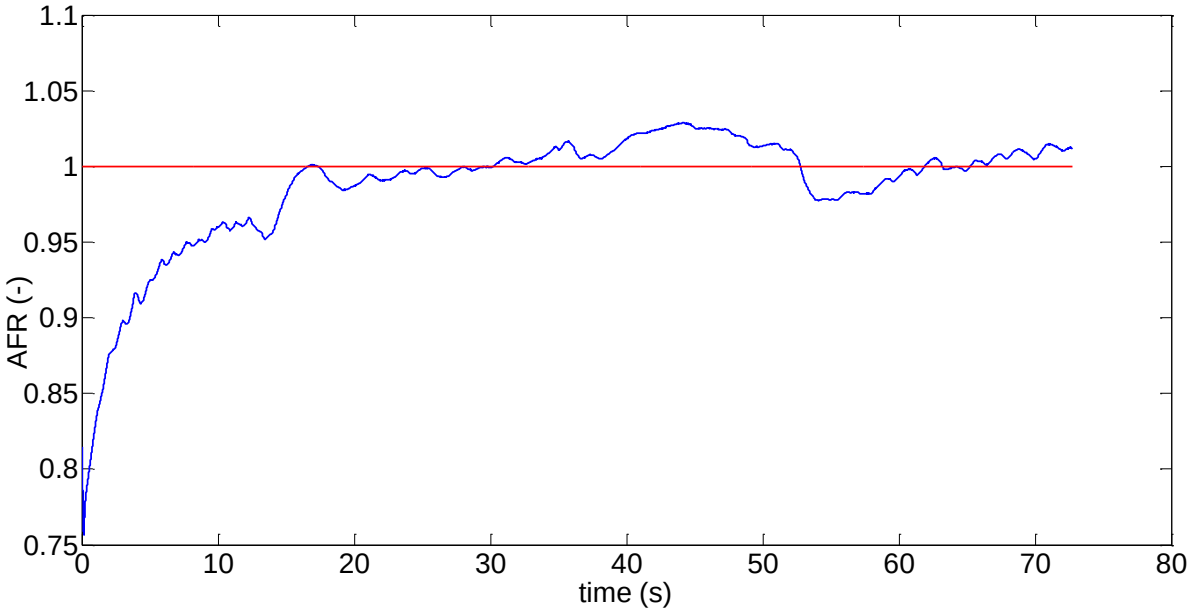

Fig. 99. Simulation result of the air-fuel ratio control by the linear state-feedback controller and the delay in the Lyapunov function

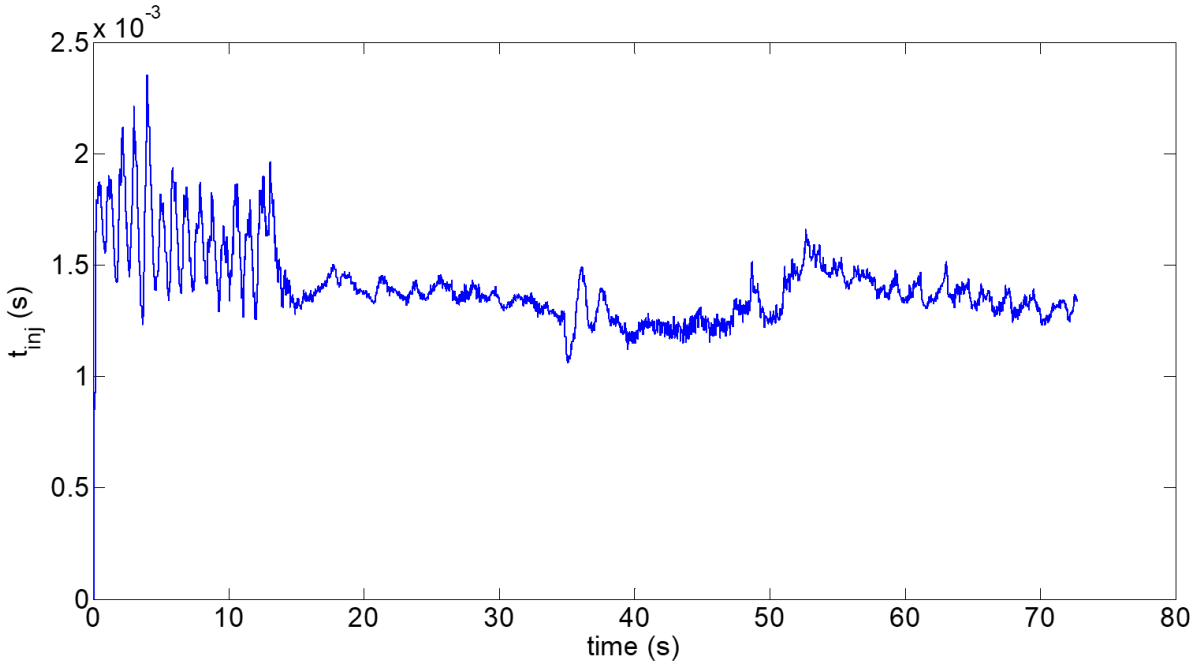

Fig. 100. Command of the injectors generated by the linear state-feedback triggered every 180 crankshaft degrees

As one can see, this first controller can maintain the air-fuel ratio around the reference $\lambda_{ref} = 1$ with an accuracy of 5%, with a control law that is computed every 180 crankshaft degrees. However, the absence of integral action does not ensure performance in transient phase. The gain $v_\lambda(k)$ that has been added (4.3.15) can only reduce the static error, but cannot guarantee any performance in dynamic phase or in case of external disturbance. Considering an idle speed dataset, the simulated controller provides satisfying performance (error <5%) in static case.

4.1.3. Experimental results

In order to validate this first methodology, this air-fuel ratio controller is implemented in the ECU of the engine test bench in addition to the idle speed controller already functioning, see Chapter 3, Section 5.2. Since this air-fuel ratio controller does not contain any integral action, an experiment is realized in the same context as the simulation, i.e. at idle speed conditions. Fig. 101 presents the results of this experiment with the measured air-fuel ratio. Fig. 102 depicts the command signal for the injection timing generated by the controller embedded in the ECU of the engine test bench.

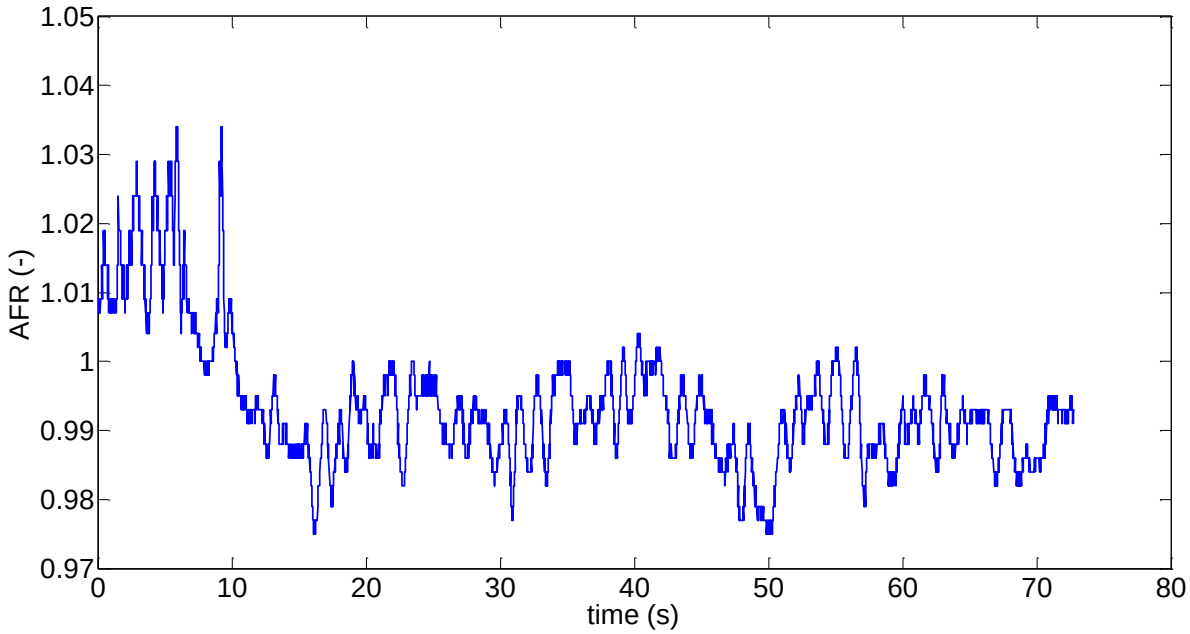

Fig. 101. Experimental result of air-fuel ratio control

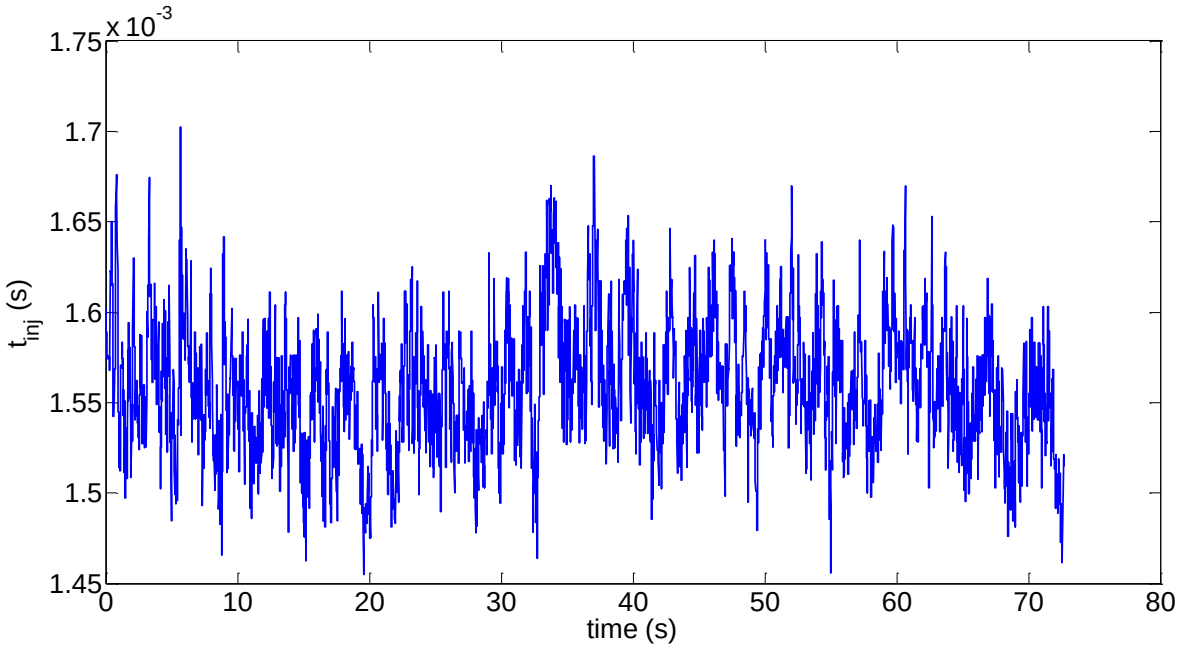

Fig. 102. Command generated by the controller embedded in the ECU of the engine test bench

As one can see, the lack of integral action makes an error appear in the reference tracking, even if the performance is satisfying (around 2% of error) on a real-work application. Since the controller is developed in the crank-angle domain, the control law is computing in function of the engine speed, making the controller robust to variations of speed, as it is the case in presence of external disturbance, as presented in the next scenario. Considering again the idle speed, a torque demand is generated at 20s with 5Nm of amplitude, and at 33s with 10Nm of amplitude. With such a torque load, the speed decreases and the air-fuel ratio controller has to recover from the disturbance. The experimental results are presented in Fig. 103 and Fig. 104. Fig. 105 depicts the measured engine

speed with both idle speed and air-fuel ratio controllers, illustrating the efficiency of the idle speed controller developed in Chapter 3 when the air-fuel ratio control is performant.

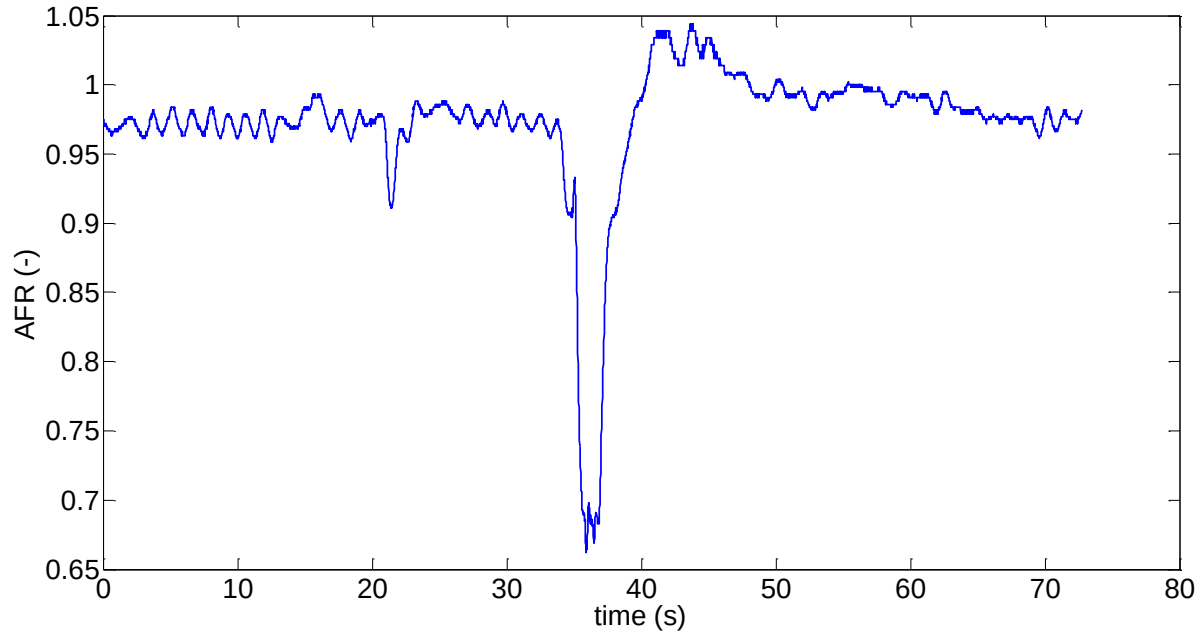

Fig. 103. Air-fuel ratio control in presence of external disturbance

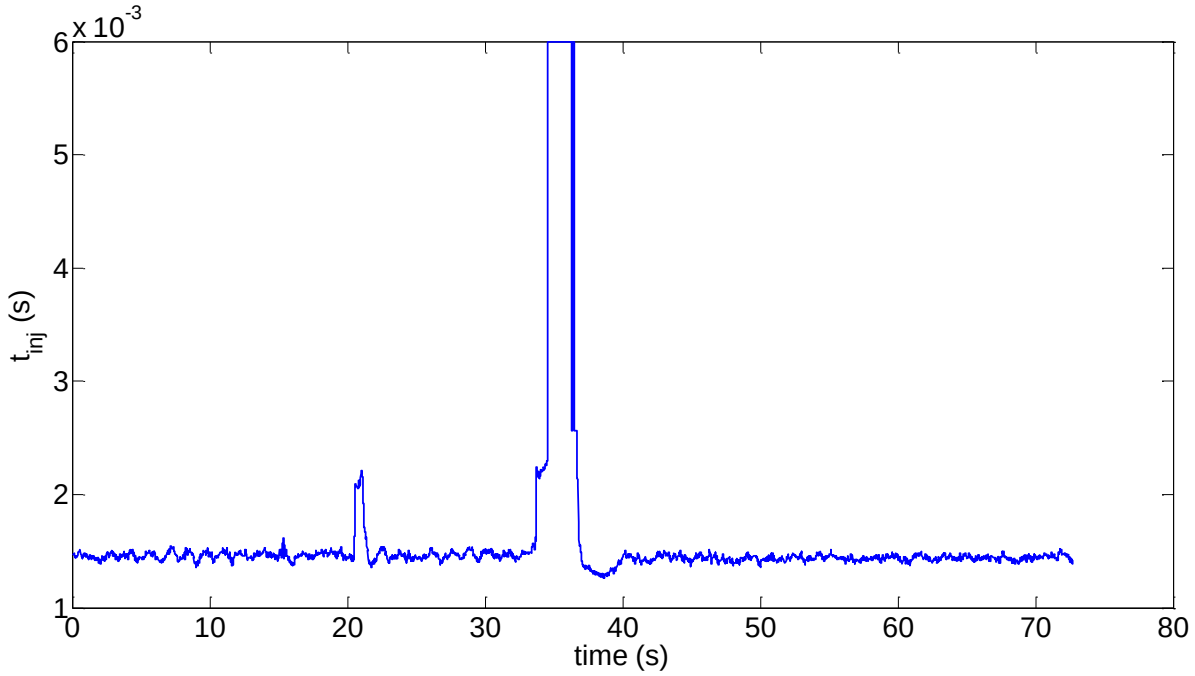

Fig. 104. Command generated by the controller facing a disturbance

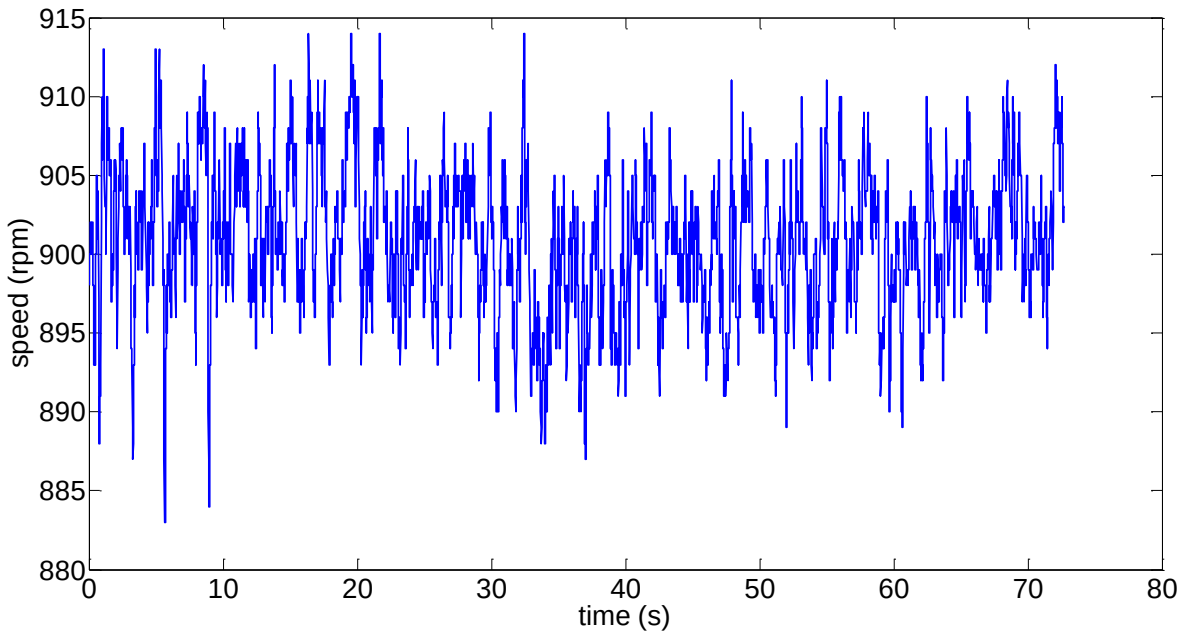

Fig. 105. Measured engine speed with both idle speed and air-fuel ratio controllers

As one can see, even without any integral action, the linear state-feedback controller, i.e. a proportional controller, succeeds in tracking the reference while an external disturbance occurs, even if the error between the measured AFR and the reference still exists. The command signal is saturated when the 10Nm disturbance appears; an integral action should react quickly, including an anti-windup structure to prevent saturations.

If this first method allows obtaining LMI conditions, it cannot find any solution while adding an integral action. The reference tracking is then difficult since the model is not exactly perfect, even if a term is added to the control law to correct the static error, see equation (4.3.15). The error still remains in real-time experiments, and the external disturbance rejection is not as performant as with an integral action.

4.2. Second methodology

4.2.1. Controller gains

Then, another methodology, less conservative, should be found. Instead of changing the control law or the relaxations, the TS model is modified such that the delay no longer appears on the control input but it is included in the state using new variables. By augmenting the state vector, so the state matrix, with as many new variables as the length of the constant delay, then the closed-loop system becomes a standard problem. Considering a quadratic Lyapunov function and the linear state-feedback, LMI conditions are obtained from the results of the literature. Thanks to the simplicity of the new conditions, an integral action can be easily added without getting unfeasible problems. The final air-fuel ratio controller can be implemented in the ECU of the engine test bench for real-time experiments:

$$u_\lambda^\theta(k) = -F_\lambda^\theta \cdot \breve{x}_\lambda^\theta(k) \tag{4.4.3}$$

with

$$\breve{x}_\lambda^\theta(k)^T = \left[x_\lambda^\theta(k)^T \quad u_\lambda^\theta(k-4)^T \quad u_\lambda^\theta(k-3)^T \quad u_\lambda^\theta(k-2)^T \quad u_\lambda^\theta(k-1)^T \quad e_\lambda^\theta(k)^T \right]^T \quad (4.4.4)$$

inside the domain of validity previously mentioned (4.4.2). The controller gain can be obtained while fixing the decay-rate to $\beta = 0.985$:

$$F_\lambda^\theta = \begin{bmatrix} 2675.1 & 0.4307 & 0.4166 & 0.3956 & 0.39 & -4340.3 \end{bmatrix} \quad (4.4.5)$$

4.2.2. Simulation results

First, the controller is validated through simulation results. Similarly to the first presented method, the controller is applied on the continuous-time model, and both the controller and the model are fed with measured signals from engine test bench datasets, so the signals already have sensor noise. In order to validate the controller, a first experiment is realized using an idle speed dataset. Since the throttle is controlled by the TS fuzzy controller developed in Chapter 3, the engine speed stays very close to the reference $n_{ref} = 900rpm$. Fig. 106 depicts the air-fuel ratio from the lambda sensor considering the idle speed conditions. Fig. 107 presents the command generated by the air fuel ratio controller. The control law is computed every engine cycle, i.e. every 180 crankshaft degrees. As one can see, the static error no longer appears since the controller includes an integral action. The error between the measured signal and the reference is less than 1%.

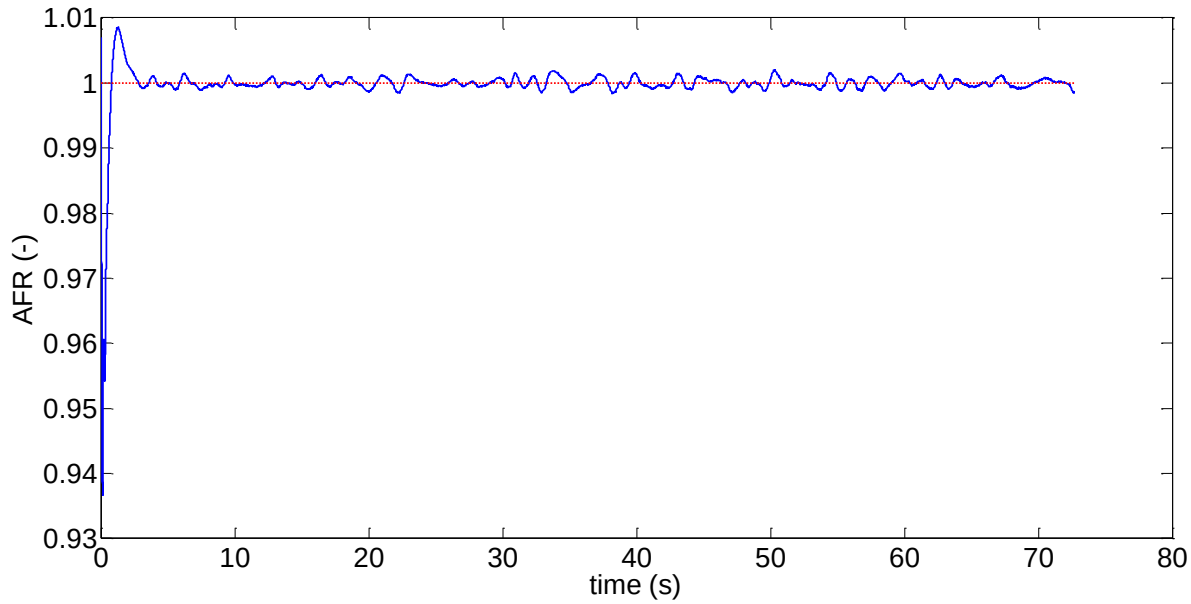

Fig. 106. Simulated air-fuel ratio in idle speed conditions

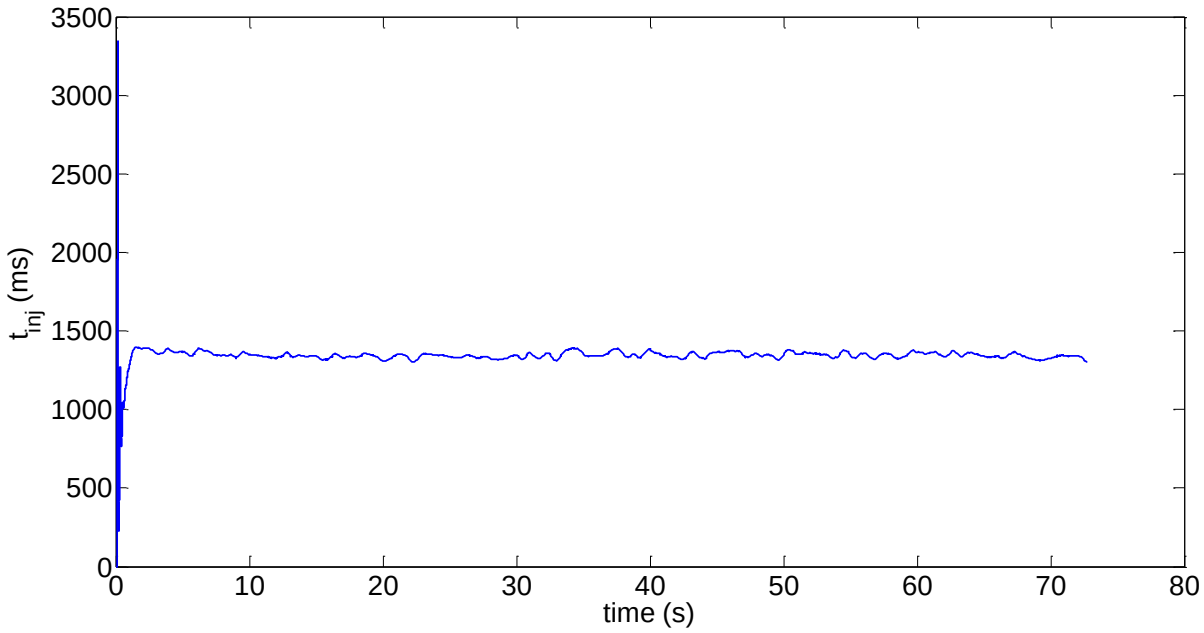

Fig. 107. Command generated by the air-fuel ratio controller

Now that the controller includes an integral action, it is possible to compare its performance with a PI controller equipped with a Smith predictor-based structure. Indeed, the Smith predictor structure has to be adapted for the case of variable delay. As a matter of first comparison, the inconvenient of the PI+Smith controller is the model involved in the Smith predictor structure. This model has to be very well identified, i.e. parametric uncertainties can make the closed-loop system unstable. Moreover, this model has to be embedded in the Electronic Control Unit and computed at every clock sample, which will be a limit for experimental applications. Finally, the PI+Smith controller can only control a system that is already stable.

For the comparison, let us consider the following PI controller:

$$u_{PI}(t) = K_p \cdot \left(1 + \frac{1}{T_i \cdot p}\right) \tag{4.4.6}$$

with $K_p = -3000$ and $T_i = 0.25$. The structure of the Smith predictor is added with the variable delay (since the expression is known from (4.1.1)). Fig. 108 presents the comparison of the output between two models, one controlled by our controller and the other one controlled by a PI+Smith controller, showing that the proposed controller has better performance in term of reference tracking than a PI controller with a Smith predictor structure.

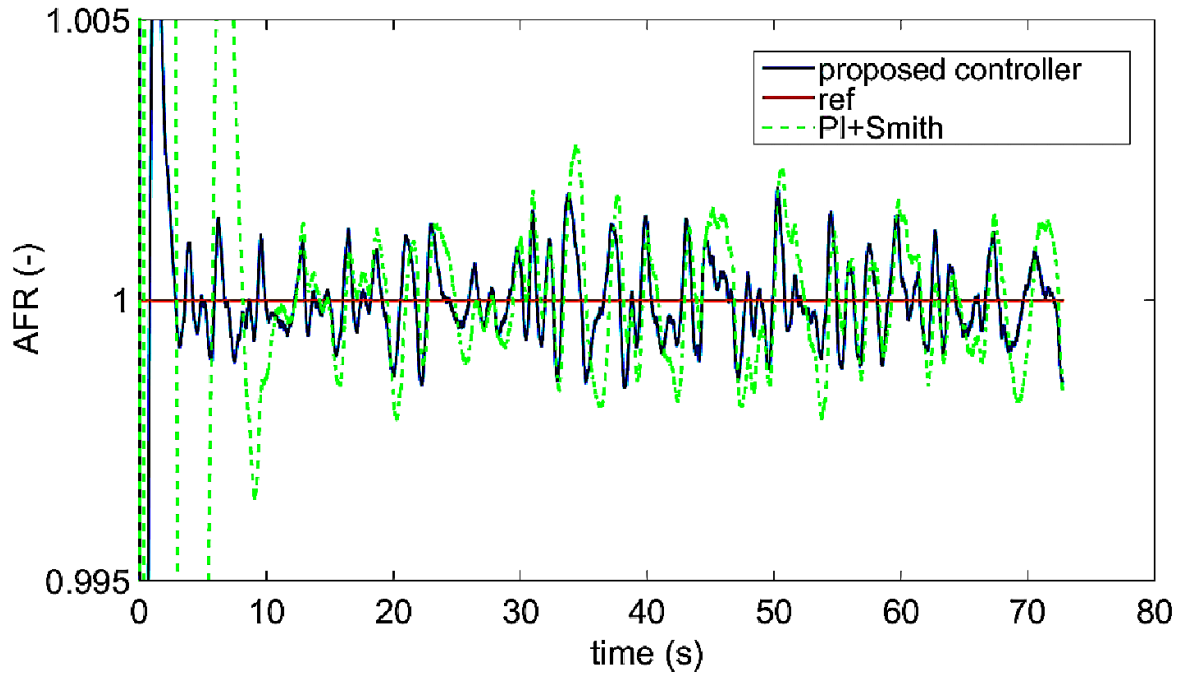

Fig. 108. Output of the air-fuel ratio models controlled by the PI+Smith controller and the TS-based controller

The second part of the Challenge #1 of air-fuel ratio control is disturbance rejection. Once the air-fuel ratio is stabilized around the reference value $\lambda_{ref} = 1$ in idle speed conditions, disturbances are applied. Fig. 109 presents the engine speed from the second dataset used to validate the proposed controller with simulation results. Even if the disturbance is applied on the speed using the torque brake and the speed is maintained at the idle speed reference by the idle speed controller from Chapter 3, the air-fuel ratio model receives an air mass flow directly impacted by the disturbance, so the air-fuel ratio is disturbed as well.

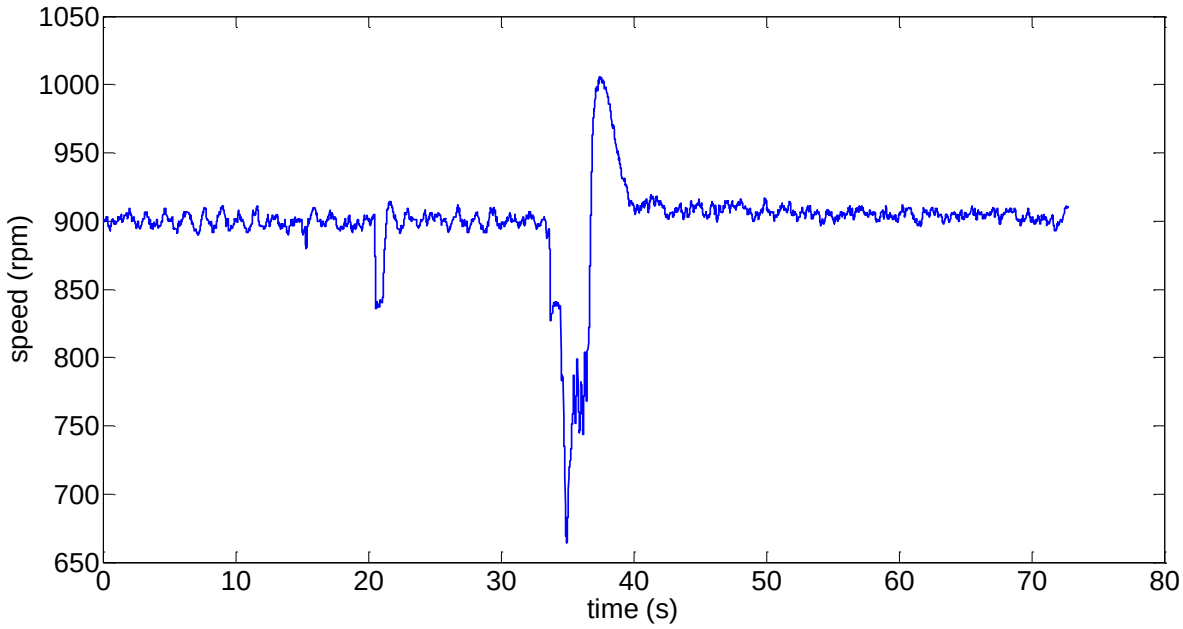

Fig. 109. Engine idle speed with external disturbance from the considered dataset

The results of the simulation are presented in the next figures. Fig. 110 presents the output of the two models controlled either by the proposed TS-based controller or the PI+Smith controller. As one can see, the designed controller has better performance in term of disturbance rejection than the PI+Smith controller, highlighting the efficiency of the proposed methodology. Fig. 111 presents the command signal sent to the model to stabilize the air-fuel ratio around the reference and to reject external disturbances.

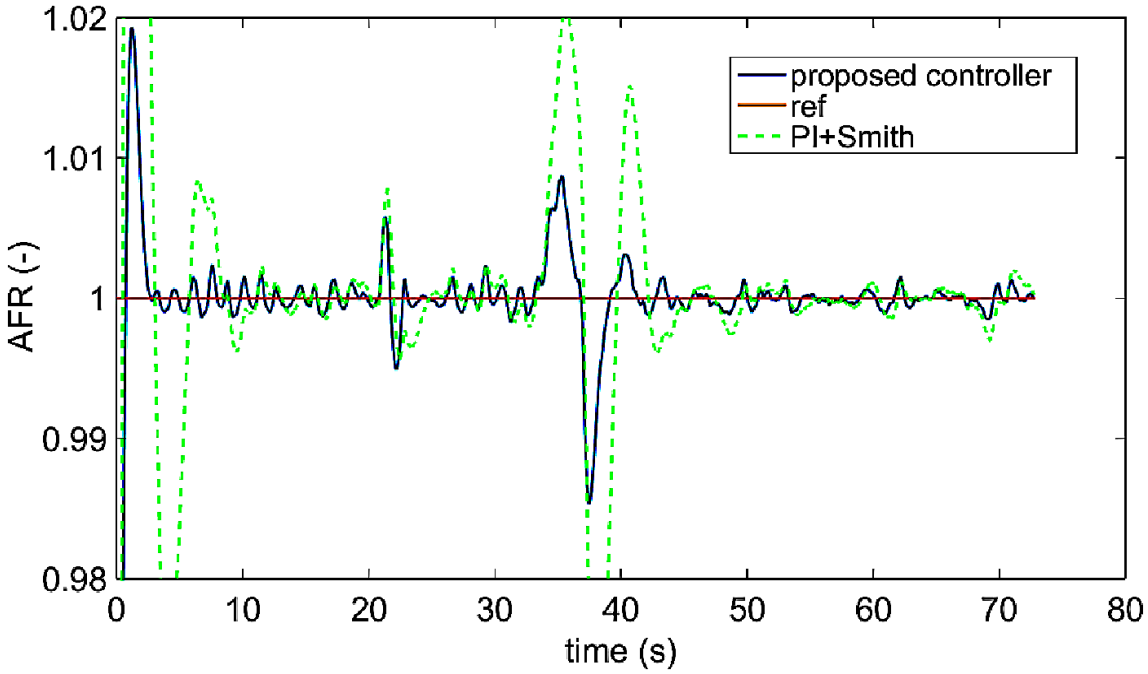

Fig. 110. Simulation results of the air-fuel ratio control

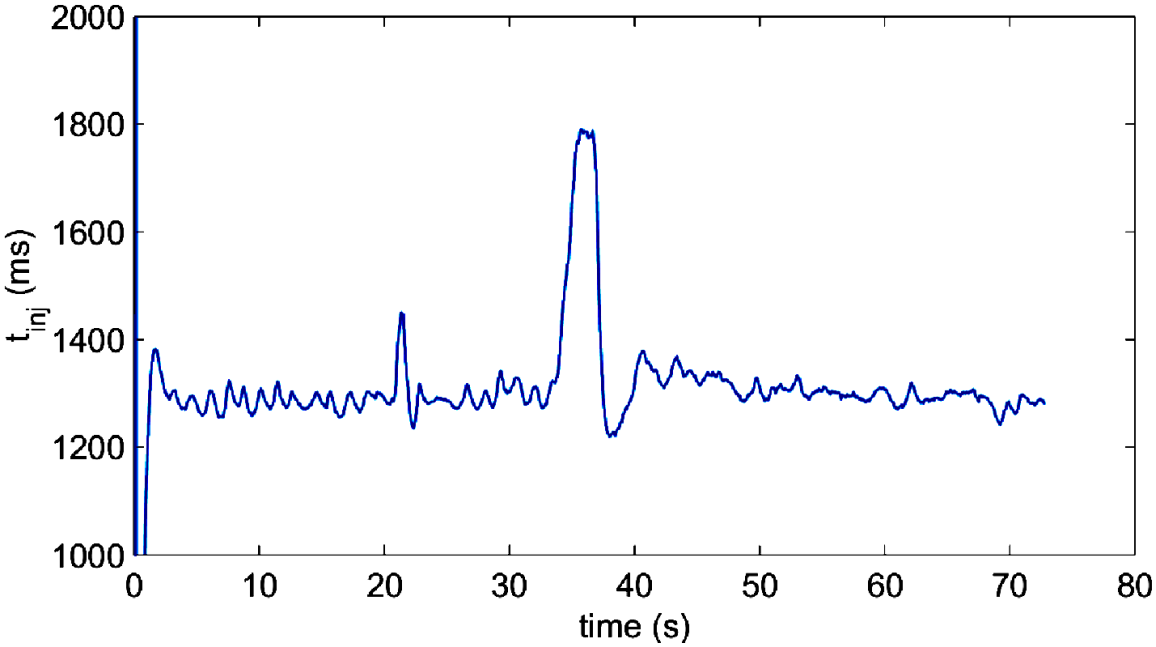

Fig. 111. Command generated by the air-fuel ratio controller to face disturbances

Now that the Challenge #1 of the air-fuel ratio has been validated in simulation, let us validate the Challenge #2. In order to verify that the proposed methodology to deal with variable transport delays is efficient, a third dataset is used to feed the simulation model. It is based on a variable engine speed, so the delay is more varying than in idle speed conditions. Fig. 112 presents the considered dataset. As one can see, the speed is varying, offering a time-varying delay as depicted in Fig. 97, transient dynamics and a 'realistic driver' behavior, making this scenario more valuable for validating the controller before experimental tests and real world implementation. However, one can notice that the speed has been kept inside the domain of validity of the Takagi-Sugeno controller (2.6.11). Fig. 113 depicts the simulation results of the air-fuel ratio control. Even if the PI controller is improved with a Smith predictor structure, the variations of the delay disturb the reference tracking of the model controller by the PI+Smith controller. Each change of speed involves an error around 5% for the PI+Smith controller, while the proposed methodology handles delay variations with less than 2%.. Fig. 114 depicts the command generated every 180 crankshaft degrees by the proposed controller. As a reminder, this means that the control law is computed every 0.01 second when the engine is running at 3000 rpm, contrary to the PI+Smith controller that provides worse performance while it is triggered every 0.001 second (simulation sampling time). This simulation results validate the efficiency of the methodology presented in Section 3.4 of this chapter. Now that the simulation has highlighted that the controller can solve both Challenge #1 and #2 of reference tracking, disturbance rejection and variable transport delay management, experimental tests can be realized.

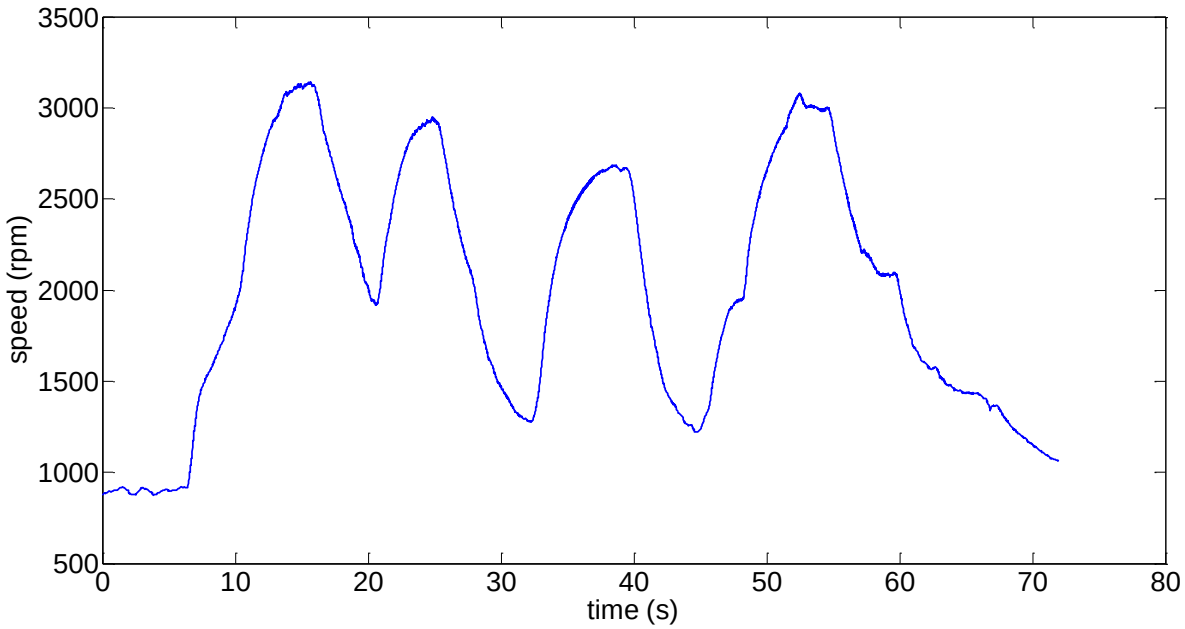

Fig. 112. Considered dataset with variable engine speed

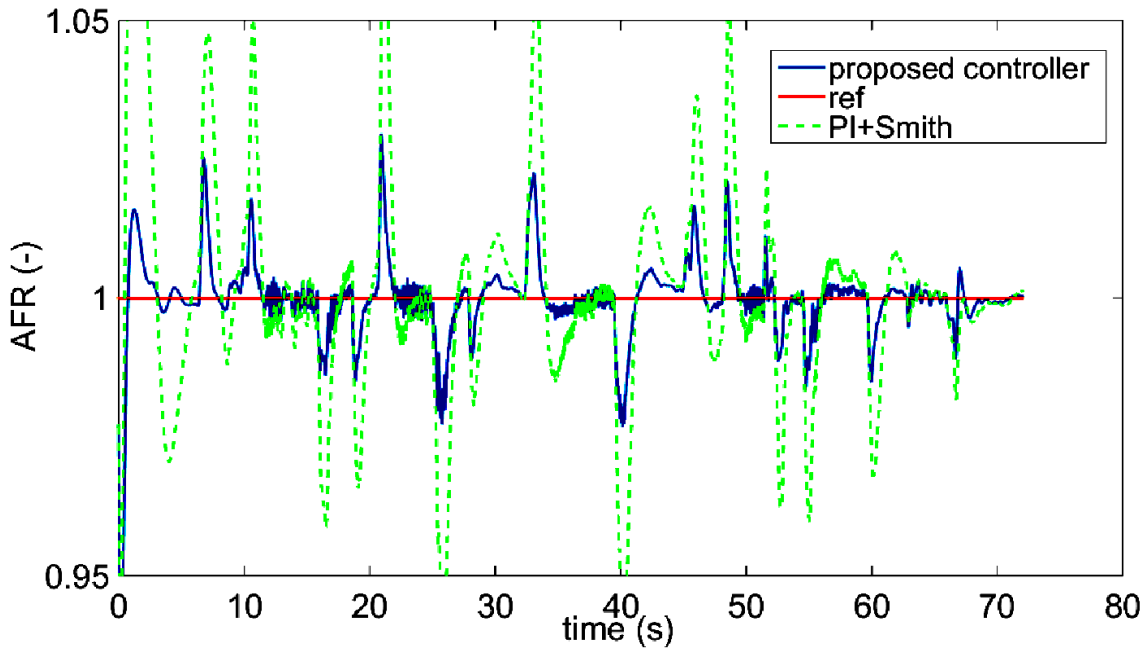

Fig. 113. Simulation results of air-fuel ratio control with varying speed

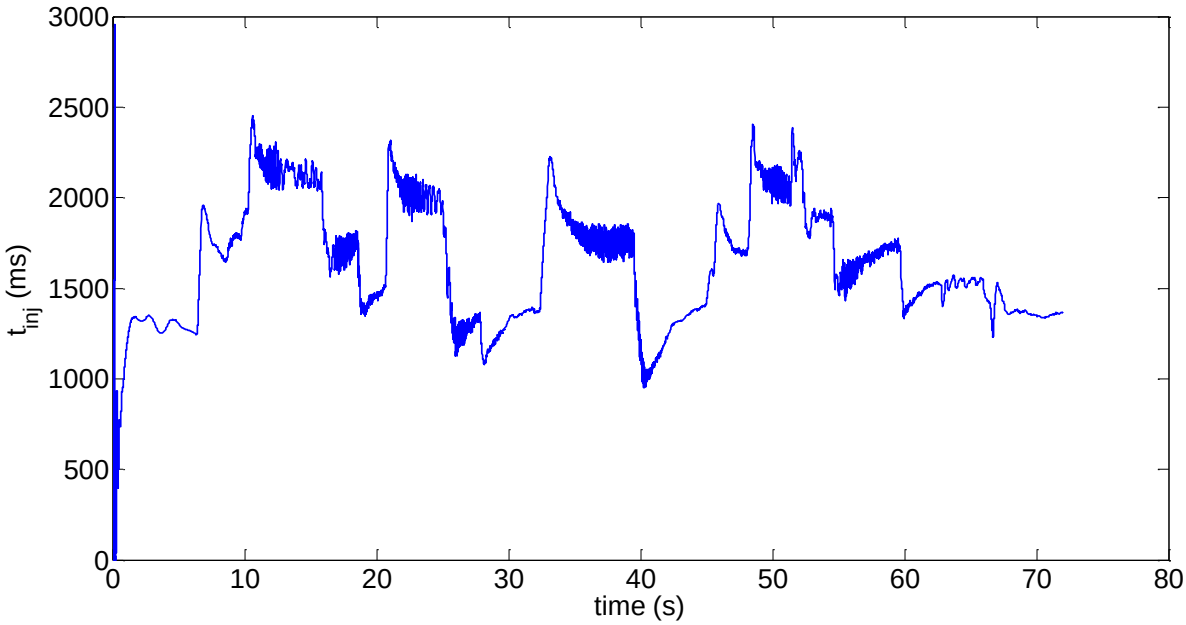

Fig. 114. Command generated by the air-fuel ratio controller to handle variable transport delay

4.2.3. Experimental results

The proposed air-fuel ratio controller (4.4.3) with the gains (4.4.5) is then implemented in the Electronic Control Unit of the engine test bench located in Valenciennes, in addition to the idle speed controller already implemented in Chapter 3. However, the cold start remains a problem, so a switch is realized to commute between the proposed controller and the maps-based controller. As already mentioned, the cold start controller should be designed in a specific module since the air-fuel ratio model is valid only for hot temperatures, see Chapter 2.

When implementing the proposed controller and the PI designed in simulation, the gains appear to be too big, so the controllers too fast. Then, it is impossible to stabilize the closed-loop system since the air-fuel ratio oscillates between the bounds of the saturation until the engine stalls. The gains of the air-fuel ratio controller need to be reduced, limiting the oscillations around the reference but decreasing the response time (systematic trade-off in control between accuracy and rapidity). After several trials, the new gains are obtained by an empirical way:

$$F_{\lambda}^{\theta} = \begin{bmatrix} 140.3 & 0.056 & 0.058 & 0.059 & 0.059 & -140.8 \end{bmatrix} \tag{4.4.7}$$

These gains allow stabilizing the air-fuel ratio around the reference value. However, these gains do not ensure any stability: They need to solve the LMI problem detailed in (4.3.24). Then, by finding a Lyapunov function with these gains, the closed-loop system is ensured to be stable. This guarantee of the closed-loop system stability is the strength of model-based controllers, since it is mathematically proved, contrary to model-free controllers such as maps or heuristic methodologies.

A first trial is considered to validate experimentally the new controller. The engine is running at idle speed $n_{idle} = 1000 rpm$, i.e. the driver pedal is not used and the engine speed is regulated with the idle speed controller developed in Chapter 3. Fig. 115 presents the experimental results by depicting the measured air-fuel ratio from the lambda sensor of the engine. Notice that this sensor is the same as the ones equipped in commercial cars, so the lack of accuracy of the sensor has to be taken into account while analyzing the results. As one can see, the air-fuel ratio is tracking the reference $\lambda_{ref} = 1$ with an error around 2%. The new gains, smaller than the simulation ones, are not big enough to handle variations of the air mass flow without oscillating. Fig. 116 depicts the command generated by the air-fuel ratio controller. The control law is computed every engine cycle, i.e. every 180 crankshaft degrees, however, it is recorded every 10 ms from the ECU.

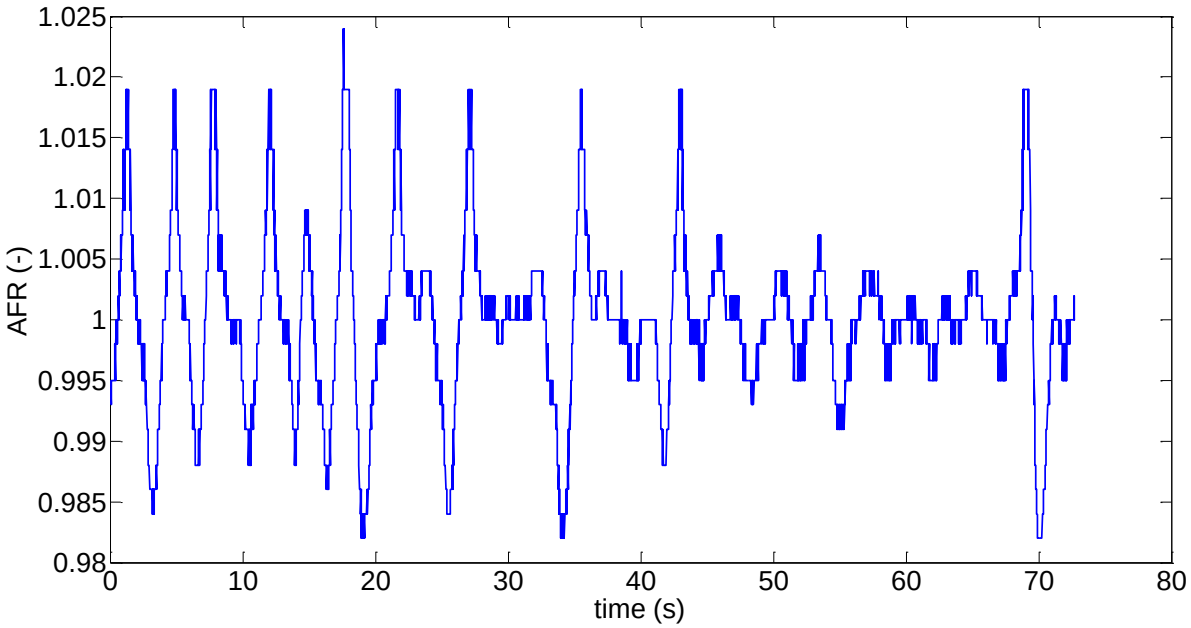

Fig. 115. Measured air-fuel ratio for idle speed conditions

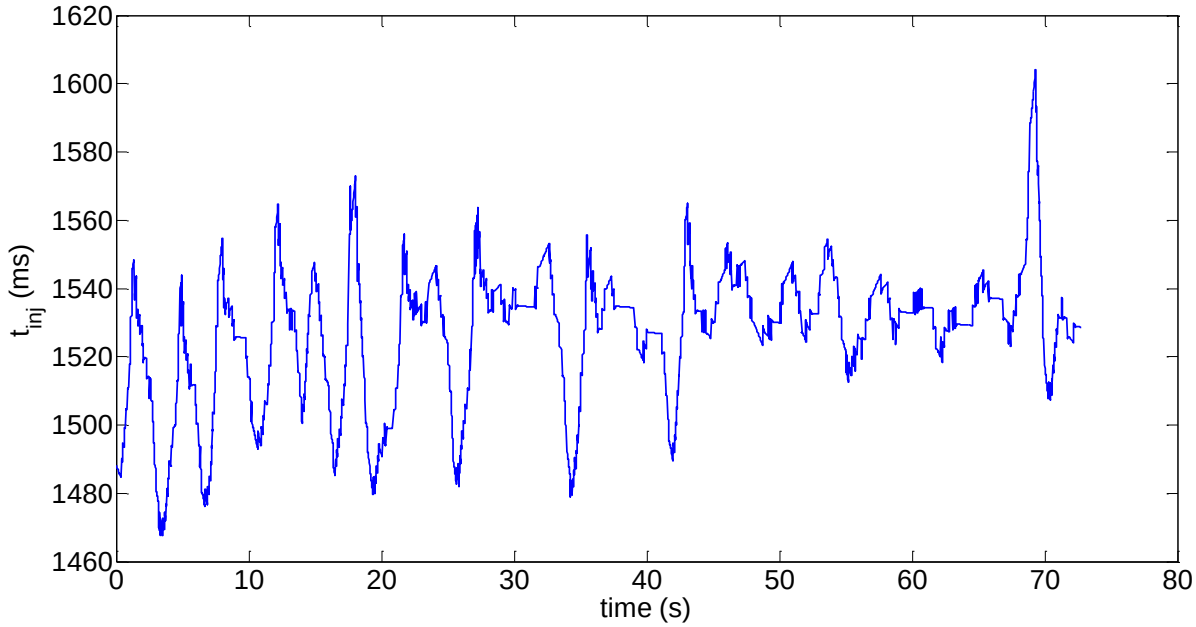

Fig. 116. Command generated by the air-fuel ratio controller

The second trial presents the experimental results of air-fuel ratio control while the engine speed is varying. The variations of speed are realized by changing the reference for the idle speed controller among $n_{ref} = \{800, 720, 1000, 1200\}$ as depicted in Fig. 117. The difficulty for the idle speed controller is the width of the operating range which is close to the bounds of the Takagi-Sugeno representation. Fig. 118 presents the measured air-fuel ratio for this case of varying idle speed. As one can see, since the controller includes an integral action, the air-fuel ratio tracks the reference. However, the change of speed, so the change of air mass flow, impacts the air-fuel ratio with peaks until 20% of error. This is due to the controller gains that are too small to handle fast changes of air mass flow, i.e. fast external disturbances, but these gains cannot be higher since it does not stabilize the closed-loop system anymore, see the command signal in Fig. 119.

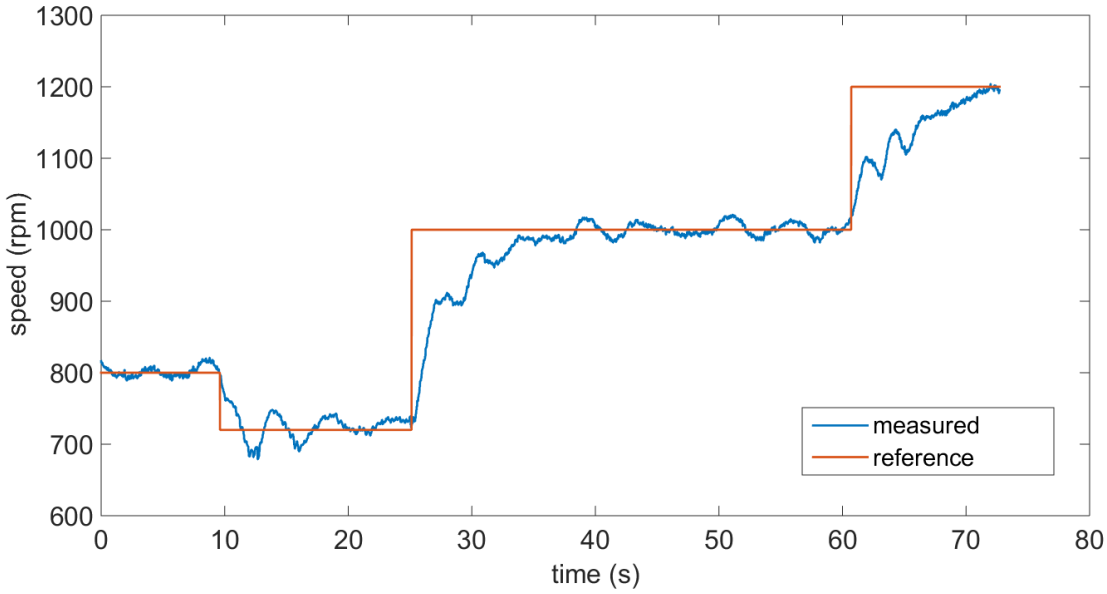

Fig. 117. Idle speed variations

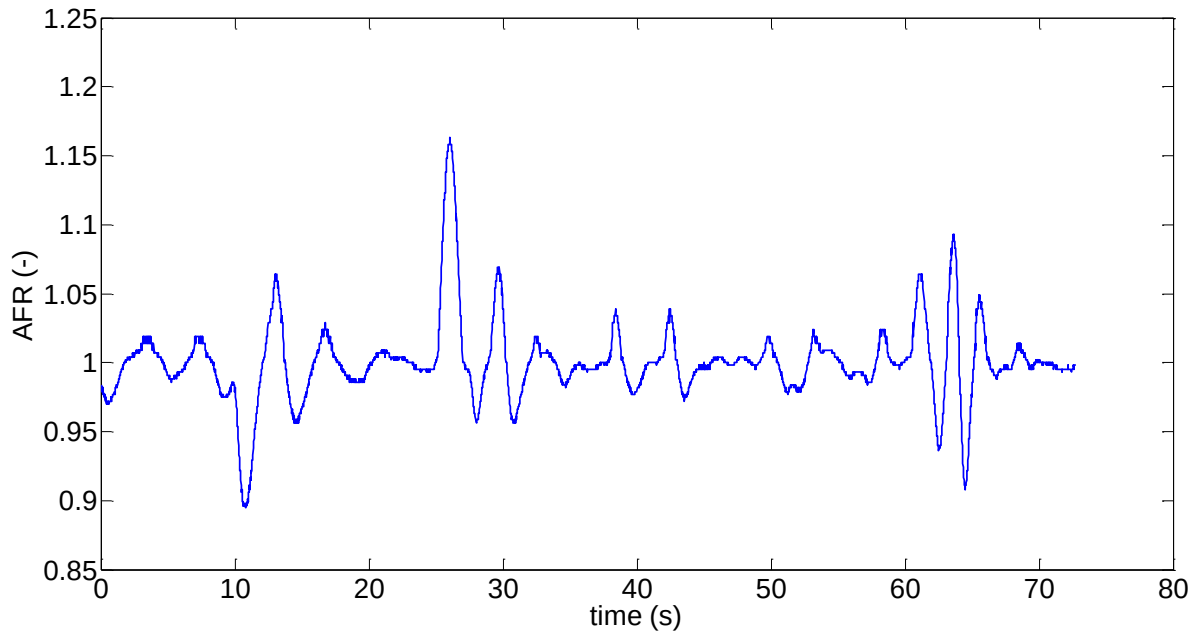

Fig. 118. Measured air-fuel ratio for varying idle speed

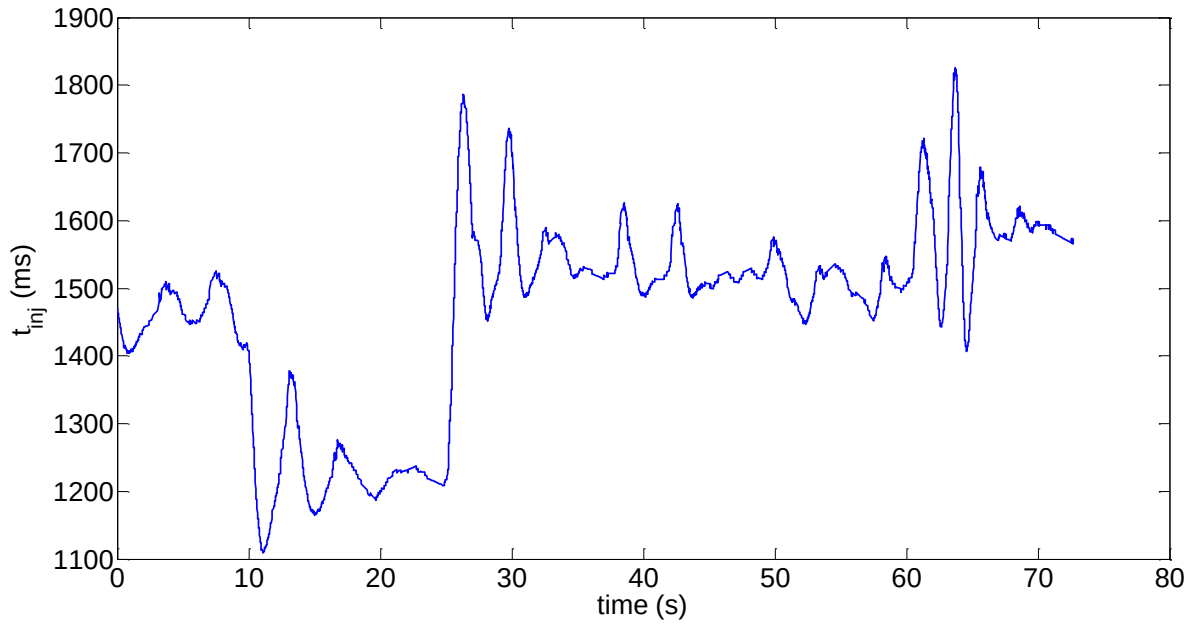

Fig. 119. Command generated by the air-fuel ratio controller for varying idle speed

The reference tracking of the Challenge #1 of air-fuel ratio is ensured by the integral action. However, the disturbance rejection is not efficient enough when the change of air mass flow is too fast since the controller structure does not include any information about air mass flow. A solution could be to include the membership functions inside the controller structure since the nonlinearities are function of the air mass flow. Then, a PDC controller should be considered.

4.2.4. PDC controller

A PDC controller can be designed similarly to the structure presented in (4.3.26). By solving the LMI conditions (4.3.32) based on the relaxation of Tuan, the gains can be obtained. Since the integral action makes a new nonlinearity appear, i.e. $\frac{T_s^\theta}{6 \cdot n^\theta(k)}$, the Takagi-Sugeno model includes three nonlinearities, so $r = 8$. The eight gains are then obtained:

$$\begin{aligned}
F_1 &= \begin{bmatrix} 241.8818 & 0.0141 & 0.0488 & 0.0456 & 0.0467 & -193.3296 \end{bmatrix} \\
F_2 &= \begin{bmatrix} 233.9040 & 0.0142 & 0.0488 & 0.0455 & 0.0465 & -193.2461 \end{bmatrix} \\
F_3 &= \begin{bmatrix} 241.8218 & 0.0659 & 0.0488 & 0.0456 & 0.0466 & -193.2912 \end{bmatrix} \\
F_4 &= \begin{bmatrix} 234.1567 & 0.0659 & 0.0488 & 0.0456 & 0.0467 & -193.3049 \end{bmatrix} \\
F_5 &= \begin{bmatrix} 248.5125 & 0.0141 & 0.0488 & 0.0456 & 0.0468 & -193.3462 \end{bmatrix} \\
F_6 &= \begin{bmatrix} 240.8205 & 0.0141 & 0.0488 & 0.0456 & 0.0468 & -193.3458 \end{bmatrix} \\
F_7 &= \begin{bmatrix} 248.4991 & 0.0659 & 0.0488 & 0.0456 & 0.0467 & -193.3292 \end{bmatrix} \\
F_8 &= \begin{bmatrix} 240.8013 & 0.0659 & 0.0488 & 0.0456 & 0.0467 & -193.3265 \end{bmatrix}
\end{aligned} \tag{4.4.8}$$

These gains are implemented in the Electronic Control Unit. Since the membership functions are computed every 180 crankshaft degrees like the control law, the controller includes the air mass flow in its structure. In order to assess the PDC controller, experimental scenarios are realized. The first trial considers idle speed conditions with varying reference, similarly to what has been presented in Fig. 117 and as depicted in Fig. 120. Fig. 121 presents the experimental results of the air-fuel ratio control with varying engine speed, and Fig. 122 depicts the command generated by the PDC controller to control the air-fuel ratio. As one can see, the reference tracking is still ensured by the integral action, i.e. the air-fuel ratio always comes back to the reference $\lambda_{ref} = 1$.

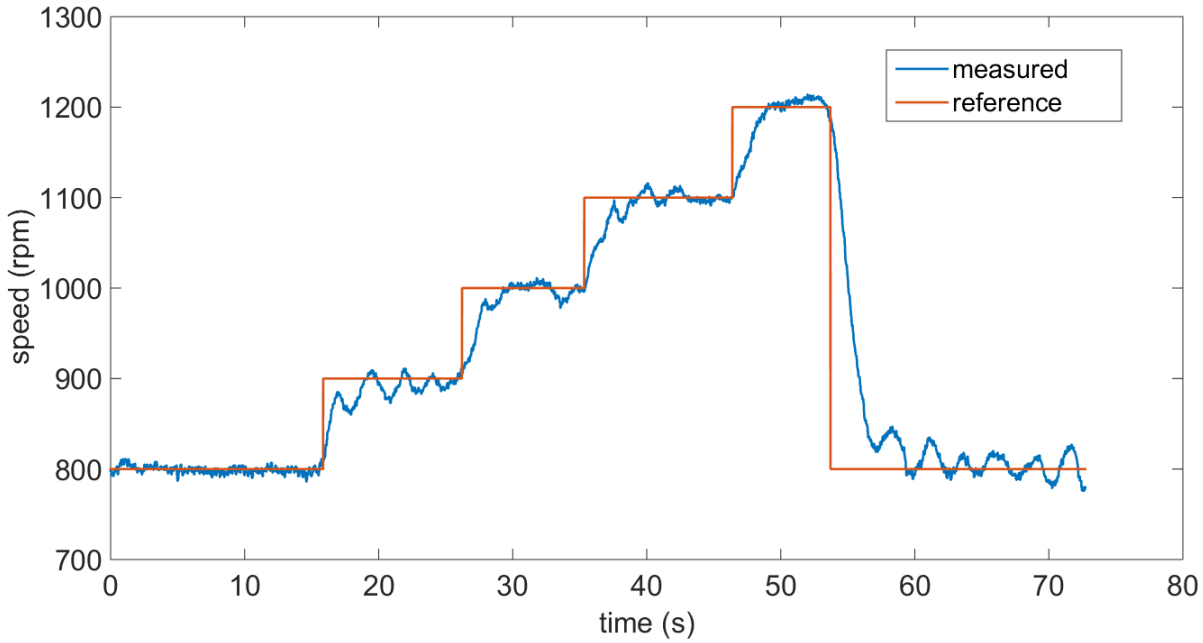

Fig. 120. Varying idle speed to assess the PDC controller

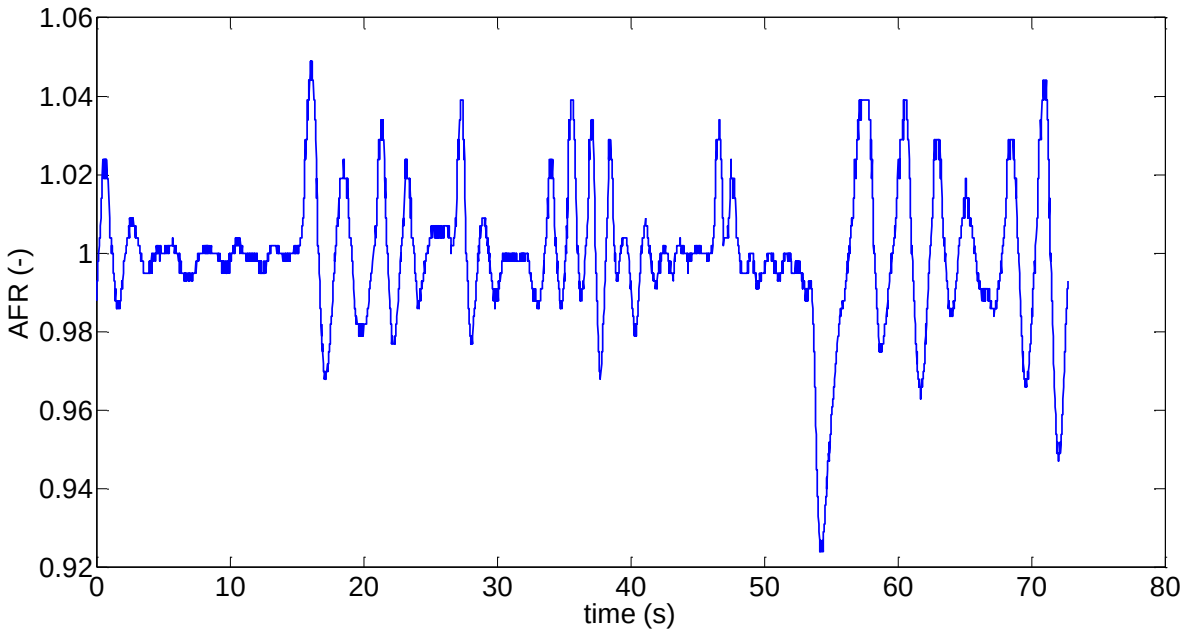

Fig. 121. Measured air-fuel ratio with the PDC controller

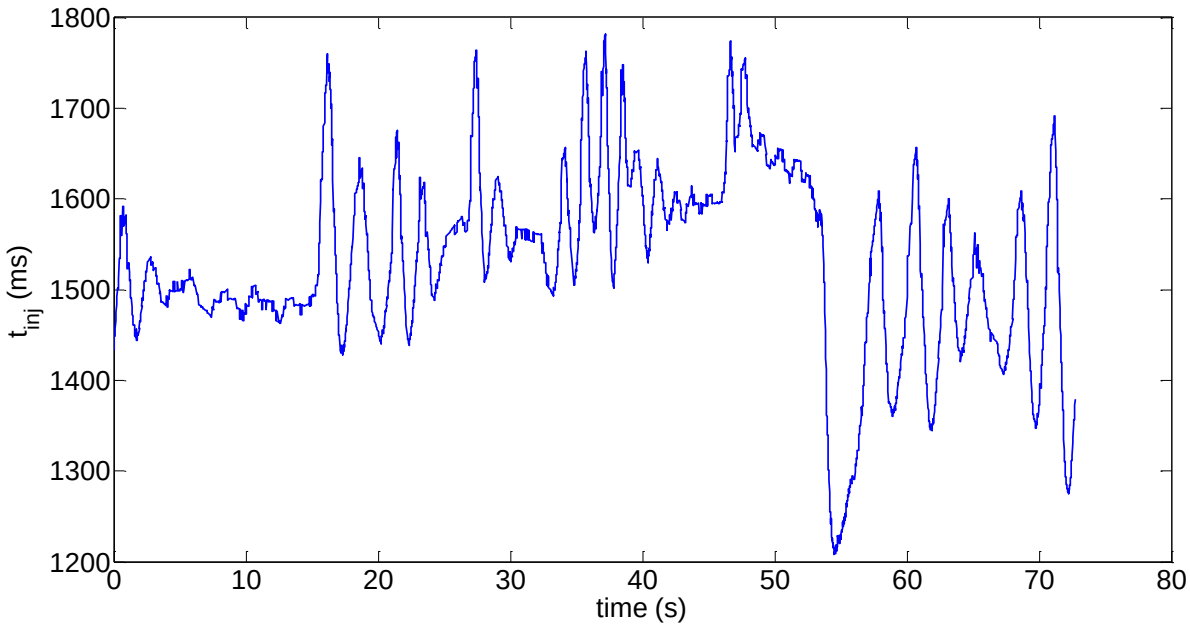

Fig. 122. Command generated by the PDC controller

Moreover, the disturbance rejection is more efficient since the controller now includes the air mass flow inside the membership functions. Indeed, during the acceleration phases, the controller succeeds in keeping the air-fuel ratio around the reference with around 6% of error (contrary to 20% for the linear state feedback previously presented). This validates the hypothesis that including the air mass flow through the membership functions can provide better results considering the Challenge #1 of the air-fuel ratio control as well as the Challenge #2 of handling the variable transport delay since the speed is constantly changing.

However, the results could be better. Indeed, as presented along the Chapter 1 while introducing the engine control, three main elements need to be controlled: the throttle valve (in idle speed context), the injectors and the spark plugs. The idle speed controller validates the three challenges of idle speed control, and the fuel injection controller presented in this chapter validates both Challenge #1 and #2. However, the spark advance control, a critical element since it is involved in the torque production of the engine, remains controlled by empirical maps. As an example, let us consider the previous trial. As one can see, when the engine speed comes back to 800 rpm (at $t = 60s$), the air-fuel ratio is clearly disturbed (important oscillations with an amplitude of 4%). Since the idle speed controller maintains the speed at $n_{ref} = 800rpm$ and the air-fuel ratio controller at $\lambda_{ref} = 1$, and both controllers include an integral action in their structure, how can these last 20 seconds be so disturbed? The answer remains in the spark advance control realized by open-loop static maps. The value of the spark advance (in degrees before top-dead center) for the trial considered in Fig. 120 to Fig. 122 is depicted in Fig. 123. As one can see, due to the static behavior of look-up tables, the spark advance control cannot ensure any reference tracking, so it can act very differently for two similar conditions (idle speed, $t = [0,15]$ and $t = [60,75]$). A first solution before considering any closed-loop spark advance control could be to apply a filter on the spark advance signal to see if the impact is reduced and both air-fuel ratio and idle speed are less oscillating.

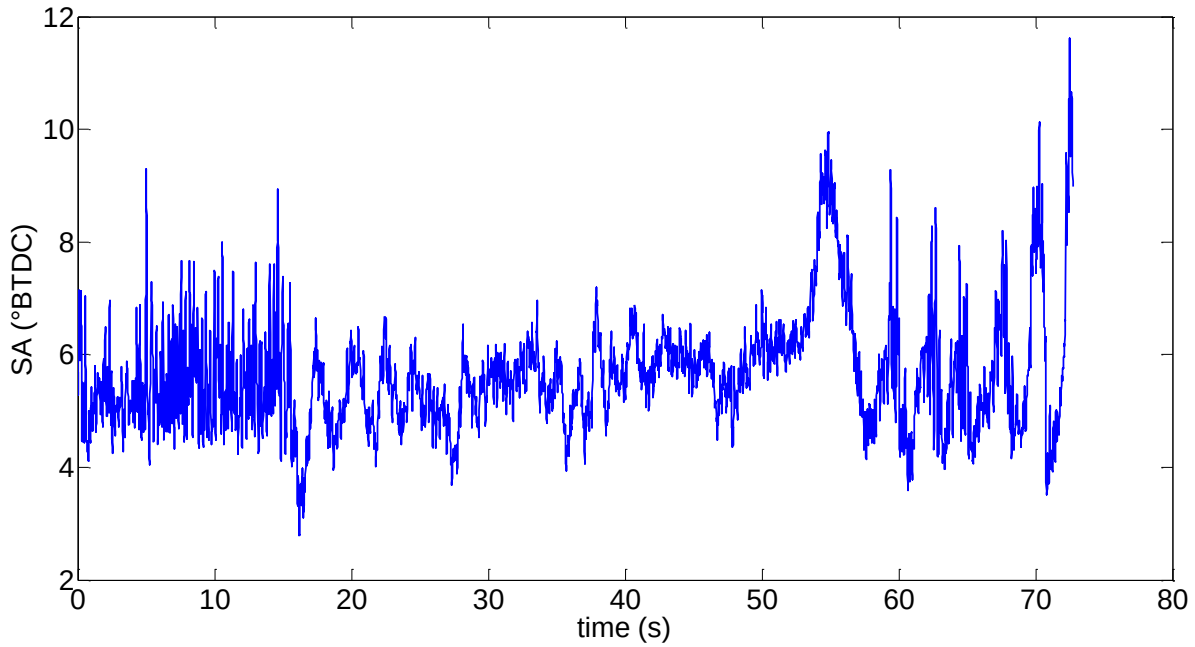

Fig. 123. Spark advance control in degrees before top-dead center

CONCLUSIONS

The process of science doesn't work unless young scientists have the freedom to attack and tear down old dogmas.

N. Stephenson, *Cryptonomicon*

This thesis is dedicated to the gasoline engine control. Since it is a crucial component of the automotive powertrain system, its control has to be efficient in order to reduce pollution and consumption. Chapter 1 presented the literature results about the specific parts of the engine control that are considered in this work. This analysis highlighted that several techniques have been developed from look-up table approaches or basic controllers such as PI ones to complex control structure. Definitively techniques based on look-up tables are time consuming to obtain (it can take weeks for tables with thousands of breakpoints) and only catches the static behavior of the system. Dealing with model-based control design, a compromise must be found between complexity (difficult to implement in a real ECU) and performances which cannot be guaranteed for all the range of operating points. Our goal was to provide a solution to this dilemma by developing dynamic controllers implemented on an ECU with good performances. The model-based method has been chosen in order to be able to establish some achievements. More specifically, the Takagi-Sugeno representation was adopted because it allows dealing with nonlinearities, is relatively easy to implement (extension of linear case) and had been successfully applied in the same context (Lauber, 2003; Khiar, 2007; Kerkeni, 2011; Nguyen, 2013).

The control of the engine is made through three main components: the throttle that is controlled in the special case of the idle speed, where the driver does not apply any command on the pedal, the fuel injection that needs to be controlled to keep the air-fuel ratio in stoichiometric proportions such that the catalytic converter is working in perfect chemical conditions, and the spark plugs that are responsible for the optimization of the torque production, so the fuel consumption.

As said previously, model-based approaches are proposed, so our first contribution detailed in Chapter 2 is to provide a nonlinear control-based model of the engine which is adapted from a hybrid model. This model is expressed in a particular discrete-time domain whose sampling value depends on the crankshaft degrees: The crank-angle domain. The idle speed model involves the throttle position as a control input and the spark advance, providing space for future improvements. In the crank-angle domain, the torque production – which is not measured – can be expressed as a function depending on measured values from previous samples. The air-fuel ratio is modelled as a first-order system involving a variable transport delay, which represents one of the main challenges of fuel injection control. Both idle speed and air-fuel ratio models have been identified and validated with experimental datasets from the engine test bench located at Valenciennes.

Based on this model, two controllers have been designed, one for the throttle (idle speed controller) and the other one for the injection timing (air-fuel ratio controller). Since both controllers need to achieve performance in term of reference tracking and external disturbance rejection, an integral

action is included in each controller structure. Chapter 3 presented the case of the idle speed controller design. To meet the requirements, a non-PDC controller had been developed which contained a time varying matrix inversion. This calculus can be very costly for an industrial controller with limited performance like an ECU. To cope with this reality, an alternative controller involving a multiple-sums fuzzy matrix had been designed. Simulations illustrated that the advanced fuzzy inversion-based controller can stabilize the idle speed around the reference and reject disturbances. Then, the alternative controller gains are obtained. Since it does not involve real-time matrix inversion anymore, the idle speed controller can be embedded in the open ECU of the engine test bench. Experimental results highlighted the efficiency of using TS fuzzy controller in application to the idle speed control, by providing reference tracking and disturbance rejection in both static and transient phases.

Chapter 4 addressed the second problem considered in our work, the air-fuel ratio control. As already mentioned, one of the main challenges relies on the variable transport delay. However, by converting the model into the crank-angle domain, since the transport delay is function of the angular speed and the crankshaft angles, it becomes fixed when expressed in the crank-angle domain and described as a constant delay on the input, i.e. an input delayed by several samples. By this transformation, the delay becomes constant and it avoids using complex control laws and Lyapunov functions for time-varying delays. Then, a first methodology for the controller design has been investigated. Since it is constant, the delay is included inside the Lyapunov function. A linear state-feedback is designed, and the gain is provided by applying the Lyapunov direct method on the closed-loop system. After having solved the LMI problem, both simulation and experimental results are presented to discuss the advantage and inconvenient of the method. Since the LMI conditions are unfeasible whenever an integral action is added to the structure of the controller, a second methodology has been investigated. The constant delay is then directly included in the state space vector, providing less conservative results for the LMI problem. The linear state feedback including an integral action has been considered in simulation framework fed with measured datasets. After having validated the methodology in simulation, real implementation of the ECU of the engine test bench has been realized. The experimental results show the success of achieving the challenges of the air-fuel ratio, however, in order to improve the performance, the linear state-feedback is changed for a PDC controller. As depicted with experimental acquisitions, the PDC controller provides better results for all the scenarios.

The different contributions of the thesis are summarized in the following table.

Throttle control	Spark advance control	Fuel injection control
• Throttle #1: Reference tracking, disturbance rejection • Throttle #2: Nonlinear behavior • Throttle #3: Engine torque not measured	• Spark #1: Optimization but avoiding knocking • Spark #2: Nonlinear behavior • Spark #3: Individual control	• Fuel #1: Reference tracking, disturbance rejection • Fuel #2: Variable transport delay • Fuel #3: Individual control

In green are depicted the challenges achieved by the fuzzy controllers that have been designed, and in red are depicted the challenges that were not considered in this work, for example the control of the spark advance. As one can see, there is still room for improvements; some possible tracks are presented in the Perspectives section.

PERSPECTIVES

Every revolution begins with a spark.

Katniss (J. Lawrence) in *Hunger Games: Catching Fire*

The Perspectives Section is divided into three parts: The first one is dedicated to short term perspectives, i.e. methodologies that can be designed and implemented in real-time in a short period of time. Mid-term perspectives are detailed in a second part, investigating the possible research directions that can be taken after the thesis. Finally, long-term perspectives are in the spotlight of the third part, extending the work to the whole automotive research area as well as the transport domain in general.

Short-term perspectives

As a short-term perspective, the different unsolved challenges can be achieved. Indeed, since the idle speed model already contains the spark (considered as an external disturbance from now), the problem can be written as a MISO problem and a spark advance control strategy can be designed. The experimental results of the idle speed controller have highlighted the fact that this throttle position controller can work efficiently even if the spark advance is changing all the time. A common empirical spark advance control that could be designed is to set the spark advance reference at a non-optimal point, i.e. the throttle controller is compensating. When a disturbance appears, the spark advance can be set very quickly to the optimal point to compensate the disturbance. As already mentioned, the spark can contribute quickly to the torque production, but with small amplitude, contrary to the air entering through the throttle that contributes in an important part of the torque production, but slowly taking into account the air path of the engine. By designing such a model-based control, the two first challenges of the spark advance control can be handled, since the Takagi-Sugeno representation can manage the nonlinear behavior and TS fuzzy controllers can provide performance without reaching the knocking point.

An example is given with simulation results. The simulation framework is the same as the one used for simulation results of Chapter 3, i.e. the continuous-time engine model is fed with measured data for the air-fuel ratio. The CATS controller is implemented to control the throttle position, and the speed reference is set to $n_{ref} = 900rpm$. Two disturbances occur, as presented in Fig. 124. For the second one, a simple spark advance strategy increases the spark advance value when the disturbance occurs, as presented in Fig. 125. The simulation results of the engine speed (plus a zoom around the reference) and the command from the controller are depicted in Fig. 126 and in Fig. 128 respectively. As one can see, the spark advance control strategy based on increasing the spark advance, i.e. going closer to the optimal point, when a disturbance occurs can help the idle speed controller reject the disturbances. The engine speed is less decreasing, meaning that the reference can be set lower, so the fuel consumption can be reduced.

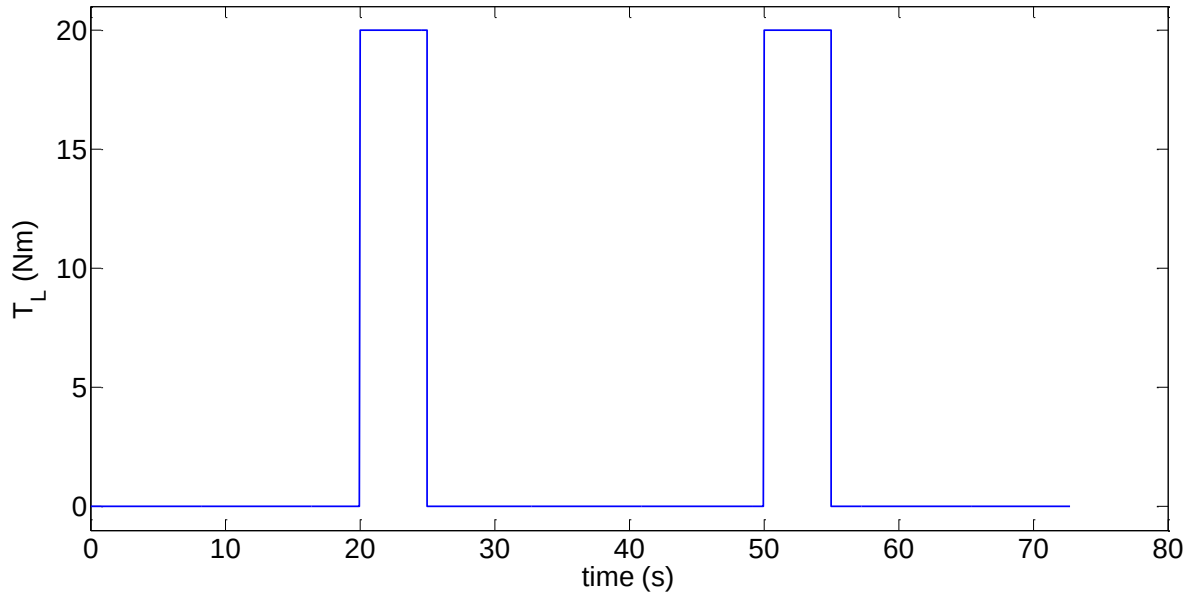

Fig. 124. Load torque signal used to simulate external disturbances

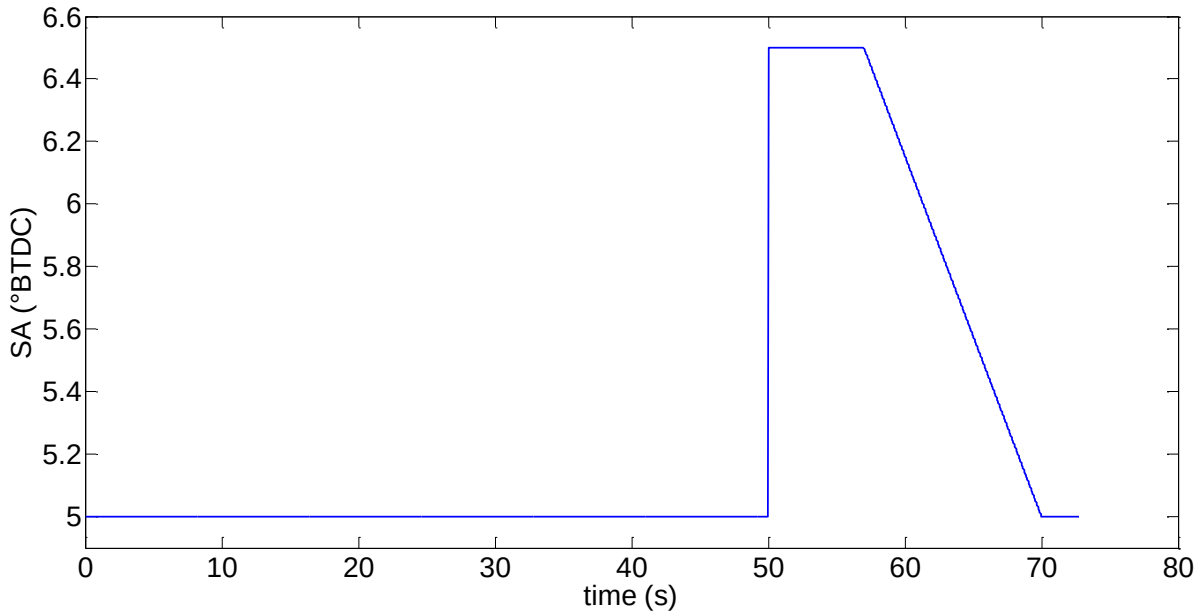

Fig. 125. Spark advance control strategy

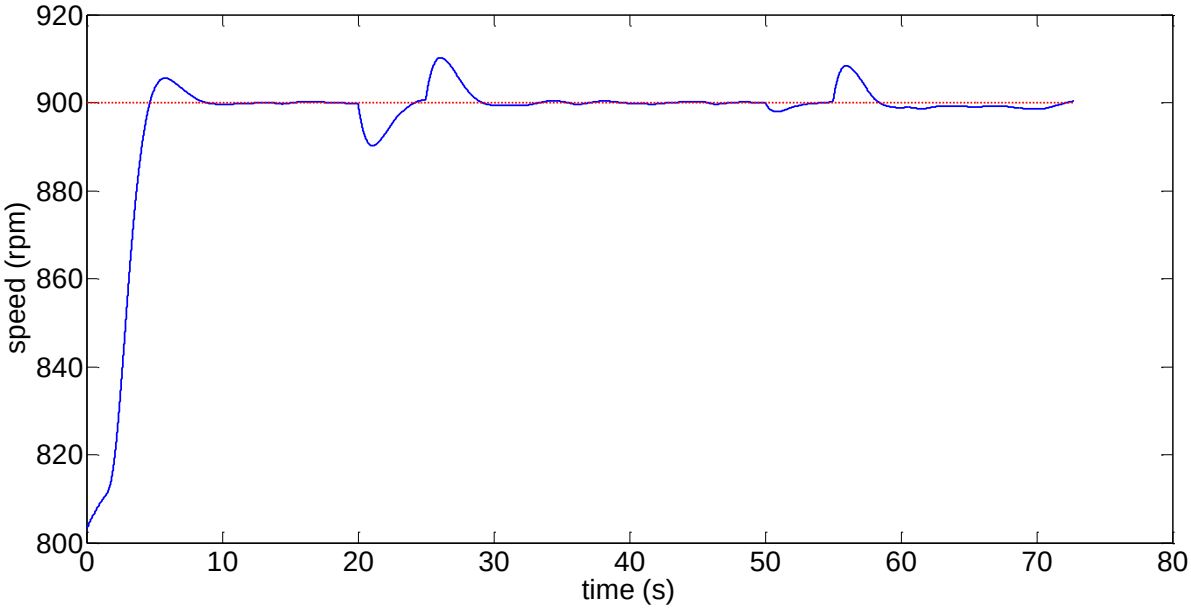

Fig. 126. Simulation results of the engine speed with two disturbances and a spark control strategy

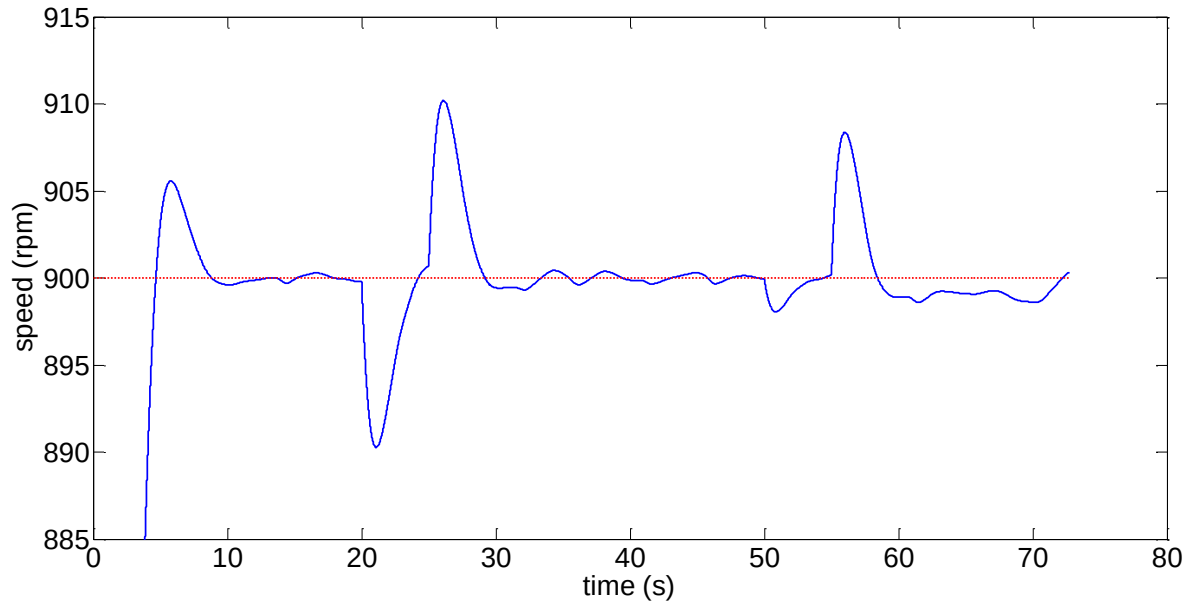

Fig. 127. Zoom around the idle speed reference

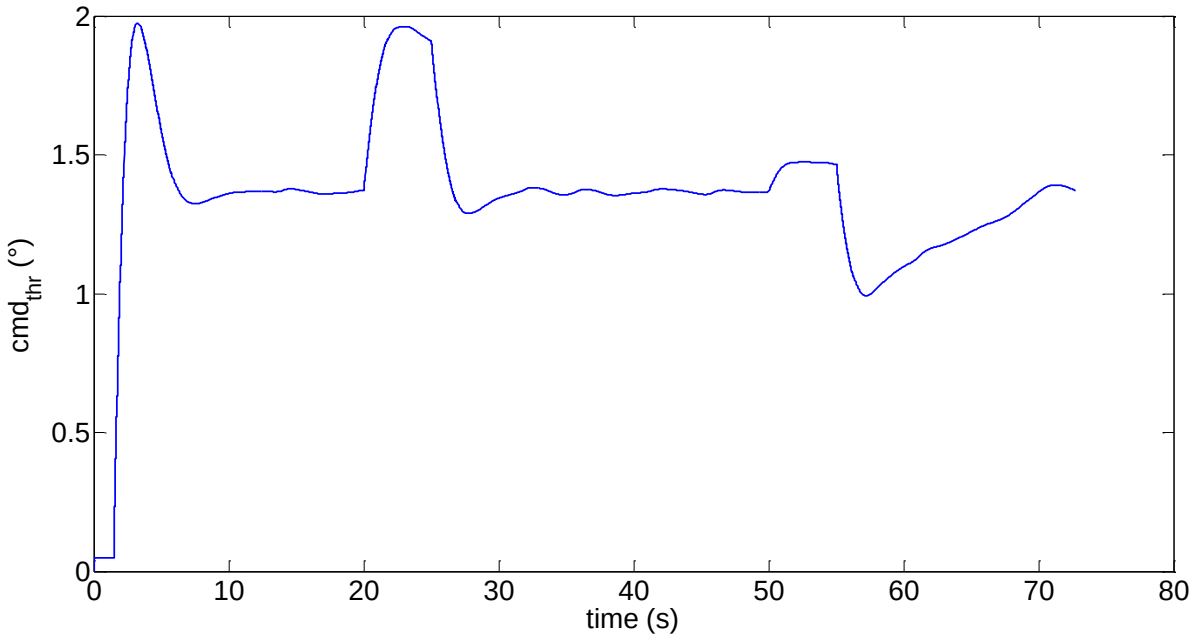

Fig. 128. Command generated by the CATS controller

A second short-term perspective that can be investigated is how to achieve the challenges of individual control (for the injectors, i.e. Challenge Fuel#3 and for the spark plugs, i.e. Challenge Spark#3). In order to control individually each cylinder, since they are not exactly equivalent, two different methodologies can be explored: Designing a controller for each cylinder, or designing one periodic controller. Indeed, the periodic behavior of the engine has been included in the sampling value of the crank-angle domain ($T_s^\theta = 180$ crankshaft degrees, so every engine turn). However, some theoretical tools have been developed for the design of controllers and observers of periodic systems, in both continuous-time and discrete-time (Bittanti and Colaneri, 2000; Colaneri, 2005; Bittanti and Colaneri, 2009). Particularly, controlling and observing periodic TS models have been recently considered, from a theoretical point of view in (Kerkeni et al., 2009; Lendek et al., 2013) and also from an application point of view since periodic observers have already been developed for estimating unmeasured values in the IC engine in (Chauvin et al., 2007; Kerkeni et al., 2010; Laurain et al., 2015a, 2015b). This could be very helpful to design for instance an individual fuel injection control since the observers can provide the individual air-fuel ratio of each cylinder.

As an example, if a system can be written as a $p-$periodic Takagi-Sugeno representation in the crank angle domain:

$$x^\theta(k+1) = A_z^{\theta,l} \cdot x^\theta(k) + B_z^{\theta,l} \cdot u^\theta(k) \tag{5.1.1}$$

then, a periodic TS observer can be designed based on (Guerra et al., 2012b):

$$\hat{x}^\theta(k+1) = A_z^{\theta,l} \cdot \hat{x}^\theta(k) + B_z^{\theta,l} \cdot u^\theta(k) + \left(S_z^{\theta,l}\right)^{-1} \cdot K_z^{\theta,l} \cdot \left(y(k) - \hat{y}(k)\right) \tag{5.1.2}$$

where l denotes the period index, $l \in \{0, \ldots, p-1\}$.

Remark (Periodic RATS observer): As one can see, this periodic TS observer implies a real-time matrix inversion due to the term $\left(S_z^{\theta,l}\right)^{-1}$. The results on design of alternative RATS observers in (Laurain et al., 2016d) should be extended to the case of periodic TS models.

Then, the accuracy of the estimation provided by the observer can be calculated from the estimation error:

$$\tilde{x}^{\theta}\left(k\right) = x^{\theta}\left(k\right) - \hat{x}^{\theta}\left(k\right) \tag{5.1.3}$$

The dynamics of this estimation error $\tilde{x}^{\theta}\left(k+1\right)$ can be established considering equations (5.1.1) and (5.1.2):

$$\tilde{x}^{\theta}\left(k+1\right) = \left(A_z^{\theta,l} - \left(S_z^{\theta,l}\right)^{-1} \cdot K_z^{\theta,l} \cdot C_z^{\theta,p}\right) \cdot \tilde{x}^{\theta}\left(k\right) \tag{5.1.4}$$

By applying the direct Lyapunov method, the estimation error is ensured to be converging to zero. The Lyapunov candidate function is a quadratic periodic one such that:

$$V^{l}\left(k\right) = \tilde{x}^{\theta}\left(k\right)^{T} \cdot P^{l} \cdot \tilde{x}^{\theta}\left(k\right) \tag{5.1.5}$$

Then, by following the proof in (Kerkeni et al., 2009), the following inequality should be verified:

$$V^{0}\left(k\right) > V^{1}\left(k+1\right) > \ldots > V^{p-1}\left(k+\left(p-1\right)\right) > V^{0}\left(k+p\right) \tag{5.1.6}$$

Then, LMI conditions can be obtained through relaxations. The theory behind periodic TS observers can be applied to the engine. Several values are unmeasured, however, they are crucial for an efficient control (such as the produced torque) or in order to optimize the behavior of each cylinder (such as the air mass inside each cylinder or the individual air-fuel ratio). The theoretical contributions of periodic TS observers have been applied to these engine problematics in (Laurain et al., 2015a, 2015b). The first application subject was to observe the spark advance contribution in each cylinder. In order to achieve such estimation, a cascaded observers structure is designed. One periodic TS observer is dedicated to estimate the amount of air inside each cylinder from the measured values of speed, pressure and throttle position. An unknown input observer is designed to reproduce the produced torque in function of the speed and the load torque (assumed to be known since it is a demand from the starter). Finally, a second periodic TS observer is realized to estimate the spark contribution of each cylinder based on the results of the two first observers, as depicted in the Fig. 129.

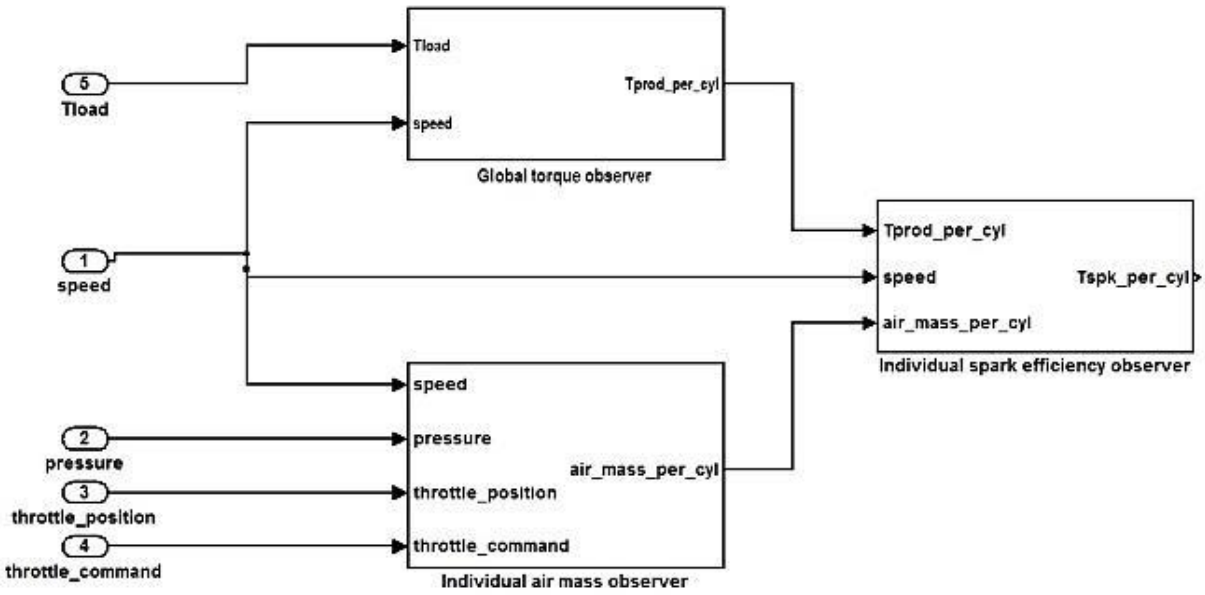

Fig. 129. Structure of the cascaded observers

Simulations are realized to present the results of this observer structure and the interest of periodic TS observers in engine applications. The engine speed is maintained at the idle speed by the controller designed in Chapter 3. The preliminary results of the first observer, i.e. the individual air mass observer, are presented in Fig. 130. They depict the air mass inside each cylinder during a transient phase (beginning of the simulation, where the speed goes from the initial speed $n_{init} = 700rpm$ until the reference speed $n_{ref} = 800rpm$).

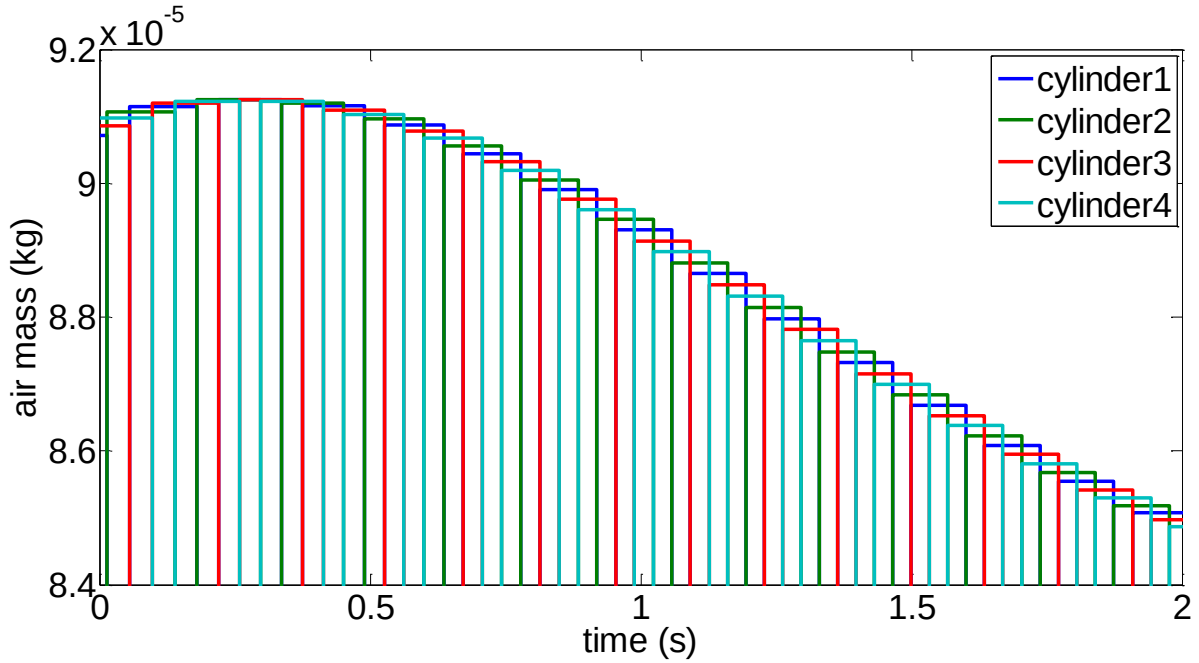

Fig. 130. Individual amount of air estimated by a periodic TS observer

Thanks to the periodic TS observer, the amount of air inside each cylinder can be estimated since it is not measured. With the knowledge of such a value, other unmeasured values can be obtained, such

as the individual air-fuel ratio (knowing the amount of fuel as a function of the injection timing) and then design a periodic controller that can provide a custom control law for each cylinder, optimizing the amount of fuel need to be injected and the air-fuel ratio of each cylinder, improving the functioning of the three-ways catalytic converter and the emitted pollution. By combining the results of this first periodic TS observer with an unknown input observer estimating the produced torque, the spark advance contribution inside each cylinder can be estimated. This can be useful in case of a fault on a spark plug. A simulation scenario has been realized considering two faults, simulated by a decrease of the spark advance command signal: One on the first cylinder (-20°) and another one on the third cylinder (-10°). The results of the individual spark advance contribution observer are presented in Fig. 131. As one can see, with the cascaded structure, the periodic TS observer is able to reconstruct the value of the spark advance contribution inside each cylinder, based on the individual air mass flow and the produced torque previously estimated. With such knowledge, the fault can be detected, located and then corrected by adjusting the control signal of each spark plug to compensate the faults.

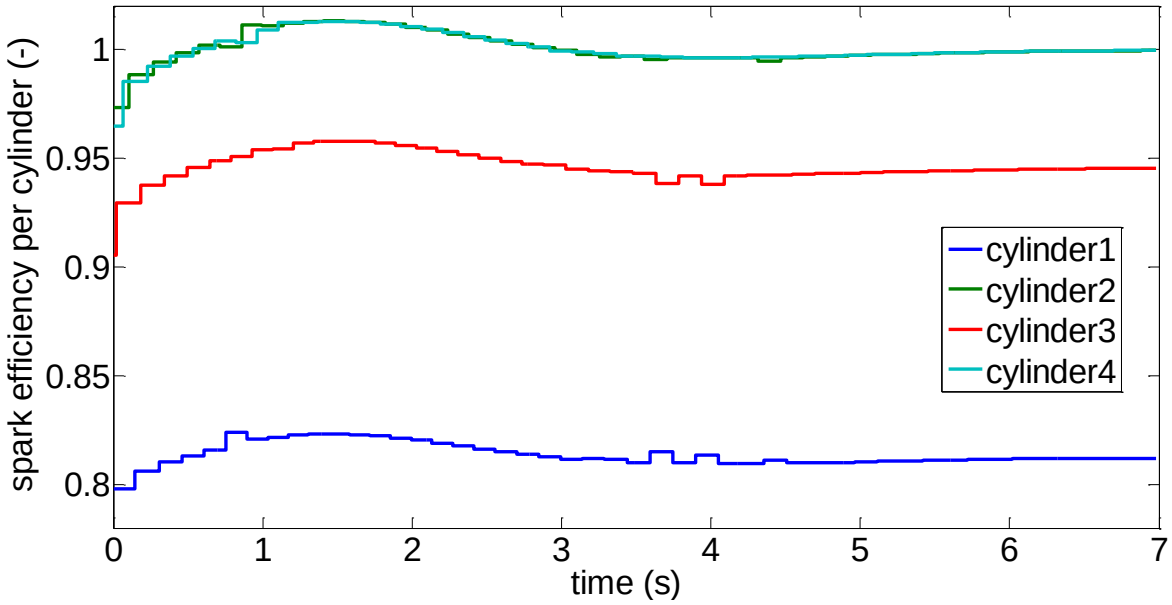

Fig. 131. Simulation results of the estimation of the spark advance contribution of each cylinder, with faults on the spark plugs

However, these periodic TS observers present the inconvenient of being dependent of the accuracy of the model. The spark advance model, as well as the produced torque model, is among the hardest parts of the engine to be identified, since no sensor can measure these values. The identification process of these models remains the major limit of the use of periodic TS observers for engine application.

Mid-term perspectives

Since the identification of the spark advance contribution model is a scientific challenge of the design of periodic TS observers in the context of engine control, several directions have to be investigated. Identification methods dedicated to periodic systems have already been developed, see for instance (Karam et al., 2003; Allen, 2009; Allen et al., 2011). These methodologies should be adapted to the

application case of the IC engine to identify the polynomial functions representing the spark advance contribution or the produced torque.

With an identified model, a fault detection module can be implemented in the ECU of the engine test bench. Fault management is realized in three main steps: Fault Detection, Identification and Reconfiguration (FDIR). Fault detection consists on the second mid-term perspective of this thesis since faults always occur in IC engines. FDIR in automotive context has been subject to many researches, for example with Driving Assistance in (Isermann et al., 2002), with combustion diagnosis in (Cavina et al., 2016) or in idle speed control context in (Montes-Solano and Pisu, 2009). Detection, identification and reconfiguration are challenging, since the engine is a very complex system. Detecting abnormal situations with a nonlinear system can be hard; identifying the location of the fault is challenging since the engine is periodically running and the values are interdependent; reconfiguration is crucial since the engine controller should be able to correct minor faults, at least be able to ensure minimum functions even in abnormal situations in order to prevent accidents and increase safety.

Two different approaches have been investigated in FDIR, as presented in the overview (Hwang et al., 2010): Robust residual generation and robust residual evaluation methods. The first category is based on filters and observers, i.e. a model is needed to design model-based fault detectors Examples of model-based FDIR are the individual spark advance contribution observer previously detailed (Laurain et al., 2015b), the one based on Parsimonious Gaussian mixture models (PGMM) (Nakamura et al., 2017) or considering input and output faults for an IC engine in (Montes-Solano and Pisu, 2009). Fault Detection, Identification and Reconfiguration techniques have been extended to the LPV systems (Blesa et al., 2010; Rotondo et al., 2014) and quasi-LPV systems, such as the Takagi-Sugeno models (Chadli et al., 2013; Ichalal et al., 2014). Particularly, FDIR of uncertain TS models has been considered using a L_2 gain observer in (Sing Kiong Nguang et al., 2007) or a sliding mode observer in (Akhenak et al., 2008).

These techniques are efficient as long as the model is accurate and well identified. In order to avoid parametric errors, the second category, robust residual evaluation, is based on measured signals: it is commonly called data-driven methods (de Bessa et al., 2016). It is based on techniques such as fuzzy/Bayesian network formulation (D'Angelo et al., 2011, 2014, 2016) or particle filters (Cosme et al., 2017). Since the engine has a periodic behavior, a perspective could be to adapt data-driven techniques to periodic systems by integrating the behavior aspect in the FDIR algorithms, i.e. to develop periodic data-driven fault detection systems.

Another mid-term perspective can focus on saturation. Indeed, in mechanical systems such as the IC engine, physical constraints and saturation exist and they have to be taken into account. Particularly, the case of constrained inputs has to be studied. From now in this thesis, anti-windup structures have been used to avoid divergence of the integral action when a bound is reached. However, better performance can be achieved by considering these saturations directly during the controller design (Nguyen et al., 2015, 2016, 2017a, 2017b). As an example, let us consider a discrete TS model with saturated input:

$$x(k+1) = A_z \cdot x(k) + B_z \cdot sat(u(k)) \tag{5.1.7}$$

Then, considering a non-PDC controller such that:

$$u(k) = -F_z \cdot H_z^{-1} \cdot x(t) \tag{5.1.8}$$

The closed-loop system combining (5.1.7) and (5.1.8) can be written:

$$x(k+1) = \left(A_z - B_z \cdot F_z \cdot H_z^{-1}\right) \cdot x(k) - B_z \cdot \psi(k) \tag{5.1.9}$$

with $\psi(k) = u(k) - sat(u(k))$. Then, the direct Lyapunov method can be applied to ensure the stability of the closed-loop system even when the control input signal reaches saturated bounds. The standard LMI conditions for TS systems controlled by non-PDC controllers are then improved with new conditions to ensure that the controller can handle bounded disturbance (either in energy or in amplitude) even if the control input is saturated. Including saturation directly in the design can provide less conservative conditions as well as less complex conditions, i.e. less number of variables in the LMI conditions. This systematic methodology to design advanced TS fuzzy controllers for constrained systems can be applied to the control of the IC engine since all the control inputs are saturated.

A last mid-term perspective is to finalize the experiments on the engine test bench located in Valenciennes. Indeed, this thesis has highlighted the efficiency of the proposed idle speed and air-fuel ratio controllers. By designing the spark advance controller as mentioned in the short-term perspectives, the whole engine control is achieved in a large case of situations (idle speed, disturbance rejection, normal driving conditions…). Moreover, fault-tolerant control can be designed based on the fault detection algorithms previously presented. However, some modules in the ECU are still missing to pretend having a full program that can be implemented in a commercial car. For instance, as presented in the Chapter 2, the cold start is a particular functioning case since the chemistry of the air-fuel mixture is changed. That is why the engines are now controlled by static maps when cold conditions are detected. The current implemented strategy in the engine test bench is to inject more fuel than needed, i.e. rich air-fuel ratio mixture in spite of the efficiency of the three ways catalytic converter, in order to increase the temperature of the engine and to reach quickly normal hot conditions. By designing a cold start controller that can handle this particular case, static maps could be definitively removed from the ECU. Then, a solution could be provided to handle all the control challenges of an IC engine using TS fuzzy methodology and proof of the stability using the Lyapunov direct method. Experimental results could be realized to highlight the efficiency of TS fuzzy controllers for every problematic of the internal combustion engine. Moreover, the open ECU of the engine test bench in Valenciennes is also equipping a commercial vehicle, so results can be obtained in road driving conditions, i.e. the most realistic experiments to validate the methodology for commercial cars.

Long-term perspectives

As long-term perspectives, the methodology could be extended to the case of a 3-cylinders engine. Indeed, engine constructors are currently tending to downsizing, i.e. reducing the size of the engine and keeping the same power and performance. In this context, 3-cylinders engines are becoming more popular. Since the periodic behavior of the engine model proposed in the thesis is based on a 4-cylinders engine, switching for a 3-cylinders engine make the model no longer valid. Most of the

theoretical contributions of the thesis can be used, or adapted. For example, the expression of the produced torque in function of measured values presented in Chapter 2 should be revised since the sampling value of the transformation to the crank-angle domain should be different. Fixing the time-varying delay of the air-fuel ratio control problem by using the transformation should also be adapted for the case of three cylinders. Once a 3-cylinders engine model is obtained, controllers can be designed for the different control inputs (throttle, fuel injectors and spark plugs). In order to validate the new controllers on an engine test bench, it is possible to consider the particular conditions of cylinder disable on a 4-cylinders engine. Indeed, the engine test bench of Valenciennes can be used by disabling one of the four cylinders. This technique of cylinder disable could improve the performance of 4-cylinders engines by changing their functioning to 3-cylinders behavior. Otherwise, another engine test bench could be used. Since this thesis is a partnership between the University of Valenciennes (UVHC), France and the Federal University of Minas Gerais (UFMG), Brazil, a collaboration can be realized with the Center for Technology and Mobility (CTM) located at UFMG. Recently, CTM purchased open controllers for their different engine test benches, including three, four, six and eight cylinders engines. A future collaboration can be realized to design advanced control systems in Valenciennes and implement them in specific engines in Belo Horizonte.

The situation of internal combustion engines in the future commercial cars can be discussed. Indeed, several countries, including France, aim to remove definitively gasoline and diesel cars for 2030. The feasibility of such a plan is not discussed, however, governments tend to remove fuel engines in profit of electric and hybrid cars. In that context, the whole engine control developed along this thesis can be used since a gasoline engine is part of a hybrid powertrain structure. Moreover, this engine is often playing the role of power generator, i.e. an engine running at idle speed conditions to reload the batteries. It is also the case of alternative power suppliers such as the ones used in hospitals and so on. In addition, including advanced engine control in trucks or boats can be considered, particularly since marine transport is not suffering any governmental constraints yet. The hypothesis of future laws on pollution emissions and fuel consumptions for marine vehicles has to be taken into account.

The advanced controllers developed along this document will probably be forgotten, adapted or changed; however, I hope that this thesis has illustrated the interest of considering nonlinear methods to control nonlinear systems such as internal combustion engines. In the future, one will see if the automotive industries decide to use appropriate tools to regulate pollution and consumption, otherwise one will not see anything since we are running to an ecological disaster.

REFERENCES

Any way you look at it, all the information that a person accumulates in a lifetime is just a drop in the bucket.

Batou in Masamune Shirow's *Ghost in the Shell*

By alphabetical order:

Abdi, J., Khalili, A. F., Inanlosaremi, K., and Askari, A. (2011). Air fuel ratio control in spark injection engines based on neural network and model predictive controller. in *IEEE Australian Control Conference (AUCC)* (Melbourne, Australia), 142–147.

Akhenak, A., Chadli, M., Ragot, J., and Maquin, D. (2008). Fault detection and isolation using sliding mode observer for uncertain Takagi-Sugeno fuzzy model. in *IEEE Mediterranean Conference on Control and Automation (MED)* (Ajaccio, France), 286–291.

Akram, M. A., Bhatti, A. I., and Ahmed, Q. (2013). Air/Fuel Ratio Estimation of SI Engine Using Higher Order Sliding Mode. in *IFAC Symposium on Advances in Automotive Control (AAC)* (Tokyo, Japan), 501–506.

Albertoni, L., Balluchi, A., Casavola, A., Gambelli, C., Mosca, E., and Sangiovanni-Vincentelli, A. L. (2005). Idle Speed Control of Port-Injection Engines via the polynomial equation approach. in *IFAC World Congress* (Prague, Czech Republic), 886–891.

Al-Hadithi, B. M., Jiménez, A., and Perez-Oria, J. (2015). New incremental Takagi–Sugeno state model for optimal control of multivariable nonlinear time delay systems. *Engineering Applications of Artificial Intelligence* 45, 259–268.

Alippi, C., Russis, C. de, and Piuri, V. (2003). A neural-network based control solution to air-fuel ratio control for automotive fuel-injection systems. *IEEE Transactions on Systems, Man, and Cybernetics, Part C (Applications and Reviews)* 33, 259–268.

Alkemade, U. G., and Schumann, B. (2006). Engines and exhaust after treatment systems for future automotive applications. in *International Conference on Solid State Ionics, Part II* (Baden-Baden, Germany), 2291–2296.

Allen, M. S. (2009). Frequency-Domain Identification of Linear Time-Periodic Systems Using LTI Techniques. *Journal of Computational and Nonlinear Dynamics* 4.

Allen, M. S., Sracic, M. W., Chauhan, S., and Hansen, M. H. (2011). Output-only modal analysis of linear time-periodic systems with application to wind turbine simulation data. *Mechanical Systems and Signal Processing* 25, 1174–1191.

Andersson, P., and Eriksson, L. (2005). Observer-based Feedforward Air-Fuel Ratio Control of Turbocharged SI Engines. in *IFAC World Congress* (Prague, Czech Republic: IFAC), 200–205.

Arsie, I., Pianese, C., and Sorrentino, M. (2006). A procedure to enhance identification of recurrent neural networks for simulating air–fuel ratio dynamics in SI engines. *Engineering Applications of Artificial Intelligence* 19, 65–77.

Arsie, I., Sorrentino, M., and Pianese, C. (2007). A neural network air-fuel ratio estimator for control and diagnostics in spark-ignited engines. in *IFAC Symposium on Advances in Automotive Control (AAC)* (Monterey, California, USA), 227–234.

Ashok, B., Denis Ashok, S., and Ramesh Kumar, C. (2016). A review on control system architecture of a SI engine management system. *Annual Reviews in Control* 41, 94–118.

Bailey, D. H., Lee, K., and Simon, H. D. (1991). Using Strassen's algorithm to accelerate the solution of linear systems. *The Journal of Supercomputing* 4, 357–371.

Balenovic, M., and Backx, T. (2001). Model-based predictive control of a three-way catalytic converter. in *IEEE International Conference on Control Applications (CCA)*, 626–631.

Ball, J. K., Bowe, M. J., Stone, C. R., and McFadden, P. D. (2000). Torque estimation and misfire detection using block angular acceleration. SAE Technical Paper.

Balluchi, A., D'Apice, C., Gaeta, M., Piccoli, B., Sangiovanni-Vincentelli, A. L., and Zadarnowska, K. (2010). A hybrid feedback for a benchmark problem of idle speed control. *International Journal of Robust and Nonlinear Control* 20, 515–530.

Barbarisi, O., Alessandro, G., and Luigi, G. (2002). An Extended Kalman Observer for the In-Cylinder Air Mass Flow Estimation. in *International Workshop on Diagnostics in Automotive Engines and Vehicles*, 1–14.

Bengea, S. C., Li, X., and DeCarlo, R. A. (2004). Combined Controller-Observer Design for Uncertain Time Delay Systems With Application to Engine Idle Speed Control. *Journal of Dynamic Systems, Measurement, and Control* 126, 772.

Bickel, J., Odendall, B., Eigenberger, G., and Nieken, U. (2017). Oxygen storage dominated three-way catalyst modeling for fresh catalysts. *Chemical Engineering Science* 160, 34–53.

Bittanti, S., and Colaneri, P. (2000). Invariant representations of discrete-time periodic systems. *Automatica* 36, 1777–1793.

Bittanti, S., and Colaneri, P. (2009). *Periodic Systems: Filtering and Control*. Springer Science & Business Media.

Blandeau, M., Estrada-Manzo, V., Guerra, T.-M., Pudlo, P., and Gabrielli, F. (2017). Fuzzy unknown input observer for understanding sitting control of persons living with spine cord injury. *Engineering Applications of Artificial Intelligence (EAAI)*.

Blandeau, M., Guerra, T. M., Pudlo, P., Gabrielli, F., and Estrada-Manzo, V. (2016). How a person with spinal cord injury controls a sitting situation Unknown input observer and delayed feedback control with time-varying input delay. in *IEEE International Conference on Fuzzy Systems (FUZZ-IEEE)* (Vancouver, Canada: IEEE), 2349–2356.

Blesa, J., Puig, V., and Bolea, Y. (2010). Fault detection using interval LPV models in an open-flow canal. *Control Engineering Practice* 18, 460–470.

Bohn, C., Bohme, T., Staate, A., and Manemann, P. (2006). A nonlinear model for design and simulation of automotive idle speed control strategies. in *IEEE American Control Conference (ACC)*, 3272–3277.

Bortolet, P., Merlet, E., and Boverie, S. (1997). Fuzzy modeling and control of an engine air inlet with exhaust gas recirculation. *Control Engineering Practice* 7, 1269–1277.

Bouarar, T., Guelton, K., and Manamanni, N. (2009). Static output feedback controller design for Takagi-Sugeno systems-a fuzzy Lyapunov LMI approach. in *IEEE Conference on Decision and Control (CDC) / IEEE Chinese Control Conference (CCC)* (Shanghai, China), 4150–4155.

Bougrine, S., Richard, S., Michel, J.-B., and Veynante, D. (2014). Simulation of CO and NO emissions in a SI engine using a 0D coherent flame model coupled with a tabulated chemistry approach. *Applied Energy* 113, 1199–1215.

Bourahala, F., Guelton, K., Khaber, F., and Manamanni, N. (2016). Improvements on PDC Controller Design for Takagi-Sugeno Fuzzy Systems with State Time-Varying Delays. in *IFAC International Conference on Intelligent Control and Automation Sciences (ICONS)* (Reims, France), 200–205.

Bowman, C. T. (1975). Kinetics of pollutant formation and destruction in combustion. *Progress in energy and combustion science* 1, 33–45.

Boyd, S., El Ghaoui, L., Feron, E., and Balakrishnan, V. (1994). *Linear matrix inequalities in system and control theory*. Studies in Applied Mathematics. Society for Industrial and Applied Mathematics (SIAM).

Bunch, J. R., and Hopcroft, J. E. (1974). Triangular factorization and inversion by fast matrix multiplication. *Mathematics of Computation* 28, 231–236.

Carbot-Rojas, D. A., Escobar-Jiménez, R. F., Gómez-Aguilar, J. F., and Téllez-Anguiano, A. C. (2017). A survey on modeling, biofuels, control and supervision systems applied in internal combustion engines. *Renewable and Sustainable Energy Reviews* 73, 1070–1085.

Cavina, N., Businaro, A., Rojo, N., De Cesare, M., Paiano, L., and Cerofolini, A. (2016). Combustion and Intake/Exhaust Systems Diagnosis Based on Acoustic Emissions of a GDI TC Engine. *Energy Procedia* 101, 677–684.

Cavina, N., Corti, E., and Moro, D. (2010). Closed-loop individual cylinder air–fuel ratio control via UEGO signal spectral analysis. *Control Engineering Practice* 18, 1295–1306.

Ceschini, L., Morri, A., Balducci, E., Cavina, N., Rojo, N., Calogero, L., et al. (2017). Experimental observations of engine piston damage induced by knocking combustion. *Materials & Design* 114, 312–325.

Chadli, M., Abdo, A., and Ding, S. X. (2013). Fault detection filter design for discrete-time Takagi–Sugeno fuzzy system. *Automatica* 49, 1996–2005.

Chamaillard, Y., and Perrier, C. (2001). Air-Fuel Ratio Control by Fuzzy Logic, Preliminary Investigation. in *IFAC Symposium on Advances in Automotive Control (AAC)* (Karlsruhe, Germany), 211–216.

Chang, C.-F., Fekete, N. P., Amstutz, A., and Powell, Jd. (1995). Air-fuel ratio control in spark-ignition engines using estimation theory. *IEEE Transactions on Control Systems Technology* 3, 22–31.

Chang, W.-J., Ku, C.-C., and Chang, C.-H. (2012). PDC and Non-PDC fuzzy control with relaxed stability conditions for contintuous-time multiplicative noised fuzzy systems. *Journal of the Franklin Institute* 349, 2664–2686.

Chauvin, J., Corde, G., Moulin, P., Castagné, M., Petit, N., and Rouchon, P. (2004). Real-time combustion torque estimation on a diesel engine test bench using time-varying Kalman filtering. in *IEEE Conference on Decision and Control (CDC)* (Atlantis, Bahamas), 1688–1694.

Chauvin, J., Corde, G., Petit, N., and Rouchon, P. (2007). Periodic input estimation for linear periodic systems: Automotive engine applications. *Automatica* 43, 971–980.

Colaneri, P. (2005). Theoretical aspects of continuous-time periodic systems. *Annual Reviews in Control* 29, 205–215.

Connolly, F. T., and Rizzoni, G. (1994). Real time estimation of engine torque for the detection of engine misfires. *ASME Journal of Dynamic Systems, Measurement, and Control* 116, 675–675.

Corti, E., Cavina, N., Cerofolini, A., Forte, C., Mancini, G., Moro, D., et al. (2014). Transient Spark Advance Calibration Approach. *Energy Procedia* 45, 967–976.

Cosme, L. B., D'Angelo, M. F. S. V., Caminhas, W. M., Yin, S., and Palhares, R. M. (2017). A novel fault prognostic approach based on particle filters and differential evolution. *Applied Intelligence*, 1–20.

Croz, J. J. D., and Higham, N. J. (1992). Stability of Methods for Matrix Inversion. *IMA Journal of Numerical Analysis* 12, 1–19.

Czarnigowski, J. (2010). A neural network model-based observer for idle speed control of ignition in SI engine. *Engineering Applications of Artificial Intelligence* 23, 1–7.

Daasch, A., Schulz, E., and Schultalbers, M. (2016). Intrinsic Performance Limitations of Torque Generation in a Turbocharged Gasoline Engine. in *IFAC Symposium on Advances in Automotive Control (AAC)* (Norrköping, Sweden), 714–721.

Dambrine, M., and Richard, J. P. (1993). Stability analysis of time-delay systems. *Dynamic Systems and Applications* 2, 405–414.

D'Angelo, M. F. S. V., Palhares, R. M., Camargos Filho, M. C. O., Maia, R. D., Mendes, J. B., and Ekel, P. Y. (2016). A new fault classification approach applied to Tennessee Eastman benchmark process. *Applied Soft Computing* 49, 676–686.

D'Angelo, M. F. S. V., Palhares, R. M., Cosme, L. B., Aguiar, L. A., Fonseca, F. S., and Caminhas, W. M. (2014). Fault detection in dynamic systems by a Fuzzy/Bayesian network formulation. *Applied Soft Computing* 21, 647–653.

D'Angelo, M. F. S. V., Palhares, R. M., Takahashi, R. H. C., and Loschi, R. H. (2011). Fuzzy/Bayesian change point detection approach to incipient fault detection. *IET Control Theory and Applications* 5, 539–551.

Däubler, L., Bessai, C., and Predelli, O. (2007). Tuning strategies for online-adaptive PI controllers. *Oil & Gas Science and Technology-Revue de l'IFP* 62, 493–500.

de Bessa, I. V., Palhares, R. M., D'Angelo, M. F. S. V., and Chaves Filho, J. E. (2016). Data-driven fault detection and isolation scheme for a wind turbine benchmark. *Renewable Energy* 87, 634–645.

De Oliveira, F. S. S., Souza, F. O., and Palhares, R. M. (2017). PID Tuning for Time-Varying Delay Systems Based on Modified Smith Predictor. in *IFAC World Congress* (Toulouse, France).

De Oliveira, M. C., and Skelton, R. E. (2001). "Stability tests for constrained linear systems," in *Perspectives in robust control* Lecture Notes in Control and Information Sciences. (Springer), 241–257.

De Santis, E., Di Benedetto, M. D., and Pola, G. (2006). Digital idle speed control of automotive engines: A safety problem for hybrid systems. *Nonlinear Analysis: Theory, Methods & Applications* 65, 1705–1724.

Demesoukas, S., Caillol, C., Higelin, P., Boiarciuc, A., and Floch, A. (2015). Near wall combustion modeling in spark ignition engines. Part B: Post-flame reactions. *Energy Conversion and Management* 106, 1439–1449.

Desheng, H., Yunfeng, H., and Hong, C. (2014). Model-based calibration for torque control system of gasoline engines. in *IEEE International Conference on Mechatronics and Control (ICMC)*, 1774–1779.

Di Cairano, S., Yanakiev, D., Bemporad, A., Kolmanovsky, I. V., and Hrovat, D. (2012). Model Predictive Idle Speed Control: Design, Analysis, and Experimental Evaluation. *IEEE Transactions on Control Systems Technology*.

Di, N., Kai, S., Junhui, H., and Jiajun, S. (2010). Individual Spark Advance Adjusting in a Multi-Cylinder Spark Ignition Engine. in *IEEE International Conference on Electrical and Control Engineering (ICECE)* (Wuhan, China), 1192–1195.

Dickinson, P. B., Rivara, N., and Shenton, A. T. (2009). A Dynamically Identified Algebraic NARX Air-to-Fuel Ratio Estimator. in *IFAC Workshop on Engine and Powertrain Control, Simulation and Modeling (E-COSM)* (Rueil-Malmaison, France), 248–254.

Ding, B., Sun, H., and Yang, P. (2006). Further studies on LMI-based relaxed stabilization conditions for nonlinear systems in Takagi–Sugeno's form. *Automatica* 42, 503–508.

Donghui, X. (2016). Study on Chaotic Time Series LS-SVM Prediction of Gasoline Engine Transient Air Fuel Ratio. in *IEEE International Conference on Robots Intelligent System (ICRIS)* (Zhangjiajie, China), 402–408.

Donghui, X., Yuelin, L., and Zhouzhe (2014). Study on Transient Air-Fuel Ratio Predictive Model of Gasoline Engine Based on Artificial Intelligence. in *IEEE International Conference on Intelligent Computation Technology and Automation (ICICTA)* (Changsha, China), 742–745.

Dongliang, W., Kaisheng, H., Xiaozhong, W., and Yinhui, W. (2011). The impact of oxygen sensor degradation on air-fuel ratio and emissions. in *IEEE International Conference on Electric Information and Control Engineering (ICEICE)* (Wuhan, China), 2773–2776.

Ebrahimi, B., Tafreshi, R., Masudi, H., Franchek, M., Mohammadpour, J., and Grigoriadis, K. (2012). A parameter-varying filtered PID strategy for air–fuel ratio control of spark ignition engines. *Control Engineering Practice* 20, 805–815.

Efimov, D. V., Javaherian, H., and Nikiforov, V. O. (2010). Iterative learning air-fuel ratio control with adaptation in spark ignition engines. in *IEEE American Control Conference (ACC)* (Baltimore, USA), 2063–2068.

Efimov, D. V., Nikiforov, V. O., and Javaherian, H. (2014). Supervisory control of air–fuel ratio in spark ignition engines. *Control Engineering Practice* 30, 27–33.

Enang, W., and Bannister, C. (2017). Modelling and control of hybrid electric vehicles (A comprehensive review). *Renewable and Sustainable Energy Reviews* 74, 1210–1239.

Eriksson, L. (1999). *Spark advance modeling and control*. Linköping: Studies in Science and Technology.

Eriksson, L., and Nielsen, L. (2000). Non-Linear Model-Based Throttle Control. *SAE Technical Paper*.

Fiengo, G., Grizzle, J. W., Cook, J. A., and Karnik, A. Y. (2005). Dual-UEGO active catalyst control for emissions reduction: design and experimental validation. *IEEE Transactions on Control Systems Technology* 13, 722–736.

Fontaras, G., Zacharof, N.-G., and Ciuffo, B. (2017). Fuel consumption and CO2 emissions from passenger cars in Europe – Laboratory versus real-world emissions. *Progress in Energy and Combustion Science* 60, 97–131.

Fridman, E. (2014). Tutorial on Lyapunov-based methods for time-delay systems. *European Journal of Control* 20, 271–283.

Fridman, E., and Dambrine, M. (2009). Control under quantization, saturation and delay: An LMI approach. *Automatica* 45, 2258–2264.

Fridman, E., Dambrine, M., and Yeganefar, N. (2008). On input-to-state stability of systems with time-delay: A matrix inequalities approach. *Automatica* 44, 2364–2369.

Gao, J., Wu, Y., and Shen, T. (2015). Combustion Phase Control of SI Gasoline Engines Using Hypothesis Test. in *IFAC Workshop on Engine and Powertrain Control, Simulation and Modeling (E-COSM)* (Rueil-Malmaison, France), 153–158.

García-Nieto, S., Salcedo, J., Martínez, M., and Laurí, D. (2009). Air management in a diesel engine using fuzzy control techniques. *Information Sciences* 179, 3392–3409.

Gerasimov, D. N., Belyaev, M. E., Nikiforov, V. O., Javaherian, H., Li, S., and Hu, Y. (2016). Inverse adaptive air-fuel ratio control in spark ignition engines. in *IFAC IEEE European Control Conference (ECC)* (Aalbotrg, Denmark), 1253–1258.

Gerasimov, D. N., and Pshenichnikova, E. I. (2012). Neural network data-driven engine torque and air-fuel ratio control. in *IEEE Mediterranean Electrotechnical Conference (MELECON)* (Yasmine Hammamet, Tunisia), 524–527.

Ghaffari, A., and Shamekhi, A. H. (2005). Fuzzy Control of Spark Advance by Ion Current Sensing. in *SAE World Congress*.

Ghaffari, A., Shamekhi, A. H., Saki, A., and Kamrani, E. (2008). Adaptive fuzzy control for air-fuel ratio of automobile spark ignition engine. *World Academy of Science, Engineering and Technology* 48, 284–292.

Goldberg, D. (1991). What Every Computer Scientist Should Know About Floating-point Arithmetic. *ACM Computing Surveys* 23, 5–48.

Grizzle, J. W., Dobbins, K. L., and Cook, J. A. (1991). Individual cylinder air-fuel ratio control with a single EGO sensor. *IEEE Transactions on Vehicular Technology* 40, 280–286.

Guardiola, C., Olmeda, P., Pla, B., and Bares, P. (2017). In-cylinder pressure based model for exhaust temperature estimation in internal combustion engines. *Applied Thermal Engineering* 115, 212–220.

Guerra, T.-M., Bernal, M., Guelton, K., and Labiod, S. (2012a). Non-quadratic local stabilization for continuous-time Takagi–Sugeno models. *Fuzzy Sets and Systems* 201, 40–54.

Guerra, T.-M., Kerkeni, H., Lauber, J., and Vermeiren, L. (2012b). An efficient Lyapunov function for discrete T–S models: observer design. *IEEE Transactions on Fuzzy Systems* 20, 187–192.

Guerra, T.-M., Kruszewski, A., Vermeiren, L., and Tirmant, H. (2006). Conditions of output stabilization for nonlinear models in the Takagi–Sugeno's form. *Fuzzy Sets and Systems* 157, 1248–1259.

Guerra, T.-M., and Vermeiren, L. (2004). LMI-based relaxed nonquadratic stabilization conditions for nonlinear systems in the Takagi–Sugeno's form. *Automatica* 40, 823–829.

Guzzella, L., and Onder, C. H. (2010). *Introduction to Modeling and Control of Internal Combustion Engine Systems*. Berlin, Heidelberg: Springer Berlin Heidelberg.

Guzzella, L., Simons, M., and Geering, H. P. (1997). Feedback linearizing air/fuel-ratio controller. *Control Engineering Practice* 5, 1101–1105.

Haghani, A., Jeinsch, T., Roepke, M., Ding, S. X., and Weinhold, N. (2016). Data-driven monitoring and validation of experiments on automotive engine test beds. *Control Engineering Practice* 54, 27–33.

Hanus, R. (1980). A new technique for preventing control windup. *Journal A* 21.

Hara, T., Shen, T., and Mutoh, Y. (2012). Iterative learning-based air-fuel control of gasoline engines with unknown off-set. in *IEEE International Conference Intelligent Systems (IS)* (Sofia, Bulgaria), 304–309.

Hasan, A. O., Abu-jrai, A., Al-Muhtaseb, A. H., Tsolakis, A., and Xu, H. (2016a). Formaldehyde, acetaldehyde and other aldehyde emissions from HCCI/SI gasoline engine equipped with prototype catalyst. *Fuel* 175, 249–256.

Hasan, A. O., Abu-Jrai, A., Al-Muhtaseb, A. H., Tsolakis, A., and Xu, H. (2016b). HC, CO and NOx emissions reduction efficiency of a prototype catalyst in gasoline bi-mode SI/HCCI engine. *Journal of Environmental Chemical Engineering* 4, 2410–2416.

Hazell, P. A., and Flower, J. O. (1971). Discrete modelling of spark-ignition engines for control purposes. *International Journal of Control* 13, 625–632.

He, B., Shen, T., Kako, J., and Ouyang, M. (2008). Input Observer-Based Individual Cylinder Air-Fuel Ratio Control: Modelling, Design and Validation. *IEEE Transactions on Control Systems Technology* 16, 1057–1065.

Hendricks, E., Poulsen, J., Olsen, M. B., Jensen, P. B., Fons, M., and Jepsen, C. (1996). Alternative observers for SI engine air/fuel ratio control. in *IEEE Conference on Decision and Control (CDC)* (Kobe, Japan), 2806–2811.

Higham, N. (1992). Stability of a Method for Multiplying Complex Matrices with Three Real Matrix Multiplications. *SIAM Journal on Matrix Analysis and Applications* 13, 681–687.

Hillesland, K., and Lastra, A. (2004). GPU floating-point paranoia. *Proceedings of GP2* 318.

Hrovat, D., Cairano, S. D., Tseng, H. E., and Kolmanovsky, I. V. (2012). The development of Model Predictive Control in automotive industry: A survey. in *IEEE International Conference on Control Applications (CCA)* (Dubrovnik, Croatia), 295–302.

Hrovat, D., and Sun, J. (1997). Models and control methodologies for IC engine idle speed control design. *Control Engineering Practice* 5, 1093–1100.

Hu, Y., Fan, Y., Liang, Y., and Chen, H. (2014). Data-driven model predictive control of Air-fuel Ratio for PFISI engine. in *IEEE World Congress on Intelligent Control and Automation (WCICA)* (Shenyang, China), 4577–4582.

Huber, J., Kopecek, H., and Hofbaur, M. (2015). Nonlinear model predictive control of an internal combustion engine exposed to measured disturbances. *Control Engineering Practice* 44, 78–88.

Hwang, I., Kim, S., Kim, Y., and Seah, C. E. (2010). A Survey of Fault Detection, Isolation, and Reconfiguration Methods. *IEEE Transactions on Control Systems Technology* 18, 636–653.

Ichalal, D., Marx, B., Ragot, J., and Maquin, D. (2014). Fault detection, isolation and estimation for Takagi–Sugeno nonlinear systems. *Journal of the Franklin Institute* 351, 3651–3676.

Isermann, R., Schwarz, R., and Stolzl, S. (2002). Fault-tolerant drive-by-wire systems. *IEEE Control Systems Magazine* 22, 64–81.

Isermann, R., and Sequenz, H. (2016). Model-based development of combustion-engine control and optimal calibration for driving cycles: general procedure and application. in *IFAC Symposium on Advances in Automative Control (AAC)* (Norrköping, Sweden), 633–640.

Jankovic, M., and Magner, S. (2011). Disturbance attenuation in time-delay systems; A case study on engine air-fuel ratio control. in *IEEE American Control Conference (ACC)* (San Francisco, USA), 3326–3331.

Jansri, A., and Sooraksa, P. (2012). Enhanced model and fuzzy strategy of air to fuel ratio control for spark ignition engines. *Computers & Mathematics with Applications* 64, 922–933.

Ji, C., Yu, M., Wang, S., Zhang, B., Cong, X., Feng, Y., et al. (2016). The optimization of on-board H2 generator control strategy and fuel consumption of an engine under the NEDC condition with start-stop system and H2 start. *International Journal of Hydrogen Energy* 41, 19256–19264.

Jia, G., Gong, J., Deng, Y., Fu, J., and Yu, M. (2011). Intelligent control study of engine air-fuel ratio co-simulation based on information fusion. in *IEEE International Conference on Electric Information and Control Engineering (ICEICE)* (Wuhan, China), 2282–2285.

Jiao, X., and Shen, T. (2011). Lyapunov-design of adaptive air-fuel ratio control for gasoline engines based on mean-value model. in *IEEE Chinese Control Conference (CCC)* (Yantai, China), 6146–6150.

Jordaan, S. M., Romo-Rabago, E., McLeary, R., Reidy, L., Nazari, J., and Herremans, I. M. (2017). The role of energy technology innovation in reducing greenhouse gas emissions: A case study of Canada. *Renewable and Sustainable Energy Reviews* 78, 1397–1409.

Kahveci, N. E., Impram, S. T., and Genc, A. U. (2014a). Adaptive Internal Model Control for Air-Fuel Ratio regulation. in *IEEE Intelligent Vehicles Symposium (IV)* (Ypsilanti, USA), 1091–1096.

Kahveci, N. E., Impram, S. T., and Genc, A. U. (2014b). Air-fuel ratio regulation using a discrete-time internal model controller. in *IEEE Conference on Intelligent Transportation Systems (ITSC)* (Qingdao, China), 2459–2464.

Kahveci, N. E., and Jankovic, M. J. (2010). Adaptive controller with delay compensation for Air-Fuel Ratio regulation in SI engines. in *IEEE American Control Conference (ACC)* (Baltimore, USA), 2236–2241.

Kang, M., Alamir, M., and Shen, T. (2016). Nonlinear Constrained Torque Control for Gasoline Engines. in *IFAC Symposium on Nonlinear Control Systems (NOLCOS)* (Monterey, California, USA), 784–789.

Kang, M., Shen, T., and Jiao, X. (2014). Continuation/GMRES Method based Nonlinear Model Predictive Control for IC Engines. in *IFAC World Congress* (Cape Town, South Africa), 5697–5702.

Karam, M., Fadali, M. S., and White, K. (2003). A Fourier/Hopfield neural network for identification of nonlinear periodic systems. in *Proceedings of the 35th Southeastern Symposium on System Theory, 2003.*, 53–57.

Karvountzis-Kontakiotis, A., and Ntziachristos, L. (2016). Improvement of NO and CO predictions for a homogeneous combustion SI engine using a novel emissions model. *Applied Energy* 162, 172–182.

Kerkeni, H. (2011). Analyse et synthèse des modèles non linéaires périodiques : application au moteur à allumage commandé.

Kerkeni, H., Lauber, J., and Guerra, T. M. (2010). Estimation of Individual In-cynlinder air mass flow via Periodic Observer in Takagi-Sugeno form. in *IEEE Vehicle Power and Propulsion Conference (VPPC)* (Lille, France), 1–6.

Kerkeni, H., Lauber, J., and Guerra, T.-M. (2009). Some results about stabilization of periodic takagi-sugeno models. in *IEEE International Conference on Fuzzy Systems (FUZZ-IEEE)* (Jeju, Korea), 814–819.

Kerkeni, H., Lauber, J., Lendek, Z., and Guerra, T. M. (2008). Individual cylinder air/fuel ratio observer on IC engine using Takagi-Sugeno's fuzzy model. in *IEEE Vehicle Power and Propulsion Conference (VPPC)* (Harbin, China), 1–6.

Keynejad, F., and Manzie, C. (2011). Cold start modelling of spark ignition engines. *Control Engineering Practice* 19, 912–925.

Khajorntraidet, C., Ito, K., and Shen, T. (2015). Adaptive time delay compensation for air-fuel ratio control of a port injection SI engine. in *IEEE Annual Conference of the Society of Instrument and Control Engineers of Japan (SICE)* (Hangzhou, China), 1341–1346.

Khajorntraidet, C., and Shen, T. (2016). Simple adaptive air-fuel ratio control for lean combustion of commercial SI engines. in *IEEE Conference on Control Applications (CCA)* (Buenos Aires, Argentina), 881–885.

Khalil, H. (1996). *Nonlinear Systems*. New Jersey: Prentice Hall.

Khiar, D. (2007). Modélisation et commande d'un moteur thermique à allumage commandé.

Killingsworth, N. J., Aceves, S. M., Flowers, D. L., Espinosa-Loza, F., and Krstic, M. (2009). HCCI Engine Combustion-Timing Control: Optimizing Gains and Fuel Consumption Via Extremum Seeking. *IEEE Transactions on Control Systems Technology* 17, 1350–1361.

Kiwitz, P., Onder, C., and Guzzella, L. (2012). Control-oriented modeling of a three-way catalytic converter with observation of the relative oxygen level profile. *Journal of Process Control* 22, 984–994.

Kumar, M., and Shen, T. (2017). In-cylinder pressure-based air-fuel ratio control for lean burn operation mode of SI engines. *Energy* 120, 106–116.

Kumar, P., Gu, T., Grigoriadis, K., Franchek, M., and Balakotaiah, V. (2014). Spatio-temporal dynamics of oxygen storage and release in a three-way catalytic converter. *Chemical Engineering Science* 111, 180–190.

Laila, D. S., and Gruenbacher, E. (2016). Nonlinear output feedback and periodic disturbance attenuation for setpoint tracking of a combustion engine test bench. *Automatica* 64, 29–36.

Lam, H. K., and Leung, F. H. F. (2007). LMI-Based Stability and Performance Conditions for Continuous-Time Nonlinear Systems in Takagi-Sugeno's Form. *IEEE Transactions on Systems, Man and Cybernetics, Part B (Cybernetics)* 37, 1396–1406.

Lang, J., Zhou, Y., Cheng, S., Zhang, Y., Dong, M., Li, S., et al. (2016). Unregulated pollutant emissions from on-road vehicles in China, 1999–2014. *Science of The Total Environment* 573, 974–984.

Lauber, J. (2003). Moteur à allumage commandé avec EGR: modélisation et commande non linéaires.

Lauber, J., Guerra, T. M., and Dambrine, M. (2011). Air-fuel ratio control in a gasoline engine. *International Journal of Systems Science* 42, 277–286.

Lauber, J., Guerra, T.-M., and Perruquetti, W. (2003). Disturbance rejection using Takagi-Sugeno fuzzy model: application to an IC engine. in *IEEE Computational Engineering in Systems Applications (CESA)* (Lille, France).

Lauber, J., Khiar, D., and Guerra, T. M. (2007). Air-Fuel Ratio Control for an IC Engine. in *IEEE Vehicle Power and Propulsion Conference (VPPC)* (Arlington, USA), 718–723.

Laurain, T., Lauber, J., and Palhares, R. M. (2015a). Observer design to control individual cylinder spark advance for idle speed management of a SI engine. in *IEEE Conference on Industrial Electronics and Applications (ICIEA)* (Auckland, New Zealand), 262–267.

Laurain, T., Lauber, J., and Palhares, R. M. (2015b). Periodic Takagi-Sugeno Observers for Individual Cylinder Spark Imbalance in Idle Speed Control Context. in *IEEE International Conference on Informatics in Control, Automation and Robotics (ICINCO)* (Colmar, France), 302–309.

Laurain, T., Lauber, J., and Palhares, R. M. (2016a). Advanced model based air path management using a discrete-angular controller in idle-speed context. in *IFAC Symposium on Advances in Automative Control (AAC)* (Norrköping, Sweden), 611–618.

Laurain, T., Lauber, J., and Palhares, R. M. (2016b). Counterpart of Advanced TS discrete controller without matrix inversion. in *IFAC International Conference on Intelligent Control and Automation Sciences (ICONS)* (Reims, France), 182–187.

Laurain, T., Lauber, J., and Palhares, R. M. (2016c). Estimation-based control law for appproximating Takagi-Sugeno-based controller. in *IEEE International Conference on Automation, Quality and Testing, Robotics (AQTR)* (Cluj-Napoca, Romania), 1–6.

Laurain, T., Lauber, J., and Palhares, R. M. (2016d). Replica of an Advanced Takagi-Sugeno discrete observer without matrix inversion. in *IEEE International Conference on Fuzzy Systems (FUZZ-IEEE)* (Vancouver, Canada), 2206–2211.

Laurain, T., Lauber, J., and Palhares, R. M. (2017a). Avoiding the matrix inversion in Takagi-Sugeno-based advanced controllers and observers. *IEEE Transactions on Fuzzy Systems*.

Laurain, T., Lendek, Z., Lauber, J., and Palhares, R. M. (2017b). A new air-fuel ratio model fixing the transport delay: Validation and control. in *IEEE Conference on Control Technology and Applications* (Hawaii, USA).

Lehmann, D., and Johansson, K. H. (2012). Event-triggered PI control subject to actuator saturation. *IFAC Proceedings Volumes* 45, 430–435.

Lendek, Z., Guerra, T.-M., and Lauber, J. (2015). Controller Design for TS Models Using Delayed Nonquadratic Lyapunov Functions. *IEEE Transactions on Cybernetics* 45, 439–450.

Lendek, Z., Lauber, J., and Guerra, T.-M. (2013). Periodic Lyapunov functions for periodic TS systems. *Systems & Control Letters* 62, 303–310.

Leroy, T., and Chauvin, J. (2013). Control-oriented aspirated masses model for variable-valve-actuation engines. *Control Engineering Practice* 21, 1744–1755.

Leroy, T., Chauvin, J., and Petit, N. (2008). Airpath control of a SI engine with variable valve timing actuators. in *IEEE American Control Conference (ACC)* (Seattle, USA), 2076–2083.

Li, P., and Shen, T. (2011). Individual Air-Fuel Ratio Balancing Control for Multi-Cylinder SI Engines: Modeling and Validation. in *IFAC World Congress* (Milano, Italy), 2214–2219.

Li, Z., and Shenton, A. T. (2010). Nonlinear Model Structure Identification of Engine Torque and Air/Fuel Ratio. in *IFAC Symposium on Advances in Automotive Control (AAC)* (Munich, Germany), 709–714.

Li, Z., and Shenton, A. T. (2012). Multi-Modelling of Torque and Air/Fuel Ratio Based on Engine Operating Regions. in *IFAC Workshop on Control Applications of Optimization (CAO)* 15th. (Rimini, Italy), 164–169.

Lian, Z., He, Y., Zhang, C.-K., and Wu, M. (2017). Further robust stability analysis for uncertain Takagi–Sugeno fuzzy systems with time-varying delay via relaxed integral inequality. *Information Sciences* 409, 139–150.

Ling, H., Xiu-Min, Y., Guo-Liang, L., and Nan, X. (2012). Dynamic Response of a Three-Way Catalytic Converter. *Energy Procedia* 17, 547–554.

Liu, J., Wang, H., and Zhang, Y. (2015). New result on PID controller design of LTI systems via dominant eigenvalue assignment. *Automatica* 62, 93–97.

Liu, J., Zhu, G., Fu, J., Xu, Z., Yao, J., and Zhan, Z. (2017). Quantitative study on in-cylinder combustion and heat release characteristic parameters of gasoline engine based on single variable sweeping tests. *Applied Thermal Engineering* 117, 487–500.

Liu, Z. q, and Zhou, Y. c (2010). A Fuzzy Neural Network and Application to Air-Fuel Ratio Control under Gasoline Engine Transient Condition. in *IEEE International Conference on Intelligent System Design and Engineering Application (ISDEA)* (Changsha, China), 24–26.

Liu, Y., and Shen, T. (2012). Modeling and experimental validation of air-fuel ratio under individual cylinder fuel injection for port-injection engines. in *IEEE International Conference on Automation Science and Engineering (CASE)* (Seoul, South Korea), 256–260.

Liu, Y., Shen, T., Sata, K., and Suzuki, K. (2011). Modeling of individual cylinder air-fuel ratio for IC engines with multi-cylinders. in *IEEE Chinese Control Conference (CCC)* (Yantai, China), 6151–6156.

Losero, R., Lauber, J., and Guerra, T.-M. (2015). Discrete Angular Torque Observer Applicated to the engine torque and clutch torque estimation via a dual-mass flywheel. in *IEEE International Conference on Industrial Electronics and Applications (ICIEA)* (Auckland, New Zealand), 1020–1025.

Ma, Q., Brahma, A., and Rizzoni, G. (2002). Idle-Speed Control for automotive engines with an integrated starter alternator. in *IFAC World Congress* (Barcelona, Spain), 247–252.

Majecki, P., van der Molen, G., Grimble, M. J., Haskara, I., Hu, Y., and Chang, C.-F. (2015). Real-Time Predictive Control for SI Engines Using Linear Parameter-Varying Models. in *IFAC Conference on Nonlinear Model Predictive Control (NMPC)* (Seville, Spain), 94–101.

Mallik, A., and Aryan (2015). State feedback based control of air-fuel-ratio using two wide-band oxygen sensors. in *IEEE Asian Control Conference (ASCC)* (Kota Kinabalu, Malaisia), 1–6.

Manzie, C., Keynejad, F., Andrianov, D. I., Dingli, R., and Voice, G. (2009). A control-oriented model for cold start operation of spark ignition engines. in *IFAC Workshop on Engine and Powertrain Control, Simulation and Modeling (E-COSM)* (Rueil-Malmaison, France), 216–223.

Meda-Campaña, J. A., Rodríguez-Valdez, J., Hernández-Cortés, T., Tapia-Herrera, R., and Nosov, V. (2015). Analysis of the Fuzzy Controllability Property and Stabilization for a Class of TS Fuzzy Models. *IEEE Transactions on Fuzzy Systems* 23, 291–301.

Meng, Z., and Pan, J.-S. (2016). Monkey King Evolution: A new memetic evolutionary algorithm and its application in vehicle fuel consumption optimization. *Knowledge-Based Systems* 97, 144–157.

Mingrui, W., Thanh Sa, N., Turkson, R. F., Jinping, L., and Guanlun, G. (2017). Water injection for higher engine performance and lower emissions. *Journal of the Energy Institute* 90, 285–299.

Misdariis, A., Vermorel, O., and Poinsot, T. (2015). A methodology based on reduced schemes to compute autoignition and propagation in internal combustion engines. *Proceedings of the Combustion Institute* 35, 3001–3008.

Montes-Solano, C. A., and Pisu, P. (2009). Model Based Fault Detection and Isolation in Idle Speed Control of IC Engines. in *IFAC Symposium on Fault Detection, Supervision and Safety of Technical Processes* (Barcelona, Spain), 905–910.

Moraal, P. E., Cook, J. A., and Grizzle, J. W. (1993). Single sensor individual cylinder air-fuel ratio control of an eight cylinder engine with exhaust gas mixing. in *IEEE American Control Conference (ACC)* (San Francisco, USA), 1761–1767.

Mozaffari, A., and Azad, N. L. (2015). An ensemble neuro-fuzzy radial basis network with self-adaptive swarm based supervisor and negative correlation for modeling automotive engine coldstart hydrocarbon emissions: A soft solution to a crucial automotive problem. *Applied Soft Computing* 32, 449–467.

Mozelli, L. A., Palhares, R. M., Souza, F. O., and Mendes, E. M. A. M. (2009). Reducing conservativeness in recent stability conditions of TS fuzzy systems. *Automatica* 45, 1580–1583.

Na, J., Herrmann, G., Rames, C., Burke, R., and Brace, C. (2016). Air-fuel-ratio control of engine system with unknown input observer. in *UKACC International Conference on Control* (Belfast, UK), 1–6.

Nakamura, T. A., Palhares, R. M., Caminhas, W. M., Menezes, B. R., de Campos, M. C. M. M., Fumega, U., et al. (2017). Adaptive fault detection and diagnosis using parsimonious Gaussian mixture models trained with distributed computing techniques. *Journal of the Franklin Institute* 354, 2543–2572.

Nesamani, K. S., Saphores, J.-D., McNally, M. G., and Jayakrishnan, R. (2017). Estimating impacts of emission specific characteristics on vehicle operation for quantifying air pollutant emissions and energy use. *Journal of Traffic and Transportation Engineering*.

Ngo, C., Sename, O., Bechart, H., and Koenig, D. (2014). Reduced Model of Engine Air Path System Using a LPV Approach. in *International Symposium on Advanced Vehicle Control (AVEC)* (Tokyo, Japan).

Nguyen, A., Laurain, T., Lauber, J., Sentouh, C., and Popieul, J.-C. (2015). Non-quadratic approach for control design of constrained Takagi-Sugeno fuzzy systems subject to persistent disturbances. in *IEEE International Conference on Fuzzy Systems (FUZZ-IEEE)* (Istanbul, Turkey), 1–6.

Nguyen, A.-T., Laurain, T., Palhares, R., Lauber, J., Sentouh, C., and Popieul, J.-C. (2016). LMI-based control synthesis of constrained Takagi–Sugeno fuzzy systems subject to L2 or L∞ disturbances. *Neurocomputing* 207, 793–804.

Nguyen, A.-T., Márquez, R., and Dequidt, A. (2017a). An augmented system approach for LMI-based control design of constrained Takagi-Sugeno fuzzy systems. *Engineering Applications of Artificial Intelligence* 61, 96–102.

Nguyen, A.-T., Tanaka, K., Dequidt, A., and Dambrine, M. (2017b). Static output feedback design for a class of constrained Takagi–Sugeno fuzzy systems. *Journal of the Franklin Institute* 354, 2856–2870.

Nguyen, T. A.-T. (2013). Outils de commande avancés pour les applications automobiles.

Norimatsu, H., and Isomura, S. (1981). Air-fuel ratio control system.

Oldenkamp, R., van Zelm, R., and Huijbregts, M. A. J. (2016). Valuing the human health damage caused by the fraud of Volkswagen. *Environmental Pollution* 212, 121–127.

Ozdemir, A., and Mugan, A. (2013). Stop/Start System Integration to Diesel Engine and System Modelling & Validation. in *IFAC Workshop on Advances in Control and Automation Theory for Transportation Applications* (Istanbul, Turkey), 95–100.

Pavlovic, J., Marotta, A., and Ciuffo, B. (2016). CO2 emissions and energy demands of vehicles tested under the NEDC and the new WLTP type approval test procedures. *Applied Energy* 177, 661–670.

Peyton Jones, J. C., Frey, J., and Shayestehmanesh, S. (2017). Stochastic Simulation and Performance Analysis of Classical Knock Control Algorithms. *IEEE Transactions on Control Systems Technology* PP, 1–11.

Peyton Jones, J. C., and Muske, K. R. (2009). Identification and adaptation of linear look-up table parameters using an efficient recursive least-squares technique. *ISA Transactions* 48, 476–483.

Peyton Jones, J. C., Spelina, J. M., and Frey, J. (2013). Likelihood-Based Control of Engine Knock. *IEEE Transactions on Control Systems Technology* 21, 2169–2180.

Polóni, T., Rohal'-Ilkiv, B., and Johansen, T. A. (2007). Multiple ARX model-based air-fuel ratio predictive control for SI engines. in *IFAC Workshop on Advanced Fuzzy and Neural Control* (Valenciennes, France), 73–78.

Postma, M., and Nagamune, R. (2012). Air-Fuel Ratio Control of Spark Ignition Engines Using a Switching LPV Controller. *IEEE Transactions on Control Systems Technology* 20, 1175–1187.

Powell, B. K., Cook, J. A., and Grizzle, J. W. (1987). Modeling and Analysis of an Inherently Multi-Rate Sampling Fuel Injected Engine Idle Speed Control Loop. in *IEEE American Control Conference (ACC)* (Minneapolis, USA), 1543–1548.

Premkumar, K., and Manikandan, B. V. (2015). Fuzzy PID supervised online ANFIS based speed controller for brushless dc motor. *Neurocomputing* 157, 76–90.

Rahmani, R., Rahnejat, H., Fitzsimons, B., and Dowson, D. (2017). The effect of cylinder liner operating temperature on frictional loss and engine emissions in piston ring conjunction. *Applied Energy* 191, 568–581.

Rigatos, G., Siano, P., and Arsie, I. (2014a). Flatness-based embedded adaptive fuzzy control of spark ignited engines. in *International Conference of Computational Methods in Sciences and Engineering (ICCMSE)* (Athens, Greece), 241–250.

Rigatos, G., Siano, P., and Arsie, I. (2014b). Flatness-based embedded control of air-fuel ratio in combustion engines. in *International Conference of Computational Methods in Sciences and Engineering (ICCMSE)* (Athens, Greece), 251–259.

Rotondo, D., Nejjari, F., and Puig, V. (2014). A virtual actuator and sensor approach for fault tolerant control of LPV systems. *Journal of Process Control* 24, 203–222.

Rupp, D., Onder, C. H., and Guzzella, L. (2007). Iterative adaptive air-fuel ratio control. in *IFAC Symposium on Advances in Automotive Control (AAC)* (Monterey, USA), 593–599.

Sa, E., Ferreira, J., Carvalho, A., and Borrego, C. (2015). Development of current and future pollutant emissions for Portugal. *Atmospheric Pollution Research* 6, 849–857.

Sabatini, S., Kil, I., Dekar, J., Hamilton, T., Wuttke, J., Smith, M. A., et al. (2015). A New Semi-Empirical Temperature Model for the Three Way Catalytic Converter. in *IFAC Workshop on Engine and Powertrain Control, Simulation and Modeling (E-COSM)* (Rueil-Malmaison, France), 434–440.

Sala, A., and Ariño, C. (2007). Asymptotically necessary and sufficient conditions for stability and performance in fuzzy control: Applications of Polya's theorem. *Fuzzy Sets and Systems* 158, 2671–2686.

Santos, H., and Costa, M. (2009). Modelling transport phenomena and chemical reactions in automotive three-way catalytic converters. *Chemical Engineering Journal* 148, 173–183.

Saraswati, S., Agarwal, P. K., and Chand, S. (2011). Neural networks and fuzzy logic-based spark advance control of SI engines. *Expert Systems with Applications* 38, 6916–6925.

Saraswati, S., and Chand, S. (2010). An optimization algorithm for neural predictive control of air-fuel ratio in SI engines. in *IEEE International Conference on Modelling, Identification and Control (ICMIC)* (Okayama, Japan), 527–532.

Schick, W., Onder, C., and Guzzella, L. (2011). Individual Cylinder Air-Fuel Ratio Control Using Fourier Analysis. *IEEE Transactions on Control Systems Technology* 19, 1204–1213.

Schuetzle, D., Siegl, W. O., Jensen, T. E., Dearth, M. A., Kaiser, E. W., Gorse, R., et al. (1994). The relationship between gasoline composition and vehicle hydrocarbon emissions: a review of current studies and future research needs. *Environmental health perspectives* 102, 3.

Shah, P., and Agashe, S. (2016). Review of fractional PID controller. *Mechatronics* 38, 29–41.

Shamim, T. (2004). Modeling and simulation of automotive catalytic converters. in *IEEE International Multitopic Conference (INMIC)* (Karachi, Pakistan), 560–565.

Shancita, I., Masjuki, H. H., Kalam, M. A., Rizwanul Fattah, I. M., Rashed, M. M., and Rashedul, H. K. (2014). A review on idling reduction strategies to improve fuel economy and reduce exhaust emissions of transport vehicles. *Energy Conversion and Management* 88, 794–807.

Shen, X., Zhang, Y., Shen, T., and Khajorntraidet, C. (2017). Spark advance self-optimization with knock probability threshold for lean-burn operation mode of SI engine. *Energy* 122, 1–10.

Shi, Y., Yu, D.-L., Tian, Y., and Shi, Y. (2015). Air–fuel ratio prediction and NMPC for SI engines with modified Volterra model and RBF network. *Engineering Applications of Artificial Intelligence* 45, 313–324.

Shiao, Y., and Moskwa, J. J. (1996). Model-based cylinder-by-cylinder air-fuel ratio control for SI engines using sliding observers. in *IEEE International Conference on Control Applications (CCA)* (Dearborn, USA: IEEE), 347–354.

Shirazi, N., Walters, A., and Athanas, P. (1995). Quantitative analysis of floating point arithmetic on FPGA based custom computing machines. in *IEEE Symposium on FPGAs for Custom Computing Machines*, 155–162.

Sing Kiong Nguang, Peng Shi, and Ding, S. (2007). Fault Detection for Uncertain Fuzzy Systems: An LMI Approach. *IEEE Transactions on Fuzzy Systems* 15, 1251–1262.

Solyom, S., and Eriksson, S. (2006). Mid-Ranging Scheme for Idle Speed Control of SI Engines. in *SAE World Congress*.

Souza, C. E. de, Palhares, R. M., and Peres, P. L. D. (2001). Robust H infinity filter design for uncertain linear systems with multiple time-varying state delays. *IEEE Transactions on Signal Processing* 49, 569–576.

Souza, F. O., Campos, V. C. S., and Palhares, R. M. (2014). On delay-dependent stability conditions for Takagi–Sugeno fuzzy systems. *Journal of the Franklin Institute* 351, 3707–3718.

Souza, F. O., De Oliveira, M. C., and Palhares, R. M. (2009a). Stability independent of delay using rational functions. *Automatica* 45, 2128–2133.

Souza, F. O., Mozelli, L. A., and Palhares, R. M. (2009b). On stability and stabilization of T–S fuzzy time-delayed systems. *IEEE Transactions on Fuzzy Systems* 17, 1450–1455.

Takagi, T., and Sugeno, M. (1985). Fuzzy identification of systems and its applications to modeling and control. *IEEE Transactions on Systems, Man and Cybernetics, Part B (Cybernetics)*, 116–132.

Takahashi, S., and Sekozawa, T. (1995). Air-fuel ratio control in gasoline engines based on state estimation and prediction using dynamic models. in *IEEE International Conference on Industrial Electronics, Control, and Instrumentation (IECON)* (Orlando, USA), 217–222.

Tan, Q., Divekar, P., Tan, Y., Chen, X., and Zheng, M. (2016). Engine Model Calibration Using Extremum Seeking. in *IFAC Symposium on Advances in Automative Control (AAC)* (Norrköping, Sweden), 730–735.

Tanaka, K., Ikeda, T., and Wang, H. O. (1998). Fuzzy regulators and fuzzy observers: relaxed stability conditions and LMI-based designs. *IEEE Transactions on Fuzzy Systems* 6, 250–265.

Tanaka, K., and Sano, M. (1994). A robust stabilization problem of fuzzy control systems and its application to backing up control of a truck-trailer. *IEEE Transactions on Fuzzy Systems* 2, 119–134.

Tavakoli, A. R., and Seifi, A. R. (2016). Adaptive self-tuning PID fuzzy sliding mode control for mitigating power system oscillations. *Neurocomputing* 218, 146–153.

Teixeira, M. C. M., Assuncao, E., and Avellar, R. G. (2003). On relaxed LMI-based designs for fuzzy regulators and fuzzy observers. *IEEE Transactions on Fuzzy Systems* 11, 613–623.

Theorin, A., and Hägglund, T. (2015). Derivative backoff: The other saturation problem for PID controllers. *Journal of Process Control* 33, 155–160.

Thomasson, A. (2009). *Wastegate Actuator Modeling and Tuning of a PID Controller for Boost Pressure Control*. Linköping.

Thomasson, A., Shi, H., Lindell, T., Eriksson, L., Shen, T., and Peyton Jones, J. C. (2016). Experimental Validation of a Likelihood-Based Stochastic Knock Controller. *IEEE Transactions on Control Systems Technology* 24, 1407–1418.

Thornhill, M., Thompson, S., and Sindano, H. (2000). A comparison of idle speed control schemes. *Control Engineering Practice* 8, 519–530.

Toyoda, M., and Shen, T. (2017). A receding horizon D-optimization approach for model identification–oriented input design and application in combustion engines. *Applied Mathematical Modelling* 42, 175–187.

Trimboli, S., Di Cairano, S., Bemporad, A., and Kolmanovsky, I. V. (2009). Model predictive control for automotive time-delay processes: An application to air-to-fuel ratio control. in *IFAC Proceedings Volumes*, 90–95.

Tuan, H. D., Apkarian, P., Narikiyo, T., and Yamamoto, Y. (2001). Parameterized linear matrix inequality techniques in fuzzy control system design. *IEEE Transactions on Fuzzy Systems* 9, 324–332.

Ulrich, V., Moroz, B., Sinev, I., Pyriaev, P., Bukhtiyarov, V., and Grünert, W. (2017). Studies on three-way catalysis with supported gold catalysts. Influence of support and water content in feed. *Applied Catalysis B: Environmental* 203, 572–581.

Valério, M., Raggi, K., and Sodré, J. R. (2003). Model for Kinetic Formation of CO Emissions in Internal Combustion Engines. SAE Technical Paper.

Wang, C., and Liu, Z. (2016). Estimation of Individual Cylinder Air-Fuel Ratio in Gasoline Engine with Output Delay. *Journal of Sensors* 2016, 1–9.

Wang, C.-H., and Huang, D.-Y. (2013). A New Intelligent Fuzzy Controller for Nonlinear Hysteretic Electronic Throttle in Modern Intelligent Automobiles. *IEEE Transactions on Industrial Electronics* 60, 2332–2345.

Wang, H. O., Tanaka, K., and Griffin, M. F. (1996). An approach to fuzzy control of nonlinear systems: Stability and design issues. *IEEE Transactions on Fuzzy Systems* 4, 14–23.

Wang, L., and Liu, J. (2017). Local stability analysis for continuous-time Takagi-Sugeno fuzzy systems with time delay. *Neurocomputing*.

Wang, S. W., Yu, D. L., Gomm, J. B., Page, G. F., and Douglas, S. S. (2006). Adaptive neural network model based predictive control for air–fuel ratio of SI engines. *Engineering Applications of Artificial Intelligence* 19, 189–200.

Wang, S., and Yu, D. L. (2008). Adaptive RBF network for parameter estimation and stable air–fuel ratio control. *Neural Networks* 21, 102–112.

Wang, Y., Xie, L., and de Souza, C. E. (1992). Robust control of a class of uncertain nonlinear systems. *Systems & Control Letters* 19, 139–149.

Wang, Z., and Jiao, X. (2015). Adaptive fuelling control considering effect of time-delay for air-fuel ratio regulation of spark ignition engines. in *IEEE Annual Conference of the Society of Instrument and Control Engineers of Japan (SICE)* (Hangzhou, China), 1311–1315.

Waschl, H., Kolmanovsky, I., Steinbuch, M., and del Re, L. eds. (2014). *Optimization and Optimal Control in Automotive Systems*. Springer.

Wei, H., Zhu, T., Shu, G., Tan, L., and Wang, Y. (2012). Gasoline engine exhaust gas recirculation – A review. *Applied Energy* 99, 534–544.

Wilkinson, J. H. (1960). Error analysis of floating-point computation. *Numerische Mathematik* 2, 319–340.

Wojnar, S., Honek, M., and Rohal'-Ilkiv, B. (2013). Nonlinear air-fuel ratio predictive control of spark ignited engines. in *2013 International Conference on Process Control (PC)*, 225–230.

Xie, H., Song, K., and He, Y. (2014). A hybrid disturbance rejection control solution for variable valve timing system of gasoline engines. *ISA Transactions* 53, 889–898.

Xie, X., Ma, H., Zhao, Y., Ding, D.-W., and Wang, Y. (2013). Control Synthesis of Discrete-Time TS Fuzzy Systems Based on a Novel Non-PDC Control Scheme. *IEEE Transactions on Fuzzy Systems* 21, 147–157.

Xu, F., Chen, H., Gong, X., and Hu, Y. F. (2013). Engine idle speed control using nonlinear model predictive control. in *IFAC Symposium on Advances in Automative Control (AAC)* (Tokyo, Japan), 171–176.

Xu, S., Sun, G., and Sun, W. (2017). Takagi–Sugeno fuzzy model based robust dissipative control for uncertain flexible spacecraft with saturated time-delay input. *ISA Transactions* 66, 105–121.

Ye, Z. (2007). Modeling, Identification, Design, and Implementation of Nonlinear Automotive Idle Speed Control Systems: An Overview. *IEEE Transactions on Systems, Man and Cybernetics, Part C (Applications and Reviews)* 37, 1137–1151.

Yildiz, Y., Annaswamy, A. M., Yanakiev, D., and Kolmanovsky, I. (2010). Spark ignition engine fuel-to-air ratio control: An adaptive control approach. *Control Engineering Practice* 18, 1369–1378.

Yildiz, Y., Annaswamy, A. M., Yanakiev, D., and Kolmanovsky, I. (2011). Spark-Ignition-Engine Idle Speed Control: An Adaptive Control Approach. *IEEE Transactions on Control Systems Technology* 19, 990–1002.

Yoneyama, J. (2007). New delay-dependent approach to robust stability and stabilization for Takagi–Sugeno fuzzy time-delay systems. *Fuzzy Sets and Systems* 158, 2225–2237.

Yurkovich, S., and Simpson, M. (1997). Comparative analysis for idle speed control: A crank-angle domain viewpoint. in *IEEE American Control Conference (ACC)* (Albuquerque, NM, USA), 278–283.

Yusri, I. M., Mamat, R., Najafi, G., Razman, A., Awad, O. I., Azmi, W. H., et al. (2017). Alcohol based automotive fuels from first four alcohol family in compression and spark ignition engine: A review on engine performance and exhaust emissions. *Renewable and Sustainable Energy Reviews* 77, 169–181.

Zhai, Y., and Yu, D. (2007). RBF-based feedforward-feedback control for air-fuel ratio of SI engines. in *IFAC Workshop on Advanced Fuzzy and Neural Control* (Valenciennes, France), 13–18.

Zhai, Y.-J., and Yu, D.-L. (2009). Neural network model-based automotive engine air/fuel ratio control and robustness evaluation. *Engineering Applications of Artificial Intelligence* 22, 171–180.

Zhai, Y.-J., Yu, D.-W., Guo, H.-Y., and Yu, D. L. (2010). Robust air/fuel ratio control with adaptive DRNN model and AD tuning. *Engineering Applications of Artificial Intelligence* 23, 283–289.

Zhang, C., and Sun, Z. (2016). Using variable piston trajectory to reduce engine-out emissions. *Applied Energy* 170, 403–414.

Zhang, F., and Yeddanapudi, M. (2012). Modeling and simulation of time-varying delays. in *Symposium on Theory of Modeling and Simulation* (Society for Computer Simulation International), 34.

Zhang, H., Fu, L., Song, J., and Yang, Q. (2016). Power Energy Management and Control Strategy Study for Extended-range Auxiliary Power Unit. *Energy Procedia* 104, 32–37.

Zhang, J., Shen, T., and Marino, R. (2010). Model-based cold-start speed control scheme for spark ignition engines. *Control Engineering Practice* 18, 1285–1294.

Zheng, G., Bejarano, F. J., Perruquetti, W., and Richard, J.-P. (2015). Unknown input observer for linear time-delay systems. *Automatica* 61, 35–43.

Zhi-Xiang, H. (2016). Predictive Control for Air Fuel Ratio of Gasoline Engine Based on Neural Network. in *IEEE International Conference on Smart City and Systems Engineering (ICSCSE)* (Hunan, China), 433–434.

Zhixiong, L., Zhiwei, G., Chongqing, H., and Aihua, L. (2017). On-line indicated torque estimation for internal combustion engines using discrete observer. *Computers & Electrical Engineering*.

Zope, R. A., Mohammadpour, J., Grigoriadis, K. M., and Franchek, M. (2009). Air-fuel ratio control of spark ignition engines with TWC using LPV techniques. in *ASME Dynamic Systems and Control Conference* (Hollywood, USA), 897–903.

PERSONAL REFERENCES

Conference papers

Nguyen, A., Laurain, T., Lauber, J., Sentouh, C., Popieul, J.-C., 2015. Non-quadratic approach for control design of constrained Takagi-Sugeno fuzzy systems subject to persistent disturbances, in: IEEE International Conference on Fuzzy Systems (FUZZ-IEEE). Istanbul, Turkey, pp. 1–6.

Laurain, T., Lauber, J., Palhares, R.M., 2015. Observer design to control individual cylinder spark advance for idle speed management of a SI engine, in: IEEE Conference on Industrial Electronics and Applications (ICIEA). Auckland, New Zealand, pp. 262–267.

Laurain, T., Lauber, J., Palhares, R.M., 2015. Periodic Takagi-Sugeno Observers for Individual Cylinder Spark Imbalance in Idle Speed Control Context, in: IEEE International Conference on Informatics in Control, Automation and Robotics (ICINCO). Colmar, France, pp. 302–309.

Laurain, T., Lauber, J., Palhares, R.M., 2016. Advanced model based air path management using a discrete-angular controller in idle-speed context, in: IFAC Symposium on Advances in Automative Control (AAC). Norrköping, Sweden, pp. 611–618.

Laurain, T., Lauber, J., Palhares, R.M., 2016. Replica of an Advanced Takagi-Sugeno discrete observer without matrix inversion, in: IEEE International Conference on Fuzzy Systems (FUZZ-IEEE). Vancouver, Canada, pp. 2206–2211.

Laurain, T., Lauber, J., Palhares, R.M., 2016. Estimation-based control law for appproximating Takagi-Sugeno-based controller, in: IEEE International Conference on Automation, Quality and Testing, Robotics (AQTR). Cluj-Napoca, Romania, pp. 1–6.

Laurain, T., Lauber, J., Palhares, R.M., 2016. Counterpart of Advanced TS discrete controller without matrix inversion, in: IFAC International Conference on Intelligent Control and Automation Sciences (ICONS). Reims, France, pp. 182–187.

Laurain, T., Lendek, Z., Lauber, J., Palhares, R.M., 2017. A new air-fuel ratio model fixing the transport delay: Validation and control, in: IEEE Conference on Control Technology and Applications. Hawaii, USA.

Journal papers

Nguyen, A.-T., Laurain, T., Palhares, R., Lauber, J., Sentouh, C., Popieul, J.-C., 2016. LMI-based control synthesis of constrained Takagi–Sugeno fuzzy systems subject to L2 or L∞ disturbances. Neurocomputing 207, 793–804.

Laurain, T., Lauber, J., Palhares, R.M., 2017a. Avoiding the matrix inversion in Takagi-Sugeno-based advanced controllers and observers. IEEE Transactions on Fuzzy Systems.

Abstract: My PhD in Automatic Control is part of the research theme “Transport” of the LAMIH. The objective is to improve the functioning of the gasoline engines, mainly by reducing the fuel consumption and the pollution. With this ecologic and economic challenge, and taking into account the new norms and the short-term strategies of the industry (scandal of Volkswagen...), new controllers have to be designed to control the air valve and the fuel injection inside the engine. Considering the highly nonlinear aspect of the system, the Takagi-Sugeno representation and the theoretical background of the LAMIH have been used. A first controller is designed to solve the problem of idle engine speed. However, the complexity of the system forces the use of a controller that is very costly from a computational point of view. An alternative controller is then designed in order to be implemented inside the embedded computer of the engine. A second controller is obtained to maintain the air-fuel ratio in stoichiometric proportions in order to reduce the pollution. This system being subject to a variable transport delay, a change of domain is realized to make this delay constant, and to design a simple and efficient controller. Real-time experiments have been realized on the engine test bench of the LAMIH in order to validate the presented methodology.

Keywords: Engine control; nonlinear system; idle speed; air-fuel ratio; Takagi-Sugeno representation; alternative controller; Lyapunov direct method; variable transport delay; identification; simulation results; engine test bench; experimental results

Résumé : Ma thèse en automatique s’inscrit dans la thématique de recherche «Transport» du LAMIH. L’objectif est d’améliorer le fonctionnement des moteurs thermiques (essence), notamment en réduisant la consommation et la pollution. Face à cet enjeu écologique et économique, et compte tenu des nouvelles normes et des stratégies court-termistes de l’industrie (scandale Volkswagen...), de nouveaux contrôleurs doivent être conçus pour piloter l’arrivée d’air et d’essence au sein du moteur. En considérant l’aspect hautement non-linéaire du système, la représentation Takagi-Sugeno et le background théorique du LAMIH sont utilisés. Un premier contrôleur est synthétisé pour régler le problème de la vitesse de ralenti du moteur. Cependant, la complexité du système impose l’utilisation d’un contrôleur très coûteux d’un point de vue computationnel. Un contrôleur alternatif est donc synthétisé afin d’être implémenté dans l’ordinateur embarqué du moteur. Un second contrôleur est obtenu pour maintenir la richesse en proportions stœchiométriques afin de réduire la pollution. Ce système étant sujet à un retard de transport variable, un changement de domaine est réalisé afin de rendre ce retard constant, et de concevoir un contrôleur simple et efficace. Des essais réels sur le banc d’essai moteur du LAMIH sont réalisés afin de valider la méthodologie présentée.

Mots-clefs : Contrôle moteur; système non-linéaire; vitesse de ralenti; richesse; representation Takagi-Sugeno; contrôleur alternatif; méthode directe de Lyapunov; retard de transport variable; identification; résultats de simulation; banc moteur; résultats expérimentaux